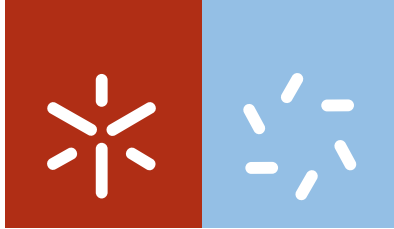**Universidade do Minho**

Escola de Ciências

Rita Maria Burguete Bacelar Marreiros Figueira

Study of use of hybrid materials obtained by sol-gel to produce efficient pre-treatments to prevent galvanized steel reinforcement corrosion

December 2014

Universidade do Minho

Escola de Ciências

Rita Maria Burguete Bacelar Marreiros Figueira

Study of use of hybrid materials obtained by sol-gel to produce efficient pre-treatments to prevent galvanized steel reinforcement corrosion

Tese de Doutoramento em Ciências
Especialidade em Química

Trabalho efectuado sob a orientação do
Professor Doutor Carlos Jorge Ribeiro da Silva
e da
Doutora Elsa Maria Vicente Dias da Silva Eustáquio Vaz Pereira

December 2014

STATEMENT OF INTEGRITY

I hereby declare having conducted my thesis with integrity. I confirm that I have not used plagiarism or any form of falsification of results in the process of the thesis elaboration.

I further declare that I have fully acknowledged the Code of Ethical Conduct of the University of Minho.

University of Minho, December, 9th, 2014

Full name: Rita Maria Burguete Bacelar Marreiros Figueira

Signature: _____

This thesis is lovingly dedicated to my husband and sons:

Hugo, Francisco and Manuel.

A person who never made a mistake never tried anything new

A. Einstein

Acknowledgements

A PhD thesis is a long journey and this work was not possible without the help of several people.

In the first place, I want to express my gratitude to my supervisors Doutora Elsa Vaz Pereira and to Professor Doutor Carlos Silva for their knowledge, inspiration and support.

I am truly thankful to Doutora Elsa Vaz Pereira for the opportunity to work in the National Laboratory for Civil Engineering (LNEC). It has been an honour to be her first PhD student. She has been supportive and has given me the freedom to pursue my projects and ambitions without objections.

I am grateful to Prof. Doutor Carlos Silva, from the first moment his presence was constant. Despite the 300 km apart, I never felt alone and he was always inspiring and supportive. I do not have words to express my thanks regarding all the hours that were devoted to reading and accompanying my work. I appreciate all his contributions of time and ideas, making my Ph.D. experience productive and stimulating. The joy and enthusiasm he has for his research was contagious and motivational for me. For all that, I am truly thankful.

I also would like to acknowledge all the people in the Metallic Materials Department that contributed immensely to my personal and professional time at LNEC. A special thanks is due to Eng.ª Ana Paula Melo. I will not forget all her support and availability in helping me to solve my daily working problems and sometimes for her availability to listen and talk about casual life stories. I will certainly miss our teatime. This group has been a source of friendships as well as good advice and collaboration. I am thankful for their technical support, in particular to Eng.ª Manuela Salta, Drª Maria João, Mrs. Paula Menezes, Eng.ª Rute Fontinha, Eng.ª Ângela Amaral and Eng.º Nuno Garcia.

I gratefully acknowledge the support of FCT (Fundação para a Ciência e Tecnologia for my PhD Grant (SFRH/BD/62601/2009).

I also thank my friends in particular Sílvia Estácio, Paula Alves, Marta Branco, Pedro Fortunato, Maria João Alves, Frederico Alves, Ana Rita Rosa and Victoria Smith for providing support and friendship that I needed.

Lastly, but not the least, I would like to thank my husband Hugo for his dedication, love, faithful support, encouragement, patience and just for being there when I needed it, without him this would be an impossible task. To my beloved sons, Francisco and Manuel, although most of the times they did not understand my absence, I am thankful for the enthusiastic way they see my work and for being terrific kids always cheering me up. To my parents, my brother Miguel and my sister Maria

Ana and Grandmother Francisca, thank you for being there when I needed you. All my defeats and accomplishments are celebrated with them.

Resumo

A corrosão de armaduras no betão armado, por carbonatação do betão ou ataque por iões cloreto, é uma das maiores causas de degradação de estruturas. A propagação da corrosão após o seu início é, em geral, rápida, podendo conduzir à deterioração das estruturas num curto espaço de tempo, com custos de reparação elevados.

A utilização do aço galvanizado é reconhecida como uma medida alternativa para aumentar o tempo de vida útil das estruturas expostas ao ataque de espécies agressivas. Imediatamente após embeber o aço galvanizado no betão fresco, que se revela como um ambiente extremamente alcalino, a camada de zinco corrói-se durante um certo período (podendo variar de apenas umas horas a alguns dias) até que a camada de passivação se forme e o betão conclua o processo de cura. Este processo de corrosão inicial pode levar a um consumo da camada de zinco que varia entre 5 e 10 μm. Simultaneamente, ocorre produção de hidrogénio que pode originar perda de aderência entre o aço de reforço e o betão. Para minimizar e/ou bloquear esta reacção inicial, usam-se vários procedimentos tais como o aumento do teor de cromatos no cimento ou aquando da preparação do betão, a adição de água com cromatos dissolvidos. Adicionalmente, a deposição de camadas de conversão química à base de crómio na superfíce do aço galvanizado também foi um método amplamente utilizado. Consequentemente, este tipo de medidas tornaram-se rotina na prevenção da evolução do hidrogénio e proteção das armaduras galvanizadas. No entanto, devido à toxicidade dos iões Cr(VI), os cimentos Portland actualmente comercializados possuem na sua composição quantidades reduzidas de Cr(VI) e a aplicação de camadas de conversão química à base de crómio tem vindo a ser evitada.

O método sol-gel é um processo versátil que envolve a utilização de uma ampla diversidade de precursores permitindo a incorporação de componentes adicionais que introduzem funcionalidades complementares tais como resistência à humidade, aderência, proteção da corrosão juntamente com o aumento das propriedades mecânicas, térmicas e ópticas. As vantagens deste processo são numerosas e além dos componentes orgânicos outros aditivos como os inibidores podem ser incorporados no sistema sol-gel melhorando a resistência à corrosão dos substratos metálicos.

O presente estudo enquadra-se no desenvolvimento de revestimentos híbridos "amigos" do ambiente produzidos pelo método sol-gel para aço galvanizado de modo a minimizar a corrosão do zinco e a evolução de hidrogénio quando em contacto com meios cimentícios. Os pré-tratamentos propostos representam alternativas viáveis na substituição de pré-tratamentos à base de Cr(VI) utilizados para controlar a reação inicial entre o zinco e o betão fresco.

Sintetizaram-se matrizes híbridas, baseadas em ureiasilicatos e aminoálcool-silicatos, que foram testadas na sua forma pura e após dopadas com um agente inibidor (Cr(III)). Os revestimentos foram depositados no aço galvanizado pelo método *dip-coating*. A eficiência dos diferentes híbridos enquanto barreira de protecção, em contacto com materiais que mimetizam as propriedades físico-químicas do betão (pastas cimentícias e argamassas) foi estudada e avaliada por diversas técnicas eletroquímicas e por técnicas de análise de superfície.

Os resultados evidenciaram que os revestimentos híbridos obtidos pelo método sol-gel possuem propriedades promissoras para serem utilizados como pré-tratamentos "amigos" do ambiente no aço galvanizado em contacto com meios cimentícios. Os revestimentos estudados permitem, efetivamente, mitigar os efeitos adversos das reações iniciais entre o aço galvanizado e os materiais cimentícios. Estes pré-tratamentos revelaram-se alternativas promissoras à utilização de camadas químicas de conversão baseadas em cromatos.

Abstract

The corrosion of steel in concrete is one of the major causes of structures degradation, requiring expensive rehabilitation. The use of hot dip galvanized steel (HDGS) has been recognized as an effective measure to increase the service life of reinforced concrete structures exposed to carbonation or to chloride ions. Immediately after the HDGS is embedded in fresh concrete, a highly alkaline environment, the zinc coating corrodes for a limited period (from several hours to a few days) until passivating surface layers are formed and the concrete hardens. This initial corrosion process may lead to zinc consumption between 5 to 10 μm. At the same time, hydrogen is produced which may lead to the loss of adherence between the steel and the concrete. Common procedures such as increasing the chromate content of the cement or adding water-soluble chromates into this preparation and the use of chromate conversion coatings (CCC) has a favourable effect on blocking initial zinc corrosion. Consequently, these have been trivial procedures employed to prevent hydrogen gas evolution and to protect the hot-dip galvanized rebars. However, due to the toxicity of Cr(VI) ions, current commercialized Portland cements have limited the content of Cr(VI) in their composition and the use of CCCs are currently being avoided.

The sol–gel method is a versatile process involving the use of a large diversity of precursors, allowing the incorporation of additional components. This introduce complementary functionalities of the material, such as moisture resistance, adhesion and corrosion protection, along with the enhancement of mechanical, thermal and optical properties. The advantages of this technology are numerous and besides the organic component, other additives, such as inhibitors could be incorporated into the sol–gel system increasing the corrosion resistance of the metal substrates.

This study is focused on the development of OIH coatings for HDGS reinforcement in contact with cementitious media. OIH sol-gel matrices doped and undoped with inhibitors, ureasilicate and alcohol-aminosilicate, were synthesized. The coatings were deposited on HDGS by a dipping process. The barrier efficiency of the different OIH sol-gel coatings was studied and assessed by several electrochemical techniques and surface analysis, when in contact with cementitious materials (cement pastes and mortar). The results show that the OIH sol-gel coatings studied effectively allow the mitigation of harmful effects of the initial excessive reaction between cementitious materials and the HDGS, showing promising properties to be used as eco-friendly pre-treatments on HDGS in contact with cementitious media.

Table of Contents

4. Ureasilicate Hybrid Coatings for Corrosion Protection of Galvanized Steel in Cementitious Media 113

Preface

This thesis represents a culmination of work and learning that has taken place over a period of four years (September 2010 – December 2014).

The work presented in this thesis is organized in five chapters, corresponding each to a paper previously published. The state of the art presented in this thesis (chapters 1 and 2) is the result of two review papers. The first paper (chapter 1) was published in a journal in the field of coatings (*Journal of Coatings Technology and Research*) and is entitled "Organic-inorganic Hybrid Sol-gel Coatings for Metal corrosion Protection: A Review of Recent Progress". This review provides a synopsis of the most recent work performed in the field of the sol-gel coatings for corrosion protection on the different metallic substrates. The second paper (chapter 2) was published in *Corrosão e Protecção de Materiais* and is entitled "Corrosion of Hot-dip Galvanized Steel Reinforcement". In this review is given an overview of the coatings and pre-treatments studied on hot-dip galvanized steel (HDGS) together with the corrosion mechanisms of HDGS in contact with high alkaline environments. The role of Cr(VI) in inhibiting the initial zinc corrosion process was also discussed.

In the following chapters, are presented the results of the research conducted during this PhD thesis. This section comprises three papers that were published in journals in the field of electrochemistry, respectively:

"Electrochemical system for assessing hybrid coatings for corrosion protection of hot dip galvanized steel in mortar" published in *Portugaliae Electrochimica Acta*. In this paper (chapter 3), an electrochemical system to assess the organic-inorganic hybrid sol-gel coatings, was studied and discussed.

"Ureasilicate Hybrid Coatings for Corrosion Protection of Galvanized Steel in Cementitious Media" published in *The Journal of The Electrochemical Society* (chapter 4). In this paper, the synthesis, the electrochemical behaviour and the morphology characterization of the ureasilicate based coatings was studied in contact with a mortar.

"Alcohol-aminosilicate Hybrid Coatings for Corrosion Protection of Galvanized Steel in Mortar" published in *The Journal of The Electrochemical Society* (chapter 5). In this paper, the synthesis, the electrochemical behaviour and morphology characterization of the alcohol-aminosilicate based coatings was studied in contact with a mortar.

Besides the papers mentioned, the work carried out for this PhD thesis was presented in scientific meetings as eight conference presentation and three poster communications.

1. Organic-inorganic Hybrid Sol-gel Coatings for Metal Corrosion Protection: A Review of Recent Progress

Organic-inorganic Hybrid Sol-Gel Coatings for Metal Corrosion Protection: A Review of Recent Progress

R. B. Figueira[a,b,*], C. J. R. Silva[b], E. V. Pereira[a]

[a]LNEC, Laboratório Nacional de Engenharia Civil, Av. Brasil 101, 1700-066 Lisbon, Portugal

[b]Centro de Química, Universidade do Minho, Campus de Gualtar 4710 - 057 Braga, Portugal

* Corresponding Author: rmfigueira@lnec.pt

Abstract

This paper is a review of the most recent and relevant achievements (from 2001 to 2013) on the development of organic-inorganic hybrid (OIH) coatings produced by sol-gel derived methods to improve resistance to oxidation/corrosion of different metallic substrates and their alloys. This review is focused on the research of OIH coatings based on siloxanes using the sol-gel process conducted at an academic level and aims to summarize the materials developed and identify perspectives for further research.

The fundamentals of sol-gel are described, including OIH classification, the interaction with the substrate, their advantages and limitations. The main precursors used in the synthesis of OIH sol-gel coatings for corrosion protection are also discussed, according to the metallic substrate used. Finally, a multilayer system to improve the resistance to corrosion is proposed, based on OIH coatings produced by the sol-gel process, and the future research challenges are debated.

Keywords

1. Introduction

Corrosion protection of metallic substrates using coatings is an active and important research area in materials science and in industry. Through the application of coatings, corrosion can be minimized and controlled by one of three main mechanisms (or by a combination of these), namely: a barrier effect preventing the contact between the corrosive medium and the metallic substrate and preventing ion migration among the coatings; a cathodic protection where the coating material acts as a sacrificial anode; the use of inhibition/passivation species, including cases of anodic or/and cathodic protection, that inhibit the action of the external corrosive agents.

Technological development has led to the production of a large variety of coatings and materials that have an efficient barrier effect preventing corrosion, namely inorganic coatings, paints and other surface treatments. Chromate and similar hexavalent chromium compounds are effective substances used as inhibitors and are usually incorporated in anticorrosive pre-treatments of a wide range of metals and alloys. The high corrosion resistance offered by the use of chromate films is due to the presence of Cr^{6+} ions. One important example is chromate based chemical conversion coatings (CCCs), as this surface treatment shows an enhanced corrosion resistance and improves coating adhesion. Nonetheless, the use of hazardous compounds, such as CCCs, VOCs (Volatile Organic Compounds) and HAPs (Hazardous Air Pollutants), has been restricted after studies about their impact on natural environments and human health showed them to be toxic and carcinogenic. As such, their application is heavily regulated by most environmental legislation.

The need for alternative environmental friendly materials and processes has been investigated, leading to an enormous effort in the search for novel materials. These materials must provide good corrosion protection performance as well the recommended environmental targets. During this period, researchers from civil and mechanical engineering, chemistry, materials and corrosion sciences have tested a large variety of non-toxic and environmentally friendly processes and among them the sol–gel method has demonstrated to be an efficient alternative for the replacement of existing CCC technology.

Osborne[1] in 2001 reported the application of sol-gel methods for the production of gel coatings for metal corrosion protection purposes. The article entitled "*Some observations on chromate conversion coatings from a sol–gel perspective*" confirmed that new chromate-free materials obtained by sol–gel methods allowed flexible control of coating morphology and constituent oxide materials leading to enhanced properties of the conversion coatings. This report showed that the organic-inorganic hybrid (OIH) coatings produced exhibited promising properties of adhesion and

corrosion protection. The obtained data also suggested that the OIH gel formulation might be tuned to contain non-soluble chromium inhibitors regulating their effective concentrations within the coating layer.[1] The quick evolution of this specific research area and the potential contribution of sol–gel coatings as a corrosion inhibition system for metal substrates has led to several review publications[2,3]. As alternatives to the use of chromate for corrosion protection of aluminium aerospace alloys,[4] the use of sol–gel derived coatings for improved corrosion resistance of aluminium and steel metal surfaces[5,6] and magnesium alloys[7] have also been debated.

OIHs obtained by sol-gel methods are a new generation of multifunctional materials with a broad spectrum of useful properties and a diversity of application potential. The name itself indicates the presence of both organic and inorganic components within the common matrix support. The inorganic part is formed from silicon or transition metal alkoxides via hydrolysis, while the organic part could be based on a diversity of molecules, and depending on how the matrix structure is produced, they can be segments of a quasi-continuous macromolecular domains grafting or bonding the inorganic skeleton. These two components (hydrophilic oxides and hydrophobic organic molecules) are normally difficult to combine within the composite network, and to achieve the interaction between them special reaction conditions must be applied.

The sol-gel OIH coatings are complex matrices where the intermolecular interactions between the macromolecular existing structures and metallic surface are extremely relevant to material properties, like low porosity and rigidity and adhesion to substrate. The conjugation of these interactions results in materials with enhanced protective properties against oxidation, corrosion, erosion and good thermal and electrical insulation properties. Another technological advantage of these materials arises from their ability to be produced at room temperature conditions on an industrial scale using well established and low-cost methods like spray, dip and spin coating, flow coating, roll coating, doctor blading and capillary coating processes or using any combination thereof.[8] Altogether, the reagents involved to produce such matrices have very low environmental impacts. The tested corrosion protection processes and materials based on sol-gel technology demonstrate positive performances when several properties are considered, such as: corrosion resistance, adhesion, fatigue resistance, reliability and quality control. Although some of the possible alternatives demonstrate promise for corrosion protection, continuous efforts are being made in improving the production of OIH materials with improved properties, the understanding of the mechanisms involved in coating production and consequently their corrosion protection performance.

OIH materials represent an important part of the R&D activities and technology portfolio in companies such as Bayer, Boeing GE, Honeywell, BASF, AkzoNobel, Sumitomo, ASAHI Kasei, ASAHI Glass, Dow-Corning, etc. They are also important in more specialized enterprises (Henkel, Procter&Gamble, Wacker, Nissan Chemicals, Shin-Etsu, Toppan, Mitsubishi Chemicals, NEPES, Merck, MicroResistTechnologies, etc). However, the present review is focused mainly on OIHs based on siloxane (i.e., at least one of the precursors used is a siloxane) gels produced by sol-gel derived methods to improve resistance to oxidation/corrosion or to modify/activate the surface properties of metallic substrates, taken from studies at an academic level in the past few years (2001-2013).

2. Sol-Gel Process Fundamentals and OIHs Classification

The sol-gel process is a low temperature synthetic route and is generally used as a chemical route to synthesize OIH materials. It is particularly advantageous in the production of coatings as it provides an excellent control of precursor stoichiometry and as there are a large number of precursor reagents with tuned functional groups, a diversity of OIH gels could be produced following the same trends. This process also allows the incorporation of additional components that introduce complementary functions of the material such as UV protection, anti-fouling, anti-reflection, moisture resistance, corrosion inhibition and adhesion protection. Moreover, sol-gel process enables coating deposition on substrates with a large surface area involving simple and inexpensive equipment.

The definition of sol-gel method itself has undergone some changes over time. There are many authors with significantly different definitions, for example Dislich[9] considered that the sol-gel procedures are only those that take into account multicomponent oxides which are homogeneous at an atomic level. Under different circumstances, Segal[10] introduced the sol-gel method as the production of inorganic oxides in the form of colloidal dispersion or in the form of metal alkoxides. Others[11], considered that the sol-gel process was any chemical process whose starting point was a solution resulting in a solid phase whether or not precipitate (even though the system did not result in a strong network). Given the diversity of definitions found, a broader sol-gel method definition was considered[12]: "*every process that starts from precursor's solutions with intermediate stages including a gel and/or a sol*".

To begin the sol-gel process, the chemical compounds known as the *precursors* (Table 1), must be selected and dissolved in a certain liquid solvent (where necessary) where they will be chemically transformed forming a *sol*. *Sols* are stable suspensions of colloidal particles within a liquid[13,14]. This

first step is a typical chemical transformation aiming at the formation of a *sol* of colloidal particles or a solution of oligomers (small polymers). As *sol* is a fluid it can be cast in a mould, or be applied on the substrates using various shaping techniques[8] and can be stored for a certain time before further casting. After this process a *gel* is formed and to achieve gelation, the chemical transformations in a *sol* must be allowed to proceed until a rigid and interconnected network forms, only limited by the walls of the container[11].

Another important step in the sol–gel art is the drying, which is a very critical one. When drying occurs under normal conditions, it usually results in a contraction of the gelled network. The resulting dry gel, commonly referred as *xerogel*, can be reduced in volume between five to ten times when compared with the initial wet gel[11,13]. This phenomenon involves the contraction deformation processes of the network and the transport of liquid through the pores of structure. If the gel is dried in wet supercritical conditions, the shrinkage will be minimal, and the resulting product is known as an *aeroge*l. If the smallest dimension of the gel is more than a few millimeters, the material is classified as a *monolith* and when the gelation occurs by fast evaporation of the solvent, films and fibers will be produced (Figure 1). However, owing to the loss of volatile by-products formed in the hydrolysis–condensation reactions, it is difficult to control sample shrinkage during three-dimensional network formation[10,11,13,15–18].
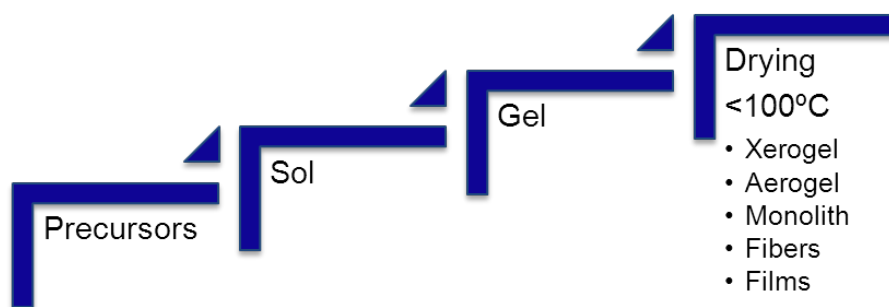
Figure 1. Main steps to obtain materials by sol-gel processing (temperatures < 100ºC) (adapted from Hench and West[14]).

According to Hench and West[14] there are three approaches used to produce sol-gel *monoliths*:

Method 1 – Gels obtained from gelation of colloidal solutions;

Method 2 – Hydrolysis and polycondensation of alkoxide or nitrate precursors followed by hypercritical drying of gels;

Method 3 – Hydrolysis and polycondensation of alkoxide precursors followed by aging and drying under ambient atmospheres.

Figure 2 shows the different routes of the sol-gel processing and their relation with the three systematic approaches proposed by Hench and West.[14] The properties of an OIH gel material are not the simple addition of each individual contribution of its components. It depends on the chemical nature, on the size and morphology as well as on the synergies established between each component. The diverse composition of these materials has led to specific classifications within OIHs. The influence of the interface is very important so its nature have been used to classify these materials. In one of the earliest papers, published by Sanchez and Ribot,[19] OIH networks were divided into two general classes; class I and II.[19] Later, Wojcik and Klein[20] introduced a classification of three main classes based on OIH chemical structures.
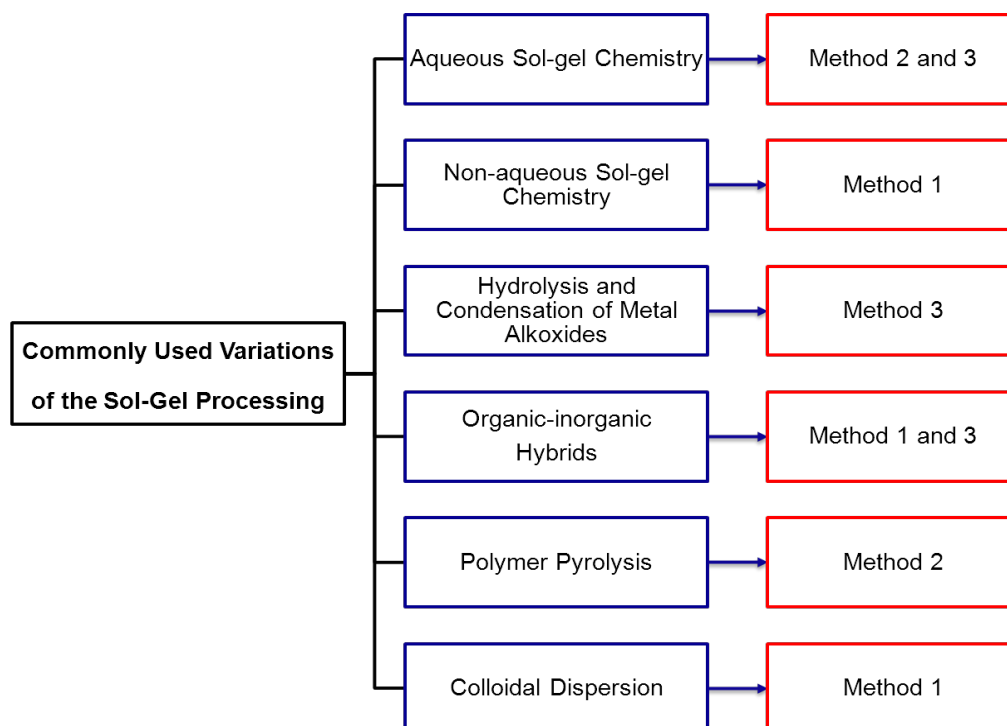
Figure 2. Different routes of the sol-gel process and their relation with the three systematic approaches proposed by Hench and West.[14]

Class I includes the OIHs where the organic and inorganic components interact via hydrogen bonds, Van der Waals forces or ionic bonds (Figure 3).

Class II includes OIHs where the inorganic and organic components are connected by covalent bonds (as shown in Figure 4). The support network is formed by condensation of chemical structural units (called gel precursors) where organic and inorganic components coexist. During the gel process the addition of the precursor's structure replicates a stable macromolecular network where these two basic components are chemically bonded.

The sol-gel synthesis of OIHs class II based on siloxanes can be easily synthesized because $Si-C_{sp}^{3}$ bonds are rather covalent and therefore quite stable toward attack by nucleophilic species such as water, alcohols, and hydroxylated ligands, among others.
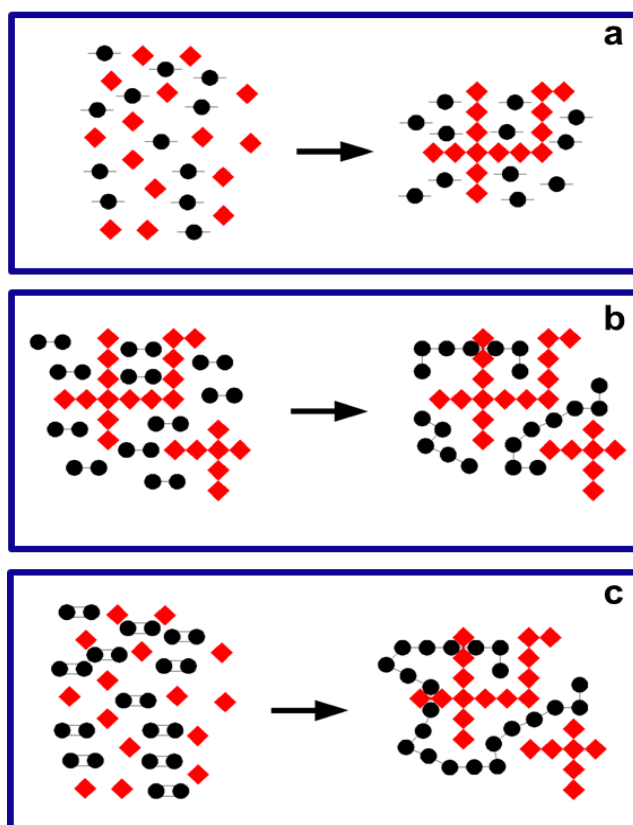
Figure 3. Interactions established between the organic and inorganic components for OIHs class I. a) ● Organic molecules immobilized in an inorganic network◆◆; b) ●●Organic molecules embedded in an inorganic network ◆◆ followed by polymerization forming a semi-interpenetrating network; c) Simultaneous formation of two networks from organic molecules ●●● and inorganic precursors ◆ forming an interpenetrating network (adapted from Prado et al.[21]).

The *precursors* of these compounds are organo-substituted silicic acid esters of general formula $R'_nSi(OR)_{4-n}$, bridged precursors of silesquioxanes $X_3Si-R'-SiX_3$ (X = Cl, Br, OR) in which R' can be any

organofunctional group and n is generally 1 or 2. Organic groups R' may bind to an inorganic network with two distinct purposes, namely: as *network modifiers* or as *network formers*. If R' is a simple non-hydrolyzable group, it will have a network modifying effect. On the other hand, if R' bears any reactive group that can, for instance, polymerize or co-polymerize (e.g., methacryloyl, epoxy, or styryl groups) or undergo hydrolysis-condensation (trialkoxysilyl groups), it will act as a *network former*.[16] The synthesis of this class of OIHs usually involves polycondensation reactions between di-, tri- or poly- functional organosiloxanes and metal alkoxides (*e.g.* $Si(OR)_4$, $Ti(OR)_4$, $Zr(OR)_4$, etc).
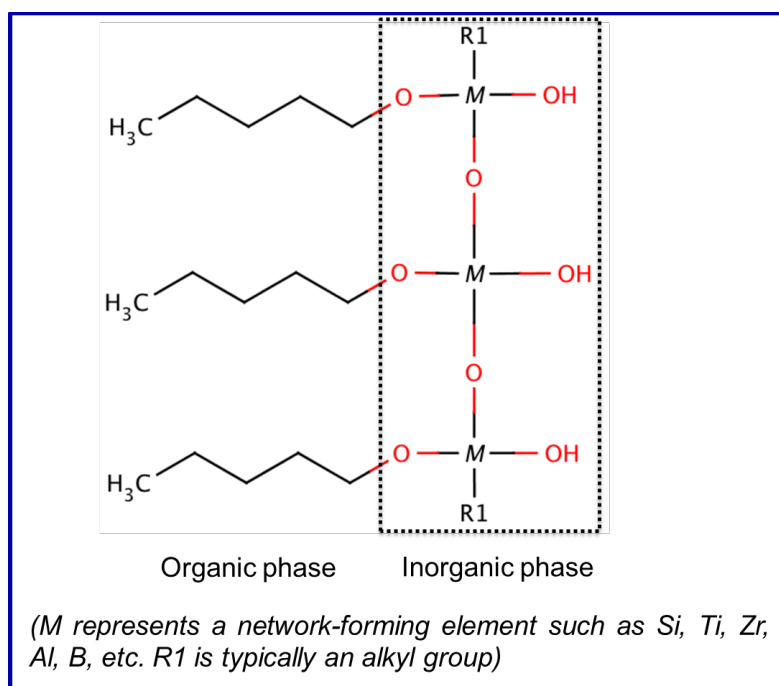
Figure 4. Organic-inorganic interactions for OIHs class II (adapted from Prado et al [21]).

Poly-functional alkoxysilanes and metal alkoxides are effective crosslinkers allowing producing OIHs materials with mechanical and thermal properties between those of polymers and glasses. The result of hydrolysis and poly-condensation of these precursors are organo-polysiloxanes that have properties such as hydrophobicity, corrosion protection, low dielectric constants or good scratch resistance.[21] Due to the chemical and physical properties of the OIHs class II that are suitable to prevent corrosion/oxidation of the metallic substrates these are the main focus of this review.

Table 1. Chemical name, empirical formula, structure and common abbreviation of some of the most commonly used precursors for the preparation of coatings by sol–gel method.
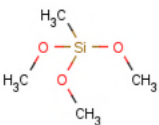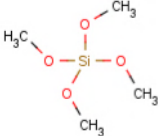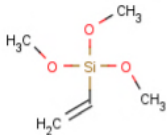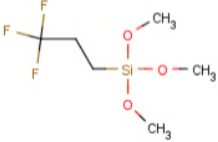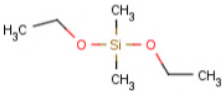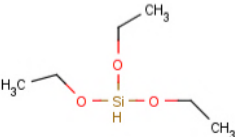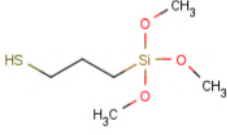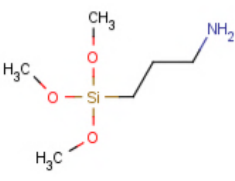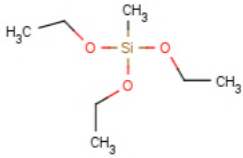
Chemical name	Empirical formula	Structure	Abbreviation
Methyltrimethoxysilane	$C_4H_{12}O_3Si$		MTMS
Tetramethylorthosilicate	$C_4H_{12}O_4Si$		TMOS
Vinyltrimethoxysilane	$C_5H_{12}O_3Si$		VTMS
3,3,3–trifluoropropyltrimethoxysilane	$C_6H_{13}F_3O_3Si$		TFPTMOS
Diethoxydimethylsilane	$C_6H_{16}O_2Si$		DEDMS
Triethoxysilane	$C_6H_{16}O_3Si$		TEOS
Γ–Mercaptopropyltrimethoxysilane	$C_6H_{16}O_3SSi$		MPTMS
3–Aminopropyltrimethoxysilane	$C_6H_{17}NO_3Si$		APTMS
Methyltriethoxysilane	$C_7H_{18}O_3Si$		MTES

Table 1. (*Continued*)
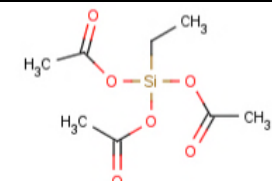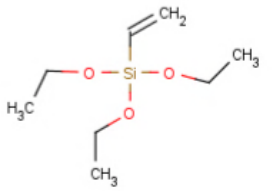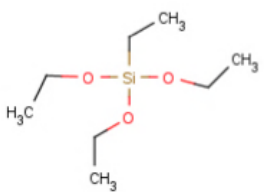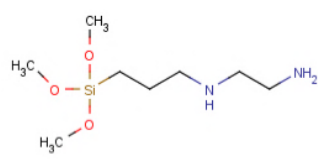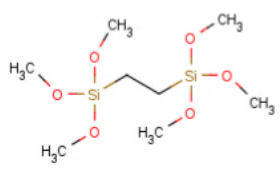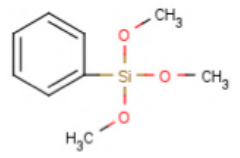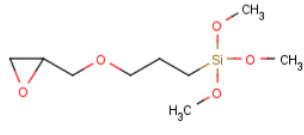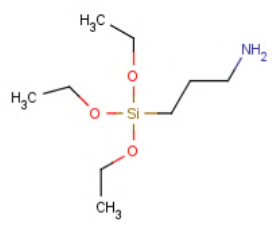
Chemical name	Empirical formula	Structure	Abbreviation
Ethyltriacetoxysilane	$C_8H_{14}O_6Si$		ETAS
Vinyltriethoxysilane	$C_8H_{18}O_3Si$		VTES
Tetraethoxysilane	$C_8H_{20}O_4Si$		TEOS
N–(2-aminoethyl)3-aminopropyltrimethoxy-silane	$C_8H_{22}N_2O_3Si$		AEAPS
Bis(trimethoxysilyl)ethane	$C_8H_{22}O_6Si_2$		BTMSE
Phenyltrimethoxysilane	$C_9H_{14}O_3Si$		PTMS
3–Glycidoxypropyltrimethoxysilane	$C_9H_{20}O_5Si$		GPTMS
3–Aminopropyltriethoxysilane	$C_9H_{23}NO_3Si$		APTES

Table 1. (*Continued*)
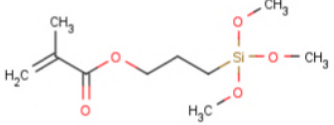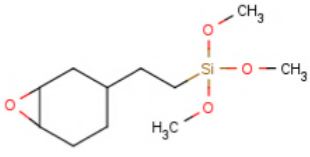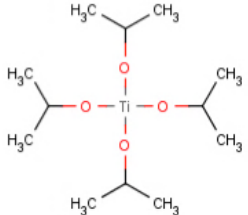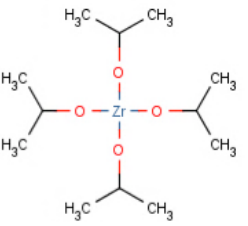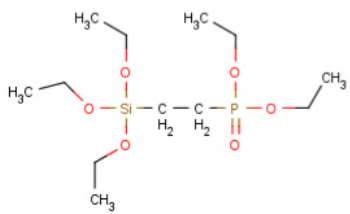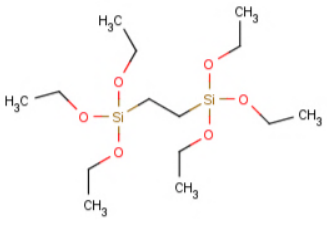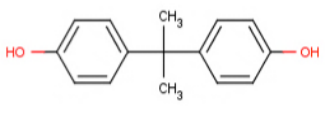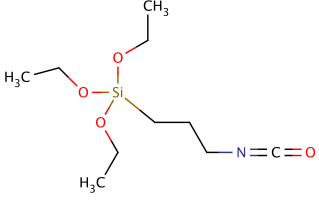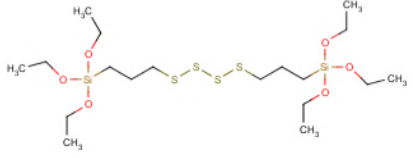
Chemical name	Empirical formula	Structure	Abbreviation
Γ−Methacryloxypropyltrimethoxysilane	$C_{10}H_{20}O_5Si$		MAPTS
2−(3,4-epoxycyclohexyl)−ethyl-trimethoxy-silane	$C_{11}H_{22}O_4Si$		ECHETS
Titanium (IV) tetra−1−propoxide	$C_{12}H_{28}O_4Ti$		TIPT
Zirconium (IV) tetra-1-propoxide	$C_{12}H_{28}O_4Zr$		ZrTPO
Diethylphosphonatoethyltriethoxysilane	$C_{12}H_{29}O_6Psi$		PHS
Bis−1,2−[triethoxysilyl]−ethane	$C_{14}H_{34}O_6Si_2$		BTSE
2,2−bis−(4−hydroxylphe-nyl)−propane	$C_{15}H_{16}O_2$		BPA

Table 1. (*Continued*)

Chemical name	Empirical formula	Structure	Abbreviation
3–isocyanatopropyltriethoxysilane	$C_{10}H_{21}O_4NSi$		ICPTES
Bis–[3–(triethoxysilyl)-propyl] tetrasulfide	$C_{18}H_{42}O_6S_4Si_2$		BTSTS

The synthesis reaction involved usually results from the conjugation of two mechanisms, namely[12,13,16]: hydrolysis of metal alkoxides (Step 1 Figure 5) to produce hydroxyl groups in the presence of stoichiometric water (generally in the presence of acid or base catalyst) followed by polycondensation of the resulting hydroxyl groups and residual alkoxyl groups to form a three-dimensional network (Step 2 Figure 5).
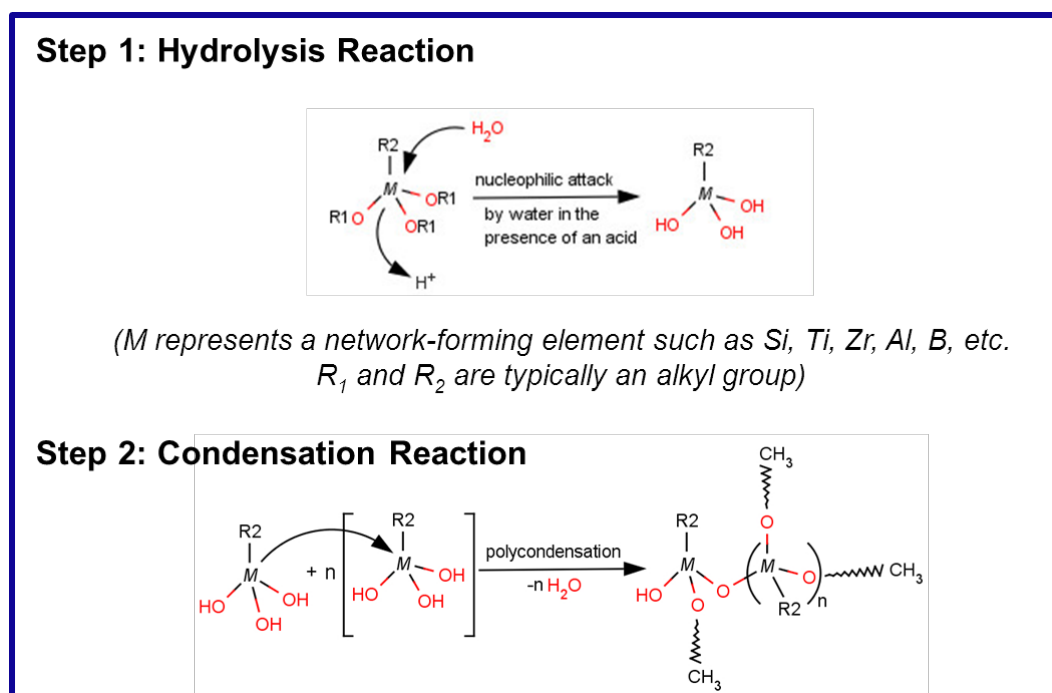
Figure 5. Generic reactions involved in the preparation of OIH materials through sol-gel method (adapted from Brinker and Scherer[11]).

18

The first step is the formation of a covalent bond between the organic and inorganic components giving rise to the "seed" precursor molecule. The conversion of the precursors into OIH materials proceeds via the formation of siloxane (Si-O-Si) bonds. This process takes place by hydrolysing monomeric tetrafunctional alkoxide precursors employing a mineral acid (e.g., HCl) or base (e.g., NH_3) as a catalyst.
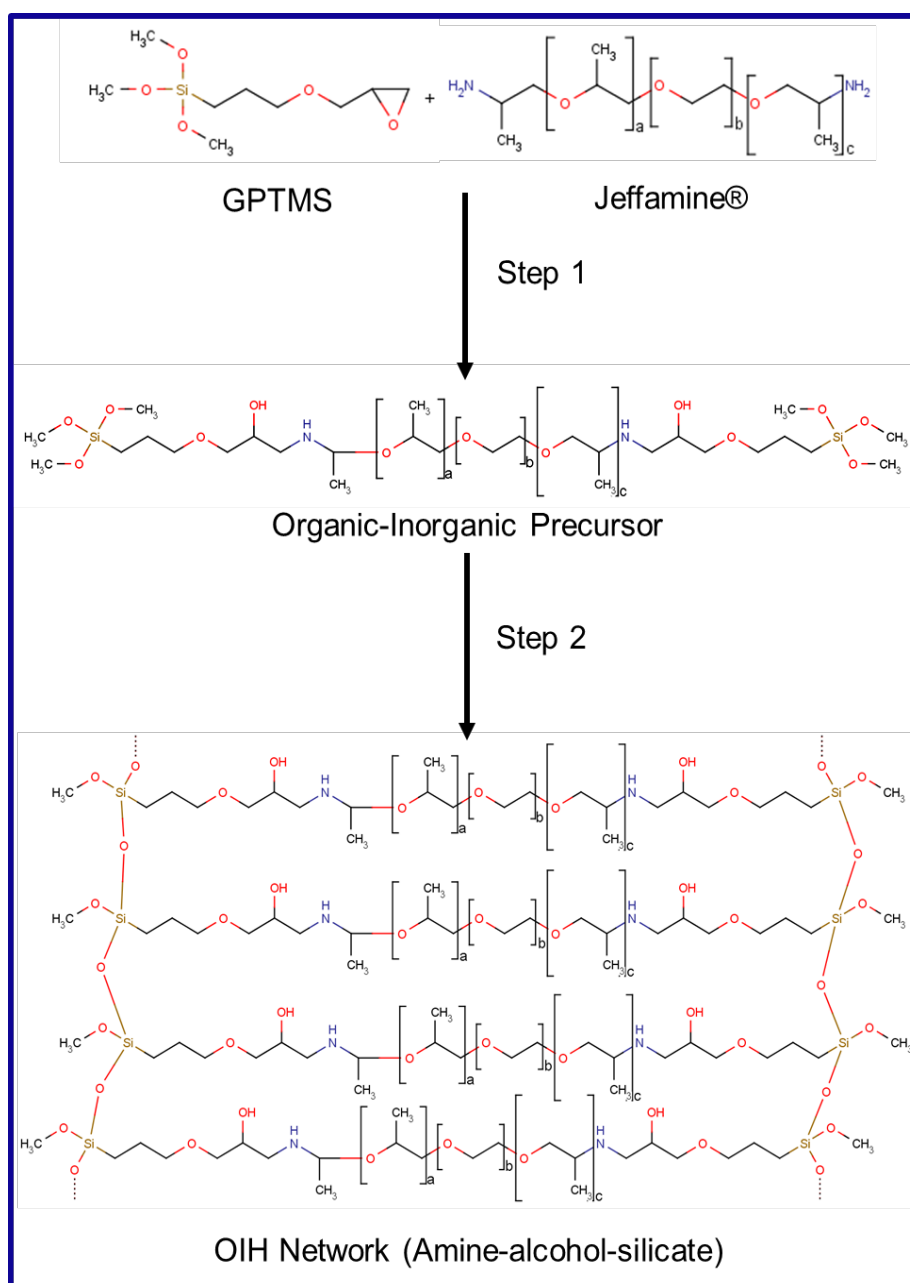
Figure 6. Practical example of the generic steps involved in the preparation of OIH materials.[22]

Figure 6 shows a schematic of a practical example including the generic steps in the preparation of a particular example of class II OIH material involving the incorporation of a polyether oligomer within the gel matrix[22]. Class III (Figure 7) includes OIHs that are based on the combination of both types of interactions assigned to classes I and II. An example of this kind of hybrid is the material obtained by an organic polymer containing hydrolysable alkoxylanes (SiOR)$_3$ and hydrogen acceptor groups such as carbonyls, amines and imides.[21]

(M represents a network-forming element such as Si, Ti, Zr, Al, B, etc.
R$_1$ is typically an alkyl group)
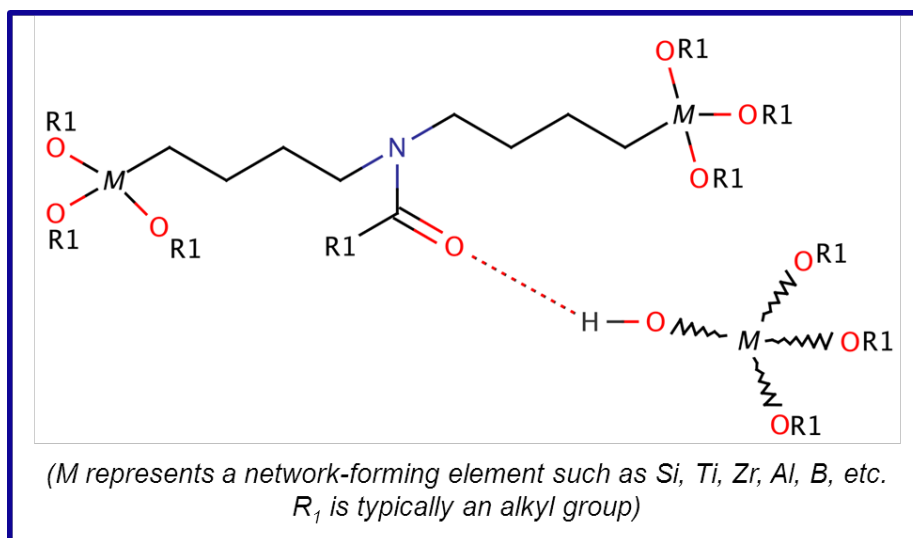
Figure 7. Organic-inorganic interactions for OIHs class III (adapted from Prado et al.[21])

3. Sol-Gel Coatings for Metals

Corrosion protection of metallic substrates has long been one of the key roles performed by organic coatings, one of the most cost-effective means of providing practical protection from corrosion to easily corrodible metallic structures and items. The production of eco-friendly sol-gel coatings to prevent corrosion on metallic substrates was one of the emerging areas of application, competing with conventional chromate and phosphate CCCs.

Corrosion protective coatings are not just a barrier layer between the object and its environment. They should act to: protect small and local areas of exposed substrate and stop the spread of damage; limit the passage of current on the substrate; slow/inhibit oxygen (and other oxidants') mobility towards the metal surface; minimize water and electrolyte penetration and release embedded inhibitor species that contribute to substrate passivation or block corrosion reactions[23–28]. Coating application or further removal processes should be performed with hazard-free procedures

and environmentally friendly reagents as well as producing eco-friendly residues.[29] The use of sol–gel method to produce coatings for corrosion protection fulfils the main requirements of what should be an environmentally friendly process. It is a waste-free method, excludes any washing stage, and is able to produce coatings with high specific pore volume, specific surface areas and high purity. Due to low temperature synthesis (frequently close to room temperature) the thermal volatilization and degradation of entrapped species (such as organic inhibitors) is minimized. As liquid precursors are used in the synthesis, it is therefore possible to cast coatings in complex shapes and produce thin films without the need for machining or melting.

Processing of sol-gel-derived film coatings and their applications have been extensively reviewed before 2001[4,30]. Metroke (2001) and co-workers[5] reviewed the recent advances in the use of sol–gel derived coatings for improved corrosion resistance of aluminium and steel metal surfaces. Later, in 2005, the pioneering work of W. J. van Ooij and co-workers[6] demonstrated the applications of functionalized trialkoxysilanes to produce OIH gels, as a prospective to solve the problems of the metal finishing industry[31]. The traditional metal plating process in this industry involves for instance, the use of CCC, lead, cadmium and cyanide in plating baths. These authors have shown that distinct terminal organic groups of the functionalized siloxanes have a key role in the improvement of coating adhesion while the continuous inorganic network formed, largely silicate, provides the coating's mechanic strength and hydrophobicity[6], minimizing/avoiding the hazards associated with traditional metal plating baths especially when it comes to heavy metals and cyanide.

In 2002 Gray and Luan[7] reviewed some the most relevant processes applied to the protection of magnesium alloys, namely: electrochemical plating, conversion films, anodizing, gas-phase deposition, laser surface alloying/cladding[7]. Since then, the research and progress on Mg alloys have improved rapidly across the world, as highlighted in the paper published by Wu and Zhang (2011)[32] where a detailed review is given about the state of the art methods of corrosion protection as well the patents regarding the protection of magnesium alloys[32]. The authors found that although the magnesium alloy-related patents exhibit a steady increase in the last 20 years, only a small amount were applied in industries[16]. In 2012 Hu et al. reviewed the progress in corrosion protection of magnesium alloys. The authors focused on the several types of existing coatings and on the techniques used to evaluate the corrosion performance of those coatings[33].

4. Organic-Inorganic Hybrid (OIH) Sol-Gel Coatings for Corrosion Protection

Organic-inorganic hybrid materials are the new generation of multifunctional materials with a broad spectrum of useful properties and diverse applications. The combination of inorganic with organic and/or bioactive components in a single material has led to many interdisciplinary scientific advances which can be seen as a large number of publications. Searches in *Science Direct*, *Springerlink*, *ECS Digital Library* and *ACS Publications*, including the keywords "hybrid" and "sol-gel", returned approximately 21000 scientific articles that were published since 1990. A bar chart of the number of identified scientific publications (Figure 8) shows that the number of publications in 2013 is about forty-five times the number of those published in 1990.
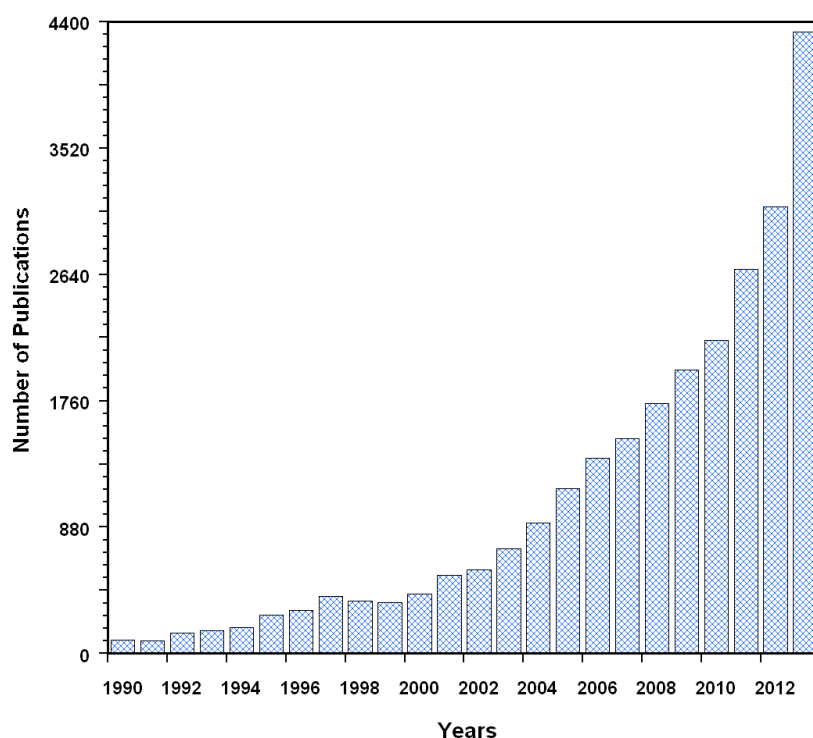
Figure 8. Bar chart of scientific publications published from 1990 until 2013 found in *Science Direct*, *Springerlink*, *ECS Digital Library* and *ACS Publications* [38] using the key words "organic-inorganic hybrids".

In the last few decades, the growing interest in developing new materials has led to the preparation of several organically modified silicates as potential metal corrosion coating materials.

Many material scientists and chemists, such as Schmidt[34] and Wilkes[35], started to synthesize OIH materials by sol–gel processes and published a series of pioneering research articles. Since then, a

diversified number of sol–gel based protective coatings have been produced and tested. In the last few decades the use of pre-treatments based on siloxanes has been widespread due to their properties, namely the low cost and low environmental impact. Several studies have been carried out extensively since the early 1990s[6,8,36,37] and it has been demonstrated that siloxanes can be effective in protecting metallic substrates against corrosion (i.e. steel, aluminium alloys, zinc alloys, copper and magnesium alloys). However, the need for tuned materials for specific purposes has led towards the production and development of new OIH gel materials which combine both the advantages of organic polymers (flexibility, lightweight, good impact resistance) and the features of inorganic material components (processability, high mechanical strength, excellent chemical resistance and thermal stability). Particular types of OIH materials have also been named, either as ORMOSILs (acronym generated from ORganically MOdified SILicates) or OMOCERs (from ORganically MOdified CERamics) depending on the precursors used (Table 1) and synthesis method.

The most effective approach in the production of OIH materials seems to be the sol-gel technique with its specific ability to create a spacious network (macromolecular network) containing M–O bonds under mild (room temperature) synthesis conditions either with or without a solvent[21,38]. Their properties are highly dependent on the degree of mutual phase dispersion (therefore dependent on the organic/inorganic ratio), the reactivity of cross-linking alkoxide reagents, the processing steps and the solvents[39].

The presence of polymeric chains within the OIH matrix contributes to the material's high electrical resistivity and impermeability, providing similar properties to the usual painting materials. The hybrid structure maximizes the preparation of materials that could lead to efficient coatings against corrosion as well as ensuring primary technological needs[40]. Over time, several review papers have been periodically published about OIH gels, giving an up-to-date description of state of the art contributions. The most important reviews published since 2000 are listed chronologically in Table 2.

Table 2. The main review articles about sol-gel processes since 2000

Year	Authors	Discussed subject matter
2000	Mackenzie and Bescher[41]	Review of the physical properties of sol-gel coatings.
2002	Attia *et al.*[42]	Overview of sol-gel derived coatings, namely the processes and optical applications.
2007	Mackenzie and Bescher[43]	Usefulness of the sol–gel process in the synthesis of materials comprising nanoscale architectures. Description of the processing of semiconducting, metallic, ferroelectric, or scintillating nanoparticles in various oxide matrices.
	Niederberger[44]	Review of non-aqueous sol–gel routes to produce metal oxide nanoparticles.
2008	Sakka[45]	Review of the effects of the starting solution composition on the reaction in alkoxysilane solutions for the formation of bulk and fibrous materials, and the microstructure of a particular film coating.
	Dimitriev *et. al.*[46]	Summary of the most significant research achievements in sol-gel science and technology.
2009	Kozhukharov[47]	Discussion of basic concepts related to sol-gel technologies, as well as the most important problems. Correlation of the properties of obtained products, synthesis conditions and the features of the methods applied.
	Wang and Bierwagen[38]	Introduction of the basic chemistry involved in sol–gel processes, the progress and development of sol–gel protective coatings on metal substrates and alloys until 2007. Summary of the most relevant limitations of sol–gel coatings.
	Benvenutti *et. al.*[48]	Discussion of the properties and characteristics of hybrid materials related to experimental synthesis conditions.
2011	Pandey and Mishra[49]	Description of synthesis routes to produce hybrid composite materials derived by combining the sol-gel approach and organic polymers.
	Sanchez *et al.*[15]	Discussion of the major applications of OIH (biological based) materials.
2012	Balgude and Sabnis[50]	Description of potential of sol-gel derived hybrid coatings processes for the production of multifunctional pre-treatments for metallic substrates.
2013	M. Abdolah Zadeh *et al.*[51]	Discussion of the most relevant existing works on self-healing sol-gel coatings.
	Chaturvedi and Dave[52]	Discussion of the methods to design nanomaterials where emphasis was given to the sol-gel method.

In the nineties,[53] the OIH concept firmly emerged and an increased number of papers focusing on this area were published within a short period of time.

In 2001 several important review papers on this subject were published. Schottner[54] and Walcarius[55] reviewed the perspectives of the hybrid sol-gel derived polymers and reported the applications of OIH materials in the various fields of electrochemistry. Mitzi[56] selected examples of OIH films and discussed the techniques used on the deposition of OIH sol-gel materials.

Several authors focused the review papers on aspects related with gel synthesis processes, like Hay and Raval[57] who reported the use of the non-hydrolytic sol-gel route to synthesize OIHs. Arkhireeva *et al.*[58] synthesized in 2004 OIHs using both the hydrolytic and non-hydrolytic sol-gel routes. The authors showed that both routes produced OIHs. However, an improved control of the shape and particle size was obtained using the hydrolytic process. In the same year, Castelvetro *et al.*[40] reviewed and discussed the synthetic approaches to produce nanostructured OIH materials. The main focus was on processes and products that can be carried out in an aqueous medium, even though non-aqueous systems have also been discussed.

Later in 2005, Sanchez *et al.*[59] summarized the general chemical pathways to prepare OIH materials and presented remarkable examples of applications of functional OIHs in several areas. The authors highlighted the use of protective coatings based on phenylsilsesquioxanes on structures for naval aircrafts and silsesquioxane–polyester mixtures in coil coating applications. The use of an OIH multilayer system on a mosaic panel of the 14th century ''Last Judgment Mosaic'' can be seen in the St Vitus cathedral in Prague. The OIH multilayer system, highlighted by the authors is composed by a functional layer of organo-alkoxysilanes and oxide nanoparticles, placed between the substrate and a fluoropolymer coating[59]. The intense research efforts on this particular area have justified, almost yearly, a detailed review paper reporting state-of-art OIHs.

The fundamental review papers were written by Innocenzi *et al.* [60], Dash *et al.* [61], Lebedev [62] and Sanchez *et al.*[63].Multilayer systems combining different sol-gel layers with different functions are also an area with high potential and have started to be exploited.

The first detailed use of OIHs was a bilayer system to prevent corrosion of metallic substrates by the combination of a super-hydrophobic OIH coating and an OIH coating doped with corrosion inhibitors, proposed by Zheng and Li[64] in 2010.

4.1. OIH Coatings for Corrosion Protection of Iron Based Alloys

Steel is the most common and versatile metal currently applied and can be classified either as carbon steel (CS) or steel alloy (SA). SA materials cover an extensive range of steels including low-steel alloys, stainless steel (SS), heat-resistant steels, and tool steels[65]. SS can be produced with a wide range of properties and can be used in many different industrial fields, owing to their mechanical and corrosion properties[65].

Steel surface substrates are traditionally passivated by the use of conversion coatings, phosphating and chromating. These treatments produce a layer of corrosion products – passivation layer – capable of resisting furthering chemical attack. However, due to the high toxicity associated to the use of chromates, several efforts are being made all over the world to find environmentally friendly treatments. OIHs obtained through sol-gel method are potential candidates as the presence of the metal oxides, on the treated steel surfaces, allows covalent bonding between the inorganic parts of the OIHs based on siloxanes (Si – O – metal oxide), as shown in Figure 9, and making them suitable alternatives to the conventional conversion coatings.

The most relevant information and conclusions gathered from the analysed papers about the use of OIH gels based on siloxane (i.e., at least one of the precursors used is based on siloxanes) coatings are summarized in Table 3, which is organized according to date of publication. By analysing the content of the collected bibliography it was concluded that the study of alternative precursors for the production of new OIH materials, using sol-gel technology, seems to have slightly evolved when compared with the amount of precursors available in the market.

The corrosion resistance behaviour of sol–gel coatings or thin films deposited onto these particular metallic substrates has been extensively studied. The studies performed, were mainly aimed at testing the capability of sol-gel coatings to improve oxidation and corrosion resistance of the substrate.

Considering all the data gathered in Table 3 and Figure 10, it is shown that only 13% of the OIH (class II) based on siloxanes were produced without the precursors TEOS, GPTMS, MAPTS, MTES and MMA. It is also shown that TEOS is used in the majority of the publications found for these substrates.
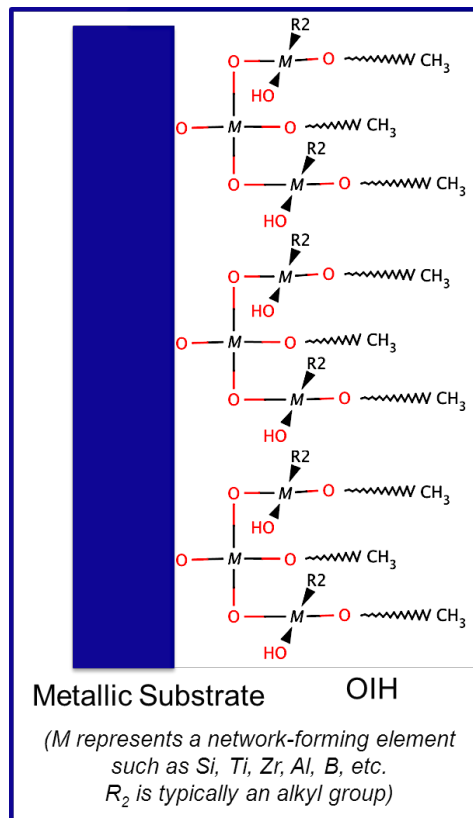
Figure 9. Schematic representation of the interactions between OIHs class II and the metallic substrate adapted from Prado et al.[21]).
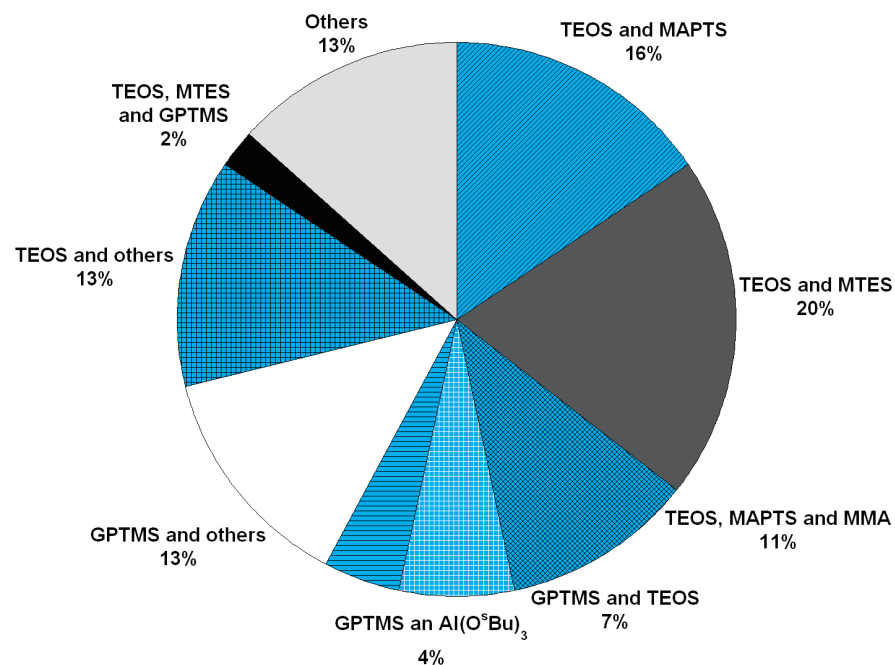
Figure 10. Distribution of publications according to the type of precursors used for the production of OIH (class II) gel coatings based on siloxanes (i.e., at least one of the precursors used is based on siloxanes) for carbon steel and iron based alloys (2001-2013).

Table 3. Studies on corrosion protection using OIH (class II) sol-gel coatings on carbon, steel alloys and SS substrates (2001-2013)

Year	Precursors	Results and Conclusions	Ref.
2001	TEOS, MAPTS	OIH coating enhanced corrosion protection, excellent film adhesion and flexibility.	66
2002	DGEBA, APTMS	OIH coatings studied offered corrosion protection.	67
2003	TEOS, MAPTS	Uniform and defect-free coatings that enhanced corrosion protection.	68
	GPTMS, AEAPS, APTES, MAPTS	Efficient coatings in protecting surfaces from external influences.	69
2004	TEOS, MTES	OIH coatings showed high stability and resistance to pitting in simulated body fluids.	70
	MTES, TIPMS, TIBMS	OIH coatings were thermally stable and the refractive index decreased with organic groups.	71
2005	TEOS, MTES	Homogenous and crack-free OIH coatings exhibited enhanced corrosion resistance.	72
	TEOS, MTES	OIH coating adherence on the substrate surface was good and corrosion resistance of bare material improved.	73
2006	GPTMS, TEOS	Passivation of the substrate was enhanced.	74
	TEOS, MAPTS (SiO_2 gel/Dacromet)	Precursors produced a crack-free surface and enhanced the erosion–corrosion resistance of Dacromet.	75
	TEOS, MTES	Crack free and continuous coatings. Effective barrier against corrosive environments.	76
2008	TEOS, MTES, GPTMS	OIH coatings exhibited good anticorrosion properties.	77
	TEOS, MTES,$AlCl_3.6H_2O$,	Multi-layer hydrophobic OIH coating with doped cerium nitrate provided good corrosion resistance.	78
2009	TEOS, MTES	OIH coatings effectively protected the surface of the substrate against corrosion.	79
	Silicone-epoxide resin (Silikopon EF)	OIH coating provided good corrosion resistance for substrates against alkaline, acidic and saline conditions.	80
	TEOS, MAPTS, MMA	OIH coating provided good corrosion resistance at OCP conditions.	81
2010	TEOS, MAPTS	Best corrosion resistance for OIH coatings obtained with TEOS/MAPTS molar ratio = 2.	82
	TEOS, MAPTS	OIH coatings increased the hydrophilic properties of the substrate surface and significantly improved the corrosion resistance in physiological media.	83
	TEOS, MAPTS	OIH coatings with defect-free, smooth surface and good substrate adhesion improved corrosion resistance.	84
	TEOS, MAPTS, MMA	OIH film improved the barrier effect against corrosion.	85
	GPTMS, ZrTPO	Coatings increased the corrosion resistance of substrate	86
	MAEP, MAPTS	Coating improved corrosion resistance when compared with the uncoated samples.	87
2011	TIPT, PAPTES	Coatings were dense, uniform, defect-free and provide protection to the substrate against corrosion.	88
2012	TEOS, VTES	OIH coatings showed to be a promising drug delivery system that can be applied to metallic implants.	89
	TEOS, LDF	OIH produced showed a barrier action against different corrosive media.	90
	TEOS, MTES	OIH films including 10 and 50 nm silica nanoparticles were produced and exhibited low corrosion current density.	91
	GPTMS, TIPT	Silane-titania hybrid coating with inhibitor loaded nanocontainers showed the best performance.	92
	TEOS, MAPTS, MMA	OIH coatings prepared protected the substrate against corrosion.	93
	GPTMS, $Al(O^sBu)_3$	Influence of cerium concentration on behaviour against corrosion of the OIH coating was studied.	94
	TEOS, MAPTES	Barrier properties of the OIH coating were improved by the incorporation of inorganic fillers.	95
	TEOS, MAPTS, MMA	Anticorrosion properties of the OIH improved when the MAPTS was added to the formulations.	96
	n-PTMS, TEOS	Both pure OIH and copper oxide-OIH coatings improved the corrosion resistance of the substrate	97
	TEOS, MTES, PTMS	OIH coatings derived from methyl substituted organically modified silane exhibited superior barrier properties.	98

Table 3. (*Continued*)

Year	Precursors	Results and Conclusions	Ref.
2012	GPTMS, BPA	Cerium doped OIH coatings protected the substrate effectively.	99
	TEOS, ZrTPO	Corrosion behaviour of the substrate was enhanced.	100
2013	TEOS, MAPTS	Addition of polyethyleneglycol within the OIH allowed improving the barrier effect and the corrosion behaviour of the coating.	101
	TEOS, MAPTS, MMA	Smooth, crack-free, adherent OIH coatings containing carbon nanotubes protected the substrate against corrosion.	102
	GPTMS, Al(O^{s}Bu)$_3$	Correlation of the influence of temperature on the chemical and structural transformation of the xerogel with the mechanical properties.	103
	GPTMS, MTMS	OIH coatings had excellent substrate adhesion and improved corrosion behaviour.	104
	GPTMS, OTES, ZrBTO	OIH coatings were produced and prevented the oxidation of the substrate.	105
	TEOS, MPTMS	OIH coating synthesized with Ce(NO$_3$)$_3$ as catalyst showed improved corrosion behaviour of the substrate.	106
	GPTMS, TEOS	Thermally cured cashew nut shell liquid based OIH coatings were developed and increased corrosion resistance properties.	107
	GPTMS, TEOS	Corrosion resistance of the OIH films was improved when a phosphoric acid pre-treatment was done.	108
	TEOS, MTES	OIH coatings enhanced the corrosion resistance of samples.	109
	ER, APTES	OIH coatings studied showed good corrosion resistance performance in neutral and acidic environments	110

Although the number of publications has increased significantly over the past 4 years, the research for this type of substrates is still confined to a few precursors and this is especially notable when compared to studies published before 2008. This unusual behaviour may be due to the search for the OIH coating with the optimum performance since the sol-gel method allows, with simple changes in the synthesis parameters, to obtain OIH materials with very distinct properties. The corrosion protection properties of OIH coatings are strongly dependent on their processing conditions, such as aging, reaction pH, curing temperature and molar ratio of precursors. The statistic data referred to above suggests that the research efforts were more focused in optimizing the synthesis process instead of testing and studying new precursors.

The publications found focused mostly on the use of TEOS, GPTMS, MAPTS and MTES including, in some cases, the performance of coating materials with embedded corrosion inhibitor species. Generally, the reported studies showed that those OIH coatings exhibit a promising performance in protecting the carbon steel and iron based alloys against corrosion. However a comparative study between the properties of the OIH coatings obtained by each author was not possible since the methods and conditions used to evaluate the OIH coatings performance were not the same and the results itself were not comparable. The extensive use of TEOS may be due to the fact that this precursor was studied in detail and its properties and reactivity are quite well known at different pH and temperatures[11,111]. Furthermore, it is less toxic when compared to TMOS,[112] it is available with a higher purity grade at a relatively low price and has a relatively slow and controllable rate of reaction[49]. OIHs based on TEOS can produce, at low temperatures, homogeneous films on large areas of substrates[113] and its addition improves the transparency of the OIH materials[112,114]. Moreover, OIHs based on TEOS are low cost as this reagent is about 4 times cheaper than GPTMS and half of the price of MTES, for similar purity grades.

4.2.   OIH Coatings for Corrosion Protection of Aluminium Based Alloys

Aluminium based alloys are a group of materials with a wide range of applications due to their physical and processability properties, namely: low density, easy shaping (in rolling, drawing and extrusion), high corrosion resistance in different environments, easy machining, colourless and non-toxic corrosion products and high thermal and electrical conductivity together with low aluminium cost, less than 2000 USD/ton. Those characteristics make aluminium based alloys of remarkable economical and industrial importance[38,65].

Examples of applications using aluminium based alloys include building structures, panels, machined components, electro–mechanical components, vehicles and accessories, tools, machine making, shipbuilding, packing, architecture, etc. Aluminium alloys are chosen in these applications due to its natural tendency to form a passivation Al_2O_3 layer, which can also be artificially generated by anodizing the substrate. Nevertheless, this passivation layer deteriorates when in contact with aggressive media, such as those containing chloride ions (particularly seaside environments) resulting in pitting corrosion[38]. To overcome this drawback CCC treatments are usually used due their effectiveness in corrosion protection of these alloys. However, as stated before, conversion layers based on Cr(VI) should be avoided and substituted by coatings environmentally friendly. OIH class II sol-gel coatings are potential candidates because in addition to the OIHs coating properties, these materials can provide a stable Si – O – Al (Figure 9) bonding between the inorganic functionality of these materials and the formed passivation layer (Al_2O_3)[115].
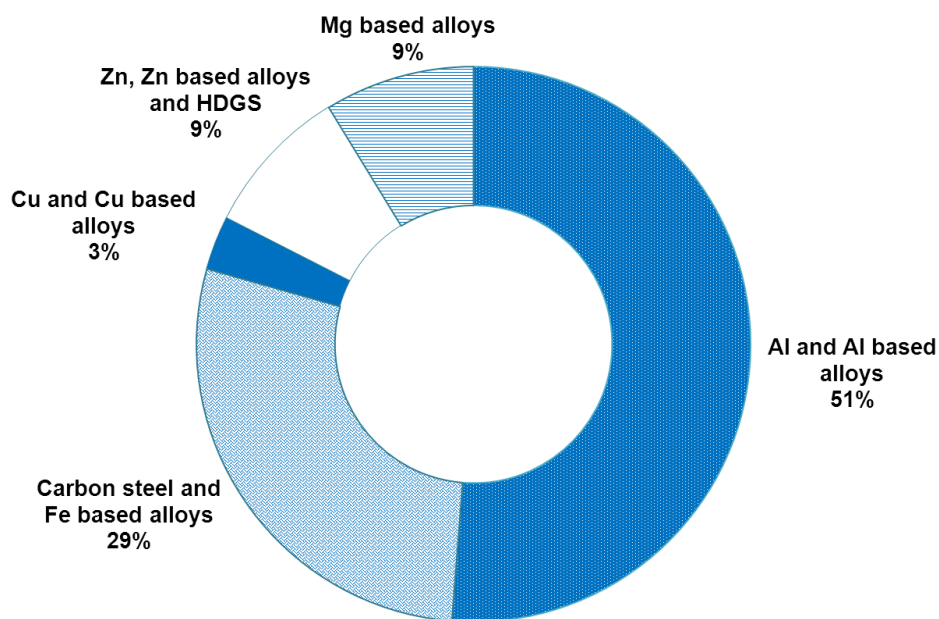
Figure 11. Reported substrates coated with OIH (class II) gel coatings based on siloxanes (i.e., at least one of the precursors used is based on siloxanes) (2001-2013).

Table 4 gathers the information collected from the published papers where OIH class II sol-gel coatings based on siloxanes (i.e., at least one of the precursors used is based on siloxanes) have been produced and tested on aluminium based alloys. As shown (Table 4), research efforts in coating development for this specific set of materials are particularly strong and are not only focused on corrosion protection but also on aspects such as changing surface hydrophobicity/hydrophobility.

For aluminium-based alloys more precursors were tested than for carbon steel and steel based alloys substrates (Table 4). Considering the information gathered, half of the published papers were applied to aluminium-based alloys (Figure 11). It should also be noted that the extensive research in seeking protective coatings for aluminium based alloys against corrosion has been extensively championed by the aviation industry since is the most commonly used material.
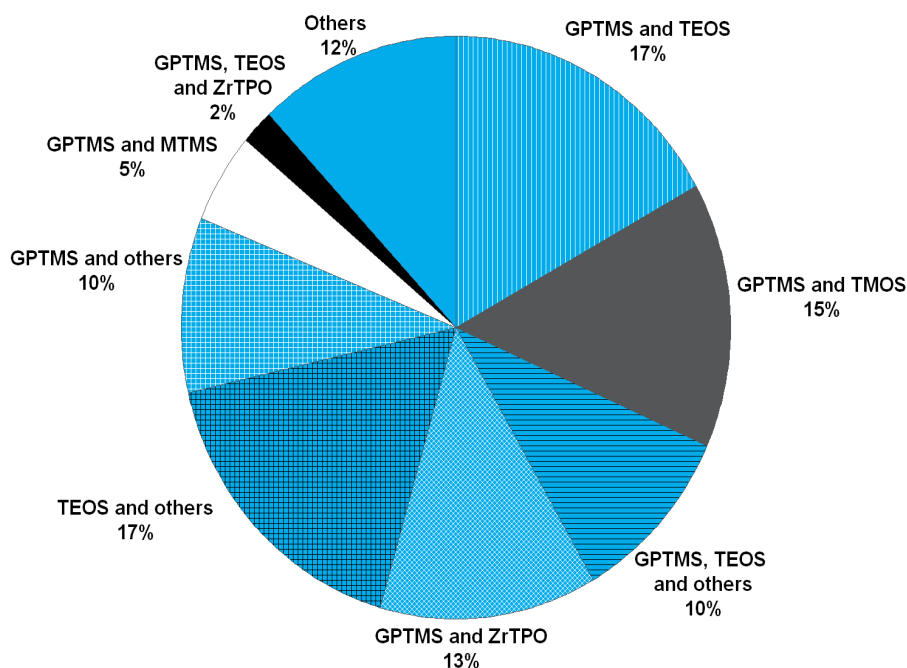
Figure 12. Precursors used for the production of OIH (class II) gel coatings based on siloxanes (i.e., at least one of the precursors used is based on siloxanes) for aluminium based alloys (2001-2013).

Considering all the information gathered in Table 4, Figure 12 shows that 12 % of the OIHs (class II) based on siloxanes reported were produced without using TEOS, GPTMS, TMOS, ZrTPO and MTMS precursors. It is also shown that TEOS is present in 46 % and GPTMS in 72 % of the publications found for aluminium based alloys. The collected data also shows that the research focuses mostly on the use of TEOS, GPTMS, TMOS and ZrTPO and includes, in some cases, the performance of coating materials with embedded corrosion inhibitor species and the deposition of multilayers produced by several deposition-curing cycles.

Table 4. Studies on corrosion protection using OIH (class II) sol-gel coatings on aluminium based alloys substrates (2001-2013)

Year	Precursors	Results and Conclusions	Ref.
2001	GPTMS, TEOS	Comparative studies showed that OIH film provided better corrosion protection than the CCCs	116
	GPTMS, TMOS	Incorporation of cerium into sols appears promising for protection against substrate corrosion.	117
2002	GPTMS, TEOS	Curing agents were studied. The amine curing agent produced films with good corrosion resistance.	118
	GPTMS, TMOS	Nature of the curing agent significantly influences film structure and the corrosion resistance properties of the OIH film (curing agents studied: CF_3SO_3H, HPF_6, DETA, TETA, TEPA).	119
2003	GPTMS, TMOS	Thin and dense protective surface OIH coatings doped with corrosion inhibitors improved corrosion protection.	120
	GPTMS, TEOS, MTES	Addition of particles to OIH coatings notably improved the final corrosion protection properties.	121
	GPTMS, AEAPS, APTES, MAPTS	OIH polymers were efficient in protecting surfaces from external influences.	69
	GPTMS, TMOS.	Investigation and characterization of the SNAP coating process.	122
2004	TEOS, VTMS, MAPTS, MTMS, DMTMS, *n*-PTMS, BTMS, IBTMS, HTMS, IOTMS, OTMS	Modification of produced thin OIH films with various concentrations of alkyl-modified silanes was found to enhance the corrosion resistance properties of the films on substrates. Hexyl-modified silanes exhibited the highest pore resistance and contact angle values.	123
	TEOS, VTMS, MAPTS	Corrosion resistance characteristics depended on the nature and concentration of diluent used. The choice of solvent enables tailoring of the OIH coating structure.	124
	MTES, TIPMS, TIBMS	Films were thermally stable, remaining without cracks on the substrates after heat treatment at 800 °C.	71
2005	GPTMS, TMOS, BPA	OIH coatings were uniform, defect-free, relatively dense, presenting good adhesion and improved corrosion protection.	125
	GPTMS, BPA	Coatings obtained improved corrosion protection by forming an impenetrable barrier to water and corrosive agents.	126
	GPTMS, TMOS	Superior adhesion and corrosion protection make SNAP surface modification a promising alternative.	127
	GPTMS, TEOS, VTMS, MAPTS	OIH coatings efficiently inhibited the corrosion of the substrate.	128
	GPTMS, TMOS	Inclusion of corrosion inhibitors within the coating has a pronounced effect on reducing a corrosion attack on the substrate.	129
	GPTMS, TEOS, ZrTPO	OIH coatings with incorporated zirconium oxide nanoparticles doped with a cerium inhibitor provided long-term corrosion protection.	130
	GPTMS, ZrTPO	OIH Sol–gel systems showed potential for aerospace uses in comparison with conventional CCCs.	131
2006	GPTMS, TEOS, ZrTPO	OIH coatings provided corrosion protection and may be used as an alternative for pre-treatment of the substrate	132
	GPTMS, TMOS	Formation of resilient films with good barrier properties.	133
	GPTMS, TEOS	OIH prevented the corrosion of the substrate.	134
	HEPA, ICPTES, MAPTMS, AEA	UV-curable OIHs were synthesized and characterized with good adhesion to the substrate.	135
	GPTMS, TEOS	Film provided an impenetrable barrier to water and corrosive agents.	136

Table 4. (*Continued*)

Year	Precursors	Results and Conclusions	Ref.
2007	TEOS, MAPTS	Transparent coatings obtained by UV curing adhered well and were robust in scratch and abrasion tests.	137
	GPTMS, TEOS	OIH coatings showed good corrosion resistance in contact with a NaCl solution.	138
	GPTMS, TEOS	OIH films provided an effective barrier to water and corrosive agents with a good corrosion resistance.	139
	GPTMS, MTMS	OIH coatings were uniform, continuous, crack-free and acted as an efficient barrier against corrosive electrolytes.	140
2008	TFPTMOS, TMOS	OIH film prevented infiltration of H_2O and limited the exposure of corrosive elements to the substrate.	141
	GPTMS, TEOS	Incorporation of different inhibitors into the silane solution enhanced protection effectiveness of the OIH film.	142
	GPTMS, TEOS, APTMS	OIH coatings with good thermal stability and excellent corrosion protection under open-circuit conditions.	143
	GPTMS, ZrTPO, TIPT, TBADP	OIH films showed good anticorrosive performance and excellent adhesion.	144
	GPTMS, ZrTPO	Studies about the impact on the barrier properties of the OIH sol–gel coatings due to the addition of corrosion inhibitors.	145
	PDMSU	PDMSU/PrOH coatings showed improved corrosion behaviour when compared to PDMSU/EtOH coatings.	147
	TEOS, MAPTS, SiO_2	OIH sol–gel coatings promoted substrate corrosion protection and the presence of inhibitors was studied.	146
	GPTMS, TMOS	Creation of a dense cross-linked OIH coating improved substrate corrosion protection.	147
	GPTMS, MTMS	Uniform and crack-free coating was obtained reducing corrosion current.	148
	MAPTS, TEOS	TEOS addition into the coating enhanced the electrochemical corrosion resistance.	149
2009	TEOS, MAPTS, EGDMA, SiO_2.	Multilayer coatings enhanced the corrosion resistance.	150
	GPTMS, MTMS, PR.	Corrosion current of the coated substrates decreased when compared to the bare substrate.	151
	TEOS, MPS, HEMA	Electrochemical measurements displayed better barrier properties than the uncoated substrate.	152
	GPTMS, TEOS	OIH films created provided excellent barrier and corrosion protection compared to bare substrate.	153
	GPTMS, TEOS, MTES, BPA, SiO_2-NP	OIH gel coatings with uniform thicknesses and nanoparticle distribution reduced the corrosion rate.	154
	TEOS, MPTMS, PTMS	Addition of inhibitors to OIH coatings led to an improvement of active corrosion protection.	155
	BTMSE, MPTMS	OIH coatings improved the corrosion protection of metals.	156
	TEOS, APTMS, IPDIC, HMDIC, TDIC	OIH gel coatings showed improved corrosion resistance compared to commercial non-chromate pre-treatments.	157
2010	TEOS, MAPTS, SiO_2, EGDMA, GMA	Multilayer systems exhibited limited barrier properties due to the porous structure of the sol–gel film.	158
	GPTMS, ZrTPO	Hydrotalcite addition to sol–gel films improves the corrosion resistance of the coated substrate.	115
	GPTMS, ZrTPO	Metallic surface treatment influences the corrosion resistance of the coated substrate.	159
	MAPTS, ZrTPO	Zirconium nanoparticles significantly improved the performance of the OIH coatings.	160
	GPTMS, TMOS	Cerium nitrate was excellent for self-healing of the OIH coating, while cerium chloride had no obvious effect.	161
	GPTMS, TMOS	OIH coating showed good corrosion resistance.	162
	TEOS, APTES, ECO	Corrosion tests showed excellent performance providing protection to the substrate.	163
	GPTMS, ZrTPO	Crack-free sol–gel coatings with improved corrosion protection were produced on the alloy surface.	164
	APTMS, IOTMS, ICPTES PFOTES	OIH coatings exhibited good corrosion inhibition.	167
	(SiloXel) silane-I, silane-II, silane-III, TiPT	SiloXel acted as an invulnerable barrier against corrosion of the substrate.	165
	BTSTS	Substrate covered by film and by silane conversion coatings showed better corrosion performance.	166

Table 4. (*Continued*)

Year	Precursors	Results and Conclusions	Ref.
2011	GPTMS, ZrTPO	Addition of as-synthesized hydrotalcite to the OIH film increased the barrier properties.	167
	GPTMS, TEOS, BPA, APTES, MTES, SiO$_2$	Increasing the doping level of inhibitors did not lead to improvement of the corrosion resistance.	168
	GPTMS, TMOS	Corrosion protection of substrates by aromatic diamine cross-linked OIH sol coatings was demonstrated.	169
	GPTMS, TEOS	Coatings exhibited a good anti-corrosion performance.	170
	MAPTS, Nb(OCH$_2$CH$_3$)$_5$	Inclusion of niobium into the matrix significantly improved the coating corrosion protection properties.	171
2012	GPTMS, Al(O^{s}Bu)$_3$	Study of the inhibitor concentration influence on anti-corrosion and mechanical properties of the OIH coating.	172
	GPTMS, TMOS	Studies on synthesis and structure of an OIH coating deposited on the substrate.	173
	GPTMS, TEOS, BPA, APTES, MTES, SiO$_2$	OIH coatings doped with cerium and transition metals showed promising corrosion protection properties.	174
	GPTMS, TEOS, MTES, BPA	OIH coating without additives provided a good corrosion protection of the substrate.	175
	GPTMS, ZrTPO	Zeolite microparticles used as reservoirs for Ce(III) were introduced into OIH coatings enhancing the corrosion protection of the substrate compared to the blank OIH coating.	176,177
	GPTMS, ZrTPO	OIH coating corrosion properties were improved when red mud particles added were previously calcined	178
	GPTMS, MTMS	OIH coatings showed to improve corrosion protection of the substrate.	179
	TEOS, MTES	OIH films doped with 1 mol % of lanthanum oxide induced a delay on the corrosion of the substrate.	180
	GPTMS, DETA, ER	Coatings doped with inhibitor provided long term corrosion protection of the substrate.	181
2013	GPTMS, TEOS	OIH coatings with good mechanical and adhesive properties were produced by optimization of the process parameters.	182
	TEOS, MTMS	Investigation of dopants within the OIH system on the bond strength of the coating and the substrate.	183
	GPTMS, ZrTPO	OIH coating containing cerium molybdate nanowires improved the corrosion protection of the substrate.	184
	GPTMS, TEOS	OIH coatings showed good corrosion barrier properties and the doped ones revealed self-healing behaviour.	185
	GPTMS, MTMS	OIH showed good adhesion to the substrate and "appreciable" corrosion resistance.	186
	GPTMS, TEOS, MTES	Corrosion protection of the OIH coatings doped with sodium montmorillonite and Ce(III) was improved	187
	GPTMS, TEOS	Pre-treatment with the OIH delays the access of aggressive species to the barrier layer.	188
	GPTMS, TEOS	OIH coatings protected the substrate against corrosion	189
	MTES, SiO$_2$	OIH showed good adhesion to the substrate, smooth, crack-free and good corrosion resistance.	190
	GPTMS, TEOS	Proper choice of parameters led to OIHs that protect the substrate against corrosion.	191
	TEOS, APTES, ECO, TIPT	OIH films showed good adhesion to the substrate and good corrosion protection.	192

The intensive use of TEOS is explained by the reasons stated in the previous section, with a lower price than MTMS or ZrTPO, boosting the search for effective OIH coatings using this specific precursor.

The use of GPTMS in 72 % of the publications found for these substrates may be explained by the fact that this precursor is a combination of two different components, in particular, *glycidoxy* (organic) and silicon *alkoxy* (inorganic) groups. It can thereby form, at the same time, an organic network through the polymerization of *glycidoxy* groups and an inorganic network through the hydrolysis and subsequent condensation reactions of *alkoxy* groups[134]. Moreover, it can be used as a binder in organic–inorganic silica based systems increasing the density and improving adhesion to the substrates[125]. It should also be mentioned that this precursor has an *epoxy* terminal group that exists as a component of commercial available epoxy glues that have an intensive industrial and domestic use for a large variety of purposes and application.

The most recent publications (since 2007) also showed that the innovations for coatings on these substrates is moving towards self-healing coatings doped with nanocontainers able to release entrapped corrosion inhibitors[193–195]. The majority of the OIH coatings studied showed promising performance in protecting the aluminium based alloys against corrosion. Some of the OIH coatings studied have reached a remarkable degree of development and the next step will undoubtedly be large-scale industrial production and marketing.

4.3. OIH Coatings for Corrosion Protection of Copper Based Alloys

Copper and copper based alloys are versatile materials. This group of alloys has a wide application in sculptures, kitchen utensils, heat exchange tubes, tube sheeting, valves and piping in seawater and fresh water systems[65].

Copper shows excellent corrosion resistance and scaling, high mechanical strength, high temperature resistance and lifetime resistance to UV degradation. However, in wet environments its corrosion processes is accelerated. OIH sol–gel coatings have also been investigated for the protection of copper and the few studies found are summarized in Table 5.

Figure 12 shows that only 3% of the considered papers report tests using OIH class II based on siloxanes (i.e., at least one of the precursors used is based on siloxanes) and Table 5 shows that the most used precursor was GPTMS.

Table 5. Studies on corrosion protection using OIH (class II) sol–gel coatings on copper and copper alloys substrates (2001-2013)

Year	Precursors	Results and Conclusions	Ref.
2003	GPTMS, MTMS, SiO$_2$	OIH coatings show good resistance to UV and effectively delayed corrosion on the substrates.	41
2008	GPTMS, MPTMS	Incorporation of 5 mol % of MPTMS enhanced the corrosion resistance.	196
2009	BTMSE, MPTMS	OIH coatings have improved the corrosion protection of the substrate.	156
2013	TEOS, GPTMS	Best corrosion protection was achieved when the amount of BTAH equals to the molar number of epoxy group in the OIH coating.	197
	TEOS, TMCS, HMDS	OIH coatings prepared in alkaline conditions are more stable and those one prepared with HMDS were not affected by corrosion.	198

The reduced number of publications could be explained by several reasons. The native copper oxide layer is mechanically weak and at room temperature consists mainly of Cu_2O or both Cu_2O and CuO with a thickness of a few nanometers and is usually contaminated by carbon[199–201]. Additionally, the oxide layer is not easily wettable by the sol solution[200], therefore the adherence between OIH sol-gel coatings and the substrate is compromised. Deflorian *et al.* showed in 2008 that GPTMS does not establish an interaction with the native copper oxide layer[202]. Moreover, 1,2,3-benzotriazole (BTAH, $C_6H_5N_3$) is an effective corrosion inhibitor for copper and its alloys in different environmental media, as demonstrated by Finšgar and Milošev[203] in a paper published in 2010, where the most significant work made using BTAH was reviewed. Therefore, it is neither a huge concern nor an urgent need to search for alternatives against corrosion for this type of substrates and alloys as BTAH shows to be a very effective corrosion inhibitor.

4.4. OIH Coatings for Corrosion Protection for Zinc-Based Alloys HDGS

Zinc is used as additive in certain rubbers and paints, in the production of alloys and as coating through several methods, such as electroplating, thermal spraying, sherardizing, hot dipping, etc.

Hot dip galvanizing (HDG) is considered the most important zinc coating process to protect building structures, such as roofs and exterior walls, and constituent parts of cars and boats. Due to its superior corrosion protection by serving simultaneously as a sacrificial anode and as a physical barrier, zinc coatings are widely used. However, during contact (such as storage and transportation) with humid environments the zinc surfaces form corrosion products (white rust Figure 13) easily due to the high electrochemical reactivity.
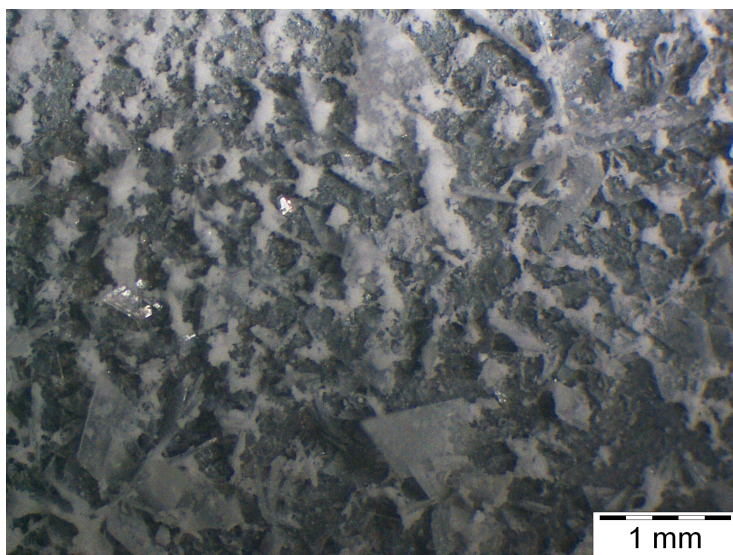
Figure 13. Stereomicroscopic observation of HDGS surface magnified 20 times showing the corrosion products (white rust).

Hot-dip galvanized steel (HDGS) used in reinforced concrete structures, is an example of the many applications of HDGS and has been recognized as an effective measure to improve the service life of reinforced concrete structures. Although, when HDGS is embedded in fresh concrete, which is a highly alkaline environment, the zinc coating corrodes until passivation occurs and the concrete hardens. Due to the initial high corrosion rate of the zinc when in contact with fresh concrete, part of the zinc layer may be removed compromising the galvanic protection of the underlying steel in the long term. Moreover, the hydrogen evolution during the corresponding cathodic half-cell reaction will increase the porosity of the adjacent cement paste and, therefore, reduce the bond strength between the rebar and the concrete. To minimize the zinc corrosion, either during storage and transportation within humid environments or when embedded in fresh concrete, CCCs have been extensively used. Nevertheless, these should be replaced in the near future due to their high toxicity.

Several studies have been made to search for viable alternatives to the use of the CCC. However, few papers have been found using OIH sol-gel technology and these are listed in Table 6. Considering all the information gathered (Table 6 and Figure 10) it was shown that only 9 % of the papers published between 2001 and 2013 tested OIH (class II) gel coatings. The most frequently used precursors were GPTMS, TEOS and MTES and their use represented 36 % of the total studies found and reported (Table 6). The small amount of published papers using OIH sol-gel coatings based on siloxanes (i.e., at least one of the precursors used is based on siloxanes) may be due to the focus on searching for new green conversion coatings[216–221] based on molybdate[216–218],

permanganate[219,220], silicate[222,222–224], titanate[225,226], rare earth salts[227–230], tungstate[231,232] and vanadate[233] compounds.

Table 6. Studies on corrosion protection using OIH (class II) sol–gel coatings on zinc, zinc based alloys and HDGS substrates (2001-2013)

Year	Precursors	Results and Conclusions	Ref
2001	ER and BPA	Results showed effective protection of the metallic substrate.	204
2004	MAPTS, TMOS	Anticorrosive performance of the Ce^{3+} ions trapped within the OIH network occurred by the self-repairing mechanism of the inhibitor.	205
2006	TEOS and PDMMS	OIH coating improved corrosion protection of the substrate.	206
	TEOS and MTES	Protective properties of OIH coating and its dependence on the sintering temperature were studied and shorter sintering times are recommended.	207
2009	GPTMS, TEOS, MTES	Results showed that the OIH ensured a barrier effect against water and oxygen and acted as an adhesion promoter between the substrate and the coating.	208
2010	GPTMS, TEOS, MTES	OIH filled with montmorillonite nanoparticles and cerium oxides enriched montmorillonite nanoparticles were tested. Cerium oxides did not improve the corrosion protection of the OIH film.	209
	GPTMS, TEOS, MTES	Effect of the EPD conditions on HDGS pre-treated with OIH was studied.	210
2011	TIPT, PAPTES	Results showed that the OIH coating offered good corrosion protection for the substrate.	88
2012	GPTMS, TEOS, MTES	Montmorillonite clay was modified to obtain Ce(III) montmorillonite clay and it was successfully incorporated in the OIH coating.	211
	AEAPS, epoxy resin	OIH coatings with nanocontainers loaded with corrosion inhibitor enhanced the anticorrosive properties compared to the coatings with empty nanocontainers or only with the inhibitor.	212
2013	GPTMS, TEOS, MTES	The beneficial effect of Na-Montmorillonite sonication on the corrosion properties of the OIH was confirmed.	104
	GPTMS, BPA	OIH coatings doped with 0.05M of cerium nitrate improved barrier properties.	213
	BTSE, ERE	Substrates coated with OIH by EPD showed improved corrosion protection than the substrates coated with OIH by immersion.	214
	ICPTES, Jeffamine®	OIH coatings minimized the H_2 evolution on the HDGS when embedded in fresh mortar.	215

4.5.   OIH Coatings for Corrosion Protection of Magnesium Based Alloys

Magnesium is employed as a structural load bearing material exploiting its chemical and metallurgical properties. These alloys are used as a sacrificial anode to protect steel against corrosion in circumstances such as the protection of underground pipelines and to increase the service life of household hot water tanks. In 2010, Guo[2] stated that due to the low weight and excellent mechanical properties of magnesium and its alloys, innovative magnesium alloys or enhanced alloys with superior properties should be developed and in-depth research should be performed. Several alloys have been developed in order to obtain a range of properties and features that can fulfil the needs of a wide range of uses.[2,65] The wide range of potential applications of magnesium and magnesium-based alloys makes it incredibly attractive for engineering uses, mainly

in the aerospace and automobile industries due to the low density and high specific stiffness. Currently magnesium-based alloys are under study and alloys referred to as AZ91D, AM60B, AM50A and AS41B have been developed for die casting processing giving rise to alloys with superior corrosion resistance when compared to the aluminium die casting alloys frequently used. In spite of these advantages their application is still limited by their high corrosion vulnerability in aqueous environments, particularly in the presence of chloride ions.[65] The publications found about the use of OIH (class II) coatings based on siloxanes (i.e., at least one of the precursors used is based on siloxanes) are summarized in Table 7.

Table 7. Studies on corrosion protection using OIH (class II) sol–gel coatings on magnesium substrates published since 2001.

Year	Precursors	Results and Conclusions	Ref
2005	MAPTS, MPTMS, SiO$_2$.	OIH coatings provided corrosion protection by sealing pores in the anodized layer and acting as a barrier. The application of multilayers eliminated the diffusion paths for corrosive species.	234
2006	TEOS, PHS	Besides the barrier coating on a metal surface, the phosphonate functionalities reacted with the surface of the substrate increasing both adhesive and corrosion resistance properties of the coatings.	235
2008	GPTMS, ZrTPO, TBADP.	A well-adhered OIH gel coating for the substrate was obtained and the effectiveness of corrosion protection was confirmed.	236
2009	TEOS, MTES, DEDMS, PHS, GPTMS.	Corrosion protection was improved by implementing an interpenetrating network coating morphology.	237
	TEOS, GPTMS	Study of the OIH coating properties, characterization and formation mechanism.	238
	GPTMS, TMOS	Phosphate conversion coating sealed with OIH coating doped with inhibitor (2-methylpiperidine) showed better corrosion resistance that undoped coating.	239
	TEOS, GPTMS	Three layers of OIH coatings totally covered the cracks produced on the molybdate conversion coating first deposited on the substrate and showing good corrosion behaviour.	240
2010	ZrTPO, GPTMS	OIH gel coatings doped with corrosion inhibitor showed improved corrosion behaviour in the protection of the films in comparison with the undoped ones.	241
	TMOS, DEDMS	OIH coatings obtained were evaluated as autonomous protective coatings as well as a pre-treatment prior to acrylic topcoat. OIH coatings doped with Ce^{3+} were effective as pre-treatments for a final acrylic coating.	242
	GPTMS, VTES	Increasing of [Ce^{3+}] on the OIH coating decreases the anti-corrosion effect.	243
2011	TEOS and MTES	Precursor ratios (X1), sol dilution (X2) and sintering temperature (X3) were studied for an OIH coating. Best conditions obtained for X1 = 3.36, X2 = 1.5 and X3 = 222 ºC.	244
2012	GPTMS, MTES	Results revealed that the surface conditioning process was a key step to achieve the required anticorrosion properties of the substrate coated with the OIH.	245
2013	GPTMS, Al(O^{s}Bu)$_3$	OIH coating showed lower thickness in some points offering inferior protection against corrosive species.	246
	DGEBA, APTES, APTMS, GPTMS, TMSPh.	OIH coatings proposed showed high corrosion resistance with considerable improvements obtained by the OIHs based on APTMS and APTES.	247

Considering all the information gathered, Figure 10 shows that 9 % of the papers were about magnesium based alloys and that in 71 % of those publications the most frequently used precursor was GPTMS in combination with others. Analysing the available research papers concerning the prevention of corrosion on magnesium alloys it seems that the research is following another path.[248–254] Most research focuses on improving the existing magnesium alloy properties[249–251] or inventing new ones,[248,252–254] instead of investigating OIH sol-gel coatings. This line of thought explains the fewer publications found when compared with the research available for aluminium or steel substrates.

5. Limitations of Organic-inorganic Hybrid Sol-Gel Coatings for Corrosion Protection

In the last two decades, the existing knowledge about sol-gel processing and relations between structure and properties has had an exceptional development. Consequently, the research efforts on this particular area of materials science have grown, allowing scientists to gain knowledge on how to develop new OIH gel materials. Despite the advantages of combining different properties, synthesis constraints still remain. The major limitations of sol-gel processing for coating metals are delamination, crackability, adhesion and thickness limits. Assuring a uniform distribution on the substrate and thermal treatments (curing/drying) are crucial factors to ensure the quality of anticorrosive coatings[3]. Cracks may affect several properties and are detrimental to the substrate in wet corrosive media. Sendova *et al.* (2003)[255] produced silicate sol-gel coating films with four different crack patterns, achieving reproducible patterns by controlling the film deposition parameters. These authors showed that the geometric characteristics of the crack patterns were related with the thickness of the film and the deposition parameters. Latella *et al.*[256] synthesized and assessed the adhesion behaviour and mechanical properties of OIH coatings. It was confirmed that the presence of a thermally grown oxide layer on the substrate, prior to the OIH sol-gel deposition, had an important role on the adhesion behaviour (quality) between the film and the substrate. They also showed that the relation between the structure of the film and the mechanical properties of the coatings were influenced by the nature/characteristics of the organic substituent. Mammeri *et al.*[39] investigated and analysed the mechanical properties of OIH gels reported by several authors and concluded that those properties were dependent on their micro- and nano- structures as well as the nature and extent of the organic–inorganic interfaces within the gel matrix. Some authors showed that when the substrate was subjected to localized plastic deformation due to impact with objects, or

extensive plastic deformation due to substrate bending, cracks and delamination developed easily in the thin films[3,55]. Others showed that electrodeposition (EPD) techniques provided fairly thick crack-free sol–gel derived coatings when compared either to dip or spin coating techniques[64,195]. Castro and co-workers[257] combined the sol-gel method and the EPD process to prepare thick coatings onto metallic substrates obtaining crack-free deposits up to 20 μm in thickness after drying and crack-free glass-like coatings of 12 μm in thickness after sintering at 500 ºC for 30 minutes[257]. The characterization of OIH materials by potentiodynamic methods showed that they have good performance against corrosion. Most of the studies reported in the literature were on planar samples and the films were deposited by dip or spin coating processes. Objects with complex shapes are far more challenging to coat using these methods, particularly if a uniform thickness is a strict requirement. For these reasons, additional coating methods besides spraying, dipping, spinning and EPD are expected to be extensively tested and developed in the near future[3]. The deposition method selected might be a limiting variable as in certain circumstances it could negatively influence the performance of the OIH coating applied on the substrate. If the deposition method chosen is not the correct one, even with an OIH material displaying excellent barrier properties, the coating performance is compromised. The available deposition methods do not ensure fully uniform coatings, particularly when dip-coating systems for the deposition of low viscosity OIH gel precursors are used. Representative SEM images and EDS analysis data obtained for the HDGS samples coated with two matrices of the OIHs synthesized and deposited on the substrate by dip coating method as described elsewhere[215] are shown in Figures 14 and 15.
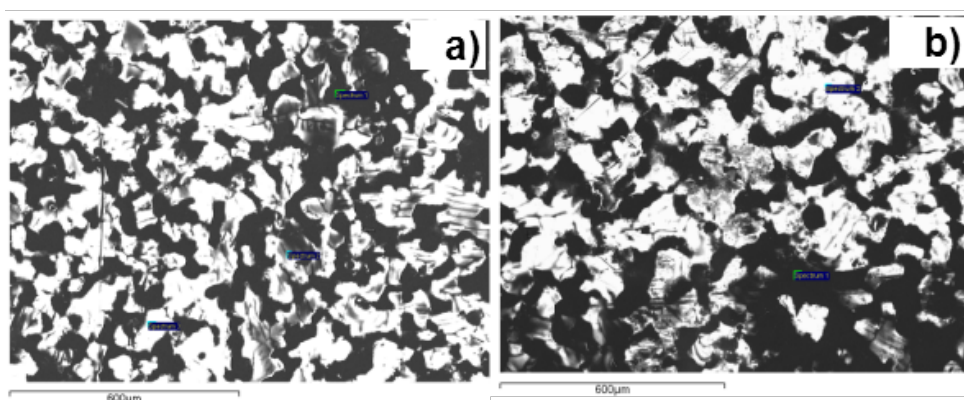
Figure 14. SEM images of HDGS samples coated with the same OIH matrix by dip step method a) one layer; b) two layers.
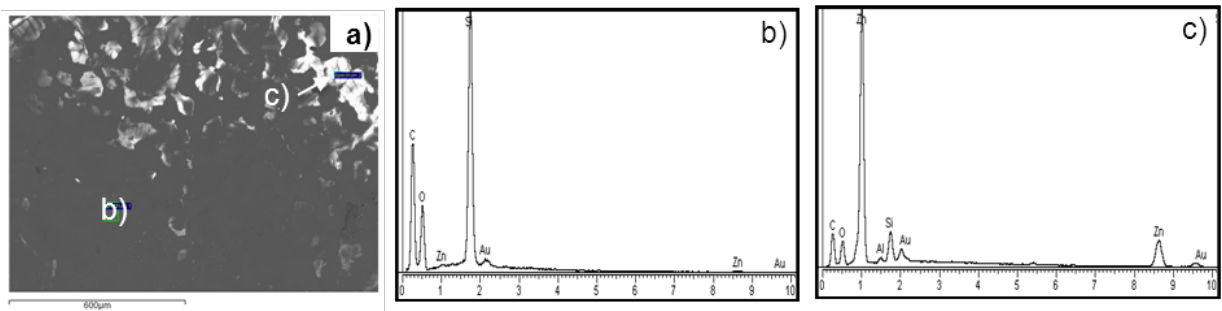
Figure 15. a) SEM image of HDGS samples coated with three layers of OIH by dip coating method; b) and c) shows EDS spectra obtained by scanning two different regions coated samples with three layers of OIH using dip coating method.

It can be observed that the distribution of the OIH coatings is not uniform. As shown by EDS analysis the grey areas correspond to the OIH coating (assigned by high peaks of C, Si and O) and the lighter areas are representative of the substrate (HDGS). In the absence of the OIH coating the peak assigned to zinc is particularly intense. It is also highlighted that it is difficult to achieve a uniform distribution even with a triple dip step process as shown in Figure 15a). Nevertheless, these obstacles can be overcome by the use of intermediate deposition and curing steps. However, the increase in the number of steps involved in coating methods make these procedures extremely complex and time consuming. As such a compromise between the improvement of the final material properties and the associated costs should be made.

Another important limitation considered by the consumer industry is the difficulty in assessing the behaviour of the coating against corrosion after being exposed to the environment. In certain cases, such as underground pipelines and storage tanks, visual observation is impossible without exceptional efforts and costs. In such situations research should be carried out by pre-evaluating the performance and lifetime of the protective coatings, on lab or at a pilot scale, to plan the adequate maintenance/replacement interventions or by the development of appropriate sensors and monitoring methods based on self-sustainable and remote control devices.

Arkles[258] in 2001 published a paper about the commercial applications of the synthesized OIH gel materials and according to him these show viability in the market either owing to uncommon properties that allow new end-use applications or significantly better cost/performance relation when compared with the available materials.

Until now, the traditional CCCs confer the best corrosion protection known at controlled costs making this area even more challenging leading to continuous research for contemporaneous OIH materials that fulfill the same properties and performances exhibited by CCCs coatings.

It is noteworthy that no report has yet been found, either in industrial or academic research, of OIH sol-gel coatings with the same production costs and of equal or superior corrosion performance to traditional conversion layers used processes (chromating and phosphating). As far as authors are aware, no systematic theoretical and experimental approach on how to evaluate the viability, efficiency and stability of OIH sol–gel coatings, has been implemented and is far from being established. The present situation demands further research and innovation efforts to guarantee the success of the application of OIH sol-gel coatings as metal corrosion protection.

6. Future and Research Challenges on Organic-Inorganic Hybrid Materials for Corrosion Protection

Nowadays, metal corrosion protection is strongly reliant on organic and organic-inorganic coating technology, as it is a cost-effective mean of providing practical protection against corrosion for easily corrodible metallic structures and objects. The quality and effectiveness of corrosion control by coatings is assumed by many users to be low cost and easy to achieve. For these reasons, the users of corrosion control coatings often choose these by cost and appearance and not by cost effectiveness, which can be measured by their performance and the lifetime of their behaviour. However, with high labour costs and the difficulties found in re-coating large, buried, complex or difficult to reach objects, more coatings users are focusing on the total costs of corrosion prevention and control. A coating system that increases the lifetime of the product but is somewhat more expensive, due to the initial application method, will pay for itself in reduced maintenance costs and reduced need for expensive recoating. Following this line of thought, the cost analysis of the corrosion protection provided by coatings must lead to further research into measuring and predicting the pot life of the protective properties of these materials.

It is undeniable that future applications and research should be focused primarily on the investigation of more environmentally friendly precursors and industrial colloid particles to replace the traditional precursors in the formation of sol–gel protective coatings without changing their general properties. Among the most critical constraints identified are the coating's mechanic strength and good adhesion to metallic substrates.

In spite of the large number of papers published on this subject, no work was found reporting the use of OIH coatings to stop and prevent corrosion on already damaged substrates as well as studies testing such materials for significant periods of time. The evaluation of whether OIH coatings have the ability to minimize/stop damage caused by corrosion and their durability over time is of extreme importance since OIHs are known for having a limited shelf life due to sluggish condensation reaction kinetics. The products developed for the protection of metallic substrates against corrosion must have a long lifetime. Another conclusion of the detailed analysis of the large set of publications was that studies on the barrier properties of the coatings over time were not found. Therefore, a relevant question that must be answered is "*How long are OIH coatings used to prevent corrosion able to maintain their barrier properties?*" As such, it is vital to undertake long-term tests in the near future as the durability/resistance of OIH coatings for corrosion prevention remains unknown.

The search for future OIH gel based coatings is oriented towards low cost, pollution-free, easily synthesized and effective corrosion protection OIH coatings that do not generate hazardous waste during their application and removal. Development of OIH coatings with self-healing properties would be a challenging innovation that will contribute in giving an added high-value to the synthesized materials.

Inspired by living organisms, materials engineers are focusing on developing materials with self-healing properties. According to Ghosh the term "self-healing" may be defined as "...*the ability of a material to heal (recover/repair) damages automatically and autonomously, that is, without any external intervention*"[259]. Several authors[195,260–272] developed and reviewed corrosion protection systems with self-healing abilities. The development of OIH coatings with those properties by incorporating the release of healing agents, reverting cross-links or using simultaneous technologies such as conductivity; shape memory effect; nanoparticle migration and co-deposition[257] might be considered as important achievements.

The development of new OIH coatings with dual behaviour (a protective barrier accumulating the OIH properties with a self-healing response) is a synergy that will bring benefits and improvements in corrosion prevention, fulfilling the requests needed by the users of coatings technology. This new concept is based on multilayer coatings where inhibitors and self-healing agents are immobilized in one of the layers being isolated from the external media and metal substrate by intermediate layers[273]. It is important that the implemented procedure to obtain these new systems assures good adhesion and similar thermal expansion coefficients between the layers. This same procedure also relies on an efficient top coating layer barrier protection. Moreover, the immobilization of both self-

healing and inhibitor agents within a layer apart from the metallic substrate, by intermediate layers, prevent side reactions and leakage that may affect the substrate.

Considering the potentialities of the sol-gel method, efficient multilayer coatings could be produced if the adhesion between the metallic substrate and the contact layer is achieved, as well as the adhesion between each one of the different upper layers. Additionally these materials show efficient barrier properties and the capacity of hosting species with different properties allows the development of an improved multilayer coating that combines corrosion inhibition and self-healing properties.

This paper proposes a model inspired by the one proposed by the authors Hughes *et al.*[273] for a multilayer coating system. The protective coating proposed is to be produced in five steps (Figure 16), using mainly sol-gel methods. The first step involves chemical activation of the metallic surface, aiming to improve further covalent interaction between the Si-O-Si groups of the OIH matrix and the oxo- and/or hidroxo- groups formed on the metallic surface. Additionally it is expected that this treatment will contribute to improving the uniformity and distribution of the first OIH sol-gel layer deposited, providing a full coverage on a smoother substrate than that given by the chemical pre-treatment.

The second step of the proposed model consists of depositing a thin layer of OIH matrix gel. The sol-gel precursors used to produce this coating material should provide good adhesion with the activated metallic substrate and adequate curing process ensuring appropriate mechanical and support properties to the deposition of a second OIH gel layer. The composition of this and the other layers should be based on the same matrix composition in order to avoid sharp differences of the properties at the interface between the different layers preventing surface/interface tensions. This strategy also contributes to minimizing the differences in thermal and mechanical properties between the different layers.

The deposition of this first layer is also necessary to ensure that the inhibitors and any other species, including self-healing agents, do not migrate towards the metallic surface except when in the presence of external aggressive agents. In this situation, the inhibitor action could be expanded to the vicinity of the metallic surface to stop the spread of corrosion.
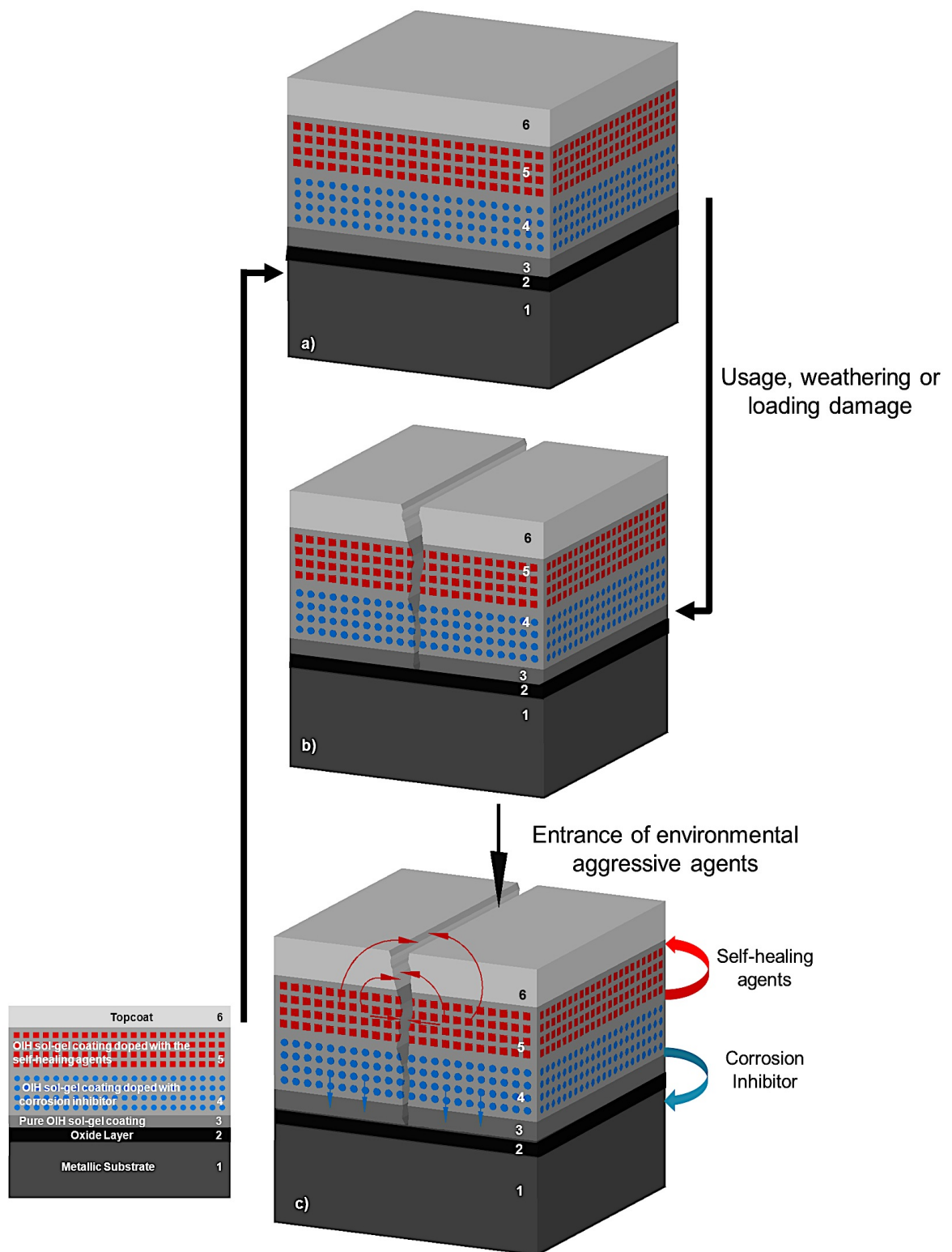
Figure 16. a) Multilayer coating system composed of five layers. 1 – Metallic substrate; 2 – Oxide layer; 3 – Pure OIH sol-gel coating; 4 – OIH sol-gel coating doped with a corrosion inhibitor ; 5 – OIH sol-gel coating doped with a self-healing agent; 6 – Topcoat. b) Multilayer coating system after damage. c) Expected behaviour of the multilayer coating system behaviour when in contact with exterior aggressive agents.

As observed by several authors the relative amount of inhibitor could compromise OIH matrix stability,[94,99,117,120,130] so the presence of the first OIH layer also contributes to additionally enhance the protection against inhibitor mobility/migration or diffusion towards the metallic surface. The layer where the inhibitor is immobilized is produced in a third step and under adequate gelling conditions to minimize the curing demanding time and optimize the immobilization of the inhibitor species within this layer. Adjusting the gelling time (viscosity) of the gel precursor (of the deposited coating) by achieving an optimum viscosity value, allows the starting of the curing process immediately and during a short time.

This methodology should also obtain a dense and smooth layer with a good adhesion to the previous OIH layer. The following step consists of producing a third OIH layer containing self-healing agents that contribute to guarantee the reversibility of the damages caused by a variety of factors such as usage, weathering or loading damage.

The reversibility mechanism could be triggered by the entrance of water and ions transported through the topcoat. This mechanism is inspired by the process that has been used for self-healing in polymer composites through the release of a polymerizable healing agent that can bridge cracks after reaction with the appropriate catalysts[274]. The synthesis procedure to obtain this layer is critical as it should ensure that the self-healing agents dispersed within this OIH layer preserve their properties and mobility after the curing treatment. Finally a highly hydrophobic topcoat layer should be deposited at mild conditions to combine the barrier effect protection and to avoid any possible degradation of the different OIH based layers that are beneath. The total thickness of this type of multilayer coating system should be about 16 μm considering the use of dip coating method that allows the production of each OIH layer with an average thickness of 4 μm. The schematic representation of the proposed multilayer coating system is displayed in Figure 16.

7. Concluding Remarks

Publications between 2001 and 2013 about OIH sol–gel coatings class II based on siloxanes, which were tested to prevent corrosion on metallic substrates, were reviewed. Since the early 1970s, academic interest in OIH materials has been accelerating and since the 1990s it has become a fast-growing and very complex subject with an almost exponential increase in the number of the scientific publications.

The main driving force in the development of OIHs class II based on siloxanes to prevent corrosion was the search for potential candidates to substitute environmentally unfriendly chromate surface treatments for metallic substrates.

The analysis of the papers published between 2001-2013 shows that it is on aluminium based alloys where higher search efforts for an efficient coating to replace CCCs has been done, followed by steel substrates, zinc and magnesium alloys, with copper alloys in last place. Regardless of the type of substrate, the most frequently used precursors were GPTMS, TEOS and TMOS.

Tested OIH materials present a large diversity of compositions and enhanced physical, mechanical and morphological properties, among others. OIH materials show strong potential and are clearly becoming a reality as serious candidates for numerous applications such as smart coatings with ''intelligent'' self-healing properties and functional protective coatings. Moreover, the OIH sol–gel process shows high potential for the production of multilayer coating systems which are promising environmentally-friendly candidates for replacement of the chromate-based pre-treatments due to a synergistic effect of good barrier properties and effective ''self-healing'' action.

Acknowledgements

References

1. J. H. Osborne, *Prog. Org. Coat.*, **41**, 280–286 (2001).

2. K. Guo, *Recent Pat. Corros. Sci.*, **2**, 13–21 (2010).

3. M. Guglielmi, *J. Sol-Gel Sci. Technol.*, **8**, 443–449 (1997).

4. R. L. Twite and G. P. Bierwagen, *Prog. Org. Coat.*, **33**, 91–100 (1998).

5. T. L. Metroke, R. L. Parkhill and E. T. Knobbe, *Prog. Org. Coat.*, **41**, 233–238 (2001).

6. W. J. van Ooij, D. Zhu, M. Stacy, A. Seth, T. Mugada, J. Gandhi and P. Puomi, *Tsinghua Sci. Technol.*, **10**, 639–664 (2005).

7. J. Gray and B. Luan, *J. Alloys Compd.*, **336**, 88–113 (2002).

8. M. A. Aegerter and M. Mennig, *Sol-gel technologies for glass producers and users*, Kluwer Academic Publishers, Boston, (2004).

9. H. Dislich, *J. Non-Cryst. Solids*, **57**, 371–388 (1983).

10. D. L. Segal, *J. Non-Cryst. Solids*, **63**, 183–191 (1984).

11. C. J. Brinker and G. W. Scherer, *Sol-gel science: the physics and chemistry of sol-gel processing*, Academic Press, Boston, (1990).

12. A. C. Pierre, in *Introduction to Sol-Gel Processing*, The Kluwer International Series in Sol-Gel Processing: Technology and Applications, p. 347–386, Springer US (1998).

13. C. Brinker, A. Hurd, P. Schunk and G. Frye, *J. Non-Cryst. Solids*, **148**, 424–436 (1992).

14. L. L. Hench and J. K. West, *Chem. Rev.*, **90**, 33–72 (1990).

15. C. Sanchez, P. Belleville, M. Popall and L. Nicole, *Chem. Soc. Rev.*, **40**, 453–1152 (2011).

16. C. Sanchez, G. J. D. A. Soler-Illia, F. Ribot, T. Lalot, C. R. Mayer, V. Cabuil, *Chem. Mater.*, **13**, 3061–3083 (2001).

17. D. G. Shchukin, A. A. Yaremchenko, M. G. S. Ferreira and V. V. Kharton, *Chem. Mater.*, **17**, 5124–5129 (2005).

18. C. F. Canto, L. A. S. de A. Prado, E. Radovanovic and I. V. P. Yoshida, *Polym. Eng. Sci.*, **48**, 141–148 (2008).

19. C. Sanchez and F. Ribot, *New J. Chem.*, **18**, 1007–1047 (1994).

20. A. Wojcik and L. C. Klein, *Appl. Organomet. Chem.*, **11**, 129–135 (1997).

21. N. M. José and L. A. S. de A. Prado, *Quimica Nova*, **28**, 281–288 (2005).

22. S. D. F. C. Moreira S. D. F. C. Moreira, C. J. R. Silva, L. A. S. A. Prado, M. F. M. Costa, V. I. Boev, J. Martín-Sánchez and M. J. M. Gomes, *J. Polym. Sci. Part B Polym. Phys.*, **50**, 492–499 (2012).

23. P. Roberge, *Handbook of Corrosion Engineering*, p. 1156, McGraw-Hill Professional, (1999).

24. T. F. O'Brien, T. V. Bommaraju and F. Hine, *Handbook of Chlor-Alkali Technology: Vol. V, Corrosion, Environmental Issues, and Future Developments*, p. 1597, Springer, (2007).

25. H. Kaesche, *Corrosion of Metals: Physicochemical Principles and Current Problems*, p. 612, Springer, (2003).

26. E. Ghali, V. S. Sastri and M. Elboujdaini, *Corrosion Prevention and Protection: Practical Solutions*, p. 580, John Wiley & Sons, (2007).

27. H. H. Uhlig and R. W. Revie, *Corrosion and Corrosion Control: An Introduction to Corrosion Science and Engineering*, p. 441, J. Wiley, (1991).

28. J. R. Davis, *Surface engineering for corrosion and wear resistance*, ASM International : Institute of Materials, Materials Park, OH, (2001).

29. H. K. Pulker, *Coatings on glass*, Elsevier, Amsterdam, New York, (1999).

30. S. Sakka and T. Yoko, in *Chemistry, Spectroscopy and Applications of Sol-Gel Glasses*, Structure and Bonding. R. Reisfeld and C. K. Jørgensen, Editors, vol. 77, p. 89–118, Springer Berlin Heidelberg (1992).

31. J. M. Magalhães, J. E. Silva, F. P. Castro and J. A. Labrincha, *J. Environ. Manage.*, **75**, 157–166 (2005).

32. C. Wu and J. Zhang, *Trans. Nonferrous Met. Soc. China*, **21**, 892–902 (2011).

33. R.-G. Hu, S. Zhang, J.-F. Bu, C.-J. Lin and G.-L. Song, *Prog. Org. Coat.*, **73**, 129–141 (2012).

34. H. Schmidt, H. Scholze and A. Kaiser, *J. Non-Cryst. Solids*, **63**, 1–11 (1984).

35. G. L. Wilkes, B. Orler and H. H. Hsin, *Polym. Prep.*, **26**, 300–302 (1985).

36. W. J. Van Ooij and A. Sabata, *J. Adhes. Sci. Technol.*, **5**, 843–863 (1991).

37. W. Yuan and W. J. van Ooij, *J. Colloid Interface Sci.*, **185**, 197–209 (1997).

38. D. Wang and G. P. Bierwagen, *Prog. Org. Coat.*, **64**, 327–338 (2009).

39. F. Mammeri, E. L. Bourhis, L. Rozes and C. Sanchez, *J. Mater. Chem.*, **15**, 3787 (2005).

40. V. Castelvetro and C. De Vita, *Adv. Colloid Interface Sci.*, **108-109**, 167–85 (2004).

41. E. Bescher and J. D. Mackenzie, *J. Sol-Gel Sci. Technol.*, **26**, 1223–1226 (2003).

42. S. M. Attia, J. Wang, G. Wu, J. Shen and J. Ma, *J Mater Sci Technol*, **18**, 211–218 (2002).

43. J. D. Mackenzie and E. P. Bescher, *Acc. Chem. Res.*, **40**, 810–8 (2007).

44. M. Niederberger, *Acc. Chem. Res.*, **40**, 793–800 (2007).

45. S. Sakka, *J. Sol-Gel Sci. Technol.*, **46**, 241–249 (2007).

46. Y. Dimitriev, Y. Ivanova and R. Iordanova, *J. Univ. Chem. Technol. Metallurgy*, **43**, 181–192 (2008).

47. S. Kozhukharov, *J. Univ. Chem. Technol.*, **44**, 143–150 (2009).

48. E. V. Benvenutti, C. C. Moro, T. M. H. Costa and M. R. Gallas, *Quím. Nova*, **32**, 1926–1933 (2009).

49. S. Pandey and S. B. Mishra, *J. Sol-Gel Sci. Technol.*, **59**, 73–94 (2011).

50. D. Balgude and A. Sabnis, *J. Sol-Gel Sci. Technol.*, **64**, 124–134 (2012).

51. M. Abdolah Zadeh, S. van der Zwaag and S. J. Garcia, *Self-Heal. Mater.*, **1**, 1–18 (2013).

52. S. Chaturvedi and P. N. Dave, *J. Mater. Sci.*, **48**, 3605–3622 (2013).

53. J. Wen and G. L. Wilkes, *Chem. Mater.*, **8**, 1667–1681 (1996).

54. G. Schottner, *Chem. Mater.*, **13**, 3422–3435 (2001).

55. A. Walcarius, *Chem. Mater.*, **13**, 3351–3372 (2001).

56. D. B. Mitzi, *Chem. Mater.*, **13**, 3283–3298 (2001).

57. J. N. Hay and H. M. Raval, *Chem. Mater.*, **13**, 3396–3403 (2001).

58. A. Arkhireeva, J. N. Hay, J. M. Lane, M. Manzano, H. Masters, W. Oware and S. J. Shaw, *J. Sol-Gel Sci. Technol.,* **31**, 31-33 (2004).

59. C. Sanchez, B. Julián, P. Belleville and M. Popall, *J. Mater. Chem.*, **15**, 3559 (2005).

60. P. Innocenzi, T. Kidchob and T. Yoko, *J. Sol-Gel Sci. Technol.*, **35**, 225–235 (2005).

61. S. Dash, S. Mishra, S. Patel and B. K. Mishra, *Adv. Colloid Interface Sci.*, **140**, 77–94 (2008).

62. E. Lebedev, *Theor. Exp. Chem.*, **46**, 391–396 (2011).

63. C. Sanchez L. Rozes, F. Ribot, C. Laberty-Robert, D. Grosso, C. Sassoye, C. Boissiere and L. Nicole, *Comptes Rendus Chim.*, **13**, 3–39 (2010).

64. S. Zheng and J. Li, *J. Sol-Gel Sci. Technol.*, **54**, 174–187 (2010).

65. B. L. Bramfitt, in *Handbook of Materials Selection*, M. Kutz, Editor, p. 25–65, John Wiley & Sons, Inc. (2007).

66. T. P. Chou, C. Chandrasekaran, S. J. Limmer, S. Seraji, Y. Wu, M. J. Forbess, C. Nguyen and G. Z. Caoa, *J. Non-Cryst. Solids*, **290**, 153–162 (2001).

67. S. Kumar, M. Alagar and V. Mohan, *J. Mater. Eng. Perform.*, **11**, 123–129 (2002).

68. T. Chou, C. Chandrasekaran and G. Z. Cao, *J. Sol-Gel Sci. Technol.*, **26**, 321–327 (2003).

69. H. Sayilkan, Ş. Şener and E. Şener, *Mater. Sci.*, **39**, 106–110 (2003).

70. J. Gallardo, A. Durán and J. J. de Damborenea, *Corros. Sci.*, **46**, 795–806 (2004).

71. T. Gunji, Y. Iizuka, K. Arimitsu and Y. Abe, *J. Polym. Sci. Part Polym. Chem.*, **42**, 3676–3684 (2004).

72. Y. Castro, B. Ferrari, R. Moreno and A. Durán, *Surf. Coat. Technol.*, **191**, 228–235 (2005).

73. A. Pepe, P. Galliano, S. Ceré, M. Aparicio and A. Durán, *Mater. Lett.*, **59**, 2219–2222 (2005).

74. L. Mascia, L. Prezzi, G. D. Wilcox and M. Lavorgna, *Prog. Org. Coat.*, **56**, 13–22 (2006).

75. L. Jianguo, G. Gaoping and Y. Chuanwei, *Surf. Coat. Technol.*, **200**, 4967–4975 (2006).

76. A. Pepe, P. Galliano, M. Aparicio, A. Durán and S. Ceré, *Surf. Coat. Technol.*, **200**, 3486–3491 (2006).

77. W. Xing, B. You and L. Wu, *J. Coat. Technol. Res.*, **5**, 65–72 (2008).

78. H. Wang and R. Akid, *Corros. Sci.*, **50**, 1142–1148 (2008).

79. A. Phanasgaonkar and V. S. Raja, *Surf. Coat. Technol.*, **203**, 2260–2271 (2009).

80. M. Qian, A. Mcintosh Soutar, X. H. Tan, X. T. Zeng and S. L. Wijesinghe, *Thin Solid Films*, **517**, 5237–5242 (2009).

81. G. Carbajal-de la Torre, M. A. Espinosa-Medina, A. Martinez-Villafañe, J. G. Gonzalez-Rodriguez and V. M. Castaño, *Open Corros. J.*, **2**, 197-203 (2009).

82. V. H. V. Sarmento M. G. Schiavetto, P. Hammer, A. V. Benedetti, C. S. Fugivara, P. H. Suegama, S. H. Pulcinelli and C. V. Santilli, *Surf. Coat. Technol.*, **204**, 2689–2701 (2010).

83. S. M. Hosseinalipour, A. Ershad-langroudi, A. N. Hayati and A. M. Nabizade-Haghighi, *Prog. Org. Coat.*, **67**, 371–374 (2010).

84. P. Hammer, M. G. Schiavetto, F. C. dos Santos, A. V. Benedetti, S. H. Pulcinelli and C. V. Santilli, *J. Non-Cryst. Solids*, **356**, 2606–2612 (2010).

85. P. H. Suegama, V. H. V. Sarmento, M. F. Montemor, A. V. Benedetti, H. G. de Melo, I. V. Aoki and C. V. Santilli, *Electrochim. Acta*, **55**, 5100–5109 (2010).

86. P. Kiruthika, R. Subasri, A. Jyothirmayi, K. Sarvani and N. Y. Hebalkar, *Surf. Coat. Technol.*, **204**, 1270–1276 (2010).

87. A. G. Kannan, N. R. Choudhury and N. K. Dutta, *J. Electroanal. Chem.*, **641**, 28–34 (2010).

88. A. K. Guin, S. K. Nayak, T. K. Rout, N. Bandyopadhyay and D. K. Sengupta, *J. Coat. Technol. Res.*, **9**, 97–106 (2011).

89. M. Hernández-Escolano, M. Juan-Díaz, M. Martínez-Ibáñez, A. Jimenez-Morales, I. Goñi, M. Gurruchaga and J. Suay, *J. Sol-Gel Sci. Technol.*, **64**, 442–451 (2012).

90. S. Ahmad, F. Zafar, E. Sharmin, N. Garg and M. Kashif, *Prog. Org. Coat.*, **73**, 112–117 (2012).

91. H. Kim and T. Hwang, *J. Sol-Gel Sci. Technol.*, **63**, 563–568 (2012).

92. C. Arunchandran, S. Ramya, R. P. George and U. K. Mudali, *J. Electrochem. Soc.*, **159**, C552–C559 (2012).

93. P. Hammer, F. C. dos Santos, B. M. Cerrutti, S. H. Pulcinelli and C. V. Santilli, *J. Sol-Gel Sci. Technol.*, **63**, 266–274 (2012).

94. J.-B. Cambon, F. Ansart, J.-P. Bonino and V. Turq, *Prog. Org. Coat.*, **75**, 486–493 (2012).

95. K. Joncoux-Chabrol, J.-P. Bonino, M. Gressier, M.-J. Menu and N. Pébère, *Surf. Coat. Technol.*, **206**, 2884–2891 (2012).

96. R. T. Sakai, F. M. Di L. da Cruz, H. G. de Melo, A. V. Benedetti, C. V. Santilli and P. H. Suegama, *Prog. Org. Coat.*, **74**, 288–301 (2012).

97. R. Subasri, R. Malathi, A. Jyothirmayi and N. Y. Hebalkar, *Ceram. Int.*, **38**, 5731–5740 (2012).

98. N. Kumar, A. Jyothirmayi, K. R. C. Soma Raju and R. Subasri, *Ceram. Int.*, **38**, 6565–6572 (2012).

99. R. Z. Zand, K. Verbeken and A. Adriaens, *Prog. Org. Coat.*, **75**, 463–473 (2012).

100. D. Angel-López M. A. Domínguez-Crespo, A. M. Torres-Huerta, A. Flores-Vela, J. Andraca-Adame and H. Dorantes-Rosales, *J. Mater. Sci.*, **48**, 1067–1084 (2012).

101. E. Certhoux, F. Ansart, V. Turq, J. -P. Bonino, J. M. Sobrino, J. Garcia and J. Reby, *Prog. Org. Coat.*, **76**, 165–172 (2013).

102. P. Hammer, F. C. dos Santos, B. M. Cerrutti, S. H. Pulcinelli and C. V. Santilli, *Prog. Org. Coat.*, **76**, 601–608 (2013).

103. S. Rahoui, V. Turq and J.-P. Bonino, *Surf. Coat. Technol.*, **235**, 15–23 (2013).

104. M. Fedel, E. Callone, S. Diré, F. Deflorian, M.-G. Olivier and M. Poelman, *Electrochim. Acta*, **124**, 90–99 (2014).

105. K. J. Jothi and K. Palanivelu, *Ceram. Int.*, **39**, 7619–7625 (2013).

106. S. Peng, W. Zhao, Z. Zeng, H. Li, Q. Xue and X. Wu, *J. Sol-Gel Sci. Technol.*, **66**, 133–138 (2013).

107. D. Balgude, K. Konge and A. Sabnis, *J. Sol-Gel Sci. Technol.*, **69**, 155-165 (2013).

108. I. Santana, A. Pepe, E. Jimenez-Pique, S. Pellice and S. Ceré, *Surf. Coat. Technol.*, **236**, 476–484 (2013).

109. M. Hernandez, A. Barba, J. Genesca, A. Covelo, E. Bucio and V. Torres, *ECS Trans.*, **47**, 195–206 (2013).

110. G. Chawada and B. Z. Dholakiya, *Res. Chem. Intermed.*, **1**, 1-16 (2013).

111. B. Karmakar, G. De and D. Ganguli, *J. Non-Cryst. Solids*, **272**, 119–126 (2000).

112. P. B. Wagh, A. V. Rao and D. Haranath, *Mater. Chem. Phys.*, **53**, 41–47 (1998).

113. S. R. Kunst, H. R. P. Cardoso, C. T. Oliveira, J. A. Santana, V. H. V. Sarmento, I. L. Muller and C. F. Malfatti, *Appl. Surf. Sci.* **298**, 1-11 (2013).

114. A. B. Wojcik and L. C. Klein, *J. Sol-Gel Sci. Technol.*, **4**, 57–66 (1995).

115. D. Álvarez, A. Collazo, M. Hernández, X. R. Nóvoa and C. Pérez, *Prog. Org. Coat.*, **67**, 152–160 (2010).

116. R. Parkhill, E. Knobbe and M. Donley, *Prog. Org. Coat.*, **41**, 261–265 (2001).

117. L. S. Kasten J. T. Grant, N. Grebasch, N. Voevodin, F. E. Arnold and M.S. Donley, *Surf. Coat. Technol.*, **140**, 11–15 (2001).

118. T. Metroke, O. Kachurina and E. T. Knobbe, *Prog. Org. Coat.*, **44**, 295–305 (2002).

119. T. Metroke and O. Kachurina, *Prog. Org. Coat.*, **44**, 185–199 (2002).

120. N. Voevodin, V. Balbyshev, M. Khobaib and M. Donley, *Prog. Org. Coat.*, **47**, 416–423 (2003).

121. A. Conde, A. Durán and J. de Damborenea, *Prog. Org. Coat.*, **46**, 288–296 (2003).

122. M. S. Donley, R. A. Mantz, A. N. Khramov, V. N. Balbyshev, L. S. Kasten and D. J. Gaspar, *Prog. Org. Coat.*, **47**, 401–415 (2003).

123. T. L. Metroke, J. S. Gandhi and A. Apblett, *Prog. Org. Coat.*, **50**, 231–246 (2004).

124. T. L. Metroke and A. Apblett, *Prog. Org. Coat.*, **51**, 36–46 (2004).

125. R. Z. Zand, A. Ershad-langroudi and A. Rahimi, *Prog. Org. Coat.*, **53**, 286–291 (2005).

126. R. Z. Zand, A. Ershad-langroudi and A. Rahimi, *J. Non-Cryst. Solids*, **351**, 1307–1311 (2005).

127. M. S. Donley, V. N. Balbyshev and N. N. Voevodin, *Prog. Org. Coat.*, **52**, 34–38 (2005).

128. Y. Liu, D. Sun, H. You and J. S. Chung, *Appl. Surf. Sci.*, **246**, 82–89 (2005).

129. A. N. Khramov, N. N. Voevodin, V. N. Balbyshev and R. A. Mantz, *Thin Solid Films*, **483**, 191–196 (2005).

130. M. Zheludkevich, R. Serra, M. F. Montemor, K. A. Yasakau, I. M. Miranda Salvado and M. G. S. Ferreira, *Electrochim. Acta*, **51**, 208–217 (2005).

131. N. N. Voevodin, V. N. Balbyshev and M. S. Donley, *Prog. Org. Coat.*, **52**, 28–33 (2005).

132. M. L. Zheludkevich, R. Serra, M. F. Montemor, I. M. M. Salvado and M. G. S. Ferreira, *Surf. Coat. Technol.*, **200**, 3084–3094 (2006).

133. N. N. Voevodin, J. W. Kurdziel and R. Mantz, *Surf. Coat. Technol.*, **201**, 1080–1084 (2006).

134. K. H. Wu, T. C. Chang, C. C. Yang and G. P. Wang, *Thin Solid Films*, **513**, 84–89 (2006).

135. M. Vezir Kahraman, M. Kuğu, Y. Menceloğlu, N. Kayaman-Apohan and A. Güngör, *J. Non-Cryst. Solids*, **352**, 2143–2151 (2006).

136. K. H. Wu, M. C. Li, C. C. Yang and G. P. Wang, *J. Non-Cryst. Solids*, **352**, 2897–2904 (2006).

137. Y.-H. Han, A. Taylor, M. D. Mantle and K. M. Knowles, *J. Sol-Gel Sci. Technol.*, **43**, 111–123 (2007).

138. H. Wang and R. Akid, *Corros. Sci.*, **49**, 4491–4503 (2007).

139. K. H. Wu, C. M. Chao, T. F. Yeh and T. C. Chang, *Surf. Coat. Technol.*, **201**, 5782–5788 (2007).

140. S. S. Pathak, A. S. Khanna and T. J. M. Sinha, *Prog. Org. Coat.*, **60**, 211–218 (2007).

141. P. M. Barkhudarov, P. B. Shah, E. B. Watkins, D. A. Doshi, C. J. Brinker and J. Majewski, *Corros. Sci.*, **50**, 897–902 (2008).

142. T. Lampke, S. Darwich, D. Nickel and B. Wielage, *Mater. Werkst.*, **39**, 914–919 (2008).

143. A. Tiwari, J. Zhu and L. H. Hihara, *Surf. Coat. Technol.*, **202**, 4620–4635 (2008).

144. S. K. Poznyak, M. L. Zheludkevich, D. Raps, F. Gammel, K. A. Yasakau and M. G. S. Ferreira, *Prog. Org. Coat.*, **62**, 226–235 (2008).

145. K. A. Yasakau, M. L. Zheludkevich, O. V. Karavai and M. G. S. Ferreira, *Prog. Org. Coat.*, **63**, 352–361 (2008).

146. N. C. Rosero-Navarro, S. A. Pellice, A. Durán and M. Aparicio, *Corros. Sci.*, **50**, 1283–1291 (2008).

147. A. J. Vreugdenhil, V. J. Gelling, M. E. Woods, J. R. Schmelz and B. P. Enderson, *Thin Solid Films*, **517**, 538–543 (2008).

148. S. S. Pathak and A. S. Khanna, *Prog. Org. Coat.*, **62**, 409–416 (2008).

149. D. Wang, X. Chen, X. Zhang, Y. Liu and L. Hu, *J. Sol-Gel Sci. Technol.*, **49**, 293–300 (2008).

150. N. C. Rosero-Navarro, S. A. Pellice, Y. Castro, M. Aparicio and A. Durán, *Surf. Coat. Technol.*, **203**, 1897–1903 (2009).

151. S. S. Pathak and A. S. Khanna, *Prog. Org. Coat.*, **65**, 288–294 (2009).

152. N. C. Rosero-Navarro, S. A. Pellice, A. Durán, S. Ceré and M. Aparicio, *J. Sol-Gel Sci. Technol.*, **52**, 31–40 (2009).

153. N. P. Tavandashti, S. Sanjabi and T. Shahrabi, *Prog. Org. Coat.*, **65**, 182–186 (2009).

154. M. Schem, T. Schmidt, J. Gerwann, M. Wittmar, M. Veith, G. E. Thompson, I. S. Molchan, T. Hashimoto, P. Skeldon, A. R. Phani, S. Santucci and M. L. Zheludkevich, *Corros. Sci.*, **51**, 2304–2315 (2009).

155. D. Raps, T. Hack, J. Wehr, M. L. Zheludkevich, A. C. Bastos, M. G. S. Ferreira and O. Nuyken, *Corros. Sci.*, **51**, 1012–1021 (2009).

156. Y.-S. Li, W. Lu, Y. Wang and T. Tran, *Spectrochim. Acta. A. Mol. Biomol. Spectrosc.*, **73**, 922–8 (2009).

157. V. Kakde and V. Mannari, *J. Coat. Technol. Res.*, **6**, 201–211 (2009).

158. N. C. Rosero-Navarro, L. Paussa, F. Andreatta, Y. Castro, A. Durán, M. Aparicio and L. Fedrizzi, *Prog. Org. Coat.*, **69**, 167–174 (2010).

159. P. Álvarez, A. Collazo, A. Covelo, X. R. Nóvoa and C. Pérez, *Prog. Org. Coat.*, **69**, 175–183 (2010).

160. P. C. R. Varma, J. Colreavy, J. Cassidy, M. Oubaha, C. McDonagh and B. Duffy, *Thin Solid Films*, **518**, 5753–5761 (2010).

161. H. Shi, F. Liu and E. Han, *Mater. Chem. Phys.*, **124**, 291–297 (2010).

162. H. Shi, F. Liu and E. Han, *Trans. Nonferrous Met. Soc. China*, **20**, 1928–1935 (2010).

163. D. M. Becchi, M. A. Luca, M. Martinelli and S. Mitidieri, *J. Am. Oil Chem. Soc.*, **88**, 101–109 (2010).

164. Z. Feng, Y. Liu, G. E. Thompson and P. Skeldon, *Electrochim. Acta*, **55**, 3518–3527 (2010).

165. A. Tiwari and L. H. Hihara, *Prog. Org. Coat.*, **69**, 16–25 (2010).

166. A. Kumar, A. Kanta, N. Birbilis, T. Williams and B. C. Muddle, *J. Electrochem. Soc.*, **157**, C346 (2010).

167. A. Collazo, M. Hernández, X. R. Nóvoa and C. Pérez, *Electrochim. Acta*, **56**, 7805–7814 (2011).

168. A. Wittmar, M. Wittmar, H. Caparrotti and M. Veith, *J. Sol-Gel Sci. Technol.*, **59**, 621–628 (2011).

169. K. J. Croes, A. J. Vreugdenhil, M. Yan, T. A. Singleton, S. Boraas and V. J. Gelling, *Electrochim. Acta*, **56**, 7796–7804 (2011).

170. E. Roussi, A. Tsetsekou, D. Tsiourvas and A. Karantonis, *Surf. Coat. Technol.*, **205**, 3235–3244 (2011).

171. P. C. R. Varma, P. Periyat, M. Oubaha, C. McDonagh and B. Duffy, *Surf. Coat. Technol.*, **205**, 3992–3998 (2011).

172. J.-B. Cambon, J. Esteban, F. Ansart, J.-P. Bonino, V. Turq, S. H. Santagneli, C. V. Santilli and S. H. Pulcinelli, *Mater. Res. Bull.*, **47**, 3170–3176 (2012).

173. J. O. Iroh and D. Rajamani, *J. Inorg. Organomet. Polym. Mater.*, **22**, 595 – 603 (2012).

174. A. Wittmar, M. Wittmar, A. Ulrich, H. Caparrotti and M. Veith, *J. Sol-Gel Sci. Technol.*, **61**, 600–612 (2012).

175. S. Kozhukharov, V. Kozhukharov, M. Schem, M. Aslan, M. Wittmar, A. Wittmar and M. Veith, *Prog. Org. Coat.*, **73**, 95–103 (2012).

176. S. A. S. Dias, S. V. Lamaka, C. A. Nogueira, T. C. Diamantino and M. G. S. Ferreira, *Corros. Sci.*, **62**, 153–162 (2012).

177. S. A. S. Dias, A. Marques, S. V. Lamaka, A. Simões, T. C. Diamantino and M. G. S. Ferreira, *Electrochim. Acta*, **112**, 549–556 (2013).

178. A. Collazo, A. Covelo, X. R. Nóvoa and C. Pérez, *Prog. Org. Coat.*, **74**, 334–342 (2012).

179. G. Gupta, S. S. Pathak and A. S. Khanna, *Prog. Org. Coat.*, **74**, 106–114 (2012).

180. M. Abuín, A. Serrano, J. Llopis, M. A. García and N. Carmona, *Thin Solid Films*, **520**, 5267–5271 (2012).

181. E. D. Mekeridis, I. A. Kartsonakis and G. C. Kordas, *Prog. Org. Coat.*, **73**, 142–148 (2012).

182. A. H. Najafabadi, R. Mozaffarinia, H. Rahimi, R. S. Razavi and E. Paimozd, *Prog. Org. Coat.*, **76**, 293–301 (2013).

183. M. May, H. Wang and R. Akid, *J. Coat. Technol. Res.*, **10**, 407–413 (2012).

184. K. A. Yasakau, S. Kallip, M. L. Zheludkevich and M. G. S. Ferreira, *Electrochim. Acta*, **112**, 236–246 (2013).

185. E. Roussi, A. Tsetsekou, A. Skarmoutsou, C. A. Charitidis and A. Karantonis, *Surf. Coat. Technol.*, **232**, 131–141 (2013).

186. R. G. Wankhede, S. Morey, A. S. Khanna and N. Birbilis, *Appl. Surf. Sci.*, **283**, 1051–1059 (2013).

187. R. Naderi, M. Fedel, F. Deflorian, M. Poelman and M. Olivier, *Surf. Coat. Technol.*, **224**, 93–100 (2013).

188. V. R. Capelossi, M. Poelman, I. Recloux, R. P. B. Hernandez, H. G. de Melo and M. G. Olivier, *Electrochim. Acta*, **124**, 69-79 (2014).

189. H. Rahimi, R. Mozaffarinia and A. H. Najafabadi, *J. Mater. Sci. Technol.*, **29**, 603–608 (2013).

190. R. V. Lakshmi, G. Yoganandan, K. T. Kavya and B. J. Basu, *Prog. Org. Coat.*, **76**, 367–374 (2013).

191. H. Rahimi, R. Mozaffarinia, A. H. Najafabadi, R. S. Razavi and E. Paimozd, *Prog. Org. Coat.*, **76**, 307–317 (2013).

192. D. M. Bechi, M. A. D. Luca, M. Martinelli and S. Mitidieri, *Prog. Org. Coat.*, **76**, 736–742 (2013).

193. M. L. Zheludkevich, S. K. Poznyak, L. M. Rodrigues, D. Raps, T. Hack, L. F. Dick, T. Nunes and M. G. S. Ferreira, *Corros. Sci.*, **52**, 602–611 (2010).

194. D. G. Shchukin, D. G. Shchukin, S. V. Lamaka, K. A. Yasakau, M. L. Zheludkevich, M. G. S. Ferreira and H. Möhwald, *J. Phys. Chem. C*, **112**, 958–964 (2008).

195. M. L. Zheludkevich, D. G. Shchukin, K. A. Yasakau, H. Möhwald and M. G. S. Ferreira, *Chem. Mater.*, **19**, 402–411 (2007).

196. A. L. K. Tan and A. M. Soutar, *Thin Solid Films*, **516**, 5706–5709 (2008).

197. S. Peng, W. Zhao, H. Li, Z. Zeng, Q. Xue and X. Wu, *Appl. Surf. Sci.*, **276**, 284–290 (2013).

198. E. Kiele, J. Lukseniene, A. Griguceviciene, A. Selskis, J. Senvaitiene, R. Ramanauskas, R. Raudonis and A- Kareiva, *J. Cult. Herit.*, **15**, 242-249 (2014).

199. A. G. Gusakov, A. G. Voropayev, M. L. Zheludkevich, A. A. Vecher and S. A. Raspopov, *Phys. Chem. Chem. Phys.*, **1**, 5311–5314 (1999).

200. M. Honkanen, M. Hoikkanen, M. Vippola, J. Vuorinen and T. Lepistö, *J. Mater. Sci.*, **46**, 6618–6626 (2011).

201. J. C. Yang, B. Kolasa, J. M. Gibson and M. Yeadon, *Appl. Phys. Lett.*, **73**, 2841–2843 (1998).

202. F. Deflorian, S. Rossi, L. Fedrizzi and M. Fedel, *Prog. Org. Coat.*, **63**, 338–344 (2008).

203. M. Finšgar and I. Milošev, *Corros. Sci.*, **52**, 2737–2749 (2010).

204. S. González, M. Gil, J. Hernández, V. Fox and R. Souto, *Prog. Org. Coat.*, **41**, 167–170 (2001).

205. M. Garcia-Heras, A. Jimenez-Morales, B. Casal, J. C. Galvan, S. Radzki and M. A. Villegas, *J. Alloys Compd.*, **380**, 219–224 (2004).

206. M. E. P. Souza, E. Ariza, M. Ballester, I. V. P. Yoshida, L. A. Rocha and C. M. A. Freire, *Materials Research*, **9**, 59–64 (2006).

207. A. Conde, J. Damborenea, A. Durán and M. Menning, *J. Sol-Gel Sci. Technol.*, **37**, 79–85 (2006).

208. M. Fedel, M. Olivier, M. Poelman, F. Deflorian, S. Rossi and M.-E. Druart, *Prog. Org. Coat.*, **66**, 118–128 (2009).

209. F. Deflorian, S. Rossi, M. Fedel and C. Motte, *Prog. Org. Coat.*, **69**, 158–166 (2010).

210. M. Fedel, M.-E. Druart, M. Olivier, M. Poelman, F. Deflorian and S. Rossi, *Prog. Org. Coat.*, **69**, 118–125 (2010).

211. C. Motte, M. Poelman, A. Roobroeck, M. Fedel, F. Deflorian and M.-G. Olivier, *Prog. Org. Coat.*, **74**, 326–333 (2012).

212. I. A. Kartsonakis, A. C. Balaskas, E. P. Koumoulos, C. A. Charitidis and G. C. Kordas, *Corros. Sci.*, **57**, 30–41 (2012).

213. R. Z. Zand, K. Verbeken and A. Adriaens, *Int. J. Electrochem. Sci.*, **8**, 548-563 (2013).

214. D. Xue and W. J. Van Ooij, *Prog. Org. Coat.*, **76**, 1095–1102 (2013).

215. R. B. Figueira, C. J. Silva, E. V. Pereira and M. M. Salta, *J. Electrochem. Soc.*, **160**, C467–C479 (2013).

216. A. A. O. Magalhães, I. C. P. Margarit and O. R. Mattos, *J. Electroanal. Chem.*, **572**, 433–440 (2004).

217. B.-L. Lin, J.-T. Lu and G. Kong, *Corros. Sci.*, **50**, 962–967 (2008).

218. C. G. da Silva, I. C. P. Margarit-Mattos, O. R. Mattos, H. Perrot, B. Tribollet and V. Vivier, *Corros. Sci.*, **51**, 151–158 (2009).

219. V. Moutarlier, M. P. Gigandet, L. Ricq and J. Pagetti, *Appl. Surf. Sci.*, **183**, 1–9 (2001).

220. J. W. Bibber, *Met. Finish.*, **106**, 41–46 (2008).

221. M. Hara, R. Ichino, M. Okido and N. Wada, *Surf. Coat. Technol.*, **169–170**, 679–681 (2003).

222. S. Dalbin, G. Maurin, R. P. Nogueira, J. Persello and N. Pommier, *Surf. Coat. Technol.*, **194**, 363–371 (2005).

223. R. P. Socha and J. Fransaer, *Thin Solid Films*, **488**, 45–55 (2005).

224. R. P. Socha, N. Pommier and J. Fransaer, *Surf. Coat. Technol.*, **201**, 5960–5966 (2007).

225. G. Klimow, N. Fink and G. Grundmeier, *Electrochim. Acta*, **53**, 1290–1299 (2007).

226. L. Zhu, F. Yang and N. Ding, *Surf. Coat. Technol.*, **201**, 7829–7834 (2007).

227. M. Hosseini, H. Ashassi-Sorkhabi and H. A. Y. Ghiasvand, *J. Rare Earths*, **25**, 537–543 (2007).

228. S. Bernal, F. J. Botana, J. J. Calvino, M. Marcos, J. A. Pérez-Omil and H. Vidal, *J. Alloys Compd.*, **225**, 638–641 (1995).

229. M. A. Arenas, C. Casado and J. D. Damborenea, **28**, 267–275 (2007).

230. B. R. W. Hinton, *J. Alloys Compd.*, **180**, 15–25 (1992).

231. R. E. Van de Leest and G. Krijl, *Thin Solid Films*, **72**, 237–246 (1980).

232. C. G. da Silva, A. N. Correia, P. de Lima-Neto, I. C. P. Margarit and O. R. Mattos, *Corros. Sci.*, **47**, 709–722 (2005).

233. Z. Zou, N. Li, D. Li, H. Liu and S. Mu, *J. Alloys Compd.*, **509**, 503–507 (2011).

234. A. L. K. Tan, A. M. Soutar, I. F. Annergren and Y. N. Liu, *Surf. Coat. Technol.*, **198**, 478–482 (2005).

235. A. N. Khramov, V. N. Balbyshev, L. S. Kasten and R. A. Mantz, *Thin Solid Films*, **514**, 174–181 (2006).

236. S. V. Lamaka, M. F. Montemor, A. F. Galio, M. L. Zheludkevich, C. Trindade, L. F. Dick and M. G. S. Ferreira, *Electrochim. Acta*, **53**, 4773–4783 (2008).

237. A. N. Khramov and J. A. Johnson, *Prog. Org. Coat.*, **65**, 381–385 (2009).

238. X. Guo, M. An, P. Yang, C. Su and Y. Zhou, *J. Sol-Gel Sci. Technol.*, **52**, 335–347 (2009).

239. H. Shi, F. Liu and E. Han, *Prog. Org. Coat.*, **66**, 183–191 (2009).

240. J. Hu, Q. Li, X. Zhong, L. Zhang and B. Chen, *Prog. Org. Coat.*, **66**, 199–205 (2009).

241. A. F. Galio, S. V. Lamaka, M. L. Zheludkevich, L. F. P. Dick, I. L. Müller and M. G. S. Ferreira, *Surf. Coat. Technol.*, **204**, 1479–1486 (2010).

242. V. Barranco, N. Carmona, J. C. Galván, M. Grobelny, L. Kwiatkowski and M. A. Villegas, *Prog. Org. Coat.*, **68**, 347–355 (2010).

243. X. Zhong, Q. Li, J. Hu, X. Yang, F. Luo and Y. Dai, *Prog. Org. Coat.*, **69**, 52–56 (2010).

244. B. Nikrooz and M. Zandrahimi, *J. Sol-Gel Sci. Technol.*, **59**, 640–649 (2011).

245. A. Zomorodian, F. Brusciotti, A. Fernandes, M. J. Carmezim, T. Moura e Silva, J. C. S. Fernandes and M. F. Montemor, *Surf. Coat. Technol.*, **206**, 4368–4375 (2012).

246. N. V. Murillo-Gutiérrez, F. Ansart, J.-P. Bonino, M.-J. Menu and M. Gressier, *Surf. Coat. Technol.*, **232**, 606–615 (2013).

247. F. Brusciotti, D. V. Snihirova, H. Xue, M. F. Montemor, S. V. Lamaka and M. G.S. Ferreira, *Corros. Sci.*, **67**, 82–90 (2013).

248. P. Molnár, A. Ostapovets and A. Jäger, *Mater. Des.*, **56**, 509–516 (2014).

249. M. E. Alam, A. M. S. Hamouda, Q. B. Nguyen and M. Gupta, *J. Alloys Compd.*, **574**, 565–572 (2013).

250. Z. M. Li, Q. G. Wang, A. A. Luo, L. M. Peng, P. H. Fu and Y. X. Wang, *Mater. Sci. Eng. A*, **582**, 170–177 (2013).

251. J. Jiang, Y. Wang, J. Liu, J. Qu, Z. Du and S. Luo, *Trans. Nonferrous Met. Soc. China*, **23**, 576–585 (2013).

252. F. Pan, J. Zhang, J. Wang, M. Yang, E. Han and R. Chen, *Trans. Nonferrous Met. Soc. China*, **20**, 1249–1258 (2010).

253. M. E. Alam, S. Han, Q. B. Nguyen, A. M. S. Hamouda and M. Gupta, *J. Alloys Compd.*, **509**, 8522–8529 (2011).

254. T. J. Chen, W. Wang, D. H. Zhang, Y. Ma and Y. Hao, *Mater. Des.*, **44**, 555–565 (2013).

255. M. Sendova and K. Willis, *Appl. Phys. Mater. Sci. Process.*, **76**, 957–959 (2003).

256. B. A. Latella, C. J. Barbé, D. J. Cassidy, H. Li and M. Ignat, *Rev. Matér.*, **10**, 199–204 (2005).

257. Y. Castro, B. Ferrari and R. Moreno, *Sol-Gel Sci. Technol.*, **26**, 735–739 (2003).

258. B. Arkles, *MRS Bull.*, **26**, 402–408 (2001).

259. S. K. Ghosh, in *Self-Healing Materials*, S. K. Ghosh, Editor, p. 1–28, Wiley-VCH Verlag GmbH & Co. KGaA (2008).

260. W. Trabelsi, P. Cecilio, M. G. S. Ferreira and M. F. Montemor, *Prog. Org. Coat.*, **54**, 276–284 (2005).

261. D. G. Shchukin, M. Zheludkevich and H. Möhwald, *J. Mater. Chem.*, **16**, 4561–4566 (2006).

262. S. V. Lamaka, M. L. Zheludkevich, K. A. Yasakau, M. F. Montemor, P. Cecílio and M. G. S. Ferreira, *Electrochem. Commun.*, **8**, 421–428 (2006).

263. S. V. Lamaka, M. L. Zheludkevich, K. A. Yasakau, R. Serra, S. K. Poznyak and M. G. S. Ferreira, *Prog. Org. Coat.*, **58**, 127–135 (2007).

264. A. Yabuki, H. Yamagami and K. Noishiki, *Mater. Corros.*, **58**, 497–501 (2007).

265. M. F. Montemor, W. Trabelsi, S. V. Lamaka, K. A. Yasakau, M. L. Zheludkevich, A. C. Bastos and M. G. S. Ferreira, *Electrochim. Acta*, **53**, 5913–5922 (2008).

266. M. F. Montemor, R. Pinto and M. G. S. Ferreira, *Electrochim. Acta*, **54**, 5179–5189 (2009).

267. S. H. Cho, S. R. White and P. V. Braun, *Adv. Mater.*, **21**, 645–649 (2009).

268. M. L. Zheludkevich, J. Tedim, C. S. R. Freire, S. C. M. Fernandes, S. Kallip, A. Lisenkov, A. Gandinia and M. G. S. Ferreira, *J. Mater. Chem.*, **21**, 4805–4812 (2011).

269. S. J. García, H. R. Fischer, P. A. White, J. Mardel, Y. González-García, J. M. C. Mol and A. E. Hughes, *Prog. Org. Coat.*, **70**, 142–149 (2011).

270. A. P. Esser-Kahn, S. A. Odom, N. R. Sottos, S. R. White and J. S. Moore, *Macromolecules*, **44**, 5539–5553 (2011).

271. J. Carneiro, J. Tedim, S. C. M. Fernandes, C. S. R. Freire, A. J. D. Silvestre, A. Gandini, M. G. S. Ferreira and M. L. Zheludkevich, *Prog. Org. Coat.*, **75**, 8–13 (2012).

272. M. L. Zheludkevich, J. Tedim and M. G. S. Ferreira, *Electrochim. Acta*, **82**, 314–323 (2012).

273. A. E. Hughes, I. S. Cole, T. H. Muster and R. J. Varley, *NPG Asia Mater.*, **2**, 143–151 (2010).

274. S. R. White, N. R. Sottos, P. H. Geubelle, J. S. Moore, M. R. Kessler, S. R. Sriram, E. N. Brown and S. Viswanathan, *Nature*, **409**, 794–797 (2001).

2. Corrosion of Hot-Dip Galvanized Steel Reinforcement

Corrosion of Hot-Dip Galvanized Steel Reinforcement

R. B. Figueira[a,b,*], E. V. Pereira[a], C. J. R. Silva[b], M. M. Salta[a]

[a]LNEC, Laboratório Nacional de Engenharia Civil, Av. Brasil 101, 1700-066 Lisbon, Portugal

[b]Centro de Química, Universidade do Minho, Campus de Gualtar 4710 - 057 Braga, Portugal

* Corresponding Author: rmfigueira@lnec.pt

Resumo

A crescente utilização do aço galvanizado em estruturas de betão armado deve-se essencialmente ao seu baixo custo e à melhoria da resistência à corrosão quando comparado com o aço sem proteção. A composição e morfologia do revestimento de zinco é determinante para o comportamento observado nos primeiros instantes de contacto do aço galvanizado com o betão fresco, dada a natureza fortemente alcalina deste meio. Durante o processo de cura do betão, o revestimento de zinco corrói-se vigorosamente até que a passivação ocorra. Nesta fase inicial, a elevada velocidade de corrosão do zinco pode contribuir para remover uma quantidade significativa deste revestimento originando uma proteção insuficiente do aço subjacente. Em simultâneo ocorre a produção de hidrogénio (resultante da reação catódica) a qual pode originar um aumento da porosidade do betão que por sua vez pode comprometer a aderência entre as armaduras galvanizadas e o betão.

Para se minimizar esta reação inicial, entre o aço galvanizado e o betão fresco, a aplicação de cromatos foi um procedimento amplamente utilizado quer como pré-tratamento do substrato metálico em aço galvanizado quer como componente do cimento utilizado. Contudo, a elevada toxicidade do crómio hevavalente e as nefastas consequências para a saúde humana e impacto no ambiente, resultaram na implementação de legislação restringindo severamente a sua utilização. Dada a sua elevada importância como pré-tratamento inibidor de corrosão, tem-se registado um crescente esforço na pesquisa de processos e materiais alternativos para tais fins. Neste artigo apresenta-se uma síntese dos resultados mais relevantes obtidos no estudo de revestimentos e pré-tratamentos destinados a aços galvanizados publicados no período que decorre entre 2001 e 2014. As soluções desenvolvidas para descrever os mecanismos de corrosão propostos na literatura assim como a importância do Cr(VI) na inibição do processo inicial de corrosão do zinco em meios extremamente alcalinos são também apresentados e discutidos.

Palavras-Chave

Aço Galvanizado, Corrosão, Revestimento, Pré-Tratamentos

Abstract

In the past several years hot-dip galvanized steel (HDGS) has successfully been used to extend the service life of reinforced concrete structures, mainly due to its low cost and high corrosion resistance compared to mild steel. However, the initial corrosion behaviour of the galvanized coating when embedded in concrete and how that behaviour may be affected by the surface composition of the coating remains unclear. When HDGS is embedded in fresh concrete (a highly alkaline environment), the zinc coating corrodes vigorously until passivation occurs and the concrete hardens. This leads to two main concerns, namely, the high initial corrosion rate, which may remove so much zinc that this leads to insufficient galvanic protection of the underlying steel, and the hydrogen production (in the corresponding cathodic half-cell reaction) which may increase the porosity of the adjacent cement paste and reduce the bond strength between the bar and the concrete. To avoid, or at least minimize, this initial reaction the use of chromates has been implemented. However, due to the toxicity of hexavalent chromium, environmental and human health concerns have restrained their use and alternatives are being studied all over the world. In this paper, the coatings and pre-treatments studied at an academic level in the last few years (2001-2014) have been reviewed together with the corrosion mechanisms of HDGS in contact with high alkaline environments and the role of Cr(VI) in inhibiting the initial zinc corrosion process.

Keywords

1. Introduction

The corrosion of steel in concrete is one of the major causes of structure degradation, requiring expensive rehabilitation. The estimated cost of corrosion damage of reinforced concrete bridges in the United States, due to the use of de-icing salts alone, was between $325 million and $1 billion per year[1]. In Australia, Europe and the Middle East the statistical results are similar[2]. Corrosion of the reinforcement in concrete is the main cause of the failures of these structures[2]. The most effective way to minimize the risk of reinforced concrete (RC) corrosion is to ensure that the cover of the metallic reinforcement sections is of an adequate thickness and possesses a high concrete quality, with a proper mixing ratio, good compaction and curing. There are four essential materials in the production of concrete including: Portland cement, sand, aggregates (stone) and water. The ratio of aggregate and sand to cement is an essential factor in determining the compressive strength of concrete mixture. The ratio of these materials affects the production of concrete and is directly related to its performance. These two features combined cover thickness and good quality concrete; confer an excellent protection to the reinforcing steel from the environmental exposure. The concrete coating works as a physical barrier for protection against aggressive environmental agents that create conditions for the passivation of the steel.

Portlandite, the main constituent of the mineralogical components used for the fabrication of concrete, together with uncontaminated water and non-aggressive admixtures or aggregates, containing mostly K^+, Na^+, Ca^{2+}, OH- ions and dissolved O_2 (from atmospheric exposure), has an important role in the durability of the concrete as it is responsible for the high alkalinity of fresh concrete (pH > 13,5). When embedded in fresh concrete, steel is protected as the concrete provides a physical protection barrier and the high pH leads to the formation of a passivation film in the reinforced steel, protecting it from corrosion. However, during the process of hydration and hardening, tensile forces can be generated causing the formation of cracks (on concrete structures), leading to reduced efficiency of the physical barrier that protects the steel. The degradation of the concrete properties often results in a common action of external and internal factors. It is a complex process, largely determined by the physicochemical properties of the concrete (internal factor) and the atmosphere that it is exposed to (external factor). Moreover, the physical barrier provided by the concrete cover is not perfect due to the porous structure of concrete.

The existence of imperfections during concreting and curing, and the conjugation of these two factors, enable the entrance (diffusion/transport) of aggressive species into the steel/concrete interface and may cause a rupture of the passivation film, therefore initiating the corrosion of the

RC. The most frequent causes responsible for breaking down the passivation film are the inclusion of Cl^- in the film as well as the reaction of atmospheric CO_2 with the constituents of the concrete. The volume of corrosion products formed, due to the presence of aggressive species, is about 4 to 6 times higher than the steel. Therefore, the evolution of corrosion in RC structures causes forces of expansion in the vicinity of the metallic parts, which, if it exceeds the tensile strength of concrete, initially leads to cracking (Figure 3), and then spalling of the concrete cover.
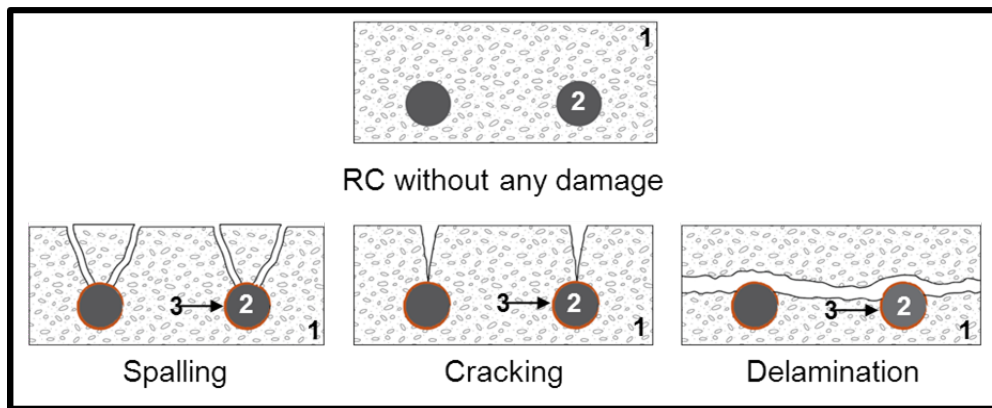
Figure 1. Spalling, cracking and delamination of RC structures adapted from[2] (1 – concrete; 2 – steel rebar; 3 – corrosion oxides).

The continuing evolution of the corrosion of RC structures subsequently causes loss of adhesion between the concrete and steel construction, loss of steel ductility and section reduction of the steel rebar that may implicate the stability of the structure. The electrochemical process of corrosion on the steel surface, where both cathodic and anodic areas are located, is explained by the following reactions:

Anodic Reaction: $\quad 2Fe \rightarrow 2Fe^{2+} + 4e^-$ (1)

Cathodic Reaction: $\quad O_2 + 2H_2O + 4e^- \rightarrow 4OH^-$ (2)

Global Reaction: $\quad 2Fe + 2H_2O + O_2 \rightarrow 2Fe(OH)_2$ (3)
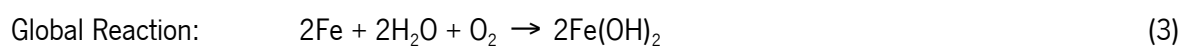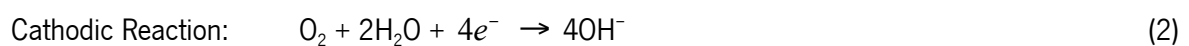
To increase the service life of RC structures, the use of hot-dip galvanized steel (HDGS) has been recognized as an effective measure[3,4]. The main cause for the widespread use of galvanized steel is the dual nature coating. As a barrier coating, the layer formed by the galvanizing process offers a resistant and metallurgically bonded zinc coating that covers the steel surface, protecting it from the corrosive action. Moreover, the zinc's sacrificial (cathodic) action protects the steel even when damage occurs in the concrete[3,4] and zinc corrosion products occupy a smaller volume than those produced from iron.

Yeomans[3] confirmed that zinc corrosion products are powdery, non-adherent and capable of migrating from the surface of the galvanized reinforcement into the concrete matrix, reducing the likelihood of zinc corrosion-induced spalling of the concrete[3,4]. Galvanized reinforced steel can withstand exposure to chloride ion concentrations several times higher (at least 4 to 5 times) than the chloride level that causes corrosion in steel reinforcement. Additionally, while steel in concrete typically depassivates below a pH of 11.5, galvanized reinforcement can remain passivated at a lower pH, thereby offering substantial protection against the effects of concrete carbonation[3]. The combination of these two factors, carbonation resistance and chloride tolerance, are commonly accepted as the basis for superior performance of galvanized reinforcement compared to steel reinforcement[5].

However, when HDGS is in contact with high alkaline environments, such as fresh concrete (pH $\geq$ 12,5), the zinc corrodes and H_2 evolution takes place. This initial corrosion process, extensively studied by several authors[6–8], may lead to zinc consumption until the formation of passivation layer (which passivates the steel reinforcement) or corrosion continues until all the zinc layer is consumed[6]. To avoid and minimize the H_2 evolution, procedures such as increasing the chromate content of the cement, adding water-soluble chromates into the preparation and chromate conversion layers have been implemented and are capable of minimizing the initial zinc corrosion. However, due to the toxicity of Cr(VI) ions, environmental and human health concerns have restrained their use and alternatives are being studied all over the world.

In this paper, potential alternatives to the use of chromium-based compounds (Cr(VI)) published in the last few years (2001-2013), were reviewed. The corrosion mechanisms of HDGS in contact with high alkaline environments and the role of Cr(VI) in inhibiting the initial zinc corrosion process were also discussed.

2. Hot-Dip Galvanized Steel (HDGS)

Hot dip galvanizing is the most important zinc coating process[4]. During this process, steel is immersed in a molten zinc bath at a temperature of $\approx$ 450 ºC. At this point, metallurgical interaction occurs between the iron and the molten zinc, forming an adherent coating that provides both an excellent barrier against iron corrosion. It also provides cathodic protection when imperfections exist or when there is local dissolution of the coating.

The hot dip galvanizing process has been widely studied and detailed information can be found in the literature[4,9–13].

Metallurgical reactions occur during the hot dip galvanizing process, leading to the formation of several intermetallic phases with increasing iron content. The intermetallic layers (from the inner phase of the substrate to the outer layer) include: γ (gamma phase), δ (delta phase), ξ (zeta phase) and η (eta phase)[9] as shown in Figure 2.
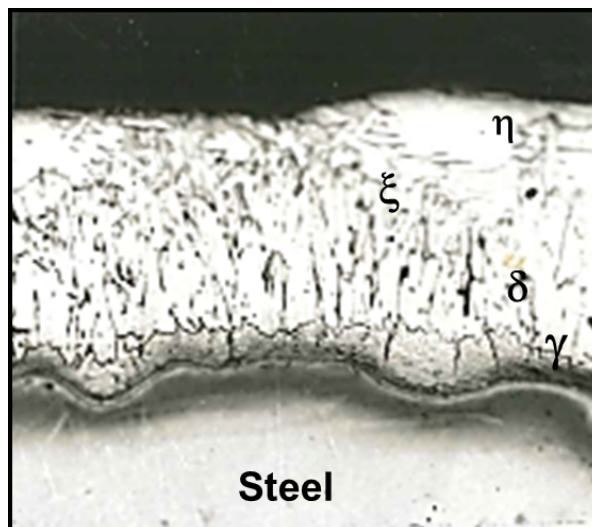
Figure 2. Intermetallic layers of HDGS

The gamma phase is a very thin layer with a cubic structure. The iron is present in a range between 21% to 28% of the layer and is often not easily identifiable. The delta layer is usually composed of two layers; an internal "compact" layer and an external "barrier" layer. The latter layer has a hexagonal structure and an iron percentage between 7 and 12%. The zeta layer is formed by asymmetric monoclinic crystals, which is less rich in iron (the range may vary from 5.8 to 6.2%). The last outer layer, eta is an external layer of almost pure zinc[9]. The composition and thickness of these

intermetallic layers depends on several factors, such as the composition of the steel substrate and surface roughness, the molten zinc bath temperature, withdrawal speed from the molten zinc bath, composition of the zinc bath and the immersion time[4,9].

The corrosion rate of zinc, in most natural environments, is 5 to 100 times slower than steel[14,15]. To minimize these effects and increase the lifetime of steel, additional protection may be provided by the use of a zinc layer. The high corrosion resistance of galvanized steel is attributed both to the galvanic action of zinc and to the barrier effect of zinc products. Zinc has a low-self corrosion rate and, due to its low position in the galvanic series, is an efficient sacrificial anode for galvanic protection of steel structures[11,14,16].

Studies on the corrosion of galvanized steel have shown that this process involves three different stages (Figure 3)[17–20].

Figure 3 – Stages of galvanized steel corrosion (adapted from [20,21]).
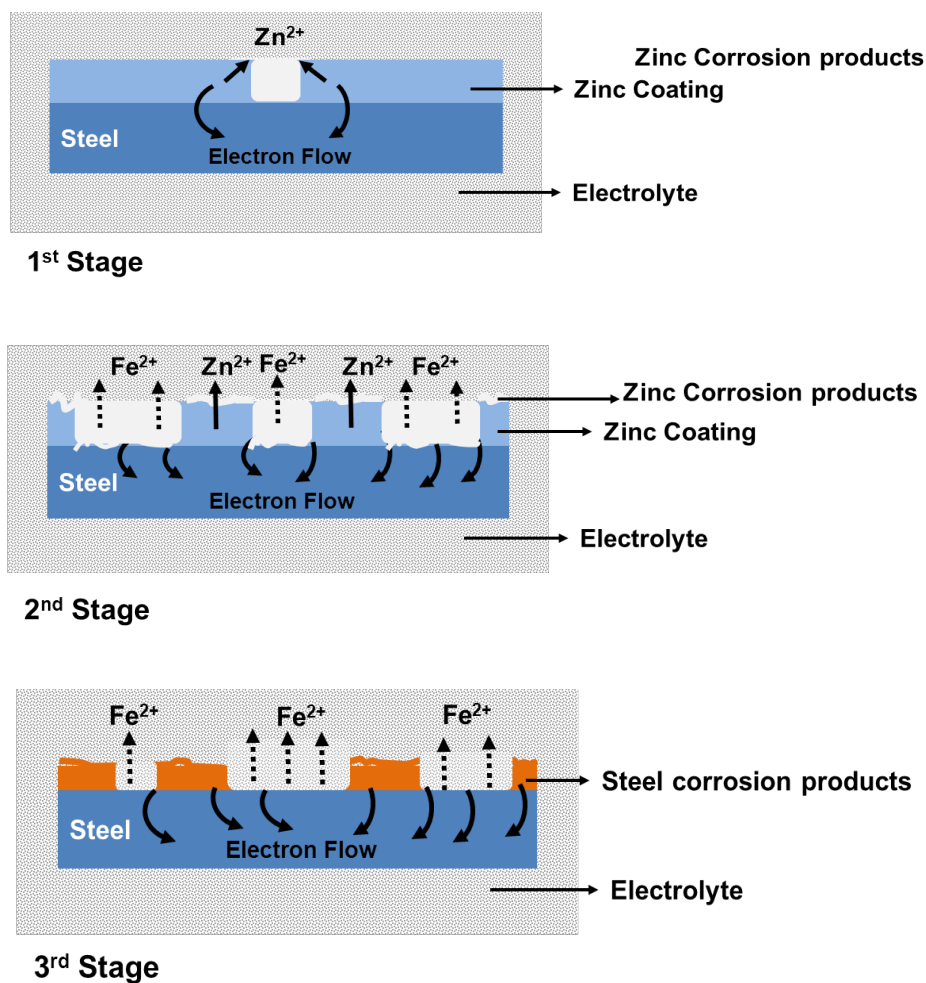
The first stage is mainly related to the dissolution of the oxide layer formed on the surface of the substrate during contact with air. The corrosion rate increases rapidly and the corrosion potential shifts towards less noble values (lower values) leading to the acceleration of the anodic process.

During the second stage, the surface of the zinc layer is covered with white rust (zinc oxide) due to partial/total dissolution of the zinc (depending on the electrolyte and the aggressive species present). Consequently, the corrosion rate decreases and the corrosion potential shifts to more noble values (higher values). In this stage, the dissolution of zinc is inhibited due to the presence of oxides and the underlying steel starts to corrode. In the third stage, the formation of red rust on the substrate surface increases. The corrosion rate remains constant and the corrosion potential continues to shift to higher values.

Even though some parts of zinc remain in the rebar, the galvanized steel shows a corrosion potential similar to that of carbon steel. At this stage, the underlying steel corrosion evolves due to the dissolution of iron and the zinc coating that remains (if no total dissolution occurred) no longer acts as sacrificial anode.

2.1. HDGS Corrosion Process in Alkaline Environments

Several studies have been carried out to understand the corrosion and passivation mechanisms of zinc in alkaline solutions. In 1964, Bird[22] showed that for a pH > 12.9 the main anodic product formed was ZnO_2^{2-}. Lieber and Gebauer[23], in 1969, were the first to recognize the formation of calcium hydroxyzincate (CAHZ) as the corrosion product of zinc in alkaline solutions rich in calcium and that it was responsible for the passivation of the substrate. One year later, Rehm and Lämmke[24] published a paper that was consistent with the studies of Lieber and Gebauer. However, the authors proposed that before the formation of CAHZ, $Zn(OH)_2$ was formed.

In 1972 Grauer and Kaesche[25] showed the formation of a ZnO layer in NaOH solutions and in the same year, Liebau *et al.* proposed the following mechanism[26]:

$$Zn + 2H_2O \rightarrow Zn(OH)_2 + H_2 \tag{4}$$

$$2Zn(OH)_2 + 2H_2O + Ca(OH)_2 \rightarrow Ca[Zn(OH)_3]_2 \cdot 2H_2O \tag{5}$$
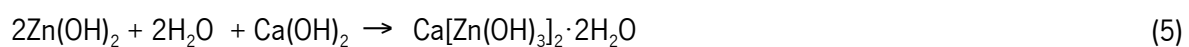
One year after, Shams El Din *et al.*[27] showed that when zinc is in contact with NaOH solutions with a concentration lower than 0.3 M, a progressive precipitation of $Zn(OH)_2$ occurs. However, in solutions

with concentrations higher than 0.3 M the zinc dioxide anion is formed as described in the following reaction:

$$Zn + 4OH^- \rightarrow ZnO_2^{2-} + 2H_2O + 2e^-$$ (6)

In 1974, Vorkapic et al. [28] studied the passivation of zinc in different concentrated solutions of KOH (1, 3, 6 and 10 M) and showed that the corrosion of zinc in the referred solutions is time dependent and a period of about 100 hours is necessary to reach a steady state. They also proposed and discussed a multi-step mechanism. Duval and Arliguie, in the same year, studied the possible reactions of zinc in contact with saturated solutions of calcium hydroxide. The influence of immersion time, surface conditions and temperature on the zinc samples was the focus of the study performed by the authors[29].
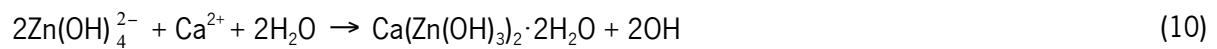
Zembura and Burzynska in 1977[30] studied the corrosion of zinc in a pH range from 1.6 to 13.3 in de-aerated solutions 0.1 M of NaCl and found that for pH values above 11 the reaction is controlled diffusionally by the ions ZnO_2^{2-} or $ZnHO_2^-$.

In 1985, Baugh and Higginson[31] showed that zinc dissolves over an extensive range of electrochemical potentials and discussed the relationship of this behaviour to other metal/metal-ion systems. Two years later, Macías and Andrade[32,33] studied the behaviour of galvanized steel in 0.001-1.5 M solutions of NaOH and KOH with or without calcium hydroxide and showed that in 12 < pH < 13.2 the zinc layer corrodes at a low rate. At pH < 12 only localized corrosion took place and for pH > 13.2 total dissolution of the zinc layer occurred without passivation. A threshold pH value was also found for the onset of H_2 evolution, which was equal to 12.8. In the same year, Macías and Andrade also discussed the morphology and composition of the corrosion products on galvanized steel immersed in 0.05 - 1.5 M solutions of KOH.

Macias and Andrade also confirmed the results obtained by Lieber and Gebauer (formation of a passivation layer of CAHZ) and showed that the surface morphology of the HDGS was dependent on the pH of the solution where the corrosion process took place[7]. The same authors also confirmed the formation of ZnO and Zn(OH)$_2$ corrosion products and it was shown that once the passive film of CAHZ was formed its stability remained even if the pH increased afterwards[7,34].

As stated previously, several studies have been devoted to understanding the corrosion and passivation mechanisms of zinc in alkaline solutions[23,26–28]. The most comprehensive work was performed by Andrade and co-workers[7,8,33–37].

Taking into consideration the results of various researchers, Andrade and Alonso[3] proposed a four step reaction mechanism to describe the corrosion process of zinc in strongly alkaline, calcium-containing solutions:

$$Zn\ (s) + 4OH^- \rightarrow Zn(OH)_4^{2-} + 2e^- \tag{7}$$

$$Zn + 2OH^- \rightarrow ZnO + H_2O + 2e^- \tag{8}$$

$$ZnO + H_2O + 2OH^- \rightarrow Zn(OH)_4^{2-} \tag{9}$$

$$2Zn(OH)_4^{2-} + Ca^{2+} + 2H_2O \rightarrow Ca(Zn(OH)_3)_2 \cdot 2H_2O + 2OH \tag{10}$$

The morphology of the passivation layer of the corrosion products on galvanized steel substrates after being in contact with an alkaline solution are shown in Figure 4. It is reasonable to assume, that due to the size of the CAHZ crystals formed in solutions of $12.5 \pm 0.1 < pH < 13.3 \pm 0.1$, the zinc surface is densely covered, providing full passivation of the substrate by the CAHZ crystals (Figure 4).
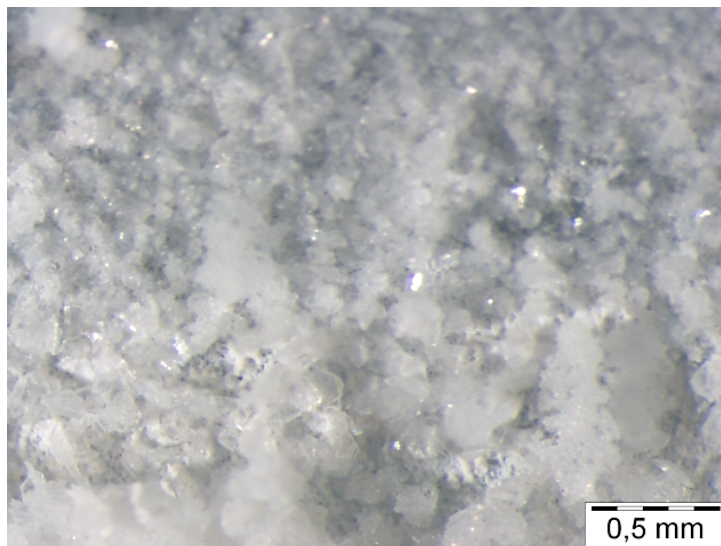

Figure 4. Stereomicroscope observation of CAHZ crystals after being in a saturated $Ca(OH)_2$ solution (60x) for 72h.

As the pH increases, the CAHZ crystal size increases, leading to crystals that do not completely cover the surface of the substrate (Figure 5). Under these circumstances, the passivation of the

surface of the substrate is difficult to reach and zinc dissolution continues until all the zinc has dissolved.
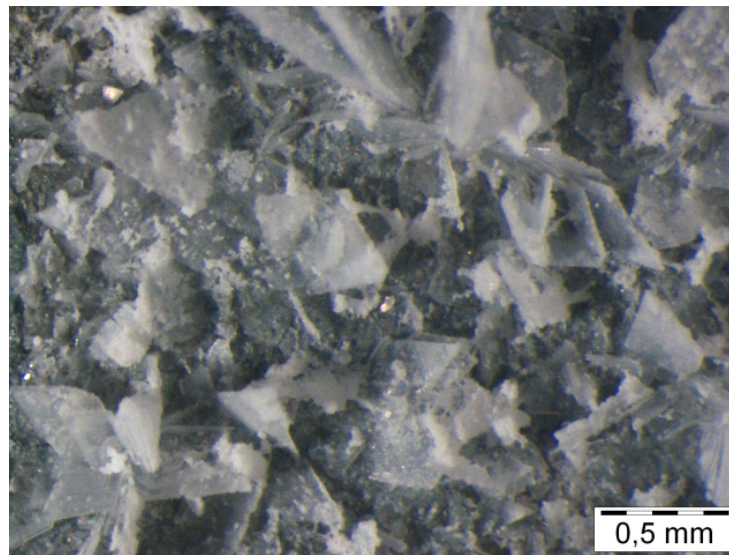
Figure 5. Stereomicroscope observation CAHZ crystals after 72h in an alkaline solution (saturated Ca(OH)$_2$ + 0.2M KOH (60x)).

Table 1 is based on the information provided by Andrade and co-workers[3,38] and briefly shows the influence of the pH on the corrosion products, whether hydrogen evolution occurs or not and if the substrate is locally attacked, corroded or passivated. Table 1 shows that for pH > 12.3 hydrogen evolution takes place and for 11.4 < pH < 13.3 the formation of CAHZ occurs.

Table 1. Inffluence of the pH on the corrosion behaviour of HDGS[3,38]

pH Range		Corrosion Products	
11 < pH < 11.4	Localized corrosion	ZnO	Without H$_2$ evolution
11.4 < pH < 12.3	Passivation	CAHZ	
12.3 < pH < 13.3	Passivation	CAHZ	H$_2$ evolution occurs
13.3 < pH < 14	Corrosion	ZnO and Zn(OH)$_2$	

2.2. HDGS Corrosion Process During Concrete Setting

Concrete is a highly alkaline environment due to the presence of calcium, sodium and potassium hydroxides (pH $\geq$ 12.6)[3]. The pH increases to values above 13 in the first several hours of curing,

reaching a maximum of 13.7 as hydration continues. Under these conditions, immediately after HDGS has been embedded in fresh concrete, and as the zinc is thermodynamically unstable at this pH, the zinc corrodes for a limited period (from several hours to a few days) until passivating surface layers are formed and the concrete hardens. Once the concrete sets, the hydrogen evolution ceases; the coating of CAHZ formed apparently provides protection to the reinforcement and no furt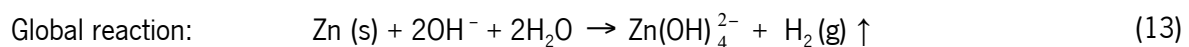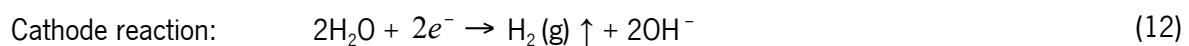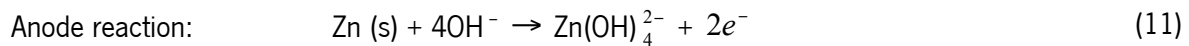her attacks take place after this initial setting is over. Nevertheless, this initial corrosion process may lead to a consumption of the zinc layer of a thickness between 5 to 10 μm [9]. At the same time, hydrogen is produced which may cause the loss of adhesion between steel and concrete.

Several corrosion studies reported the behaviour of HDGS in contact with concrete media[3,22,39–48]. However, uncertainties concerning the initial corrosion behaviour of the galvanized coating when embedded in concrete still remains. The main literature about corrosion and passivation mechanisms of zinc in concrete environments, suggest that the formation of the protective layer due to zinc oxidation takes place with water reduction and subsequent hydrogen evolution[3,6–8,26,32,33,38]. Other authors claim that the formation of protective layers is related to the presence of oxygen at the concrete/rebar interface[49,50].

The chemical equations involved in the corrosion of zinc in concrete found in the literature are[45]:

Anode reaction: $\qquad Zn\ (s) + 4OH^- \rightarrow Zn(OH)_4^{2-} + 2e^-$ $\hfill$ (11)

Cathode reaction: $\qquad 2H_2O + 2e^- \rightarrow H_2\ (g) \uparrow + 2OH^-$ $\hfill$ (12)

Global reaction: $\qquad Zn\ (s) + 2OH^- + 2H_2O \rightarrow Zn(OH)_4^{2-} + H_2\ (g) \uparrow$ $\hfill$ (13)

The conversion of zinc into CAZH is described by the reaction:

$$2\ Zn + Ca(OH)_2 + 6H_2O \rightarrow Ca[Zn(OH)_3]_2 \cdot 2H_2O + 2\ H_2\ (g) \uparrow \qquad (14)$$
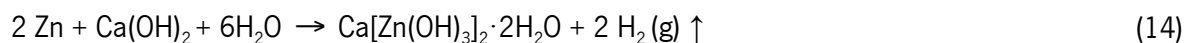
Additionally, the formation of zincate and hydrogen may occur as described by[45]:

$$Zn + 2OH^- \rightarrow ZnO_2^{2-} + H_2\ (g) \uparrow \qquad (15)$$

Zincate ion further reacts with water leading to the formation of zinc hydroxide[45]:

$$ZnO_2^{2-} + 2H_2O \rightarrow Zn(OH)_2 + 2OH^- \tag{16}$$

Studies regarding the effectiveness of the chromate treatments on HDGS when in contact with alkaline environments are limited. Short *et al.*[46,51] showed that regardless of the chromate treatments on HDGS, the zinc coating is generally dissolved when exposed to alkaline solutions. This suggests that the CCCs may not be stable in highly alkaline solutions. On the other hand, researchers have been devoted to the study of the effectiveness of CCCs on corrosion resistance of HDGS in environments containing chlorides. In this case it has been unanimously shown that CCC improves the corrosion resistance of zinc[3,42,44,52–55]. Despite these contradictory findings, the galvanizing industry believes that CCCs are necessary to hinder the hydrogen evolution and minimize the initial zinc corrosion process in fresh concrete. Common procedures such as increasing the chromate content of the cement or adding water-soluble chromates into its preparation have been implemented to protect the galvanized rebars[3,4]. The original reason behind the use of CCCs on galvanized steel is to avoid the formation of wet storage stain during the first six weeks after galvanizing, and in particular to reduce the formation of excessive amounts of zinc oxide and zinc hydroxide during that period[3].

The high corrosion resistance offered by the use of chromate compounds is due to the presence of Cr^{6+} and Cr^{3+}. Chromate ions are oxidative inhibitors that hinder hydrogen evolution in fresh concrete, leading to the formation of a passive film of zinc chromate and chromic oxide[3,45]. However, a controversial study was found[46]. The authors conclude that the chromate treatment was unnecessary and the chromate film appears to retard the formation of CAHZ and reduces the passivation of the zinc[46]. Other authors claim that the presence of chromium reduces the corrosion rate of HDGS and delays the passivation[3,44]. Despite the differing conclusions on the use of chromates, it has been reported that chromate and similar hexavalent chromium compounds are toxic and carcinogenic. Their use in industry is a common source of serious environmental issues, which has led to their application being heavily regulated by most environmental legislation. Current commercial Portland cements have a limited content of Cr(VI) in their composition and the use of CCC is currently being avoided. Thus, intense research is being undertaken to replace chromates with more ecological compounds.

2.3. Environmentally Friendly Alternatives to the Use of Chromium Based Compounds

Many consider HDGS as the oldest and most economical method used for applying zinc coatings on steel[4,56]. During the last few years, developments in this field have included new surface treatments, incorporation of composite materials into the bath and post-treatment techniques such as chromate and phosphating conversion layers.

Table 2 shows the main surface treatments on zinc substrates or metallic substrates coated with zinc used in publications between 2001 and 2013 as well as the main conclusions/achievements. Studies that were performed in order to improve the process of the production of HDGS were not taken into consideration. However, several studies have been performed[56–66], such as Sere et al. in 1999 where results showed that the addition of small concentrations of lead and antimony improved the zinc coating uniformity and its adhesion to the steel substrate[67].

In 2007, Pistofidis et al. demonstrated that the incorporation of bismuth into the galvanizing bath, at certain proportions, lead to improved adhesion and corrosion resistance of the substrate[68]. The use of metal oxides, such as ZnO, ZrO_2 and TiO_2, as bath additives have also been reported[69,70].

The current alternatives to Cr (VI) show positive and negative performances when considering properties such as corrosion resistance, adhesion, fatigue resistance, reliability and quality control. Multiple studies have been undertaken to find alternatives in order to mitigate the harmful effects of an initial excessive reaction between the cement pastes and the zinc[71–73]. However, processes with similar performances as CCC with the same associated costs have not yet been achieved. Liu et al in 2010 showed that molybdate-based CC provided a corrosion behaviour similar to the one offered by CCC however the authors also stated that the market cost of the molybdate based solution was much higher than the chromate solution[74]. An innovative study on the incorporation of silanes in the concrete admixture to protect the HDGS in RC structures was also reported[75] and the authors concluded that hydrophobic concrete protected the substrate in RC structures in the presence of cracks.

The analysis of Table 2 and Figure 5 shows that the main efforts for finding new and efficient pre-treatments to minimize the corrosion of zinc substrates were focused on testing and producing new CCs applied directly on the HDGS surface, representing 36% of the published papers mentioned. The analysis shows that the number of published papers increased significantly after 2006. This growth is closely related with the Directive 2002/95/EC on the Restriction of Hazardous Substances that was adopted in February 2003 by the European Union and took effect in July 2006.
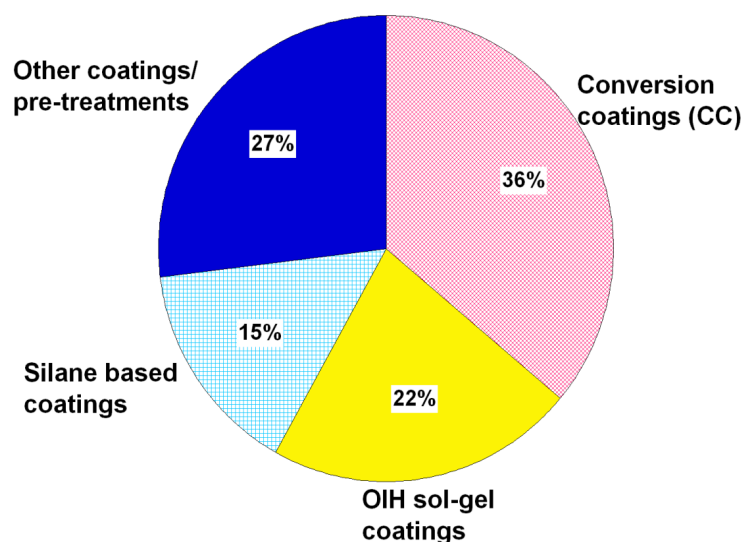
Figure 6. Distribution of the type of surface pre-treatments/coatings studied on zinc substrates and metallic substrates coated with zinc published between 2001 and 2013.

Abbreviations and Acronyms (used in Table 2)

AZC	Ammonium zirconium carbonate
APTES	3-Aminopropyltriethoxysilane
BPA	Bisphenol A
BTSE	Bis-1,2- [triethoxysilyl]ethane
BTESPT	Bis-[triethoxysilylpropyl] tetrasulfide
CAHZ	Calcium Hydroxyzincate
CC	Conversion Coating
CCCs	Chromate Conversion Coatings
ED	Electrodeposition
ER	Epoxy Resin
ERE	Epoxy-resin-ester
GPTMS	3-Glicidoxypropyltrimethoxysilane
GS	Galvanized Steel
HDGS	Hot-dip Galvanized Stee
MPTMS	γ-Mercaptopropiltrimethoxysilane
MPS	Molybdate-phosphate-silicate
MTES	Methyltriethoxysilane
NP	Nanoparticle(s)
OC	Organic Coating
OIH	Organic-Inorganic Hybrid
PANI	Polyaniline
PAPTES	N-Phenyl-3-Aminopropyltriethoxysilane
PDMMS	Polidymetilmetoxysilane
PMS	Potassium methyl siliconate
POABQ	Poly(4,4'-oxydiphtalic anhydride-co-2,5-bis(4,4'- methylenedianiline)-1,4-benzoquinone)
PPDO	Poly(pyromellitic dianhydride-co-4,4'-oxydianiline)
TEOS	Tetraethoxysilane
TMVS	Trimethoxy(vinyl)silane
TIPT	Titanium isopropoxide

Table 2. Types of pre-treatments and coatings studied on zinc substrates and metallic substrates coated with zinc (2001-2013)

Year	Type of pre-treatment/coating	Results and Conclusions	Ref
2001	OIH sol-gel coating	Effective corrosion protection of the HDGS using an OIH coating prepared with ER and BPA precursors.	76
	CC	Cerium CC decreased the corrosion rate of the GS.	77
2002	Silane containing $Na_2Si_2O_5$	Zinc pre-treated with Ce^{3+} and coated with BTSE and $Na_2Si_2O_5$ enhanced the corrosion protection of the GS.	78
2003	Colloidal silicate coating	Coating prepared with colloidal silicate, titanium sulphate and nitrate ions enhanced the corrosion resistance of the GS.	79
	Calcium–zinc phosphate	Extracts of pigments used in organic coatings for corrosion control were mixed and provided inhibitive efficiency.	80
2004	OIH sol-gel coating	Corrosion behaviour of the Ce^{3+} ions trapped within the OIH network .	81
	Organic coating	Study of the kinetics of chromate release from a polyester isocyanate primer with strontium chromate as inhibiting pigment.	82
		Study on the application of an organic coating (lacquer) containing phosphating reagents on HDGS.	83
	Silane and CCs	Pre-treatments using Ce and La CCs and BTESPT. Improved results were obtained for the La CC with or without BTESPT.	84
	CC	CCC showed better anticorrosive performance than the molybdate CC.	85
2005	CC	Resemblances between CCCs and tungstate CC were shown.	86
	Silica based coatings	Deposition of a coating from silica sol/sodium metasilicate mixture on zinc substrate showed promising results.	87
	Silane doped with inhibitor	BTESPT doped with Ce^{3+} improved the anticorrosion performance of the GS.	88
2006	OIH sol-gel coating	OIH coating prepared with TEOS and PDMMS improved corrosion protection of the substrate.	89
		OIH coating prepared with TEOS and MTES and its dependence on the sintering temperature were studied.	90
	CC	Cerium or lanthanum CCs did not hinder the H_2 evolution on HDGS in alkaline solutions.	91
		Zirconia CC acted as a physical barrier and improved corrosion behaviour when compared to uncoated GS.	92
		Rare earth aqueous solutions containing $Ce(NO_3)_3 .6H_2O$ were used to obtain CC on HDGS.	93
		CC using a mixture of Ce^{3+} and Ce^{4+} hydrated oxides/hydroxides with zinc oxide improved the corrosion resistance of HDGS.	55
	Silane doped with inhibitor	BTESPT films doped with Ce^{3+} show enhanced corrosion protection when compared to undoped ones.	94
		BTSE or BTESPT doped with Ce^{3+} or La^{3+} showed good corrosion inhibition properties.	95
	Silanes	BTSE or BTESPT modified with SiO_2 are effective pre-treatments for corrosion protection of HDGS substrates	96
2007	Epoxy coating	Epoxy coatings ED on bare HDGS with CCC showed improved results	97
	Silane	Unpainted samples showed that MPTMS does not passivate the substrate however, it does promote adhesion between the paint and the substrate.	98
	CC	Cerium CC improved the corrosion resistance of electro-galvanized steel.	99
		Titanium CC improved corrosion resistance of the electro-galvanized steel.	100
	Silane modified	BTESPT solutions modi ed with SiO_2 or CeO_2 NP activated with Ce^{3+} improved corrosion resistance.	101
2008	Silanes	Corrosion behaviour of HDGS pre-treated with BTESPT modified with alumina particles improved corrosion protection.	102
	Epoxy coatings	Epoxy coatings were ED on HDGS pre-treated with phosphate coating.	103
	Silane with CeO_2ZrO_2 NP	BTESPT films containing CeO_2. ZrO_2 NP provided good corrosion protection to the GS.	104
	CC	HDGS treated in a formulation of molybdate, phosphate, nitrate and fluoride ions enhanced the corrosion resistance.	105
2009	OIH sol-gel coating	OIHs prepared with GPTMS, TEOS and MTES ensured a barrier effect against water and oxygen.	106
	Silane and CC	GS coated with only silane, only Ce^{3+} CC, and both were tested. The best performance was for the combination of both.	107
	MPS coatings	MPS coating behaved better than the CCC in acidic and alkaline pH.	108
	TMVS and CC	Results showed that La CC and silane provided better anticorrosion performance than CCC.	109

Table 2. (*Continued*)

Year	Type of pre-treatment/coating	Results and Conclusions	Ref
2010	OIH sol-gel coating	OIH prepared with GPTMS, TEOS, MTES and filled with montmorillonite NP and cerium oxides enriched montmorillonite NP were tested. Cerium oxides did not improve the corrosion protection of the OIH film.	110
		Effect of the ED conditions on HDGS pre-treated with OIH prepared with GPTMS, TEOS, and MTES was studied.	111
	Molybdate/silane coatings	The molybdate/silane composite film enhanced the corrosion resistance of the HDGS.	112
	CC	Treatment was composed of fluorotitanic acid, manganese phosphate, phosphoric acid and an organic compound.	113
		Cr(III), Cr(VI), Co(II) and Ni(II) chemical treatments were conducted using $Cr(NO_3)_3$, CrO_3, $CoCl_2$ and $NiCl_2$ respectively.	114
		Molybdate CC on electroplated zinc improved the corrosion resistance.	74
		Cerium CC improved the corrosion resistance of the GS.	115
		Corrosion resistance of the La CC modified with citric acid on HDGS was superior to that of common La CC.	116
	Inorganic oxide thin films	Films of MgO, NiO and ZrO_2 were deposited on GS. Nickel oxide or zirconia increased corrosion resistance.	117
2011	OIH sol-gel coating	OIH coating prepared with TIPT and PAPTES offered good corrosion protection to the substrate.	118
	Polyimide coatings	POABQ and PPDO provide to the HDGS corrosion protection during the study.	119
	Polyester acrylate coatings	Corrosion of GS was improved by the presence of the UV-curing polyester acrylate resin doped with PANI.	120
	Primer	It was concluded that CCC could be successfully replaced by a primer with aluminium phosphosilicate.	121
	Epoxy-polyamide coating	Corrosion resistance and adhesion properties of an epoxy-nanocomposite on HDGS treated by Cr(III), Cr(VI), Cr(III)-Co(II) and Cr(III)-Ni(II) CCs was evaluated.	122
		Corrosion resistance of HDGS coated with an epoxy coating containing NP and micro sized ZnO particles was improved.	123
	CC	Vanadium CC was prepared on electro-galvanized steel and enhanced the corrosion protection.	124
		Silicate CC prepared on HDGS showed self-healing abilities.	125
		Lanthanum CC modified with acid citric and the corrosion resistance of the HDGS was improved.	122
2012	OIH sol-gel coating	OIH coating prepared with GPTMS, TEOS and MTES incorporated with Ce^{3+} montmorillonite clay.	126
		OIH coatings with nanocontainers loaded with corrosion inhibitor enhanced the anticorrosive properties compared to the coatings with empty nanocontainers or only with the inhibitor.	127
	CC	PMS was added into the silicate CC. The coating increased the corrosion resistance of the GS.	128
		Development of a coating in an aqueous silane mixture of GPTMS and APTES enhanced the corrosion protection of the GS.	129
	Epoxy coatings	Epoxy coatings modified with combinations of layered double hydroxides and cerium molybdate nanocontainers lled with corrosion inhibitors revealed that both types of nanocontainers could provide effective corrosion inhibition.	130
2013	OIH sol-gel coating	Beneficial effect of Na-Montmorillonite sonication on the corrosion properties of OIH (using GPTMS, TEOS, MTES) was found.	131
		OIH coatings (using GPTMS and BPA) doped with Ce^{3+} improved the barrier properties.	132
		HDGS coated with OIH (using BTSE and ERE as precursors) by electrophoretic deposition showed improved corrosion protection when compared to HDGS coated with OIH by immersion.	133
		OIH using ICPTES and Jeffamine® minimized the H_2 evolution on the HDGS when embedded in fresh mortar.	73
		OIH coating (using GPTMS and BPA) doped with Ce^{3+}. The optimal corrosion resistance was obtained for $[Ce^{3+}]=0.05M$	132
	TiO_2 sol–gel lm	Photocatalytic TiO_2 film was prepared using an alkoxide sol–gel solution (including TiO_2 NP) on HDGS. A Ce CC was used between the HDGS and TiO_2 film. The corrosion resistance of the substrate was enhanced.	69
	AZC	Promising results were obtained in using AZC in enhancing the corrosion resistance of GS.	134

3. Future and Research Challenges on Corrosion of Hot-Dip Galvanized Steel Reinforcement

According to Andrade[35], studies regarding the corrosion of RC structures started in the early 70's. During the last five decades, numerous papers have been published on this subject. However, due to controversial studies and contradictory results[3,44,46,135] further studies on the role of hexavalent chromium in hindering the hydrogen evolution should be performed. The analysis of the papers published and referred to in this article have also shown that molybdate based conversion coatings are very promising, displaying behaviour very similar to CCC. The negative aspect of this pre-treatment is that the associated cost is higher than for CCC. Therefore, the production of effective molybdate CC with lower concentration of Molybdate (to minimize the costs), is a path that will most certainly be explored. OIH coatings prepared by sol-gel process have also been used as potential corrosion protection of HDGS. The unique properties of OIHs allow new end-use applications and display a significantly better cost/performance relationship when compared with other available materials in the marketplace. Research on contemporaneous hybrid polymers has been gaining market niches, which leads the authors to believe that these materials are also another path for future success. All innovative materials, and OIHs are no exception, face many difficulties and challenges for large-scale industrial production. Several factors including capital investment, ease of manufacturing, coating performances and environment issues need to be considered when developing a coating process for industrial application. It is undeniable that future trends for coating systems need to be low cost, pollution-free, and easy to synthesize and actually be effective in preventing, minimizing and controlling the corrosion of the metallic substrates. Combined systems including the so-called "green smart materials" will be developed allowing for the capacity of regeneration and react according to the needs of the medium surrounding the substrate.

References

1. National Research Council (U.S.) and Committee on the Comparative Costs of Rock Salt and Calcium Magnesium Acetate (CMA) for Highway Deicing, *Highway deicing: comparing salt and calcium magnesium acetate*, Transportation Research Board, National Research Council, Washington, D.C., (1991).

2. H. Böhni, *Corrosion in Reinforced Concrete Structures*, H. Böhni, Woodhead Publishing Ltd, Cambridge, UK, (2005).

3. S. R. Yeomans and International Lead Zinc Research Organization, *Galvanized steel reinforcement in concrete*, Elsevier, Amsterdam, (2004).

4. F. C. Porter, *Corrosion Resistance of Zinc and Zinc Alloys*, p. 540, CRC Press, (1994).

5. B. S. Hamad and J. A. Mike, *Constr. Build. Mater.*, **19**, 275–283 (2005).

6. A. Macias, *Mater. Struct.*, **24**, 456–465 (1991).

7. M. T. Blanco, C. Andrade, and A. Macias, *Br. Corros. J.*, **19**, 41–48 (1984).

8. A. Macias and C. Andrade, *Corros. Sci.*, **30**, 393–407 (1990).

9. Comité euro-international du béton, *Coating Protection for Reinforcement: State of the Art Report*, p. 68, Thomas Telford, (1995).

10. Hot-Dip Galvanizing for Corrosion Prevention - A Guide to Specifying and Inspecting Hot-Dip Galvanized Reinforcing Steel, American Galvanizers Association, USA, (2004).

11. F. E. Goodwin, T. F. M. Committee, M. Dubois, and J. S. Kim, Proceedings of the international symposium held at the TMS Annual Meeting, February 16-19, 1998, San Antonio, Texas, p. 382, Minerals, Metals & Materials Society, (1998).

12. M. J. Hornsby, *Hot-dip galvanizing: a guide to process selection and galvanizing practice*, p. 84, Intermediate Technology Publications, by arrangement with Food and Agriculture Organisation of the United Nations, (1995).

13. P. Maass and P. Peissker, Handbook of Hot-dip Galvanization, Jonh Wiley & Sons, (2011).

14. C. J. Slunder, W. K. Boyd, T. K. Christman, and International Lead Zinc Research Organization, *Zinc: its corrosion resistance*, International Lead Zinc Research Organization, New York, (1986).

15. A. C. Stern, *Air Pollution, Vol. 6, Third Edition: Supplement to Air Pollutants, Their Transformations, Transport and Effects*, 3rd edition., p. 483, Academic Press, New York, (1986).

16. L. H. Everett, K. W. J. Treadaway, and Building Research Station (Great Britain), *The use of galvanised steel reinforcement in building*, Building Research Station, Ministry of Public Building and Works, Garston, Watford [England], (1970).

17. A. P. Yadav, A. Nishikata and T. Tsuru, *Corros. Sci.*, **46**, 361–376 (2004).

18. D. Zaarei, A. A. Sarabi, F. Sharif and S. M. Kassiriha, *J. Coat. Technol. Res.*, **5**, 241–249 (2008).

19. A. P. Yadav, A. Nishikata and T. Tsuru, *Corros. Sci.*, **46**, 169–181 (2004).

20. V. Padilla, P. Ghods and A. Alfantazi, *Constr. Build. Mater.*, **40**, 908–918 (2013).

21. G. A. El-Mahdy, A. Nishikata and T. Tsuru, *Corros. Sci.*, **42**, 183–194 (2000).

22. C. E. Bird, *The Influence of Minor Constituents of Portland Cement on the Behaviour of Galvanized Steel in Concrete*, p. 5, South African Council for Scientific and Industrial Research, (1964).

23. W. Lieber and J. Gebauer, *Zem.-Kalk-Gips*, **4**, 161–164 (1969).

24. G. Rehm and A. Lämmke, *Betonsteinzeitung*, **36**, 360–365 (1970).

25. R. Grauer and H. Kaesche, *Corros. Sci.*, **12**, 617–624 (1972).

26. F. Liebau and A. Amel-Zadeh, *Krist. Tech.*, **7**, 221–227 (1972).

27. A. M. S. El Din, F. M. A. El Wahab and S. M. A. El Haleem, *Mater. Corros.*, **24**, 389–394 (1973).

28. L. Vorkapić, D. M. Dražić and A. R. Despić, *J. Electrochem. Soc.*, **121**, 1385–1392 (1974).

29. R. Duval and R. Arliguie, *Mem. Sci. Rev. Met.*, **11**, 719-727 (1974).

30. Z. Zembura and L. Burzynska, *Corros. Sci.*, **17**, 871–878 (1977).

31. L. M. Baugh and A. Higginson, *Electrochim. Acta*, **30**, 1163–1172 (1985).

32. A. Macias and C. Andrade, *Br. Corros. J.*, **22**, 113–118 (1987).

33. A. Macias and C. Andrade, *Br. Corros. J.*, **22**, 119–130 (1987).

34. A. Macías and C. Andrade, *Mater. Construccion*, 36, 19–27 (1986).

35. C. Andrade, Reinforcement corrosion: Research needs in: Concrete Repair, Rehabilitation and Retrofitting II, Taylor & Francis Group, London, UK, (2009).

36. A. Macías and C. Andrade, *Cem. Concr. Res.*, **17**, 307–316 (1987).

37. A. Macías and C. Andrade, *Br. Corros. J.,* **18**, 82-87, (1983).

38. C. Andrade and A. Macias, *Galvanized Reinforcement in Concrete*, p. 137 in A. D. Wilson, J. W. Nicholson and H. J. Prosser (Eds.), Surface Coating vol. 2. Elsevier Applied Science, (1987).

39. T. Bellezze, M. Malavolta, A. Quaranta, N. Ruffini and G. Roventi, *Cem. Concr. Compos.,* **28**, 246–255 (2006).

40. A. S. Castela, B. S. da Fonseca, R. G. Duarte, R. Neves and M. F. Montemor, *Electrochim. Acta,* **124**, 52-68 (2014).

41. S. B. Farina and G. S. Duffó, *Electrochim. Acta*, **52**, 5131–5139 (2007).

42. I. Fayala, L. Dhouibi, X. R. Nóvoa and M. Ben Ouezdou, *Cem. Concr. Compos.*, **35**, 181–189 (2013).

43. R. Ghosh and D. D. N. Singh, *Surf. Coat. Technol.*, **201**, 7346–7359 (2007).

44. M. Raupach and Mining Institute of Materials, *Corrosion of reinforcement in concrete: mechanisms, monitoring, inhibitors and rehabilitation techniques*, Woodhead ; CRC Press, Cambridge; Boca Raton, (2007).

45. E. Sistonen, *Service Life of Hot-dip Galvanised Reinforcement Bars in Carbonated and Chloride-contaminated Concrete*, Teknillinen Korkeakoulu (2009).

46. Z. Q. Tan and C. M. Hansson, *Corros. Sci.*, **50**, 2512–2522 (2008).

47. F. Tittarelli and G. Moriconi, *Cem. Concr. Res.*, **41**, 609–614 (2011).

48. E. Sistonen, A. Cwirzen and J. Puttonen, *Corros. Sci.*, **50**, 3416–3428 (2008).

49. R. Roberge and W. Zheng, *Corros. Sci.*, **35**, 507–514 (1993).

50. E. Maahn and B. Sorensen, *Corrosion*, **42**, 187–196 (1986).

51. N. R. Short, S. Zhou and J. K. Dennis, *Surf. Coat. Technol.*, **79**, 218–224 (1996).

52. M. H. Sohi and M. Jalali, *J. Mater. Process. Technol.*, **138**, 63–66 (2003).

53. A. K. Singh, G. Jha, N. Rani, N. Bandyopadhyay and T. Venugopalan, *Surf. Coat. Technol.*, **200**, 4897–4903 (2006).

54. M. Kulka and A. Pertek, *Appl. Surf. Sci.*, **218**, 114–123 (2003).

55. M. A. Arenas, C. Casado and J. D. Damborenea, **28**, 267–275 (2007).

56. S. M. A. Shibli and F. Chacko, *Surf. Coat. Technol.*, **202**, 4971–4975 (2008).

57. H. Asgari, M. R. Toroghinejad and M. A. Golozar, *Curr. Appl. Phys.*, **9**, 59–66 (2009).

58. Y. Boonyongmaneerat, K. Saengkiettiyut, P. Rattanawaleedirojn, C. Angkaprasert, J. Wanichsampan and S. Saenapitak, *J. Iron Steel Res. Int.*, **17**, 74–78 (2010).

59. Z. A. Hamid, A. A. Aal, H. B. Hassan and A. Shaaban, *Appl. Surf. Sci.*, **256**, 4166–4170 (2010).

60. S. Le Manchet, D. Verchère and J. Landoulsi, *Thin Solid Films*, **520**, 2009–2016 (2012).

61. E. Pavlidou, N. Pistofidis, G. Vourlias and G. Stergioudis, *Mater. Lett.*, **59**, 1619–1622 (2005).

62. R. Sa-nguanmoo, E. Nisaratanaporn and Y. Boonyongmaneerat, *Corros. Sci.*, **53**, 122–126 (2011).

63. X.-L. Shang, B. Zhang, E.-H. Han and W. Ke, *Electrochim. Acta*, **65**, 294–304 (2012).

64. S. M. A. Shibli, R. Manu and S. Beegum, *Surf. Coat. Technol.*, **202**, 1733–1737 (2008).

65. S. T. Vagge and V. S. Raja, *Surf. Coat. Technol.*, **203**, 3092–3098 (2009).

66. D. Yang, J. Chen, Q. Han and K. Liu, *J. Rare Earths*, **27**, 114–118 (2009).

67. J. D. Culcasi, C. I. Elsner, A. R. D. Sarli and P. R. Sere, **122**, 143–149 (1999).

68. N. Pistofidis, G. Vourlias, S. Konidaris, El. Pavlidou, A. Stergiou and G. Stergioudis, *Mater. Lett.*, **61**, 994–997 (2007).

69. J. H. Park, W. S. Kim, D.-H. Jo, J. S. Kim and J. M. Park, *J. Ind. Eng. Chem.* **20**, 1965-1972 (2014).

70. S. M. A. Shibli, V. S. Dilimon, S. P. Antony and R. Manu, *Surf. Coat. Technol.*, **200**, 4791–4796 (2006).

71. F. J. Recio, M. C. Alonso, L. Gaillet and M. Sánchez, *Corros. Sci.*, **53**, 2853–2860 (2011).

72. A. A. O. Magalhães, I. C. Margarit and O. Mattos, *Electrochim. Acta*, **44**, 4281–4287 (1999).

73. R. B. Figueira, C. J. Silva, E. V. Pereira and M. M. Salta, *J. Electrochem. Soc.*, **160**, C467–C479 (2013).

74. D. Liu, Z. Yang, Z. Wang and C. Zhang, *Surf. Coat. Technol.*, **205**, 2328–2334 (2010).

75. F. Tittarelli and G. Moriconi, *Corros. Sci.*, **52**, 2958–2963 (2010).

76. S. González, M. Gil, J. Hernández, V. Fox and R. Souto, *Prog. Org. Coat.*, **41**, 167–170 (2001).

77. M. F. Montemor, A. M. Simões and M. G. S. Ferreira, **43**, 274–281 (2001).

78. K. Aramaki, *Corros. Sci.*, **44**, 1375–1389 (2002).

79. M. Hara, R. Ichino, M. Okido and N. Wada, *Surf. Coat. Technol.*, **169–170**, 679–681 (2003).

80. I. M. Zin, S. B. Lyon and V. I. Pokhmurskii, *Corros. Sci.*, **45**, 777–788 (2003).

81. M. Garcia-Heras, A. Jimenez-Morales, B. Casal, J. C. Galvan, S. Radzki and M. A. Villegas, *J. Alloys Compd.*, **380**, 219–224 (2004).

82. T. Prosek and D. Thierry, *Prog. Org. Coat.*, **49**, 209–217 (2004).

83. S. Feliu and V. B. Barranco, *J. Coat. Technol. Res.*, **1**, 93–102 (2004).

84. M. G. Ferreira, R. Duarte, M. Montemor and A. M. Simões, *Electrochim. Acta*, **49**, 2927–2935 (2004).

85. A. A. O. Magalhães, I. C. P. Margarit and O. R. Mattos, *J. Electroanal. Chem.*, **572**, 433–440 (2004).

86. C. G. da Silva, A. N. Correia, P. de Lima-Neto, I. C. P. Margarit and O. R. Mattos, *Corros. Sci.*, **47**, 709–722 (2005).

87. S. Dalbin, G. Maurin, R. P. Nogueira, J. Persello and N. Pommier, *Surf. Coat. Technol.*, **194**, 363–371 (2005).

88. W. Trabelsi, P. Cecilio, M. G. S. Ferreira and M. F. Montemor, *Prog. Org. Coat.*, **54**, 276–284 (2005).

89. M. E. P. Souza, E. Ariza, M. Ballester, I. V. P. Yoshida, L. A. Rocha and C. M. A. Freire, *Materials Research*, **9**, 59–64 (2006).

90. A. Conde, J. Damborenea, A. Durán and M. Menning, *J. Sol-Gel Sci. Technol.*, **37**, 79–85 (2006).

91. M. Sánchez, M. C. Alonso, P. Cecílio, M. F. Montemor and C. Andrade, *Cem. Concr. Compos.*, **28**, 256–266 (2006).

92. R. R. Pareja, R. L. Ibáñez, F. Martín, J. R. Ramos-Barrado and D. Leinen, *Surf. Coat. Technol.*, **200**, 6606–6610 (2006).

93. J. Lu, H. Wu, G. Kong, C. Che and Q. Xu, *Trans. Nonferrous Met. Soc. China*, **16**, 1397–1401 (2006).

94. A. M. Cabral, W. Trabelsi, R. Serra, M. F. Montemor, M. L. Zheludkevich and M. G. S. Ferreira, *Corros. Sci.*, **48**, 3740–3758 (2006).

95. M. F. Montemor, W. Trabelsi, M. Zheludevich and M. G. S. Ferreira, *Prog. Org. Coat.*, **57**, 67–77 (2006).

96. M. F. Montemor, A. M. Cabral, M. L. Zheludkevich and M. G. S. Ferreira, *Surf. Coat. Technol.*, **200**, 2875–2885 (2006).

97. J. B. Bajat, V. B. Mišković-Stanković, N. Bibić and D. M. Dražić, *Prog. Org. Coat.*, **58**, 323–330 (2007).

98. U. Bexell and T. M. Grehk, *Surf. Coat. Technol.*, **201**, 4734–4742 (2007).

99. M. Hosseini, H. Ashassi-Sorkhabi and H. A. Y. Ghiasvand, *J. Rare Earths*, **25**, 537–543 (2007).

100. L. Zhu, F. Yang and N. Ding, *Surf. Coat. Technol.*, **201**, 7829–7834 (2007).

101. M. F. Montemor and M. G. S. Ferreira, *Electrochim. Acta*, **52**, 6976–6987 (2007).

102. F. J. Shan, C. S. Liu, S. H. Wang and G. C. Qi, *Acta Metall. Sin. Engl. Lett.*, **21**, 245–252 (2008).

103. J. B. Bajat, V. B. Mišković-Stanković, J. P. Popić and D. M. Dražić, *Prog. Org. Coat.*, **63**, 201–208 (2008).

104. M. F. Montemor, W. Trabelsi, S. V. Lamaka, K. A. Yasakau, M. L. Zheludkevich, A. C. Bastos and M. G. S. Ferreira, *Electrochim. Acta*, **53**, 5913–5922 (2008).

105. D. D. N. Singh and R. Ghosh, *Surf. Coat. Technol.*, **202**, 4687–4701 (2008).

106. M. Fedel, M. Olivier, M. Poelman, F. Deflorian, S. Rossi and M.-E. Druart, *Prog. Org. Coat.*, **66**, 118–128 (2009).

107. G. Kong, J. Lu and H. Wu, *J. Rare Earths*, **27**, 164–168 (2009).

108. Y. Hamlaoui, L. Tifouti and F. Pedraza, *Corros. Sci.*, **51**, 2455–2462 (2009).

109. T. Peng and R. Man, *J. Rare Earths*, **27**, 159–163 (2009).

110. F. Deflorian, S. Rossi, M. Fedel and C. Motte, *Prog. Org. Coat.*, **69**, 158–166 (2010).

111. M. Fedel, M.-E. Druart, M. Olivier, M. Poelman, F. Deflorian and S. Rossi, *Prog. Org. Coat.*, **69**, 118–125 (2010).

112. G. Kong, J. Lu, S. Zhang, C. Che and H. Wu, *Surf. Coat. Technol.*, **205**, 545–550 (2010).

113. S. Le Manchet, J. Landoulsi, C. Richard and D. Verchère, *Surf. Coat. Technol.*, **205**, 475–482 (2010).

114. B. Ramezanzadeh, M. M. Attar and M. Farzam, *Surf. Coat. Technol.*, **205**, 874–884 (2010).

115. M. Olivier, A. Lanzutti, C. Motte and L. Fedrizzi, *Corros. Sci.*, **52**, 1428–1439 (2010).

116. G. Kong, L. Liu, J. Lu, C. Che and Z. Zhong, *J. Rare Earths*, **28**, 461–465 (2010).

117. R. Romero, F. Martin, J. R. Ramos-Barrado and D. Leinen, *Surf. Coat. Technol.*, **204**, 2060–2063 (2010).

118. A. K. Guin, S. K. Nayak, T. K. Rout, N. Bandyopadhyay and D. K. Sengupta, *J. Coat. Technol. Res.*, **9**, 97–106 (2011).

119. E. Huttunen-Saarivirta, V. E. Yudin, L. A. Myagkova and V. M. Svetlichnyi, *Prog. Org. Coat.*, **72**, 269–278 (2011).

120. S. Jafarzadeh, A. Adhikari, P.-E. Sundall and J. Pan, *Prog. Org. Coat.*, **70**, 108–115 (2011).

121. A. M. P. Simões, R. O. Carbonari, A. R. D. Sarli, B. del Amo and R. Romagnoli, *Corros. Sci.*, **53**, 464–472 (2011).

122. G. Kong, L. Lingyan, J. Lu, C. Che and Z. Zhong, *Corros. Sci.*, **53**, 1621–1626 (2011).

123. B. Ramezanzadeh and M. M. Attar, *Prog. Org. Coat.*, **71**, 314–328 (2011).

124. Z. Zou, N. Li, D. Li, H. Liu and S. Mu, *J. Alloys Compd.*, **509**, 503–507 (2011).

125. M. Yuan, J. Lu, G. Kong and C. Che, *Surf. Coat. Technol.*, **205**, 4507–4513 (2011).

126. C. Motte, M. Poelman, A. Roobroeck, M. Fedel, F. Deflorian and M.-G. Olivier, *Prog. Org. Coat.*, **74**, 326–333 (2012).

127. I. A. Kartsonakis, A. C. Balaskas, E. P. Koumoulos, C. A. Charitidis and G. C. Kordas, *Corros. Sci.*, **57**, 30–41 (2012).

128. J. Min, J. H. Park, H.-K. Sohn and J. M. Park, *J. Ind. Eng. Chem.*, **18**, 655–660 (2012).

129. L. Wang, C. Liu, H. Yu and C. An, *J. Iron Steel Res. Int.*, **19**, 46–51 (2012).

130. M. F. Montemor, D. V. Snihirova, M. G. Taryba, S. V. Lamaka, I. A. Kartsonakis, A. C. Balaskas, G. C. Kordas, J. Tedim, A. Kuznetsova, M. L. Zheludkevich and M. G. S. Ferreira, *Electrochim. Acta*, **60**, 31–40 (2012).

131. M. Fedel, E. Callone, S. Diré, F. Deflorian, M.-G. Olivier and M. Poelman, *Electrochim. Acta* (2013), 124, 90-99 (2014).

132. R. Z. Zand, K. Verbeken and A. Adriaens, *Int. J. Electrochem. Sci.*, **8,** 548-563 (2013)

133. D. Xue and W. J. Van Ooij, *Prog. Org. Coat.*, **76**, 1095–1102 (2013).

134. R. Sako and J. Sakai, *Surf. Coat. Technol.*, **219**, 42–49 (2013).

135. C. M. Hansson, A. Poursaee and S. J. Jaffer, *Portland Cem. Assoc.*, Skokie (2007).

3. Electrochemical System for Assessing Hybrid Coatings for Corrosion Protection of Hot-Dip Galvanized Steel in Mortar

Electrochemical system for assessing hybrid coatings for corrosion protection of hot dip galvanized steel in mortar

R. M. Figueira[a,b,*], E. V. Pereira[a], C. J. R. Silva[b], M. M. Salta[a]

[a]LNEC, Laboratório Nacional de Engenharia Civil, Av. Brasil 101, 1700-066 Lisbon, Portugal

[b]Centro de Química, Universidade do Minho, Campus de Gualtar 4710 - 057 Braga, Portugal

*Corresponding Author: rmfigueira@lnec.pt

Abstract

Corrosion of steel in concrete is one of the major causes of structure degradation, requiring expensive maintenance. The using of hot dip galvanized steel (HDGS) has been recognized as one effective measure to increase the service life of reinforced concrete structures in marine environmental. However, HDGS corrodes in contact with high alkaline environment of fresh concrete. Although this initial corrosion process allows the formation of a protecting layer barrier, the corrosion that occurs initially is harmful and chromate conversion layers are usually used to prevent it.

Due to toxicity of Cr(VI), these kinds of pre-treatments have been forbidden and hybrid coatings have been proposed as alternatives[1-3]. To evaluate the performance of these coatings, beyond the laboratory characterization, in situ tests in real conditions should be performed.

An electrochemical system to measure the macrocell current density (igal) was designed to evaluate the degradation of HDGS coated samples with different organic-inorganic hybrid films, embedded in mortar during 70 days, using an automatic data acquisition system.

This system revealed to be feasible and highly sensitive to coatings degradation. Also, allow distinguishing different hybrid coatings with different thicknesses.

Keywords

1. Introduction

To minimize the risk of corrosion of reinforced concrete structures (RCS) it should be ensured that the concrete covering the metallic reinforcement parts is of an adequate thickness and possesses a higher quality; with a proper mixing ratio, good compaction and curing. However, the physical barrier of protection provided by the concrete cover is not perfect. Due to the porous concrete structure, resulting from imperfections of concreting and curing processes, the diffusion/transport of aggressive species towards the interface steel/concrete is enabled. The conjugation of these factors may cause rupture of the film passivation and initiate rusting of steel originating failure in reinforced concrete structures. However, premature failure in RCS by reinforcement corrosion in aggressive environments, especially structures exposed to marine environments, might be mitigated if the reinforcing steel is hot dip galvanized[4-7]. The zinc coating on rebars embedded in concrete acts as a physical barrier avoiding direct contact between the coated reinforcing steel and the aggressive environment. Deposited zinc acts as sacrificial anode protecting the steel against corrosion and the zinc corrosion products provide a sealing effect on zinc coating due to discontinuities[6]. Moreover, galvanized reinforcing steel can withstand exposure to chloride ion concentrations several times higher (at least 4 to 5 times) than the chloride level, that causes corrosion in steel reinforcement[8].

While steel in concrete typically depassivates at a pH below 11.5, galvanized reinforcement can remain passivated at a lower pH, thereby offering additional substantial protection against the effects of concrete carbonation[8] The combination of these factors: carbonation resistance and chloride tolerance are commonly accepted as the basis for superior performance of galvanized reinforcement compared to steel reinforcement. In addition, zinc corrosion products occupy a smaller volume than those produced from iron causing slight or no disruption in the surrounding concrete. Yeomans[8] also confirmed that the zinc corrosion products are powdery and non-adherent making them capable of migrating from the surface of the galvanized reinforcement into the concrete matrix, reducing the likelihood of zinc corrosion-induced spalling of the concrete.

The cathodic reaction from water hydrolysis with hydrogen evolution, in contact with high alkaline environments, such as concrete, takes place, producing a continuous dissolution of the metal until the solution becomes oversaturated by these ions that precipitate as $Zn(OH)_2$ or ZnO [6]. In order to avoid those reactions the cement must contains at least 100 ppm of chromates in the final concrete mix or the hot-dip galvanized bars must be previously passivated with a chromate conversion layer to minimize the evolution of hydrogen during the reaction between zinc and fresh concrete[9-15].

The high corrosion resistance offered by the use of chromate films is endorsed to the presence of Cr^{6+} and Cr^{3+}. Chromate and similar hexavalent chromium compounds are among the most common substances used as inhibitors and are commonly incorporated in anticorrosive pre-treatments of a wide range of metals and alloys, such as steels, aluminium alloys, copper, lead and others. The original reason behind the use of chromates treatments on galvanized steel is to avoid the formation of wet storage stain during the first six weeks after galvanizing, in particular to reduce the formation of excessive amounts of zinc oxide and zinc hydroxide during that period, and reduce the consequent release of hydrogen gas[8]. The reaction of zinc with the concrete ceases in a few days and gives just sufficient corrosion products to ensure a strong and reliable bond to the concrete when fully hardened. Although the chromium-based compounds improve the corrosion resistance of zinc and minimize the hydrogen evolution, their application is heavily regulated by most environmental legislation due to their carcinogenic effects. Research efforts are being made to replace chromates and produce new ecological compounds and processes aiming good corrosion resistance, adhesion, and fatigue resistance, reliability and quality control performances. Besides some commercial available products, research developments involves a better understanding of these coatings performance beyond the laboratory scale, so *in situ* tests (in real RCS conditions) are currently performed and feasible systems being developed. As well documented by several authors[16-23] electrochemical techniques (i.e. half-cell potential measurements, polarization resistance, potentiostatic and galvanostatic transients perturbations, electrochemical impedance spectroscopy, noise analysis, multielectrode systems, etc.) offer several advantages for reinforcement corrosion monitoring. Schiessl and Raupach in 1992[24] developed a sensor to be implemented inside concrete during the construction. The developed sensor device involves the paring of a non-oxidable metal electrode, usually stainless steel, with the steel rebars used to build the construction structure, allowing measuring the galvanic current created when construction steel depassivates by action of the aggressive agents (local acidification, carbonation, ingress of chloride ions and/or depletion of O_2). Installing these sensors on critical points of the concrete structure together with an appropriate data acquisition and communication systems is possible a real-time RCS monitoring. Detecting or predicting the instant wherein the construction steel depassivates[26,27], makes possible to plan the necessary maintenance interventions in order to minimize the involved costs.

In the present work is described an electrochemical system[25] based on Schiessl and Raupach studies[24]. The main purpose of the paper is to evaluate the response of the designed electrochemical system when coated with different OIH and not to evaluate the barrier properties of the coatings. This system was tested under laboratory conditions to assess the system response to

the degradation of HDGS coated with different OIH films embedded in mortar. The developed cells allow assessing and monitoring the behaviour of HDGS protective coatings with time when in contact with mortar. The results show that the designed system implemented is suitable to evaluate the *in situ* degradation of HDGS coated with different OIH films embedded in concrete.

2. Experimental

2.1. Reagents

The OIH gel matrices were prepared following a well-established methodology described elsewhere[28-30]. Two sets of four different structural types of ureasilicate OIH gel matrices were prepared by a reaction between the isocyanate group of the derived siloxane (ICPTES) with four different di-amino functionalized polyether (Jeffamine® D-400, Jeffamine® ED-600, ED-900 and ED-2000, hereafter generically referred as Jeffamines) with different molecular weights, with and without incorporated Cr(III) ions, obtained by adding the correspondent salt aqueous solutions with a concentration of 0.01M. All the used Jeffamines and the functionalized siloxane (3-isocyanate propyltriethoxysilane) were stored protected from light and used as supplied. Ethanol (EtOH, absolute 98 %, Riedel-de-Haën), citric acid monohydrate (Merck), and chromium (III) nitrate nanohydrate (Aldrich) were also used as received. Ultra-pure water (0.055-0.060 μS/cm) obtained from a *Purelab Ultra* System (Elga) was used.

HDGS metal plates commercially available were used, with 5.0x1.0x0.1 (in cm) and with a Zn average thickness of 16 μm on both sides.

2.2. Preparation of HDGS Coated Samples

HDGS coating samples were prepared by dipping HDGS metal plates, used as received and previously degreased with acetone, in the synthesized mixture at a withdrawal speed of 10 mm min^{-1} without residence time using a dip coater (Nima, model DC Small) and subsequently placed in an incubator-compressor (*ICP*-400, Memmert) and kept at 40ºC for about two weeks. Two sets of coated HDGS samples were produced, by one and three dip steps process. The identification of the different prepared samples is in Table 1.

Table 1. Adopted codes for the coating samples prepared

HDGS OIH coated sample		
Jeffamine	Pure Matrix	Cr(III) doped
D-400 ®	U(400)	U(400)_Cr(III)
ED-600®	U(600)	U(600)_Cr(III)
ED-900®	U(900)	U(900)_Cr(III)
ED-2000®	U(2000)	U(2000)_Cr(III)

2.3. Preparation of Mortar

The corrosion behaviour of HDGS coated with the different OIH coatings were studied in mortar that was prepared according to EN 196-1 standard[31] using cement type I 42,5R (Table 2), distilled water and normalized sand (AFNOR) (Table 3) with a weight ratio of 6:2:1 (sand:cement:water).

Table 2. Characteristic values of mechanical, physical and chemical properties for cement type I 42.5R

Mechanical and physical properties:	Cement type I 42,5R
Start of binding (min)	150
Volume stability acc. to Le Chatelier (mm)	1.0
Pressure strength after 2 days (MPa)	30
Pressure strength after 28 days (MPa)	54
Chemical properties:	
SO_3 (%)	3.5
CI (%)	0.01
Loss on calcination (%)	3.0
Content of insoluble residue	1.0

Table 3. Physical and chemical properties for normalized sand

Physical and chemical properties	
Physical state	Solid
SiO_2:	> 95 %
Form:	Crystallized
Form of grains:	Subangular
Specific temperature for changes in	Fusion temperature: 1610° C
Decomposition temperature:	None
Flash Point:	Not applicable
Self-inflammation temperature:	Not applicable
Explosive characteristics:	Not applicable
Mass volume:	Absolute: 2,63 g/m³
Solubility:	insoluble in water, soluble in hydro-fluoric acid

2.4. Electrochemical Studies

To assess the reliability of the electrochemical system, macrocell current density (i_{gal})[25] measurement was performed using a system based on two electrodes (parallel rectangular metal plates with 5.0x1.0x0.1 cm), as shown in Figure 1. The working electrode (WE) was a HDGS plate, also with two cm^2 of area, and coated as described on section previously. The grey area in the Figure 1 represents the OIH coating on HDGS. The counter electrode (CE) was a stainless steel (SS, type 316L) plate with an active surface section of two cm^2. The edges of both of the electrodes plates, as well the non-active area and connecting zones were protected with a two-component epoxy resin (Araldite®). The set of the two electrodes was fixed in plastic lids that fit in a 100 mL polyethylene flask (Normax). For comparison purposes, cells using a HDGS WE without any OIH coating were prepared to be used as reference (hereafter referred generically as control cells).

To assemble the electrochemical cells used to measure i_{gal}, 120±10 g of fresh mortar was transferred to each 100 mL PE flask where the electrodes were immersed and the flask closed (mortar was prepared according to above and immediately used). Using an automatic data acquisition system (Datataker DT505, series 3), the i_{gal} measurement of the prepared cells were performed through reading the potential difference to the terminals (shunted with a 100 Ω resistor *vide* Figure 2) immediately after being embedded in fresh mortar.

Measurements were performed with a periodicity of 1 minute at the first seven days, and at each 5 minutes during the remaining time until the record was completed, at the 74th day.
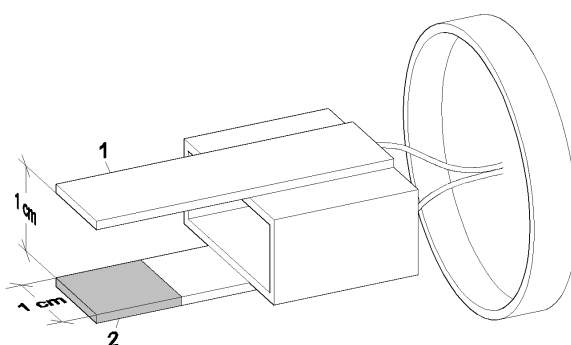

Figure 1. Schematic representation of electrochemical system developed for assess coating performance through monitoring of i_{gal}. Legend: 1. Stainless steel counter electrode (CE); 2. HDGS coated working electrode (WE), with OIH gel deposit–represented by a grey zone.
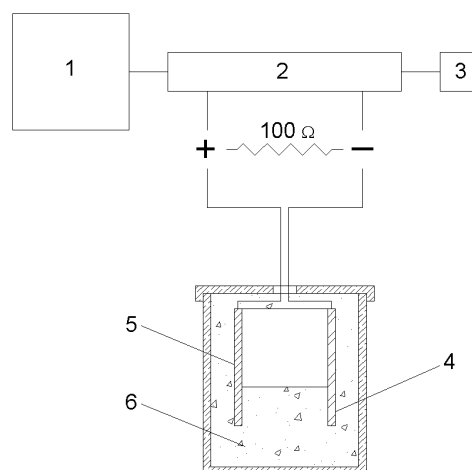
Figure 2. Schematic representation of assembled two electrodes cell. Legend: 1. PC; 2. Datataker; 3. Power supply; 4 and 5. Working and counter electrodes, respectively; 6. Mortar.

2.5. Stereoscopic Microscopy

The HDGS surfaces were thoroughly examined in the laboratory using a zoom stereomicroscope system (Olympus SZH).

2.6. Scanning Electron Microscopy (SEM/EDS)

The morphology of the OIH sol-gel coatings surface applied on HDGS specimens were performed with scanning electron microscope (SEM, JEOL JSM-6400) coupled with an EDS detector (Inca-xSight Oxford Instruments), and the surface of specimens were covered with an ultrathin coating of gold deposited by sputter coating. The SEM/EDS studies of the HDGS coated samples were performed on the substrate before and after being in contact with mortar after 74 days. After the essay was completed, the hardened cementitious materials were thoroughly broken to release the HDGS specimens and allow SEM/EDS observations.

3. Results and Discussion

Figure 3 shows the macrocell current density (i_{gal}) response collected from the different prepared electrochemical cells involving the HDGS coated samples and the control cell during 74 days[30].

The high values of i_{gal} recorded for the first days of contact with the fresh mortar are due to zinc corrosion, that in the presence of high alkaline environments it corrodes[9-15]. Nevertheless, the coated samples tend to lower values when compared to control sample. The obtained evolution of cell

current density with time shows a profile that is dependent of OIH coating matrix, the presence of Cr(III) ions and the number of dipping steps. Globally the measured current density decrease along the contact time showing in the 74th day an average value that is about two orders of magnitude lower than the initially observed. Cells based on one layer coated HDGS samples reveal a very noisy behaviour comparatively with samples with a coating produced by three dipping steps.
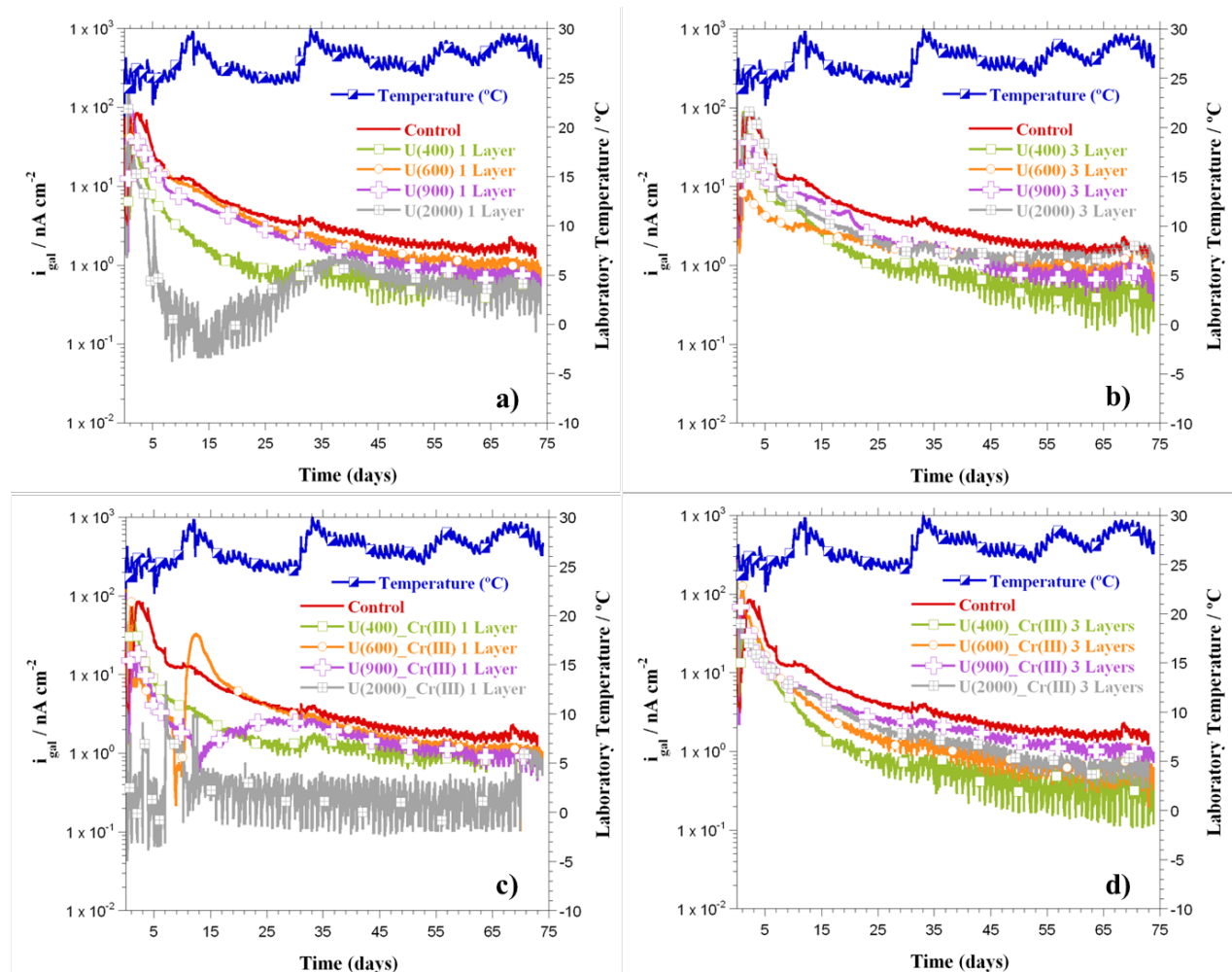

Figure 3 – Recorded galvanic current profiles.

As shown, the i_{gal} cell values are sensitive to the external laboratory temperature variation and to the composition and number of OIH deposited (one and three) layers. The collected data makes possible to distinguish between the different used OIH coatings as the output response changes with the coating composition and with the presence or absence of inhibitor (Cr(III)). It was also observed that the uncoated HDGS specimen shows the higher current density values among the all set of tested macrocells.

Figure 4 shows the images obtained with a stereomicroscope for the uncoated HDGS (control) and for HDGS coated by one dip step for U(400), U(600) and U(2000). The stereomicroscope images that show to be less attacked by the electrolyte correspond to cells where lower values of i_{gal} data were recorded. Figure 5 shows the SEM images and EDS spectra obtained for the control and for HDGS coated with U(400) by one dip step.
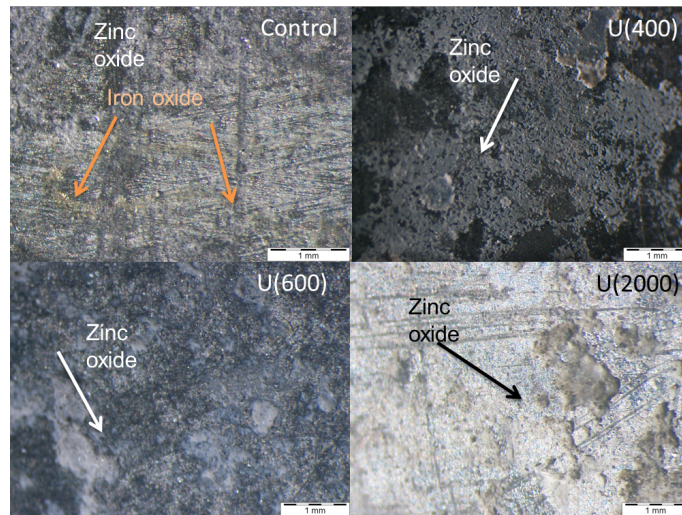

Figure 4. Observation of HDGS surfaces uncoated (control) and coated with OIH sol-gel with stereomicroscope after being embedded in mortar for 74 days, showing the presence of zinc oxide and traces of iron oxides.
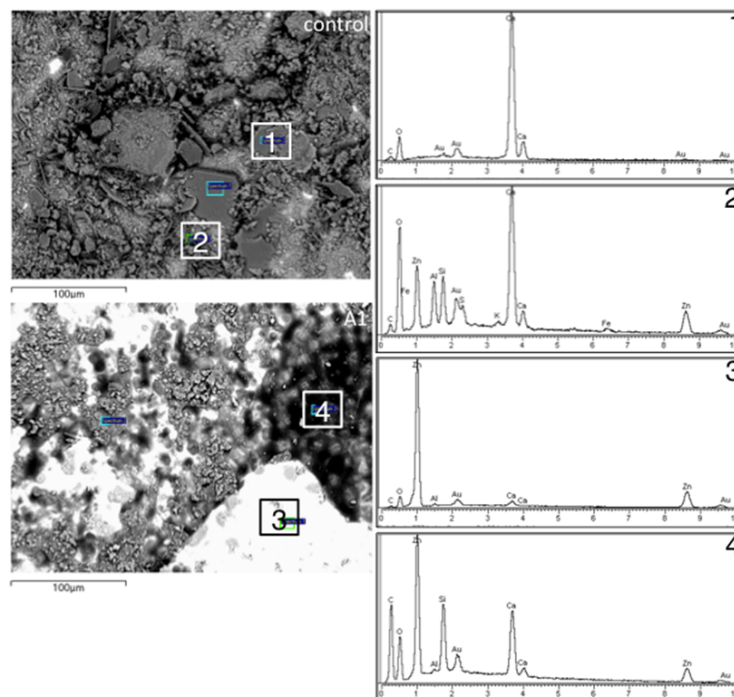
Figure 5. BSE images of the HDGS samples surface for control and HDGS coated with U(400) after being embedded in mortar for 74 days with the localization of the EDS spectra; 1, 2 EDS spectra for control; 3 and 4 EDS spectra for HDGS coated with U(400).

Figure 6 shows the SEM images and EDS spectra obtained for HDGS coated with U(600), U(900) and U(2000) by one dip step. From the analysis of the collected set of images obtained by SEM, it can be concluded that the surface of uncoated HDGS sample (control cell) reveals the most severe damages among all that were exposed to mortar. The obtained results from EDS analysis reveal the presence of iron peaks. These results are in agreement with i_{gal} data and with stereomicroscope images.
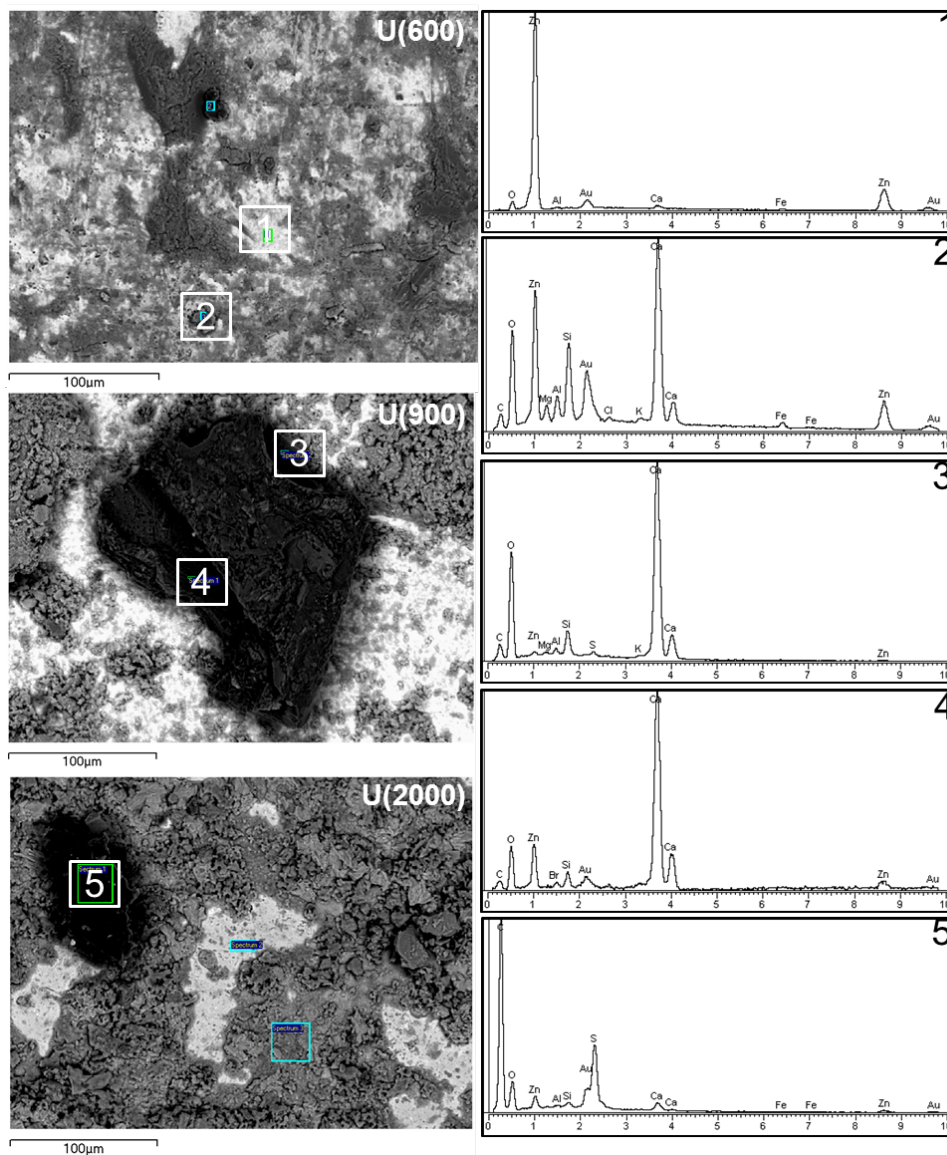

Figure 6. BSE images of the HDGS samples surface coated with U(600), U(900) and U(2000) after being embedded in mortar for 74 days with the localization of the EDS spectra; 1, 2 EDS spectra for HDGS coated with U(600); 3 and 4 EDS spectra for HDGS coated with U(900); 5 EDS spectrum for HDGS coated with U(2000).

The topic of this paper is to evaluate the response and the behaviour of the electrochemical system when testing different OIH coatings. It was observed that the HDGS coated samples do not show to be similarly affected by the corrosive action of mortar components and depend on the OIH coating applied, as observed in stereomicroscope images displayed in Figure 4. The EDS correspondent spectra show the presence of carbon and silicon on the surface indicating that the applied coating preserved their initial form. The information obtained by these two techniques confirm that the barrier stability and efficiency of the OIH gel coating contribute to minimize the recorded current density and consequently minimize the extent of HDGS corrosion process. The results obtained show that the electrochemical system is reliable and suitable to evaluate the behaviour of the OIH coatings.

4. Conclusions

The analysis of the results obtained by optical and SEM/EDS of the WE of the disassembled cells show to be consistent with the data obtained by the electrochemical technique. The behaviour of coated HDGS samples revealed to be highly sensitive to the OIH coatings composition allowing distinguishing between the distinct coatings with different thicknesses. The collected data also allows concluding that presence of Cr(III) ions within the OIH gel matrix contributes to mitigate the corrosion process in the first instants of contact with fresh concrete. The results show that the developed system allow to distinguish with high reliability OIH sol-gel coatings using the same matrix with slight variations like doping with inhibitor (Cr(III)). The system revealed to be highly sensitive to the external temperature variation since when the temperature increases the i_{gal} data also increases. The designed system implemented seems to be suitable to evaluate the *in situ* degradation of HDGS coated with different OIH films embedded in concrete. Future studies should be performed *in situ* in order to evaluate the output response to the presence of aggressive agents such local acidification, carbonation, ingress of chloride ions and/or depletion of O_2.

References

1. R. B. Figueira, C. J. R. Silva, E. V. Pereira and M. M. Salta, *Proceedings from Electrochemistry 2012 - Fundamental and Engineering Needs for Sustainable Development*, München, September 17 – 19th.

2. M. Qian, A. M. Soutar, X. H. Tan, X. T. Zeng and S. L. Wijesinghe, *Thin Solid Films*, **517**, 5237–5242 (2009).

3. A. Pepe, P. Galliano, M. Aparicio, A. Durán and S. Cere, *Surf. Coat. Tech.*, **200,** 3486–3491 (2006).

4. F. C. Porter, *Corrosion Resistance of Zinc and Zinc alloys*, New York, (1994).

5. M. Sánchez, M. C. Alonso, P. Cecílio, M. F. Montemor and C. Andrade*, Cement Concrete Comp.*, **28**, 256-266 (2006).

6. F. Tittarelli and T. Bellezze, *Corros. Sci.*, **52**, 978-983 (2010).

7. F. J. Recio, M. C. Alonso, L. Gaillet and M. Sánchez, *Corros. Sci.*, **53,** 2853-2860 (2011).

8. S. R. Yeomans, *Galvanized steel reinforcement in Concrete*, Elsevier: Amsterdam, (2004).

9. B. E. Roetheli, G. L. Cox and W. B. Littreal, *Met. Alloys*, **3**, 73-76 (1932).

10. A. Macías and C. Andrade, *Brit. Corros. J.*, **22,** 113-118 (1982).

11. A. M. S. El Din, F. M. A. El Wahab and S. M. A. El Haleem, *Werkst. Korros.* **24**, 389-384 (1973).

12. F. Liebau and A. Amel-Zadeh, *Kistall und Technick*, **7**, 221-227 (1972).

13. L. Z. Vorkapic, D. M. Drazic and A. R. Despic, *J. Electrochem. Soc.*, **121**, 1385-1392 (1974).

14. W. Lieber and J. Gebauer, *Zement-kalk-Gips,* **4**, 161-164 (1970).

15. Z. Q Tan and C. M. Hansson, *Corros. Sci.*, **50,** 2512-2522 (2008).

16. B. Elsener, *Mater. Sci. Forum*, **192,** 857–866 (1995).

17. J. H. Yoo, Z. T. Park, J. G. Kim and L. Chung, *Cem. Concr. Res.*, **33,** 2057–2062 (2003).

18. W. J. McCarter and O. Vennesland, *Constr. Build. Mater.*, **18**, 351–358 (2004).

19. H. W. Song and V. Saraswathy, *Int. J. Electrochem. Sci.*, **2**, 1–28 (2007).

20. M. Islam and S. F. Daily, *J. ASTM Int.*, **3,** 1546–1557 (2006).

21. V. Leelalerkiet, T. Shimizu, Y. Tomoda and M. Ohtsu, *J. Adv. Concr. Technol.,* **3**, 137–147 (2005).

22. J. M. Smulko, K. Darowicki and A. Zieliñski, *Russ. J. Electrochem.*, **42,** 548–552 (2006).

23. C. Andrade and C. Alonso, *Constr. Build. Mater.*, **10,** 315–328 (1996).

24. P. Schiessl and M. Raupach, *ACI Concr. Int.*, **7,** 52-55 (1992).

25. ASTM G109-07 *Standard Test Method for Determining Effects of Chemical Admixtures on Corrosion of Embedded Steel Reinforcement in Concrete Exposed to Chloride Environments.* In: Annual book of ASTM standards, 03.02, (2007).

26. E. V. Pereira, R. B. Figueira, M. M. Salta and I. T. E. Fonseca, *Sensors*, **9**, 8391-8398 (2009).

27. E. V. Pereira, *Monitorização da corrosão no betão armado*, PhD Thesis, University of Lisbon, Lisbon, (2004).

28. V. I. Boev, A. Soloviev, C. J. R. Silva, M. J. M. Gomes and D. J. Barber, *J. Sol-Gel Sci. Techn.*, **41**, 223-229 (2007).

29. S. D. F. C. Moreira, C. J. R. Silva, L. A. S. A. Prado, M. F. M. Costa, V. I. Boev, J. Martín-Sánchez and M. J. M. Gomes, *J. Polym. Sci. Pol. Phys.*, **50**, 492-499 (2012).

30. R. B. Figueira, C. J. R. Silva, E. V. Pereira and M. M. Salta, *J. Electrochem. Soc.*, **160**, C467-C479 (2013).

31. European Committee for Standardization, BS EN 196-1 (2005).

4. Ureasilicate Hybrid Coatings for Corrosion Protection of Galvanized Steel in Cementitious Media

Ureasilicate Hybrid Coatings for Corrosion Protection of Galvanized Steel in Cementitious Media

R. B. Figueira[a,b,*], C. J. R. Silva[b], E. V. Pereira[a], M. M. Salta[a]

[a]LNEC, Laboratório Nacional de Engenharia Civil, Av. Brasil 101, 1700-066 Lisbon, Portugal

[b]Centro de Química, Universidade do Minho, Campus de Gualtar 4710 - 057 Braga, Portugal

* Corresponding Author: rmfigueira@lnec.pt

* Electrochemical Society Student Member

Abstract

This study is focused on the electrochemical behaviour and surface analysis of an eco-friendly organic–inorganic hybrid (OIH) coating for hot dip galvanized steel (HDGS) in contact with cementitious media. This treatment is a proposed alternative to replace toxic Cr(VI)-based pre-treatments used to control reactions between the zinc and wet concrete. HDGS samples were coated with two different sets of OIH obtained by a sol-gel process. Five distinct OIH matrices were obtained by reaction of functionalized metal alkoxide (3-isocyanatopropyltriethoxysilane) with five different molecular weight diamine-alkylethers. One set of HDGS samples was coated with each of the five pure OIH matrices and another was coated with similar OIH matrices doped with Cr(III). The morphology of OIH coatings over HDGS surface was characterized by SEM/EDS. Similar OIH films were prepared separately and the respective resistivity was measured by electrochemical impedance spectroscopy. Polarization resistance and macrocell current density were used to evaluate the corrosion protection properties of the HDGS coated samples in contact with cementitious media for a period of 74 days. Results showed that the produced OIH coatings provide barrier properties that withstand the high pH of the electrolyte, protecting the HDGS protecting the HDGS when it first contacts cementitious media.

Keywords

1. Introduction

The corrosion of steel in concrete is one of the major causes of structures degradation, requiring expensive rehabilitation. The use of hot dip galvanized steel (HDGS) has been recognized as an effective measure to increase the service life of reinforced concrete structures exposed to carbonation or to chloride ions[1-3]. The galvanized coating is a physical barrier that hinders the contact of aggressive agents with the steel substrate and the zinc layer acts as a sacrificial anode, protecting the steel against corrosion[4-5].

Immediately after the HDGS is embedded in fresh concrete, a highly alkaline environment, the zinc coating corrodes for a limited period (from several hours to a few days) until passivating surface layers are formed and concrete hardens. This initial corrosion process may lead to zinc consumption between 5 to 10 µm[2]. At the same time hydrogen is produced which may lead to the loss of adherence between steel and concrete.

Several corrosion studies reported the behaviour of HDGS in contact with concrete media and in alkaline solutions[2-21]. However, uncertainties concerning the initial corrosion behaviour of the galvanized coating when embedded in concrete still remains. The main literature about corrosion and passivation mechanisms of zinc in concrete environments, suggest that the formation of the protective layer due to zinc oxidation takes place with water reduction and subsequent hydrogen evolution[9-11]. Other authors claim that the formation of protective layer is related to the presence of oxygen at the concrete/rebar interface[12,14,18].

Andrade and co-workers[11,22-23], found that at pH $\geqslant$ 12.5 zinc dissolution and hydrogen evolution takes place producing a continuous dissolution of the metal. However, in concrete interstitial electrolyte solutions containing Ca^{2+} ions, in the form of calcium hydroxide ($Ca(OH)_2$), the passivation of the metal surface is induced. Nevertheless, this process seems to be highly dependent on the electrolyte pH since a survey conducted by Macias and co-workers established that a pH > 13.2 is the limit value for passivation capability of galvanized steel[11]. Under these circumstances, several passivation mechanisms have been proposed[9,24,25,26,27].

According to Andrade and Alonso[27] the calcium hydroxyzincate (CAHZ) crystals $Ca(Zn(OH)_3)_2$ formed in the electrolytes with 12.5 < pH < 13.3 present a size that make them able to cover compactly the substrate surface forming an efficient passivation layer. However, at pH > 13.3, which are common values for fresh concrete, the formed CAHZ crystals present higher dimension, which compromises the formation of a compact passivation layer[11]. Common procedures such as increasing the chromate content of the cement or adding water-soluble chromates into the preparation and

chromate conversion layers (CCL) have a favourable effect on blocking initial zinc corrosion. Consequently, these have been trivial procedures employed to prevent hydrogen gas evolution and to protect the galvanized rebars[18]. However, due to the toxicity of Cr(VI) ions, actual commercialized Portland cements have limited the content of Cr(VI) in their composition and the use of CCL is currently being avoided.

Multiple studies have been performed to find alternatives to mitigate the harmful effects of an initial excessive reaction between the cement pastes and the zinc[28-33]. Nevertheless, processes with similar performances of CCL in the presence of chloride have not been achieved yet.

Sol-gel process became an important field of research during the last years and have been shown to be an adequate route to produce OIH coatings[34-40]. Several studies have demonstrated[41-44] that the mechanical and electrical properties of these materials make them suitable pre-treatments to improve the corrosion resistance of several metals and alloys.
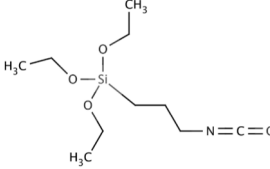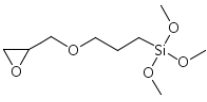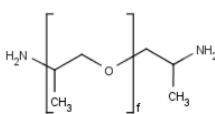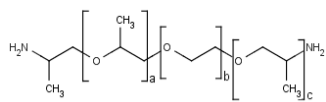
In this study, different OIH gel coatings obtained by sol-gel process were assessed as possible eco-friendly alternatives to replace the use of Cr(VI) ions to control the reactions that occur in the first instances of contact of the HDGS with fresh concrete. HDGS samples coated with the different OIH ureasilicate based gel were evaluated when in contact with cementitious media for a period of 74 days. The barrier efficiency of pure OIH coatings with similar Cr(III) doped gels were compared by using electrochemical techniques (macrocell current density, i_{gal}, and polarization resistance R_p) and surface analysis (Scanning Electronic Microscopy/Energy Dispersive Spectrometry, SEM/EDS). The implemented treatment approach was an attempt to combine two advantageous factors: the inhibition properties of the Cr(III) ion, which has comparatively lower toxicity than Cr(VI), and the enhanced mechanical properties of the support gel matrix that contributes to ion immobilization and acts as a physical barrier against corrosive external media.

2. Experimental

2.1. Reagents

The OIH gel matrices were prepared following a well-established methodology[35-36]. The structures and specifications of gel precursors are presented in Table 1.

Table 1. Structural and physical details of reagents used in OIH synthesized samples.

Chemical Name Molecular Formula	Chemical Structure	Abbreviation	M (gmol^{-1})	$\rho_{25°C}$ (gcm^{-3})
3-Isocyanatopropyltriethoxysilane C$_{10}$H$_{21}$NO$_4$Si		ICPTES (Aldrich)	247.37	1.002
3-Glycidoxypropyltrimethoxysilane C$_9$H$_{20}$O$_5$Si		GPTMS (Aldrich)	236.34	1.070
O,O'-bis(2-aminopropyl) polypropyleneglycol 130		Jeffamine D-230® (Fluka)	230$^{a)}$	0.948
O,O'-bis(2-aminopropyl) polypropyleneglycol 300	Similar	Jeffamine D-400® (Fluka)	400$^{a)}$	0.972
Poly (propyleneglycol)-block-poly (ethyleneglycol)-block-poly (propyleneglycol)-bis-(2-aminopropylether)-600		Jeffamine ED-600® (Fluka)	600$^{a)}$	1.035
Poly(propyleneglycol)-block-poly (ethyleneglycol)-block-poly (propyleneglycol)-bis-(2-aminopropylether)-900	Similar	Jeffamine ED-900® (Fluka)	900$^{a)}$	1.065
Poly(propyleneglycol)-block-poly (ethyleneglycol)-block-poly(propyleneglycol)-bis-(2-aminopropylether)-2000	Similar	Jeffamine ED-2000® (Fluka)	2000$^{a)}$	1.068

Notes: a) MW approximate value.

Five di-amino functionalized polyether (hereafter referred generically as Jeffamine) with different molecular weights were used. The Jeffamine D-230 and D-400 exhibit distinct molecular structures of Jeffamine ED-600, ED-900 and ED-2000. The polymeric chains of the first two di-amino functionalized compounds are based exclusively in propyleneglycol monomers, while the higher molecular weight are block co-polymers based on propylene-ethylene-ethylene glycols sequences. All the used Jeffamines and the functionalized siloxane (3-isocyanate propyltriethoxysilane) were stored protected from light and used as supplied.

Ethanol (EtOH, absolute 98 %, Riedel-de-Haën), citric acid monohydrate (Merck), and chromium (III) nitrate nonahydrate (Aldrich) were also used as received. Ultra-pure water (0.055-0.060 µS/cm) obtained from a Purelab Ultra System (Elga) was used.

2.2. Synthesis Procedure of OIH Ureasilicate Matrix Monoliths Discs and Coatings by Sol-Gel Method

The experimental steps involved in the synthesis of OIH matrices to produce samples (films) or coated HDGS samples are schematically described in Figure 1. The precursor (Jeffamine) was available with five different molecular weights, therefore two sets of different materials were prepared: the pure OIH matrices and the OIH matrices doped with Cr(III) ions. Each of the sets were prepared as a thin circular disk and as coating layer on HDGS (Table 2).

Table 2. Adopted representation codes for the different prepared material samples

	Specimen			
	OIH disk sample		HDGS OIH coated sample	
Jeffamine	Pure Matrix	Cr(III) doped	Pure Matrix	Cr(III) doped
D-230®	U(230)	U(230)_Cr(III)	HDGS/U(230)	HDGS/U(230)_Cr(III)
D-400 ®	U(400)	U(400)_Cr(III)	HDGS/U(400)	HDGS/U(400)_Cr(III)
ED-600®	U(600)	U(600)_Cr(III)	HDGS/U(600)	HDGS/U(600)_Cr(III)
ED-900®	U(900)	U(900)_Cr(III)	HDGS/U(900)	HDGS/U(900)_Cr(III)
ED-2000®	U(2000)	U(2000)_Cr(III)	HDGS/U(2000)	HDGS/U(2000)_Cr(III)

Both materials were produced from a single batch of precursor solution, that was obtained using 1:2 stoichiometric molar ratio of each Jeffamine molecular weight and ICPTES mixed in a glass container and stirred at 700 rpm, for 20 min. The first stage of preparation of the OIH matrix network involved the formation of urea bonds between the organic and inorganic components. The reaction between the amine end group ($-NH_2$) of Jeffamine, with different molecular weights (Jeffamine D-230®, Jeffamine D-400®, Jeffamine ED-600®, Jeffamine ED-900® and Jeffamine ED-2000®) and the isocyanate group (-N=C=O) of ICPTES, led to the formation of the precursors of future gel matrices, hereafter referred as: U(230), U(400), U(600), U(900) and U(2000).

In the second stage, 0.22 M citric acid ethanolic solution was added to set the citric acid/ICPTES molar ratio to 0.094. The mixture was stirred for 15 minutes to obtain a homogeneous mixture, and depending on the sample to be obtained, 0.01 M of Cr(III) aqueous solution was added, or not. The volume of salt solution added was adjusted to ensure that the Cr(III)/ICPTES molar ratio is set to

2.938 x10^{-4}. As the total volume of reaction media was equal to 8 mL, so the final added volume of water was dependent on the volume of added Cr(III) solution and finally the mixture was stirred for another 15 min. Part of the prepared mixture was placed into a Petri dish (polystyrene, 2 cm of diameter, supplied by Sarstedt), and this was subsequently placed in an incubator-compressor (*ICP-400*, Memmert) and kept at 40 ºC for about two weeks to ensure a precise control and reproducibility conditions of hydrolysis/condensation reactions as well the evaporation of the remaining solvents.

Figure 1 highlights the implemented preparation conditions that led to samples that were highly transparent and to homogeneous disks free of cracks in which the flexibility increased with higher molecular weight of Jeffamine used.

Coated HDGS samples were prepared by using a dip coater (Nima, model DC Small). HDGS metal plates were dipped in the remaining part of the prepared mixtures at a withdrawal speed of 10 mm min^{-1} without residence time. It should be pointed out that a total of 10 different OIH gel compositions were produced consisting of two sets of coated HDGS samples with one and three dip steps. Used HDGS metal samples with dimensions of 5.0x1.0x0.1 (in cm) and with a Zn average thickness of 16 μm on both sides were obtained from commercially available plates. The curing of the coated HDGS samples was performed following the same conditions used to obtain the gel disks.

2.3. Preparation of Mortar and Cement Paste

The corrosion behaviour of HDGS coated with the different OIH coatings was studied in mortar and cement pastes. The mortar was prepared according to EN 196-1 standard[44] using cement type I 42,5R, distilled water and normalized sand (AFNOR) with a weight ratio of 6:2:1 (sand:cement:water). The cement paste was prepared using the same cement type used in mortar preparation and a weight ratio of cement:water equal to 2:1.
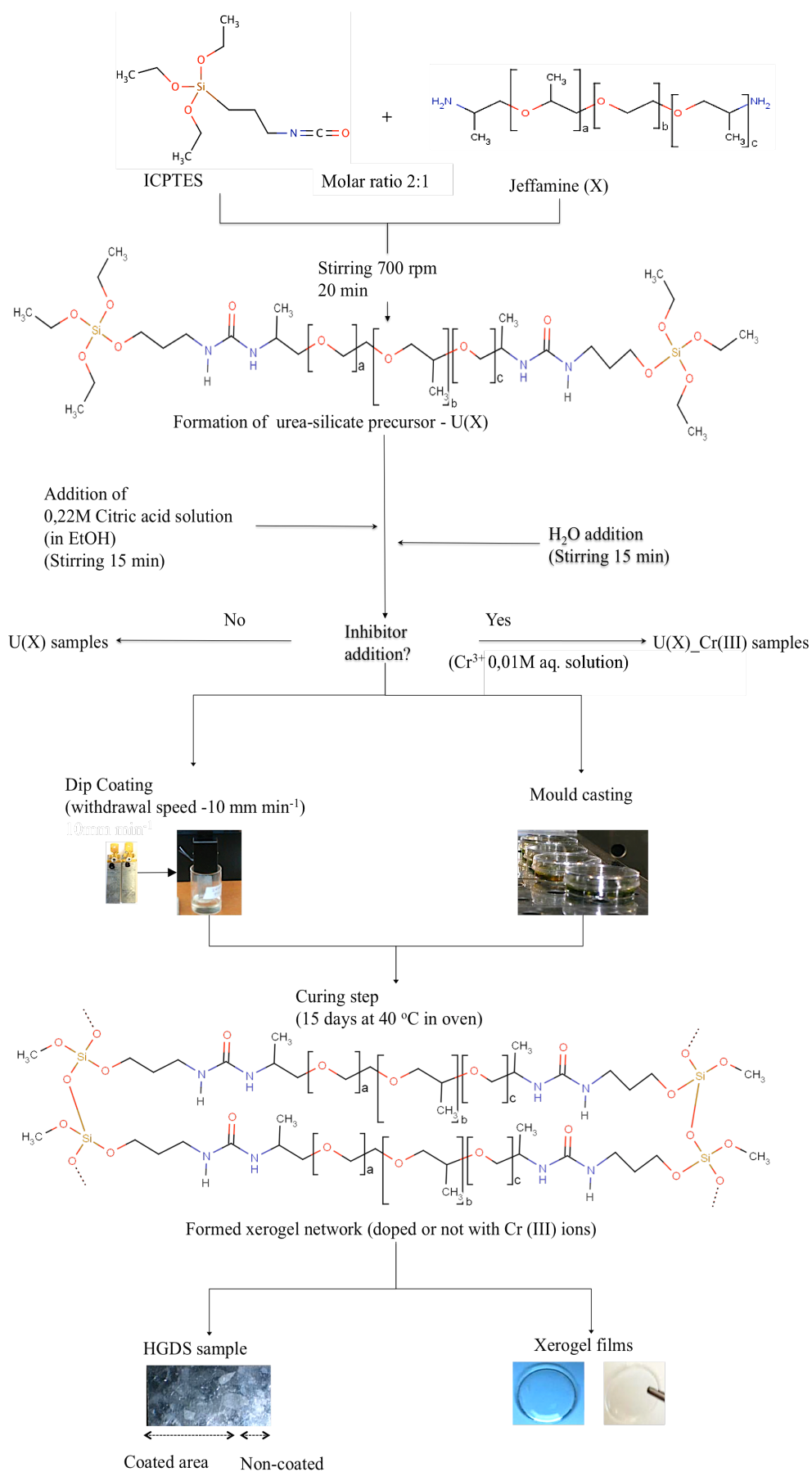
Figure 1. Schematic representation of the main steps involved in the production of OIH films and coatings.

2.4. Electrochemical Studies

The corrosion behaviour of the HDGS coated with OIH was assessed by polarization resistance (R_p) measurements and macrocell current density (i_{gal})[45]. OIH gel samples (disks) were also characterized by electrochemical impedance spectroscopy (EIS) measurements.

2.4.1. Electrochemical Impedance Spectroscopy (EIS)

EIS measurements were carried out to characterize electrical resistivity and capacitance of the prepared OIH disk films, using two Au disc electrodes (10 mm diameter and 250 µm thickness) and a support cell adapted from a previously used model[46]. Measurements were performed at room temperature using an Impedance/Gain-Phase Analyzer (Model 1260A, Solartron-Schumberger) and a Potentiostat/Galvanostat (Model 1287A, Solartron-Schlumberger) controlled by a PC using Zplot software (Solartron-Schlumberger, version 2.9c). Measurements were taken by applying a 10 mV (peak-to-peak, sinusoidal) electrical potential within a frequency range from $1x10^5$ Hz to 0.01 Hz (10 points per decade) between the two Au electrodes at open circuit potential. The frequency response data of the studied electrochemical cells were displayed in a Nyquist plot, using ZView software (Solartron-Schlumberger, version 2.9c) that was also used for data fitting purposes.

2.4.2. Macrocell Current Density (i_{gal})

The i_{gal} measurements were performed using a system based on two parallel electrodes (rectangular metal plates with dimensions of 5.0x1.0x0.1 cm). The working electrode (WE) was a HDGS plate with an active area of 2 cm^2 coated as described previously. The counter electrode (CE) was a stainless steel (SS, type 316L) plate with an active surface section of 2 cm^2. The edges of both of the electrode plates, as well the non-active area and connecting zones were protected with dual-component epoxy resin (Araldite®)[47-48]. The set of two electrodes was fixed in plastic lids that fit in a 100 mL polyethylene flask (Normax). For comparison purposes, cells prepared with non-coated HDGS WE electrodes were used as a reference (hereafter referred generically as control). To assemble the electrochemical cells used to measure i_{gal}, 120±10g of fresh mortar was transferred to a 100 mL polyethylene flask, subsequently the electrodes were immersed and the flask closed.

Using an automatic data acquisition system (Datataker DT505, series 3), i_{gal} measurements of prepared cells, were performed through reading the potential difference to the terminals (shunted with a 100 Ω resistor). Measurements were performed at one-minute intervals during the first seven

days, and at each five minutes during the remaining time until the record was completed, on the 74th day.

2.4.3. Polarization Resistance (R_p)

The R_p measurements were performed with a three-electrode electrochemical cell system using a previously established protocol[47-48]. The CE and WE electrodes were assembled and protected as described previously. Titanium-activated wire with a length of one cm was used as reference electrode (RE). The electrodes were connected to an isolated copper cable and the cutting zone of the tip of the titanium electrode was covered with epoxy resin. For comparison purposes, cells with non-coated HDGS WE electrodes were prepared and used as reference (hereafter referred generically as control). The R_p values were estimated by the potentiostatic method using a potentiostat/galvanostat (Voltalab PGZ 301) according to the referred protocol[47-50].

2.5. Scanning Electron Microscopy (SEM/EDS)

The morphology of the OIH sol-gel coating surface applied on HDGS specimens was analysed with a scanning electron microscope (SEM, JEOL JSM-6400) coupled with an EDS detector (Inca-xSight Oxford Instruments), and the surface of specimens were covered with an ultrathin coating of gold deposited by sputter coating. The SEM/EDS studies of the HDGS coated samples were performed on the substrate before and after being in contact with cement paste for 7 and 14 days and after 74 days in contact with mortar. The hardened cementitious materials were carefully 239 broken to release the HDGS specimens and SEM/EDS observations 240 were made promptly.

3. Results and discussion

3.1. Electrochemical Studies

3.1.1. EIS Measurements

EIS is commonly used for the characterization of protective properties of coating on corrodible metal[51-54]. Many studies were focused on the change in the impedance of coated metals as they undergo either natural or artificial exposure to conditions that cause corrosive failure of such

systems[54-57]. Some articles suggest that if the resistance of the coating is $< 10^7$ Ω cm^2, then such coatings no longer offer protection[57-59].

Figures 2 and 3 present the Nyquist complex impedance plots obtained from the EIS analysis of prepared film samples. Due to different obtained behaviour plots for the U(600) and U(600)_Cr(III) films, EIS data are displayed in Figure 2. The results obtained for U(900), U(900)_Cr(III), U(2000) and U(2000)_Cr(III) films are plotted in Figure 3.
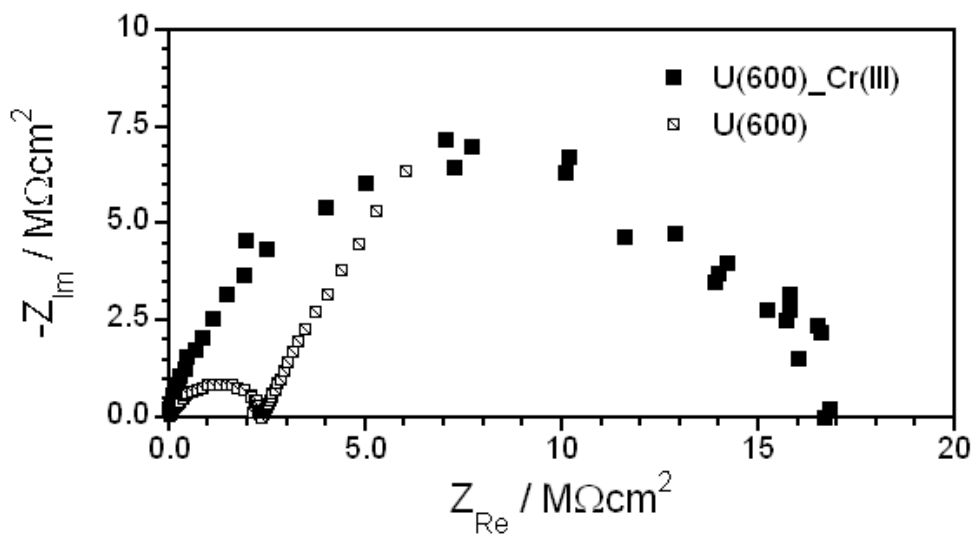

Figure 2. Typical complex plane impedance plots obtained for OIH films based on U(600) matrix

Figures 2 and 3 show that at higher applied frequencies both graphs describe a semicircle, which intercepts the x-axis.

The amplitude of the semi-circles changes with sample composition indicating that this is assigned to the dielectric characteristics of the OIH gel sample such as resistivity and capacitance. Data obtained at lower applied frequencies describes a line suggesting another electrochemical process probably assigned to Au/OIH interfacial phenomena.
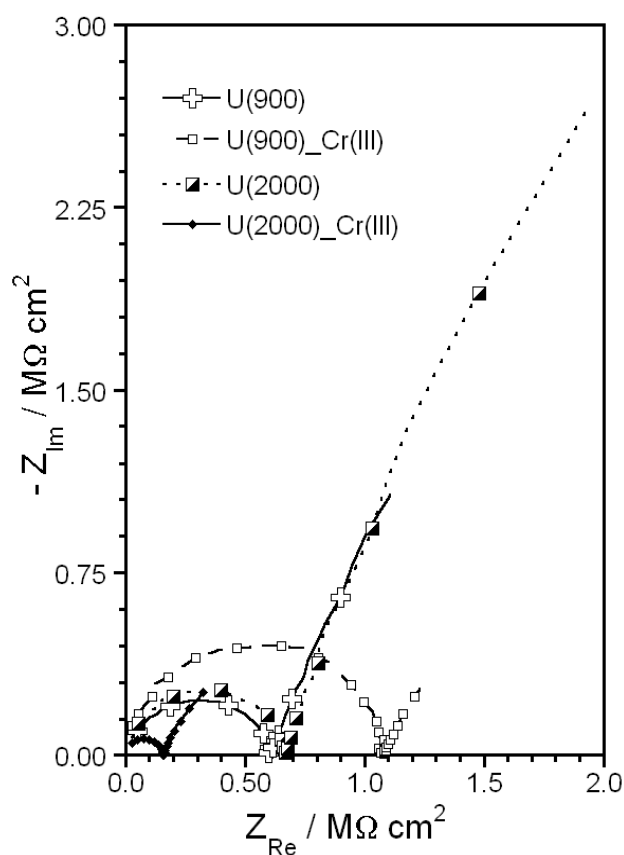
Figure 3. Typical complex plane impedance plot obtained for OIH films based on U(900) and U(2000) matrices.

An equivalent circuit as shown in Figure 4 was used to describe the observed impedance response of the cell configuration used in these measurements. This was built by the association of two sets of resistances and capacitors connected in parallel. These circuit components are identified as the association of two distinct behaviours: the dielectric response of the OIH gel (electrolyte) and the two identical established Au/OIH blocked interfaces. The OIH behaviour is characterized by the conjugation of a high resistivity, assigned to charge transport across the gel material, and the geometric capacity derived from the dielectric behaviour of the support matrix. The two processes are described by an equivalent circuit involving the association of a resistance (R_{sample}) in parallel with a capacitance (C_{sample}).
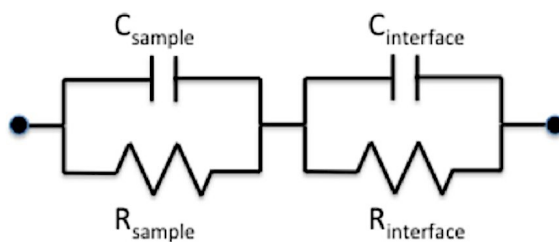
Figure 4. Equivalent circuit used to describe the observed impedance response of the cell configuration developed for measurements of OIH films electric properties.

Concerning the inertness of Au electrodes and the low value of the potential applied, the Au/OIH gel interfaces could be described by a similar association, in parallel, of the interfacial resistance ($R_{interface}$) and capacitor ($C_{interface}$), which describe, respectively, the interfacial charge transfer and the capacity that arises from the charge established at the Au/OIH interface. When the time constants for the two regions are similar, the consequent responses in frequency are overlapped and a single electric sub-element could be used. The two semicircles observed at distinct applied frequency ranges result from capacitance time constants with large differences associated with the charge transport across the OIH and the charge relaxation that occurs at the interfaces.

The use of EIS analysis to obtain resistivity data about OIH disk films based on U(230) and U(400) matrices, with and without Cr(III), could not be performed. This may be due to the combination of the high rigidity and the low conductivity of these materials that contribute to a poor electric contact between the OIH film and the Au electrode disks. It is suggested that the resistance of the electrical interface is higher than the operational measuring range of the equipment used for EIS analysis.

The values of resistivity (ρ) and the capacitance (C), were normalized to cell geometry dimensions and to the cross section area of the Au electrode, respectively. The obtained values were calculated using the following equations (where A_{Au} is the area of the gold electrodes and d_{sample} the thickness of the analyzed OIH film sample):

$$\rho = R_{sample} \times A_{Au} / d_{sample} \tag{1}$$

$$C = C_{sample} \times A_{Au\ disk} \tag{2}$$

The values of R_{sample} and C_{sample} were obtained by fitting the data corresponding to the high frequency semi-circle data to a RC equivalent circuit following the commonly used procedure[36].

Table 3 shows the average values of the logarithm of resistivity (log ρ) and normalized capacitance from five samples of each OIH film (uncertainty is expressed for 95% confidence).

Table 3. Resistivity (ρ) and normalized capacitance (C) of analyzed OIH film samples.

Specimen	log ρ/ log (Ω cm)	C/ nF cm (a)
U(600)	7.72±0.36	0.117±0.018
U(600)_Cr(III)	8.07±0.06	0.024±0.008
U(900)	7.06±0.10	0.050±0.013
U(900)_Cr(III)	6.92±0.24	0.021±0.004
U(2000)	6.77±0.24	0.030±0.004
U(2000)_Cr(III)	5.93±0.26	0.016±0.003

Note (a) Capacitance values normalized to cell constant

Table 3 demonstrates that for all analyzed OIH film samples, ρ is between 10^6 and 10^8 Ω cm. It is predicted that OIH films based on U(230) and U(400) matrices could have higher ρ values than those obtained for the other OIH. Pure and Cr(III) doped OIH samples show a negligible difference of (log ρ) when the same Jeffamine was used. The resistivity of Cr(III) OIH doped gels decreases by two orders of magnitude when the Jeffamine molecular weight is changed from 600 to 2000.

These results are very promising, as the inclusion of Cr(III) ions does not significantly change the resistivity of the OIH films, preserving their barrier efficiency. Data from Table 3 also shows that the capacitance of the produced OIH samples seems not to be significantly affected by the presence of Cr(III) with exception of OIH based on U(600) matrices.

3.1.2. i_{gal} Measurements

Figure 5 shows the macrocell current density (i_{gal}) collected from the 20 different prepared electrochemical cells involving the HDGS coated samples plus the control that were embedded in the mortar during a period of 74 days.

All the measured macrocell current densities show higher values during the first seven days and a gradual decrease to lower values with time. It was also verified that the control (OIH coating free HDGS sample) shows higher i_{gal} values compared to those involving HDGS OIH coated samples.

129

The difference of i_{gal} values between the control and the OIH based on U(400) pure matrix (Figure 5b) show to be the highest of all sets of samples coated with OIH pure matrices. Concerning the HDGS samples coated with Cr(III) doped OIH matrices the lowest i_{gal} values were obtained for the sample coated by one dipping step of U(2000)_Cr(III) OIH gel (Figure 5e).

The lowest i_{gal} values, taken from all sets of samples after 28 days, were obtained for HDGS coated with OIH matrices based on U(230) matrix (Figure 5a). Although a slight increase is observed with time, i_{gal} behaviour evolves with time to lower values after 70 days. It is also observed that Cr(III) doped OIH coatings present higher i_{gal} values and have a similar behaviour during the first 28 days regardless of the number of deposited layers. Although the Jeffamine precursor used have different structures and compositions, they show the same two terminal amine groups. After reaction with functionalized siloxane (ICPTES), two urea bonds are formed between each terminal amine (from Jeffamine) and the isocyanate groups (from ICPTES). The final structure of the OIH gel could be described as two blocks co-existing within a network: the rigid inorganic (silicate based) backbones (which give enhanced mechanical properties to the final material) are spaced by flexible organic (polyether) chains linked by the mentioned urea bonds (Figure 1). When the sol-gel precursor is applied on HDGS surfaces, a new interface is formed between the components of the ureasilicate network and the metal surface.

The nature of the gel precursors suggests that interaction between the network components and HDGS substrate happens preferentially with the silicate groups. The organic part of the OIH is somehow kept away from the metal surface due to its predominant hydrophobic characteristics. Considering this hypothesis, the role of Jeffamine is essential to minimize cracking of the deposited gels during the curing process (due to network stress as the formation of silicate regions involves the release of EtOH molecules).

Overall, the obtained i_{gal} data highlights that OIH gels based on high Jeffamine molecular (Figures 5c, 5d and 5e) weights reveal a less efficient barrier effect when compared to lower molecular weights (Figures 5a and 5b). This effect could also be related to the observed decrease of reactivity between ICPTES and Jeffamine, as confirmed by the observation of a reduced exothermic reaction. The increase in molecular weight suggests that less extensive bonds between these two reagents occur and consequently a less compact network is formed, compromising the barrier properties.
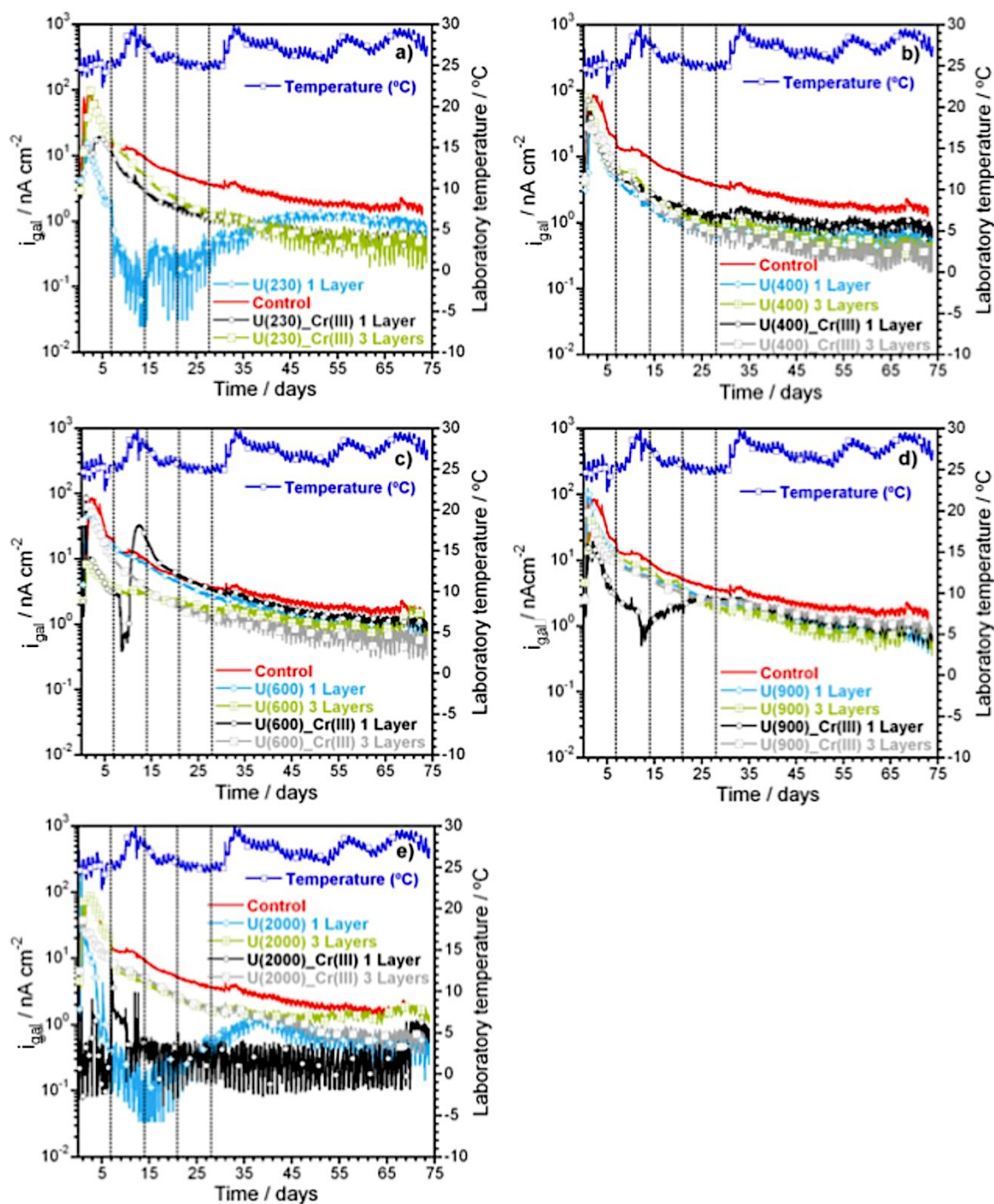
Figure 5. Plots of the variation macrocell current density (i_{gal}) and laboratory temperature with time recorded for the different coated HDGS sample cells (kept embedded in mortar for 74 days). Displayed graphs correspond to the five different used OIH ureasilicate matrices: a) U(230); b) U(400); c) U(600); d) U(900) and e) U(2000).

The obtained data suggests that coatings deposited with a single layer (with and without Cr(III) ions) are shown to provide better barrier protection properties to HDGS when compared to coatings with three layers. These differences are most likely explained by the varied amount of gel precursors that

were deposited over the HDGS, when one or three dips were performed. The probability of the coating thickness changing along the length of the sample is influenced by the amount of precursor solution deposited on the sample's surface, the sol viscosity, the dip-coating procedure and the period of time necessary for gelation and curing processes. The above-mentioned factors could not be controlled in this experiment to a satisfactory level to obtain reproducible samples when a triple dip step was used. Further experiments have to be performed to validate this hypothesis, particularly when high molecular weight Jeffamines are involved. Future research should take into account modifications on gel synthesis by controlling sol viscosity, on gel deposition such as dip-coating procedures (optimizing dipping speed and residence time) and on HDGS OIH gel coating curing conditions.

3.1.3. R_p Measurements

The determination of the R_p values was performed once a day during the first seven days and then on the 10th, 21st and 70th day. The results obtained for the cells of all five sets of HDGS coated samples are presented in Figure 6. The value of $10^6\ \Omega\ cm^2$ has been considered as a threshold limit value above which steel is passivated in cementitious materials[3,9,18,50], and is represented by a horizontal line on all the plots.

Table 4 summarizes the relevant data about some of the characteristic of R_p evolution along an elapsed time for all the studied cells.

The following information is gathered in this table: the observed time (in days) necessary for R_p to reach passivation threshold values, the evolution of polarization resistance after the threshold moment and the R_p value at the end of the monitoring period (74 days).

As observed from the collected results, with the exception of HDGS samples coated with three layers of OIH U(2000) (Figure 6e), all the coated samples achieved passivation threshold earlier than the control samples. In the studied conditions, HDGS coated with OIH reach passivation earlier than the control, which is in agreement with i_{gal} data measurements.

Generally, lower R_p values were obtained for all cells during the first seven days, suggesting that zinc corrosion occurred, which is also in agreement with i_{gal} results. After this period, the HDGS coated samples show higher R_p values when compared to the control. On the 70th day, the R_p passivation threshold value ($10^6\ \Omega\ cm^2$) is overcome for all the OIH coated samples.

Analysing the data obtained for HDGS coated with OIH U(230) (Figure 6a), it is observed that the substrate with one layer of OIH gel passivates after seven days, but suddenly drops to values under the limit of passivation for the period between the 10th and 21st day, rising again to R_p values above the passivation limit by the 74th day. Samples with one and three layers of OIH U(230)_Cr(III) passivate only after 21 days of exposure. Control and HDGS coated with pure OIH U(230) samples present a very similar behaviour along time but demonstrate differences in the magnitude of recorded R_p values. These results might arise from the coating heterogeneity over the substrate surface. Due to the roughness of the zinc layer, the thin OIH U(230) coating does not cover the substrate uniformly and the small uncovered areas could be susceptible to the high pH of the electrolyte.

Table 4. Systematic presentation of observed R_p values variation on the studied cells.

Matrix	Control [a]	Pure		Cr(III) doped	
		(1 layer)	(3 layers)	(1 layer)	(3 layers)
U(230)	t = 56 [b]	t = 8	n. a.	t = 18	t = 15
	$\Delta R_p > 0$ [c]	$\Delta R_p > 0$		$\Delta R_p > 0$	$\Delta R_p < 0$
	$R_{p70} = 1.34$ [d]	$R_{p70} = 2.14$		$R_{p70} = 3.33$	$R_{p70} = 4.32$
U(400)	t = 56	t = 10	t = 14	t = 19	t = 13
	$\Delta R_p > 0$	$\Delta R_p < 0$	$\Delta R_p < 0$	$\Delta R_p > 0$	$\Delta R_p < 0$
	$R_{p70} = 1.34$	$R_{p70} = 4.52$	$R_{p70} = 3.44$	$R_{p70} = 7.90$	$R_{p70} = 2.67$
U(600)	t = 56	t = 14	t = 12	t = 48	t = 18
	$\Delta R_p > 0$	$\Delta R_p > 0$	$\Delta R_p < 0$	$\Delta R_p > 0$	$\Delta R_p > 0$
	$R_{p70} = 1.3$	$R_{p70} = 15.2$	$R_{p70} = 1.92$	$R_{p70} = 1.59$	$R_{p70} = 5.33$
U(900)	t = 56	t = 12	t = 45	t = 16	t = 19
	$\Delta R_p > 0$	$\Delta R_p < 0$	$\Delta R_p > 0$	$\Delta R_p < 0$	$\Delta R_p > 0$
	$R_{p70} = 1.3$	$R_{p70} = 2.83$	$R_{p70} = 3.03$	$R_{p70} = 1.51$	$R_{p70} = 5.53$
U(2000)	t = 56	t = 16	t = 63	t = 14	t = 18
	$\Delta R_p > 0$	$\Delta R_p < 0$	$\Delta R > 0$	$\Delta R_p < 0$	$\Delta R_p > 0$
	$R_{p70} = 1.3$	$R_{p70} = 5.82$	$R_{p70} = 7.88$	$R_{p70} = 10.0$	$R_{p70} = 2.66$

Notes: (a) Data obtained from the cell built with uncoated HDGS working electrode (b) Time (in days) when R_p passivation threshold is achieved (value estimated by interpolation), (c) Evolution of normalized R_p value after threshold time: constant ($\Delta R_p = 0$); increasing ($\Delta R_p > 0$); decreasing ($\Delta R_p < 0$), (d) $R_p \pm 0.01$ value after 70 days (in $M\Omega$ cm^2).

It can be verified that the pure OIH U(230) (Figure 6a)) and U(400) (Figure 6b)) HDGS samples coated with one layer exhibit higher values of R_p when compared respectively with the doped matrices. This behaviour is in agreement with Zheludkevich and co-workers[60] who verified that the selection of an inhibitor and its constituent compound might be critical to the stability of the sol–gel network.
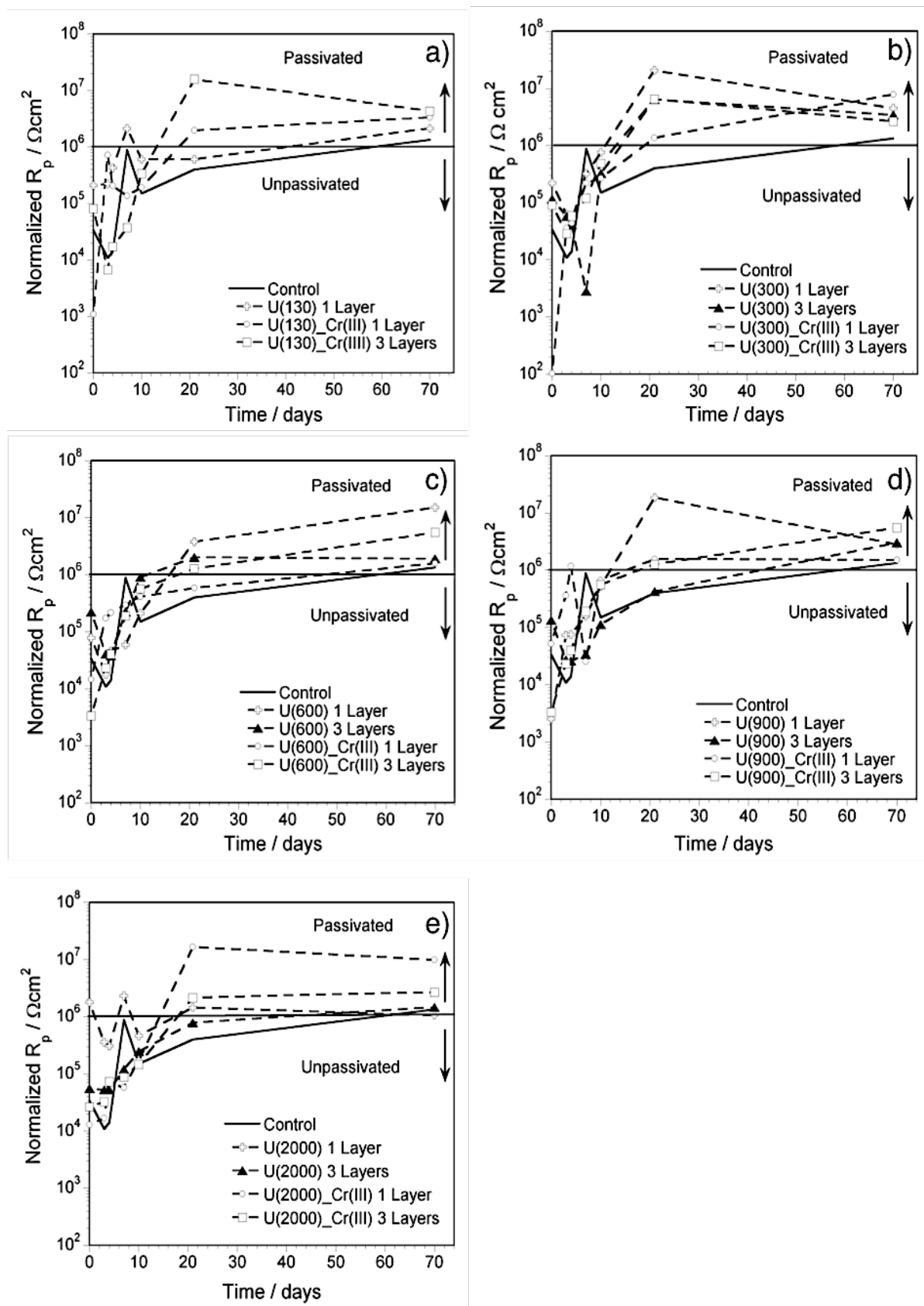
Figure 6. Plots of the variation of cell R_p, normalized polarization resistance, with time recorded for the different coated HDGS cells samples (kept embedded in mortar for 74 days). Displayed graphs correspond to the five different used OIH ureasilicate based matrices. a) U(230); b) U(400); c) U(600); d) U(900) and e) U(2000).

These arguments may justify the observed differences between the samples coated with Cr(III) doped OIH gels, as in the first stages these ions might not be in a non-free ionic form but in a more complex form involving the interaction of the available species or network functional groups. The formation of chemical bonds with free Cr(III) within the gel matrix could compromise the hybrid network stability. The evolution of R_p values of cells coated with OIH based on U(2000) matrix (Figure 6e)) are similar to the other OIH coatings. The samples coated with one layer OIH U(2000)_Cr(III) gel show the best performance (higher R_p values) of all the studied samples and passivates on the 21st day.

3.2. SEM/EDS Analyses

Surface morphology of coated HDGS samples was assessed by SEM/EDS analysis before (Figures 8 and 9) and after contact with a high alkaline environment (Figures 7, 10 and 11).

SEM analyses revealed that OIH coatings cover the HDGS substrate regardless of the number of dips and the OIH composition (Figure 8).

The results for HDGS samples coated with different OIH non-doped coatings, embedded in mortar for 74 days, are displayed in Figure 7. The obtained images and spectra show that the performance of the OIH based protective layer is significantly affected by the molecular weight of the Jeffamine incorporated into the OIH coating. OIH gels based on high Jeffamine molecular weights show traces of Fe (Figures 7d, 7e and 7f) suggesting that the OIH coating was eroded as well the Zn protective layer. However, these results demonstrate less erosion than the control (Figure 7a). Nevertheless, coatings based on U(230) and U(400) matrices (Figures 7b and 7c) were shown to provide an adequate protection since no traces of Fe were found. It has also been demonstrated that the SEM/EDS results are in agreement with the data obtained by i_{gal} and R_p measurements, where OIH with high Jeffamine molecular weights present lower R_p and higher i_{gal} values; however, the results obtained by the control showed lower and higher R_p and i_{gal} values respectively.

A detailed analysis of the morphological modifications produced on HDGS coated samples, after exposure to a highly alkaline environments, was focused on U(230) based OIH coating. The choice of this particular set of samples was supported by the evidence that this OIH formulation provides an enhanced protection when compared to the other OIH formulations.
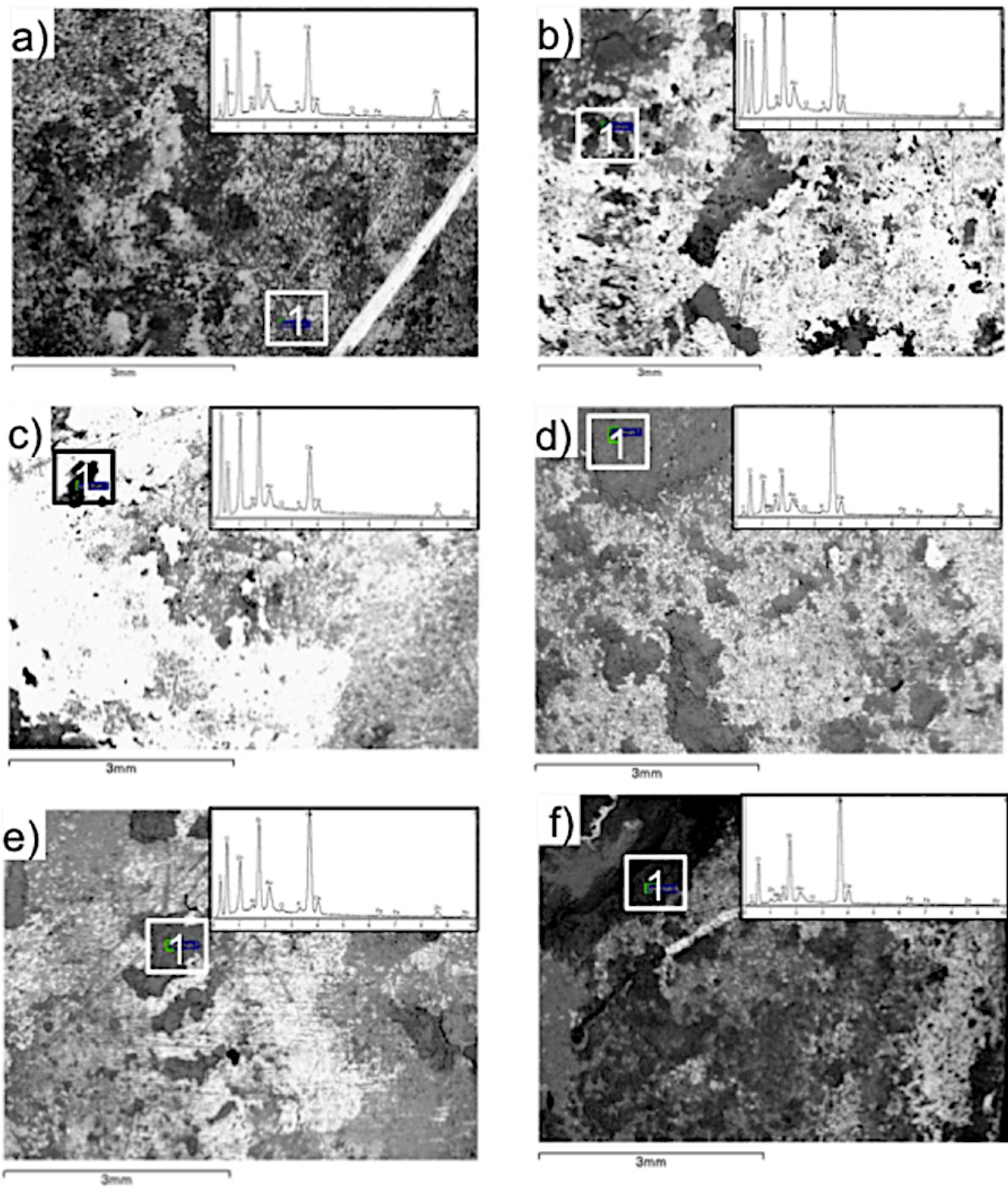
Figure 7. SEM images and EDS spectra (inset) of HDGS samples coated with different OIH compositions obtained by one dip step after being in contact with mortar for a period of 74 days: a) Control); b) U(230); c) U(400); d) U(600); e) U(900); f) U(2000).

The SEM/EDS analysis was implemented to assess the resistance of these OIH coatings after seven and 14 days respectively of contact with cement paste and after 74 days with mortar. The effect of dipping process on deposited coatings was also analyzed. Representative SEM images and EDS

analysis data obtained for the HDGS samples coated with one and three dip steps of OIH U(230), before being embedded in cement paste and/or mortar are shown in Figures 8a and 8b, respectively. The lighter areas correspond to the presence of Zn (Figure 8a.1) and the darker areas correspond to the presence of OIH U(230) (Figure 8a.2), which is shown on the EDS analysis as high intensity peaks of C, Si and O.
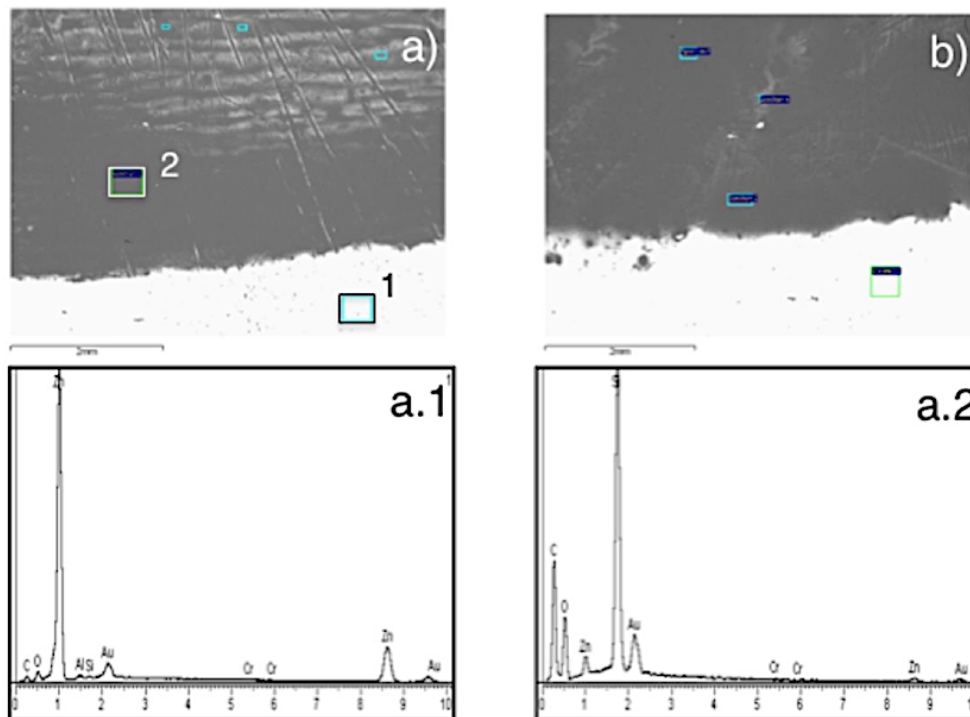

Figure 8. SEM images and EDS spectra of the HDGS sample surface coated with OIH U(230) by using: a) one dip step and b) 3 dip steps of before embedded in the electrolyte (cement paste or mortar). Images a.1) and a.2) show EDS spectra obtained by scanning two different regions of one dip step of OIH U(230) coated samples.

Figure 9 shows a higher magnification of HDGS sample coated with U(230) obtained by one dip step. The thickness of the coating on the metal surface is variable since multiple shades of grey were found. By EDS analysis it was confirmed that the darker areas present high intensity peaks of Si, C and O (Figure 9a.1), and correspond to thicker coating zones compared to light grey areas which show lower intensity peaks of Si, C, O and high peaks of Zn (Figure 9a.2) that could be interpreted as the thinnest coating area. These results are in agreement with R_p and i_{gal} values and may justify the behaviour found during the first seven days in which the R_p and i_{gal} values were

generally lower and higher, respectively. However, due to non-uniform coating, zinc corrosion may occur with a similar behaviour to the control but with values of R_p and i_{gal} of different magnitude than those obtained for the control.
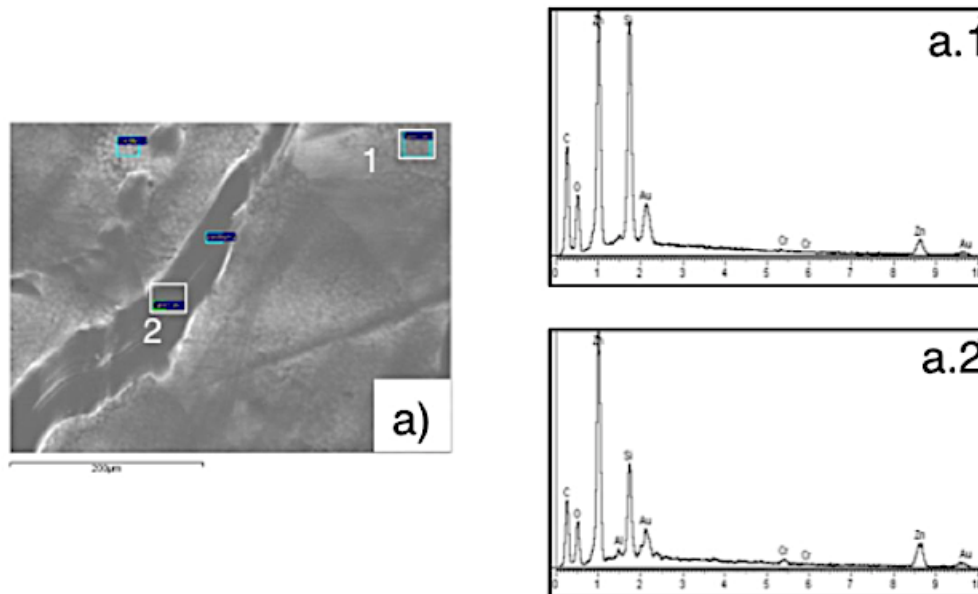

Figure 9. SEM images and EDS spectra of the HDGS sample surface coated with one dip step with higher magnification of OIH U(230) before being embedded in the electrolyte (cement paste or mortar). a.1 and a.2 shows EDS spectra obtained.

The SEM/EDS results obtained for the control and HDGS samples coated with U(230) by one dip step, after being embedded in cement paste for seven days are displayed in Figure 10.

Displayed SEM images confirmed the presence of corrosion products on the surface of the control sample (Figure 10a). According to some authors[15,16,18,23] the immersion of HDGS plates in alkaline solutions in which Ca^{2+} ions are present, such as cement paste and mortar, promotes the formation of calcium hydroxyzincate (CAHZ) therefore it is very likely that this might be present, however no further conclusions can be made about the precise corrosion products present. The distinct composition of deposits present is shown by comparing the EDS scans obtained for the control sample (Figure 10a.1) with those obtained for HDGS dipped once in OIH U(230) (Figures 10b.2 and 10b.3). The control sample shows high peaks of Fe and O and low peaks of C, which indicates that the substrate was attacked by the electrolyte (cement paste). It is postulated that the inner layers of the Zn coating were affected, namely the zeta, delta and gamma layers, which are progressively

138

richer in Fe[3]. The zinc layer was most likely partially or totally removed and iron oxides were subsequently formed (detected by high peaks assigned to their constituents).
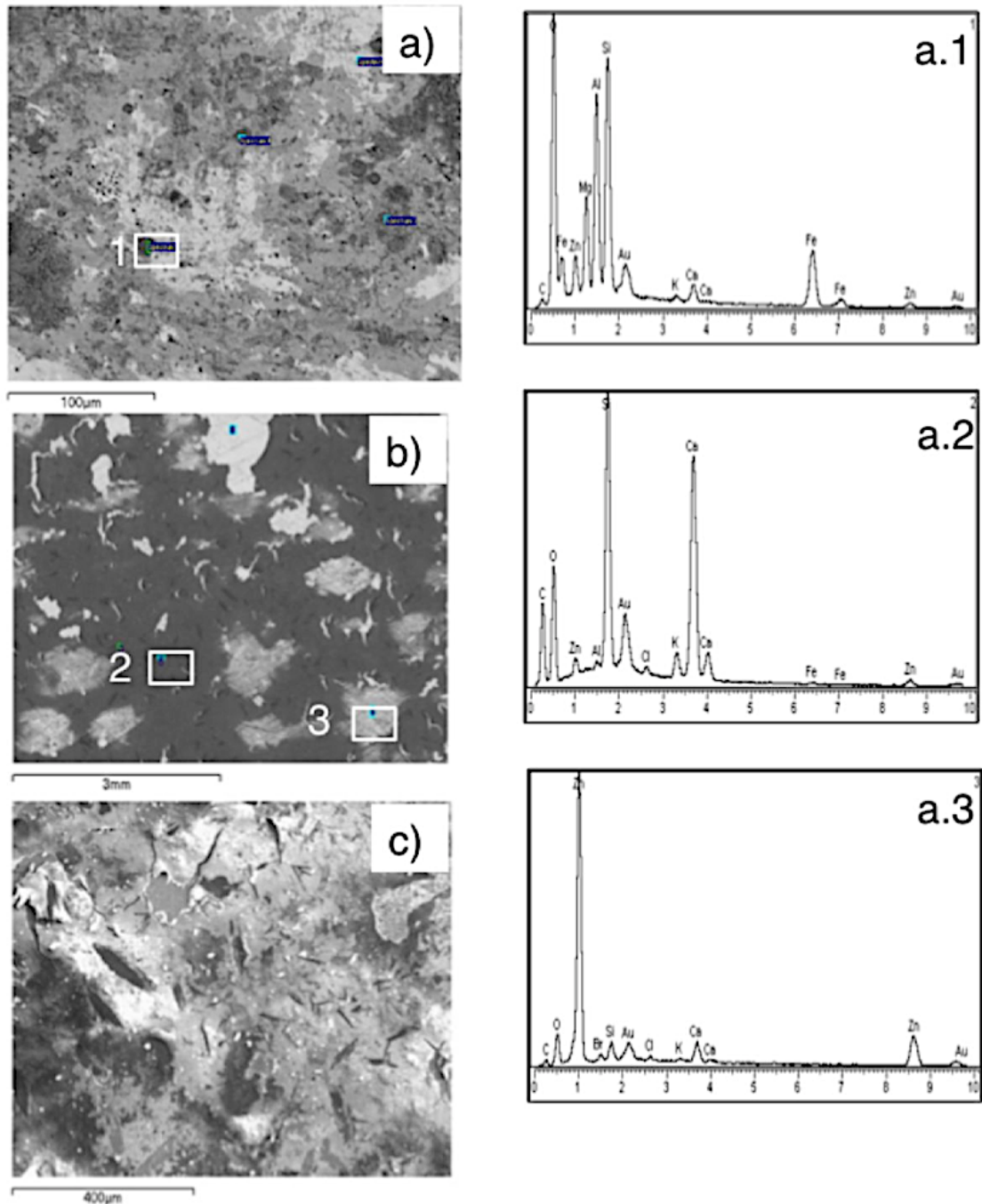

Figure 10. SEM images and EDS spectra obtained from HDGS samples seven days after embedded in cement pastes: a) Control); b) HDGS sample coated with one dip step of OIH U(230) and c) higher magnification image of HDGS coated with one dip step of OIH U(230), showing surface defects. EDS spectra were obtained from : a.1) uncoated HDGS sample; b.2) and b.3) HDGS samples coated with one dip step of OIH U(230).

EDS spectra of OIH U(230) coated samples shows the simultaneous presence of high peaks of C, Si and O (Figure 10b.2), traces of Zn (in lighter areas), zinc oxides in darker areas and very low traces of Fe (figure 10b.3). Indeed, the EDS spectrum displayed in Figure 10b.3 (collected from a lighter area of the image displayed in Figure 10b), is shown to be quite similar to that obtained by the HDGS uncoated area before being embedded in the cement paste (Figure 8a.1).

These results suggest that when the HDGS sample was removed from cement paste part of the OIH coating was pulled out. The SEM image of a coated sample with OIH U(230) by one dip step after seven days in cement paste (Figure 10c) also displays minor areas that suggest that the coating was completely removed. The different morphology of these small areas may be derived from several causes, namely: the removal of the cell from the concrete, the effect of the high pH of the electrolyte environment or the inefficiency of deposition method; however, no further conclusions could be made about the precise cause.

Figure 11 shows SEM images obtained for the control sample after being in contact with cement paste and mortar for 14 and 74 days, Figure 11a and 11b, respectively, and for the sample coated by one dip step of OIH U(230), after being embedded in mortar for 74 days, Figure 11c. EDS data obtained from the control sample after 14 days embedded in cement paste (Figure 11a.1) and after being embedded 74 days in mortar (Figure 11b.2) shows the presence of Zn, on lighter areas, and Fe and Zn oxides, on darker areas. The inner layers of the zinc layer were most likely attacked to form iron oxides and CAHZ deposits, as previously stated.

Figures 11c.3, 11c.4 and 11c.5 show the EDS spectra collected in different areas of the HDGS coated by one dip step of OIH U(230) after being embedded in mortar during 74 days. This data confirms that the OIH coating remained on the substrate as proven by the simultaneous presence of C, O and Si and absence of Fe. These results suggest that the OIH U(230) coating provides an efficient coating protection and minimizes the damage caused to the HDGS by the high pH of fresh concrete during the first moments of contact. This conclusion is due to the fact that damage to the HDGS was minimized when in contact with mortar for 74 days and with cement paste during seven days, which is a more aggressive environment than mortar. Furthermore, the chemical reaction between Zn and cement constituents is allowed for and no evidence of the creation of voids were detected in the interface between the metal and the cementitious material.
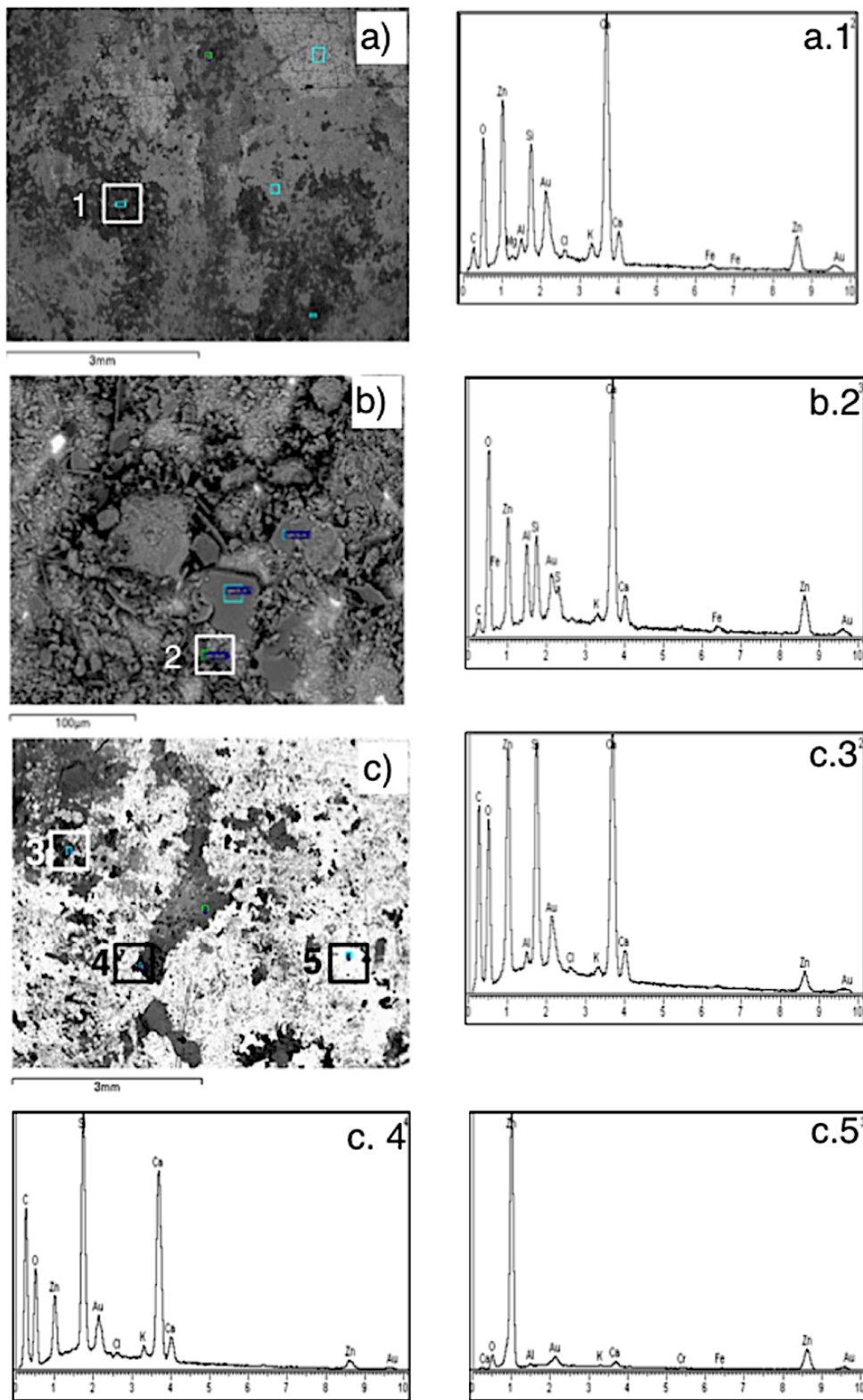
Figure 11. SEM images obtained from HDGS samples after embedded in cement paste: a) Control embedded in cement paste for 14 days; b) Control embedded in mortar for 74 days; and c) HDGS sample coated with one dip step of OIH U(230) after being embedded in mortar for 74 days. EDS spectra were obtained from: a.1) uncoated HDGS sample embedded in cement paste for 14 days; b.2) uncoated HDGS sample embedded in cement paste for 74 days; c.3), c.4) and c.5) HDGS sample coated with one dip step of OIH U(230) embedded in cement paste for 74 days.

4. Conclusions

The present work reports the corrosion protection performances of environmentally friendly OIH sol-gel based coatings for HDGS in cementitious media. These coatings were obtained from the reaction of isocyanate-derived siloxane (ICPTES) with five different diamino functionalized polyether chains with different molecular weights with and without embedded Cr(III) ions and deposited over HDGS by dip-coating methods.

From the characterization of the electric properties of pure and Cr(III) doped OIH gel, it was observed that with the exception of OIH matrix based on U(2000), these OIH materials exhibit a high resistivity ($>10^7$ Ω cm^2) and a capacitance (normalized to cell geometry) with the magnitude of low nF cm. The results suggest that the OIH materials show electric properties that are suitable for consideration as an efficient treatment. The electrochemical results obtained from cells (where the coated HDGS samples were exposed to mortar) show that all the samples display better performance when compared to control (the uncoated HDGS sample). It was also verified that the i_{gal} values are in agreement with R_p data and that both performance parameters are sensitive to the OIH composition as well as the process used to obtain the deposited coatings.

The results point to the conclusion that all the produced OIH film coatings based on ureasilicate gels have promising properties to be employed as pre-treatments to reduce corrosion activity during the initial stages of contact of the HDGS samples with the concrete alkaline environment, allowing the formation of protective layers on the surface of the substrate.

From the analysis of recorded evolution of R_p with time, it was also concluded that the OIH coatings based on U(230) and U(400) matrices achieved passivation threshold earlier than the others and consequently present better performance protecting HDGS against corrosion in the initial contact with fresh concrete. By combining SEM and EDS analysis, it was shown that the formed gel coating coverage is not continuous even when a triple dip step is used. Thus, additional experiments are necessary to study if a more uniform coating improves or worsens the performance of OIH results in preventing corrosion on HDGS without interfering in the adhesion/bond of the substrate to the concrete.

Overall, for the conditions tested in this work, the results suggest that the cathodic reaction involving hydrogen evolution was hindered or partially hindered, by the presence of OIH films.

The proposed pre-treatment shows a high potential of protection efficiency of HDGS in the early stages of contact with fresh concrete. The observed barrier effect introduced by these coatings

suggests that the thickness of deposited zinc coating may be reduced with the preservation of corrosion protection performances with an advantageous reduction of galvanization process costs and raw materials.

Acknowledgements

References

1. L. Bertolini, B. Elsener, P. Pedeferri and R. B. Polder, *Corrosion of Steel in Concrete – Prevention, Diagnosis, Repair*, p. 261, Wiley-VCH, Weinheim (2004).

2. Fédération Internationale du Béton, *Effect of zinc on prestressing steel*, FIB bulletin Nº. 64 (2012).

3. Comité Euro-International du Beton, *Coating protection for reinforcement: State of the art report*, CEB Bulletin d'Information Nº. 211 (1995).

4. A. Collazo, M. Hernández, X. R. Nóvoa and C. Pérez, *Electrochim. Acta*, **56**, 7805-7814 (2011).

5. K. J. Croes, A. J. Vreudenhil, M. Yan, T. A. Singleton, S. Boraas and V. J. Gelling, *Electrochim. Acta*, **56**, 7796–7804 (2011).

6. V. H. V. Sarmento, M. G. Schiavetto, P. Hammer, A. V. Benedetti, C. S. Fugivara, P. H. Suegama, S. H. Pulcinelli and C. V. Santilli, *Surf. Coat. Tech.*, **204**, 2689–2701 (2010).

7. H. Kaesche, *Electrochim. Acta*, **9** 383-394 (1964).

8. B. Bresler and I. Cornet, ILZRO Report No.TS-9-4 (1969)

9. W. Lieber and J. Gebauer, *Zem-Kalk-Gips*, **4**, 161-164 (1969).

10. R. Duval and R. Arliguie, *Mem. Sci. Rev. Met.*, **LXXI 11**, 719-727 (1974).

11. M. T. Blanco, C. Andrade and A. Macias, *Brit. Corros. J.*, **19**, 41–48 (1984).

12. E. Maahn and B. Sorensen, *Corrosion-NACE*, **42**, 187–196 (1986).

13. A. Macias and C. Andrade, *Corros. Sci.*, **30**, 393-407 (1990).

14. R. Robergè and W. Zheng, *Corros. Sci.,* **35**, 507-514 (1993).

15. S. R. Yeomans, *Corrosion of the zinc alloy coating in galvanized reinforced concrete*, in: Proceedings of the Corrosion'98, paper 653, NACE International, Houston, (1998).

16. M. Sánchez, M. C. Alonso, P. Cecílio, M. F. Montemor and C. Andrade, *Cement. Concrete Comp.*, **28**, 256-266 (2006).

17. R. Ghosh and D. D. N. Singh, *Surf. Coat. Tech.*, **201**, 7346–7359 (2007).

18. Z. Q. Tan and C. M. Hansson, *Corros. Sci.* **50,** 2512-2522 (2008).

19. P. H. Suegama, V. H. V. Sarmento, M. F. Montemor, A. V. Benedetti, H. G. Melo, I. V. Aoki and C. V. Santilli, *Electrochim. Acta*, **55**, 5100-5109 (2010).

20. Z. Feng, Y. Liu, G. E. Thompson and P. Skeldon, *Electrochim. Acta*, **55**, 3518-3527 (2010).

21. F. Tittarelli and T. Belleze, *Corros. Sci.*, **52**, 978-983 (2010).

22. A. Macias and C. Andrade, *Mater. Construccion*, **36**, 19-27 (1986).

23. A. Macias and C. Andrade, *Brit. Corros. J.*, **22**, 113-118 (1987).

24. A. M. S. E. Din, F. M. A. E. Wahab and S. M. A. E. Haleem, *Werkst Korros.*, **24**, 389-394 (1973).

25. F. Liebau and A. Amel-Zadeh, *Kistall und Technik*, **7**, 221-227 (1972).

26. C. Andrade and A. Macias, *Galvanized Reinforcement in Concrete*, p. 137 in A. D. Wilson, J. W. Nicholson and H. J. Prosser (Eds.), Surface Coating vol. 2. Elsevier Applied Science, (1987).

27. C. Andrade and C. Alonso, *Electrochemical aspects of galvanized steel*, p. 111, in S. R. Yeomans (Ed.), Elsevier, (2004).

28. S. B. Farina and G. S. Duffó, *Electrochim. Acta*, **52**, 5131-5139 (2007).

29. M. Mokaddem, P. Volovitch and K. Ogle, *Electrochim. Acta*, **55**, 7867-7875 (2010).

30. F. J. Recio, M. C. Alonso, L. Gaillet and M. Sánchez, *Corros. Sci.*, **53**, 2853-2860 (2011).

31. T. N. Vu, M. Mokaddem, P. Volovitch and K. Ogle, *Electrochim. Acta*, **74**, 130-138 (2012).

32. A. A. O. Magalhães, I.C.P. Margarit and O. R. Mattos, *Electrochim. Acta*, **44**, 4281-4287 (1999).

33. R. B. Figueira, C. J. R. Silva, E. V. Pereira and M. M. Salta, in: Proceedings of the Electrochemistry 2012 - Fundamental and Engineering Needs for Sustainable Development, München, (2012).

34. J. D. Mackenzie, *J. Non-Cryst. Solids*, **48**, 1-10 (1982).

35. V. I. Boev, A. Soloviev, C. J. R. Silva, M. J. M. Gomes and D. J. Barber, *J. Sol-Gel Sci. Techn.*, **41**, 223-229 (2007).

36. S. D. F. C. Moreira, C. J. R. Silva, L. A. S. A. Prado, M. F. M. Costa, V. I. Boev, J. Martín-Sánchez and M. J. M. Gomes, *J. Polym. Sci. Pol. Phys.*, **50**, 492-499 (2012).

37. A. Chiappini, C. Armellini, A. Chiasera, H. Jestin, M. Ferrari, E. Moser, G. N. Conti, S. Pelli, R. Retoux and G. C. Righini, *Opt. Mater.*, **31**, 1275-1279 (2009).

38. A. A. Saif and P. Poopalan, *Solid State Electron.*, **62**, 25-30 (2011).

39. B. Ma, S. Tong, M. Narayanan, S. Liu, S. Chao and U. Balachandran, *Mater. Res. Bull.*, **46**, 1124-1129 (2011).

40. L. Petrov, L. Spasov, P. Dimitrov and C. Vladov, *React. Kinet. Catal. Lett.*, **52**, 191-197 (1994).

41. T. P. Chou, C. Chandrasekaran, S. J. Limmer, S. Seraji, H. G. D. S. Wu, M. J. Forbes, C. Nguyen and G. Z. Cao, *J. Non-Cryst. Solids*, **290**, 153-162 (2001).

42. M. Zheludkevich, R. Serra, M. F. Montemor, K. A. Yasakau, I. M. Miranda Salvado and M. G. S. Ferreira, *Electrochim. Acta*, **51**, 208–217 (2005).

43. A. Pepe, P. Galliano, M. Aparicio, A. Durán and S. Cere, *Surf. Coat. Tech.*, **200**, 3486-391 (2006).

44. S. S. Pathak and A.S. Khanna, *Prog. Org. Coat.*, **62**, 409-416 (2008).

45. European Committee for Standardization, BS EN 196-1 (2005).

46. ASTM G109-07 *Standard Test Method for Determining Effects of Chemical Admixtures on Corrosion of Embedded Steel Reinforcement in Concrete Exposed to Chloride Environments.* In: Annual book of ASTM standards, 03.02, (2007).

47. C. J. R. Silva and M. J. Smith, *Electrochim. Acta*, **40**, 2389-2392 (1995).

48. E. V. Pereira, R. B. Figueira, M. M. Salta and I. T. E. Fonseca, *Sensors,* **9**, 8391-8398 (2009).

49. E. V. Pereira, *Monitorização da corrosão no betão armado*, PhD Thesis, University of Lisbon, Lisbon, (2004).

50. J. González, A. Molina, M. Escudero and C. Andrade, *Corros. Sci.*, **25**, 917-930 (1985).

51. C. Andrade, V. Castelo, C. Alonso and J. González, *Corrosion effect of stray currents and the techniques for evaluating corrosion of rebars in concrete*, ASTM STP 906, V. Chaker, American Society for Testing and Materials, Philadelphia (1986).

52. R. C. Bacon, J. J Smith and F. M. Rugg, *Ind. Eng. Chem.*, **40**, 161-167 (1948).

53. D. Loveday, P. Peterson and B. Rodgers, *JCT Coatings Tech.*, 46-52 (2004).

54. S. R. Taylor, *IEEE Trans. Electr. Insul.*, **24**, 787-806 (1989).

55. F. Mansfeld, H. Shih, H. Greene and C. H. Tsai In: J. Scully, D. C. Silverman and M. Kendig, ASTM STP 1181, p. 37. ASTM, Philadelphia, PA, (1993).

56. Y. T. Al-Janabi, A. M. Al-Ramis and H. M. S. Al-Mutairi, *Proceedings of NACE Corrosion*, Paper 759, (2000).

57. D. C. Silverman, *Corros. Rev.*, **10**, 31-77 (1992).

58. G. Bierwagen, D. Tallmann, J. Li, L. He and L. C. Jeffcoate, *Prog. Org. Coat.*, **46,** 149-158 (2003).

59. Jr. H. Leidheiser, *Prog. Org. Coat.,* **7**, 79-104 (1979).

60. Jr. H. Leidheiser, *J. Coat. Technol.*, **802**, 21-31 (1991).

61. M. Zheludkevich, R. Serra, M. F. Montemor, K. A. Yasakau, I. M. Miranda Salvado and M. G. S. Ferreira, *Electrochim. Acta*, **51**, 208–217 (2005).

5. Alcohol-aminosilicate Hybrid Coatings for Corrosion Protection of Galvanized Steel in Mortar

Alcohol-Aminosilicate Hybrid Coatings for Corrosion Protection of Galvanized Steel in Mortar

R. B. Figueira[a,b,*], C. J. R. Silva[b], E. V. Pereira[a], M. M. Salta[a]

[a]LNEC, Laboratório Nacional de Engenharia Civil, Av. Brasil 101, 1700-066 Lisbon, Portugal

[b]Centro de Química, Universidade do Minho, Campus de Gualtar 4710 - 057 Braga, Portugal

* Corresponding Author: rmfigueira@lnec.pt

* Electrochemical Society Student Member

Abstract

Organic-inorganic hybrid (OIH) matrices were synthesized by sol-gel method and deposited on hot-dip galvanized steel (HDGS) using a dip-coating process. These OIHs, generally called amino-alcohol-silicates, were synthesized using a functionalized siloxane, 3-glycidoxypropyltrimethoxysilane, and five oligopolymers (Jeffamine®) with different molecular weights: 230, 400, 600, 900 and 2000. Besides the five different pure OIH matrix coatings, a similar set of HDGS samples were coated with the OIH matrices doped with Cr(III), which was tested as a corrosion inhibitor. The OIH coatings were assessed using electrochemical studies, namely electrochemical impedance spectroscopy, macrocell current density, open circuit potential monitoring and polarization resistance. The studies were carried out in mortar. Analysis of the results obtained by optical and scanning electronic microscopy methods were consistent with the data obtained by electrochemical techniques. The HDGS samples coated with OIH matrices showed better performance when compared with HDGS uncoated samples.

Keywords

1. Introduction

During the last three decades, the corrosion of steel reinforcement has been widely studied and reported.[1-7] In spite of the majority of the reinforced concrete (RC) structures showing high durability, serviceability and long-term performance as well as intense research being performed in the last few years, a large number of failures have been reported due to the corrosion of the reinforcement embedded in the concrete.

The most effective way to minimize the risk of corrosion reinforcement concrete is to ensure that the cover of the metallic reinforcement parts is of an adequate thickness. The concrete should be of high quality, with a proper mixing ratio, good compaction and curing.[1,6,7] Several proven methods are known for preventing and controlling corrosion. Improving the concrete quality and increasing the concrete cover are the most economical protection measures yet are not always enough. A method that is widely accepted and recognized as efficient at providing corrosion protection of the RC, is the application of hot-dip galvanized steel (HDGS), since it is considered economically favourable when compared to others.

The use of HDGS has been recognized by several authors[7,8-12] as an effective measure to increase the service life of RC structures exposed to carbonation or to chloride ions. However, zinc in contact with fresh concrete (high alkaline environment) is oxidized and hydrogen evolution occurs, for a limited period, until passivating formation layers occur and concrete hardens. To avoid zinc corrosion and hydrogen evolution, chromate and similar hexavalent chromium compounds are among the most common substances used as inhibitors or incorporated into the preparation of the fresh concrete. However, these compounds are toxic and carcinogenic, causing serious environmental hazards and their incorporation in protective coatings is heavily regulated by most environmental legislation. Therefore, intense research all over the world is being undertaken to replace chromates with more ecological compounds.

Organic-inorganic hybrid (OIH) sol-gel films are potential alternatives to replace chromate-based pre-treatments and can be easily deposited on metallic substrates to improve either their resistance to oxidation and corrosion or to modify their surface properties.

The synthesis, characterization and application of OIH materials have advanced at a rapid pace in the last few decades. The major driving forces behind the intense activities in this area are the new and different properties of the nanocomposites, which traditional macroscale composites and conventional materials do not have. Through the combination of inorganic and organic components and the use of appropriate processing methods, various types of primary and secondary bonding

within the matrix network can be developed. This can lead to materials that meet proper technical requirements for electrical, optical and corrosion resistance applications.

The OIHs based on siloxanes using sol-gel technology allow the production of multifunctional materials with suitable properties to be applied in corrosion science. They represent a new class of materials characterized by a biphasic morphology consisting of distinct organic and inorganic domains at a nanometric level.[13-16] The organic and inorganic components are totally or partially linked through strong chemical bonds (covalent, or Lewis acid-base bonds). The chemical methods used to synthesize OIH networks depend on the relative stability of the chemical links that associate the different components.[17]

OIHs based on siloxanes can be easily synthesized from organo-substituted silicic acid esters with the general formula $R'_nSi(OR)_{4-n}$.[17] Organic groups R' may bind to an inorganic network, with two distinct purposes, namely: as *network modifiers* or as *network formers*. If R' is a simple non-hydrolyzable group, it will have a network modifying effect. On the other hand, if R' possesses any reactive groups (e.g., methacryloyl, epoxy, or styryl groups) it can polymerize or copolymerize, or undergo hydrolysis-condensation (trialkoxysilyl groups). This type of functionalized precursor will act as a *network former*.[17] The first step of the sol-gel method is the formation of a covalent bond between organic and inorganic components giving rise to the "pivotal" precursor molecule. The conversion of the precursors into OIH materials proceeds via the formation of siloxane (Si-O-Si) bonds. This process takes place by hydrolysis of monomeric tetrafunctional alkoxide precursors that can be catalysed by an acid (e.g., HCl) or alkaline compound (e.g., NH_3).

Several studies have shown[8-23] that the mechanical, thermal and electrical properties of OIH materials obtained by sol-gel methods based on siloxanes are interesting and as such, these materials can be used as pre-treatments to improve the corrosion resistance of several metals and alloys.

The combination of functionalized siloxanes and polymeric structures is a route to produce homogeneous OIH materials with enhanced properties. This is due to their capacity to host chemical species with distinct properties within the produced matrix.[13,17] This type of material opens up the possibility to produce composites that can incorporate inhibitor species, which may contribute to preventing or minimizing the corrosion of the metallic substrate.

In this study, OIH matrices were synthesized. These OIHs, hereafter called amino-alcohol-silicates, A(X), were obtained using a functionalized siloxane 3-Glicidoxypropyltrimethoxysilane (GPTMS). The

functionalized siloxane was made to react with five oligopolymers (referred to as Jeffamine®) with different molecular weights (MWs): 230, 400, 600, 900 and 2000.

The OIH coatings, obtained by sol-gel process, were assessed as possible eco-friendly alternatives to replace the use of chromate based pre-treatments. The coatings developed aim to control the reactions that occur in the first instances of contact of the HDGS with fresh concrete. The behaviour of HDGS samples coated with the different OIHs was evaluated when in contact with mortar for a period of 137 days.

The barrier efficiency of pure A(X) coatings with similar Cr(III) doped gels were compared by using electrochemical techniques, namely electrochemical impedance spectroscopy (EIS), macrocell current density (i_{gal}), open circuit potential monitoring (E_{corr}), and polarization resistance (R_p). Scanning Electronic Microscopy/Energy Dispersive Spectrometry (SEM/EDS) analyses of the coatings were performed before and after exposure to the cement based materials.
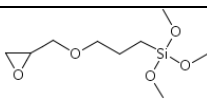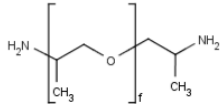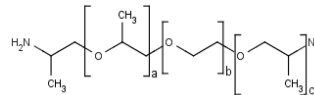
2. Experimental

2.1. Reagents

The structures and specifications of the used gel precursors are presented in Table 1. Five di-amino functionalized polyethers (hereafter referred to generically as Jeffamine®) with different MWs were used.

All the precursor reagents used, namely the different MWs of Jeffamine® and GPTMS (97%, Aldrich), were stored protected from light and used as supplied. Absolute ethanol (EtOH, absolute 98%, Riedel-de-Haën), citric acid monohydrate (Merck) and chromium (III) nitrate nonahydrate (Aldrich) were also used as received. Ultra-pure water (0.055–0.060 μS/cm) obtained from a Purelab Ultra System (Elga) was used.

Table 1. Structural and physical details of reagents used in OIH synthesized samples.

Chemical Name / Molecular Formula	Chemical Structure	Abbreviation	M (gmol^{-1})	$\rho_{25^\circ C}$ (gcm^{-3})
3-Glycidoxypropyltrimethoxysilane C$_9$H$_{20}$O$_5$Si		GPTMS (Aldrich)	236.34	1.070
O,O'-bis(2-aminopropyl) poly-propyleneglycol 130		Jeffamine D-230® (Fluka)	230[a]	0.948
O,O'-bis(2-aminopropy1) poly-propyleneglycol 300	Similar	Jeffamine D-400® (Fluka)	400[a]	0.972
Poly (propyleneglycol)-block-poly (ethyleneglycol)-block-poly (propyle-neglycol)-bis-(2-amino propylether)-600		Jeffamine ED-600® (Fluka)	600[a]	1.035
Poly(propyleneglycol)-block-poly (ethyleneglycol)-block-poly (propyle-neglycol)-bis-(2-aminopropylether)-900	Similar	Jeffamine ED-900® (Fluka)	900[a]	1.065
Poly(propyleneglycol)-block-poly (ethyleneglycol)-block-poly (propyle-neglycol)-bis-(2-aminopropylether)-2000	Similar	Jeffamine ED-2000® (Fluka)	2000[a]	1.068

Notes: a) MW approximate value.

2.2. Sol-gel Synthesis Procedure of OIH Amino-Alcohol-Ailicate Matrix Monoliths Discs and Coatings

The synthesis of A(X) matrices included several steps, as described in Figure 1. Using the same precursor (Jeffamine®) with five different MWs and using the same methodology, two sets of different materials were prepared: the pure A(X) matrices and the matrices doped with Cr(III) ions. Each set of samples was prepared as a thin circular disc and as a coating layer on HDGS (Table 2).
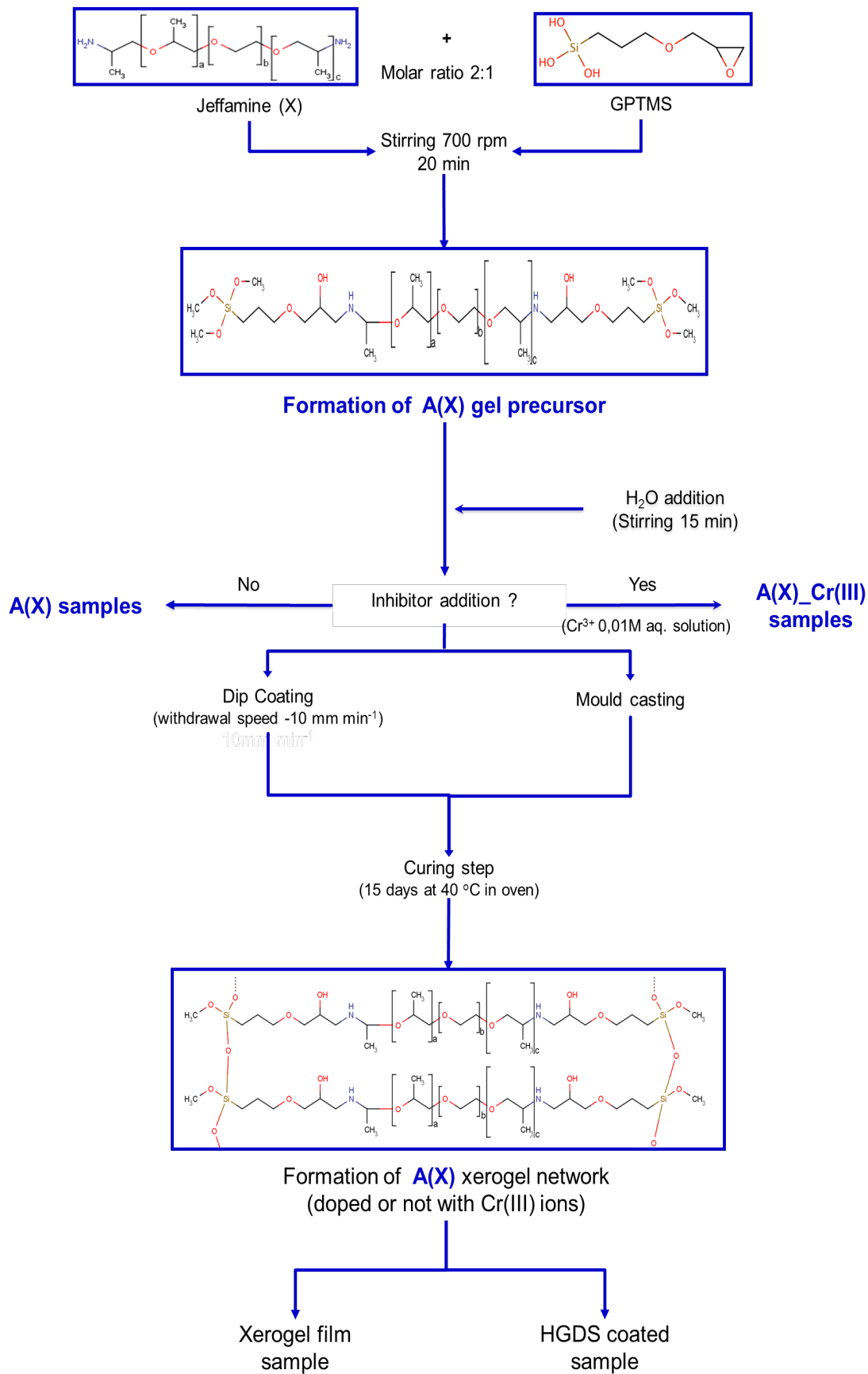
Figure 1. Schematic representation of the main steps involved in the production of OIH films and coatings based on A(X) matrices.

Both materials were produced from a batch of precursor solution that was obtained using 1:2 stoichiometric molar ratio of each Jeffamine® MW and GPTMS mixed in a glass container and stirred at 700 rpm, for 20 min. The reaction between the amine end group (–NH2) of Jeffamine with different MWs (Jeffamine® D-230, Jeffamine® D-400, Jeffamine® ED-600, Jeffamine® ED-900 and Jeffamine® ED-2000) and the epoxy group of GPTMS, led to the formation of the precursors of future gel matrices, hereafter referred to as: A(230), A(400), A(600), A(900) and A(2000).

Table 2. Adopted representation codes for the different prepared material samples

| Jeffamine | Specimen OIH disk sample | | HDGS OIH coated sample | |
	Pure Matrix	Cr(III) doped	Pure Matrix	Cr(III) doped
D-230®	U(230)	U(230)_Cr(III)	U(230)_HDGS	U(230)_Cr(III)_HDGS
D-400 ®	U(400)	U(400)_Cr(III)	U(400)_HDGS	U(400)_Cr(III)_HDGS
ED-600®	U(600)	U(600)_Cr(III)	U(600)_HDGS	U(600)_Cr(III)_HDGS
ED-900®	U(900)	U(900)_Cr(III)	U(900)_HDGS	U(900)_Cr(III)_HDGS
ED-2000®	U(2000)	U(2000)_Cr(III)	U(2000)_HDGS	U(2000)_Cr(III)_HDGS

In the second stage, 0.22 M citric acid ethanolic solution was added. The mixture was stirred for 15 minutes to obtain a homogeneous mixture, and 0.01M of Cr(III) aqueous solution was added to obtain Cr(III)-based samples. The final volume of water added was adjusted so as to obtain a total volume of 8 mL reaction media. Finally the mixture was stirred for another 15 min. Part of the prepared mixture was placed into a Petri dish (polystyrene, 2 cm of diameter, supplied by Sarstedt), and this was subsequently placed in an incubator-compressor (*ICP*-400, *Memmert*) and kept at 40 °C for two weeks. This procedure ensured precise control and reproducible conditions of hydrolysis/condensation reactions as well the evaporation of the remaining solvents. Figure 1 highlights the preparation conditions implemented that led to samples that were highly transparent and to homogeneous discs free of cracks in which the flexibility increased with MWs of Jeffamine® used. Coated HDGS samples were prepared by using a dip coater (*Nima*, model *DC Small*). HDGS metal plates were dipped in the remaining part of the prepared mixtures at a withdrawal speed of 10 mm min^{-1} without residence time. It should be pointed out that a total of 10 different OIH gel compositions were produced consisting of two sets of coated HDGS samples with one and three dip steps. The HDGS metal samples used had dimensions of 5.0 × 1.0 × 0.1 (in cm) and had an average Zn thickness of 16 μm on both sides. Samples were obtained from commercially available plates. The curing of the coated HDGS samples was performed following the same conditions used to prepare the gel discs.

2.3. Preparation of Mortar

The corrosion behaviour of HDGS coated with the different OIH coatings was studied in mortar. The mortar was prepared according to EN 196-1 standard[24] using cement type I 42,5R, distilled water and normalized sand (AFNOR) with a weight ratio of 6:2:1 (sand:cement:water).

2.4. Electrochemical Studies

The corrosion behaviour of the HDGS coated with OIHs was assessed by E_{corr}, R_p and i_{gal}.[25] OIH gel samples (discs) were also characterized by EIS measurements.

2.4.1. Electrochemical Impedance Spectroscopy (EIS)

EIS measurements were carried out to characterize resistance, electrical conductivity, and electric permittivity of the prepared OIH disc films. Capacitance of OIH film coating was also determined. Measurements were performed using two parallel Au disc electrodes (10 mm diameter and 250 μm thickness) and a support cell, adapted from a previously used model[26] providing a precise control of cell dimensions. Measurements were performed at room temperature using an Impedance/Gain-Phase Analyzer (Model 1260A, Solartron-Schumberger) and a potentiostat/galvanostat (Model 1287A, Solartron-Schlumberger) controlled by a PC using Zplot software (Solartron-Schlumberger, version 2.9c). Measurements were taken by applying a 20 mV (peak-to-peak, sinusoidal) electrical potential within a frequency range from 1×10^5 Hz to 0.01 Hz (10 points per decade) at open circuit potential. The frequency response data of the studied electrochemical cells were displayed in a Nyquist plot, using ZView software (Solartron-Schlumberger, version 2.9c) that was also used for data fitting purposes.

2.4.2. Open Circuit Potential Monitoring (E_{corr})

The E_{corr} measurements were carried out using an electrochemical cell described elsewhere.[27] A titanium-activated wire with a length of one cm was used as a reference electrode (RE) and a HDGS plate with an active area of 2 cm^2 coated with OIH was used as a working electrode (WE). The electrodes were connected to an isolated copper cable and the cutting zone of the tip of the titanium electrode was covered with dual-component epoxy resin (Araldite®). The edges of the WE plates, as well the non-active area and connecting zones, were also protected with dual-component epoxy resin

(Araldite®). The E_{corr} values were estimated with a potentiostat/galvanostat (Voltalab PGZ 301). For comparison purposes, cells with non-coated HDGS working electrodes were prepared and used as a control.

2.4.3. Macrocell Current Density (i$_{gal}$)

The i_{gal} measurements were performed using a system based on two parallel electrodes (rectangular metal plates with dimensions of $5.0 \times 1.0 \times 0.1$ cm). As a counter electrode (CE), a stainless steel (SS, type 316L) plate was used and as a WE, it was HDGS coated with the different OIHs that was used. Both electrodes had an active average area of 2 cm^2. The edges of both CE and WE plates, as well the non-active areas and connecting zones were protected with a dual-component epoxy resin (Araldite®) using a previously established protocol.[27-29] For comparison purposes, cells prepared with non-coated HDGS WE electrodes were used as control. To assemble the electrochemical cells, 120 $\pm$ 10 g of fresh mortar was transferred to a 100 mL polyethylene flask, the electrodes were subsequently immersed and the flask closed. Using an automatic data acquisition system (Datataker DT505, series 3), i_{gal} measurements of prepared cells were performed through reading the potential difference to the terminals across an external 100 Ω resistor, according to ASTM G109.[25] Measurements were performed at one-minute intervals during the first seven days, and at each five minutes during the remaining time until the record was completed, on the 137th day.

2.4.4. Polarization Resistance (R$_p$)

The R_p measurements were performed with a three-electrode electrochemical cell system using a previously established protocol.[29] A stainless steel (SS, type 316L) plate was used as a CE and HDGS coated with the different OIHs was used as a WE. Both electrodes had an active average area of 2 cm^2. The edges of both the CE and WE plates, as well the non-active areas and connecting zones were protected with a dual-component epoxy resin (Araldite®). A titanium-activated wire with a length of one cm was used as a RE and the tip of the electrode was protected as described previously. For comparison purposes, cells with non-coated HDGS WE electrodes were prepared and used as control. The R_p values were estimated by the potentiostatic method using a potentiostat/galvanostat (Voltalab PGZ 301), according to the literature.[29-31]

2.5. Scanning Electron Microscopy (SEM/EDS)

The morphology of the OIH sol-gel coating surface applied on HDGS specimens was analyzed with a SEM (JEOL JSM-6400) coupled with an EDS detector (Inca-xSight Oxford Instruments). The surface of the specimens was previously covered with an ultrathin coating of gold deposited by sputter coating. SEM investigations of the surfaces were carried out by using the back-scattered electron detector in order to emphasize the contrast for the different metallic phases. The SEM/EDS studies of the HDGS coated samples were performed on the substrate before and after 137 days in contact with mortar. The hardened cementitious materials were carefully broken to release the HDGS specimens and SEM/EDS observations were promptly performed.

3. Results and Discussion

3.1. Electrochemical Studies

3.1.1. EIS Measurements

EIS is a powerful tool that was widely used in the last few decades for the characterization of corrosion processes as well as for the assessment of the protective performance of pre-treatments, organic coatings[33-45] and OIH coatings.[46,47] This electrochemical technique is not destructive. Consequently, EIS can be used to follow the evolution of a coated system exposed to an accelerated ageing test and provide, in a short time, information about the corrosion protection properties of the materials. Figures 2-8 show the Nyquist complex impedance plots obtained from the EIS analysis of the prepared film samples based on A(X) matrices. EIS data for A(400) and A(400)_Cr(III) films are displayed in Figures 2a) and 2b). EIS data for A(600) and A(600)_Cr(III) are displayed, respectively in Figures 3 and 4. The results for A(900), A(900)_Cr(III), A(2000) and A(2000)_Cr(III) disc samples are plotted in Figures 5, 6, 7 and 8, respectively. The large diameter semicircle that is observed in all samples at the lowest studied frequency range is assigned to the electrochemical behaviour of the interface between the matrix and the Au electrodes. This part of Nyquist plot was proposed to be described by a simple R-C EEC but the fitting was not performed since it was assumed that it was not relevant for the comprehension of the electrochemical behaviour of HDGS coated samples due to the differences of their interfacial behaviour. The fitted regions are shown by solid lines in all the Nyquist plots. The insets of Figures 5-8 show a detailed view of the fitted region. With the exception of Figure 3, all the Nyquist plots show that the high frequency region resembles a semicircle intersecting the x-axis. The diameter of the semicircles changes with the sample composition, indicating that this is assigned to the dielectric characteristics of the OIH gel sample, which include

conductivity, capacitance and electric permittivity. Data obtained at lower frequencies describes a line suggesting another electrochemical process that might be assigned to Au/OIH interfacial phenomena. EIS analysis of the OIH films based on A(230), with and without Cr(III), could not be performed. This may be due to the combination of the high rigidity and the low conductivity of these materials, contributing to a poor electric contact between the OIH film and the Au electrode discs, thus disabling the electrical response.

The equivalent electrical circuit (EEC) used to describe the observed impedance response of the cell configuration in these measurements is shown as an inset in each Nyquist plot. As the semicircles show a depressed form, the analysis of all the impedance responses was based on an EEC where constant phase elements (CPE) were used instead of pure capacitance.
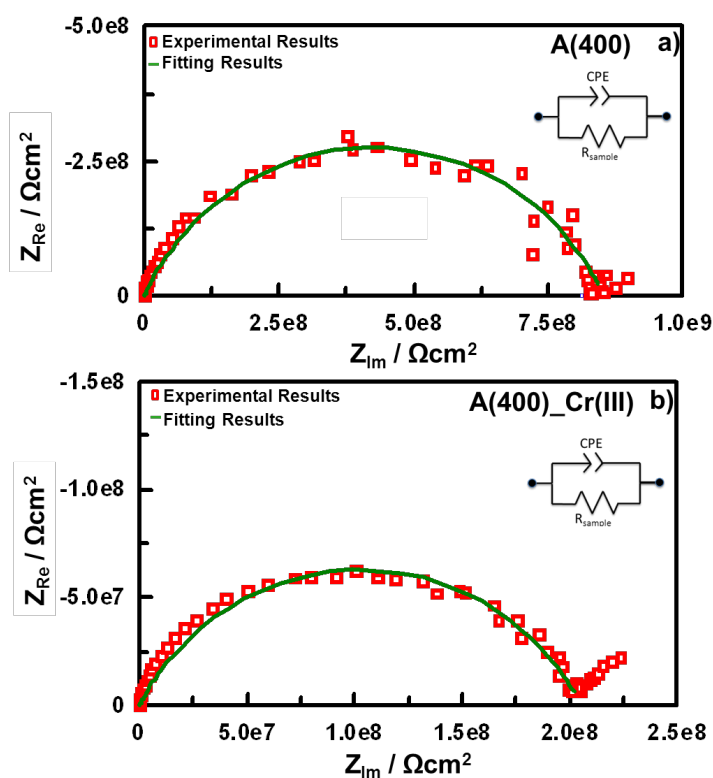

Figure 2. Typical complex plane impedance plots obtained for OIH films based on a) A(400) and b) A(400)_Cr(III) with the EEC as an inset in each plot used to analyze the EIS response.
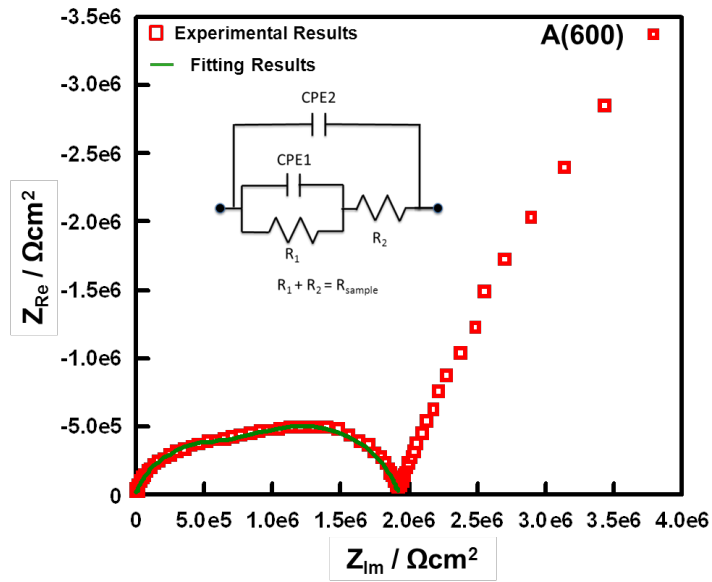
Figure 3. Typical complex plane impedance plots obtained for OIH films based on A(600) with the EEC as inset used to analyze the EIS response.
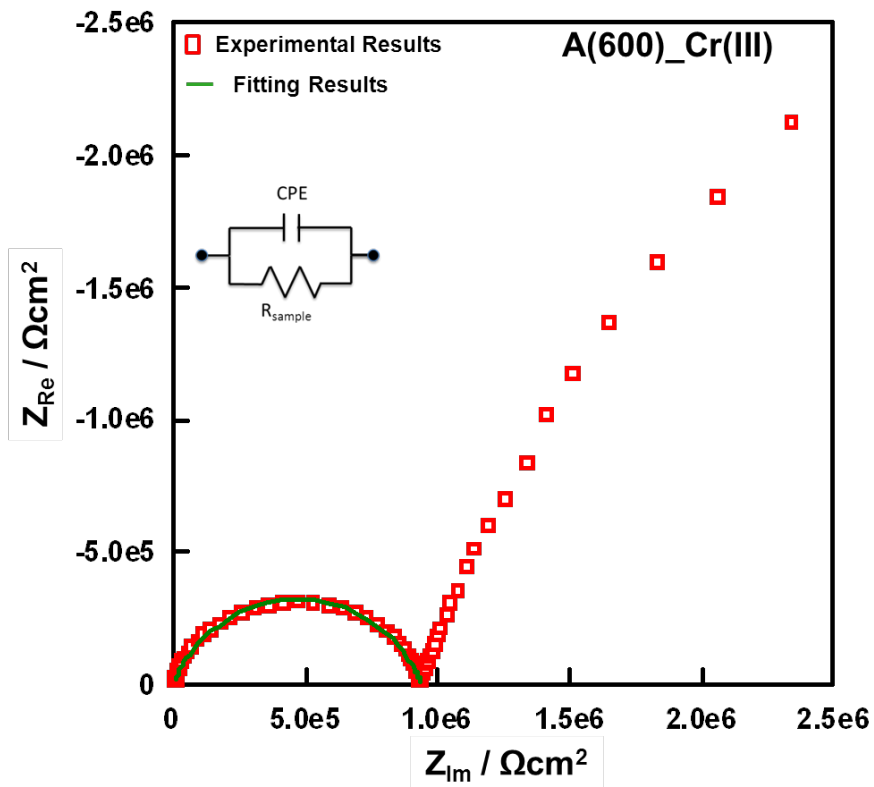

Figure 4. Typical complex plane impedance plots obtained for OIH films based on A(600)_Cr(III) with the EEC as an inset used to analyze the EIS response.

162

Figure 5. Typical complex plane impedance plots obtained for OIH films based on a) A(900) with the EEC as an inset used to analyze the EIS response; b) detail of the semicircle.

Figure 6. Typical complex plane impedance plots obtained for OIH films based on a) A(900)_Cr(III) with the EEC as an inset used to analyze the EIS response; b) detail of the semicircle.
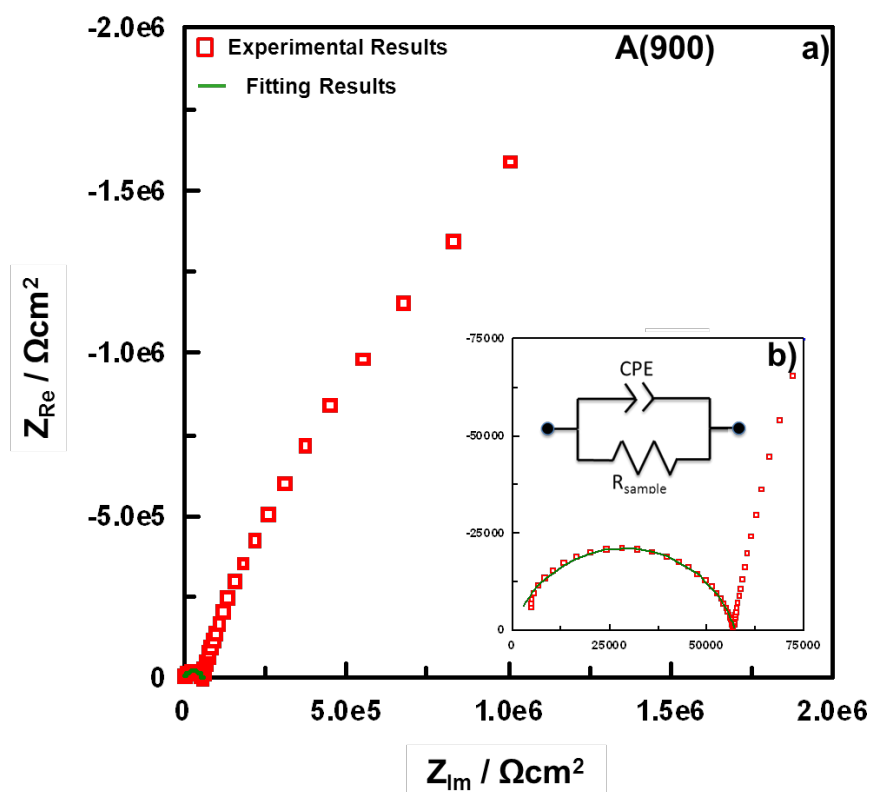
Figure 7. Typical complex plane impedance plots obtained for OIH films based on a) A(2000) with the EEC as an inset used to analyze the EIS response; b) detail of the semicircle.
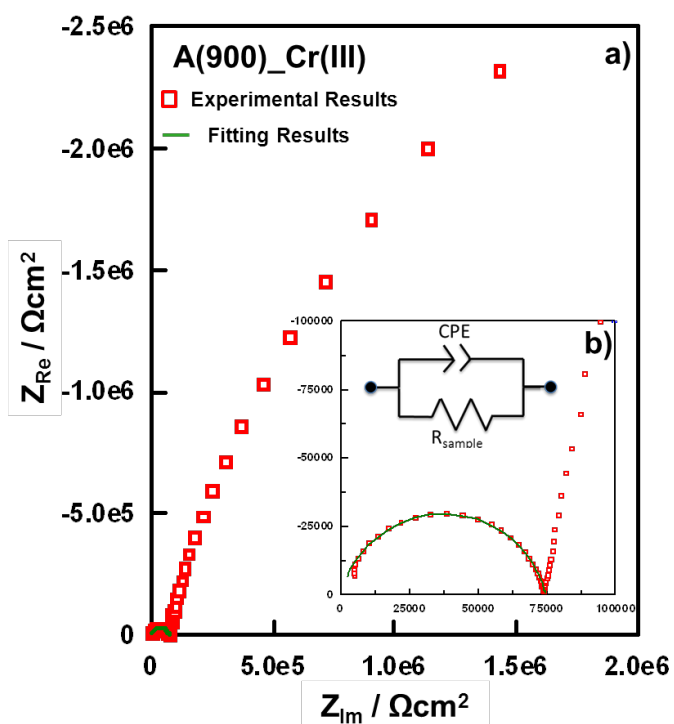

Figure 8. Typical complex plane impedance plots obtained for OIH films based on a) A(2000)_Cr(III) with the EEC as an inset used to analyze the EIS response; b) detail of the semicircle.
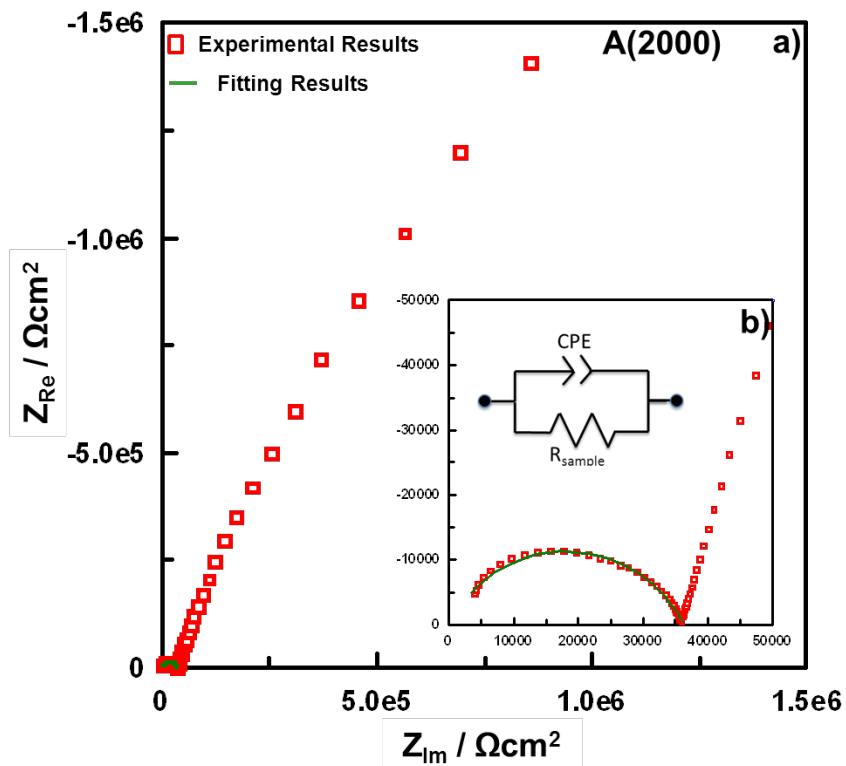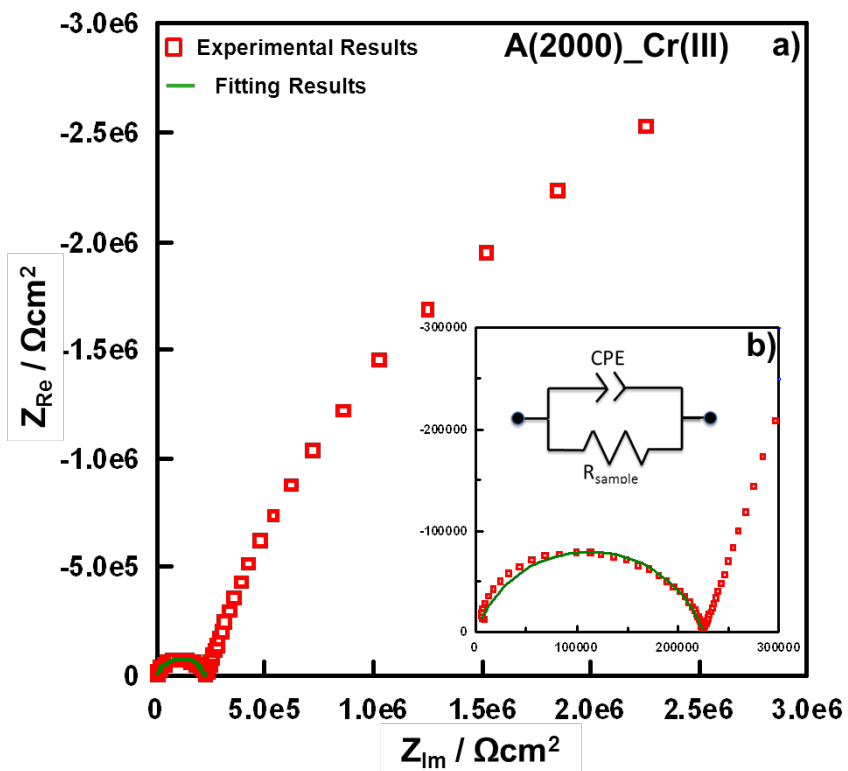
The impedance of a CPE is given by[48]:

$$Z_{CPE} = 1 \, / \, [Q(j\omega)^{\alpha}] \qquad\qquad (1)$$

Where α and Q are parameters independent of frequency.[49] When $\alpha=1$ Q represents the capacity of the interface and when $\alpha\neq1$ the system shows a behaviour that is associated to surface heterogeneity.[49] When considering a resistive-capacitive parallel circuit and using a CPE instead of an ideal capacitor ($\alpha=1$) the impedance for the EEC is determined by[49]:

$$Z_{CPE} = R_{Sample} \, / \, [1+(j\omega)^{\alpha}QR_{Sample}] \qquad\qquad (2)$$

Where R_{Sample} is the resistance in parallel with the CPE and Q and α have the same meaning previously stated.

The CPE parameter Q cannot be equated to the interfacial capacitance (C_{eff}).[49,50] To estimate the C_{eff} the relationship developed by Brug et al. cited by Orazem and Tribollet[49,50] was used:

$$C_{eff} = [QR_{sample}{}^{(1-\alpha)}]^{1/\alpha} \qquad\qquad (3)$$

The EEC used to model the Nyquist plots for all the A(X), with exception of A(600) (Figure 3), contains a simple CPE (Q) and a Resistance (R_{sample}) that is associated with the film resistance. A(600) (Figure 3) contains two CPEs (Q1 and Q2) and two resistances (R1 and R2) that are associated with the resistance of the film. Five measurements were performed for each A(X). However, only one example for each A(X) of the fitting parameters, namely R_{Sample}, Q (represented by CPE in the EEC in Figures 2 and 4-8), α parameters and the percentage of error associated to each element are shown in Table 3. The observation of the Nyquist plot obtained for A(600) (Figure 3) shows a distinctive impedance response at a higher frequency range. The two partially overlapping semicircles with different radii may be identified as two time dependent charge relaxation processes

with different time-constants. Two CPE (CPE$_1$ and CPE$_2$) contributions are included here since the system shows a frequency dispersion associated with relaxation phenomena, probably due to residual solvent still incorporated within the fill matrix. The elements R$_1$ and R$_2$ describe the sample's (bulk) resistance of these two distinct dielectric media. According to this model, the sample's bulk resistance corresponds to the sum of R$_1$ with R$_2$. The fitting parameters referred to above that correspond to the two relaxation processes, namely R$_1$, R$_2$, CPE$_1$, CPE$_2$, α_1, α_2 and the percentage of error associated to each element are also displayed in table 3. As this behaviour was only observed in this OIH film it suggests that at the molecular level the A(600) film exhibits morphological aspects that are distinct from the other A(X) films. Using the EIS response, the values of resistance (R$_{Sample}$ /Ω), Q (S$^\alpha$/Ωcm^2) and α were obtained by fitting the data corresponding to the proposed EECs.[28] Ceff (F) values were calculated using equation 3. Normalized resistance (R / Ω cm^2), normalized capacitance (C / nF cm^{-2}), conductivity (σ / S cm^{-1}) and relative permittivity (ε_r) were also determined. The R and C values were normalized to cell geometry dimensions. The values obtained were calculated using the following equations (where A$_{Au}$ is the area of the gold electrodes, d$_{Sample}$ is the thickness of the analyzed OIH film sample and ε_o represents the vacuum permittivity in nF cm^{-1}):

$$R = R_{Sample} \times A_{Au\ disc} \tag{4}$$

$$C = C_{eff} / A_{Au\ disc} \tag{5}$$

$$\sigma = (d_{Sample}/A_{Au\ disc})/R_{Sample} \tag{6}$$

$$\varepsilon_r = (C_{eff} \times d_{Sample}) / \varepsilon_o \times A_{Au\ disc} \tag{7}$$

Table 3 shows the average values of the logarithm of resistance (log R), conductivity (-log σ), C and εr obtained for the five samples of each OIH film (uncertainty is expressed for 95% confidence). Table 4 shows that for all analyzed OIH film samples based on A(X) matrices, normalized R values are between 10^4 and 10^8 Ω cm^2. It is predicted that OIH films based on A(230) matrices could have

higher values than those obtained for the other OIHs. It was found in the literature that if the resistance of the coating is < 10^7 Ω cm^2, then such coatings do not fit the conditions that are assumed to provide an effective corrosion protection.[51-53] The results showed that for OIHs based on A(X) matrices, only the ones with lower Jeffamine® MWs (A(400) with or without Cr(III)), have resistances higher than that value stated previously. The resistance of OIH matrices based on A(X) decreases by four orders of magnitude when the Jeffamine® MW changes from 400 to 2000. For Cr(III) OIH doped gels a reduction of three orders of magnitude, for the same MW change, was found.

The results show that the inclusion of Cr(III) in A(X) matrices does not significantly change the resistance of the OIH hybrids. Data from Table 4 also show that the normalized capacitance values of the produced OIH samples seem not to be significantly affected by the presence of Cr(III). The higher capacitance values were obtained for A(400)_Cr(III). This high value reflects that the distinct relaxation processes across A(400)_Cr(III) samples are interpreted as the existence of a phase with a high dielectric constant and this behaviour might be due to the synthesis conditions used to prepare these materials.

Table 3. EIS data fitting of the OIH disc samples based on A(X) matrices

OIH sample	R_{Sample} / Ω cm^2	CPE (Q) / S$^\alpha$ Ω^{-1} cm^{-2}	α
A(400)[a]	8.53 x 10^8 (±0.60%)	7.38 x 10^{-11} (±3.65%)	0.73 (±1.11%)
A(400)_Cr(III) [a]	2.05 x 10^8 (±0.37%)	1.50 x 10^{-10} (±2.84%)	0.70 (± 0.72%)
A(600)_Cr(III) [a]	9.42 x 10^5 (±0.19%)	3.92 x 10^{-10} (±3.23%)	0.76 (± 0.40%)
A(900) [a]	5.79 x 10^4 (±0.19%)	4.20 x 10^{-10} (±4.34%)	0.81 (± 0.39%)
A(900)_Cr(III) [a]	7.44 x 10^4 (±0.18%)	2.12 x 10^{-10} (±4.16%)	0.86 (± 0.35%)
A(2000) [a]	3.62 x 10^4 (±0.24%)	2.27 x 10^{-9} (±5.09%)	0.71 (± 0.53%)
A(2000)_Cr(III) [a]	2.25 x 10^5 (±0.36%)	3.26 x 10^{-10} (±7.16%)	0.78 (± 0.74%)

A(600)[b]	R_1 / Ω cm^2	R_2 / Ω cm^2	CPE$_1$ / S$^\alpha$ Ω^{-1} cm^{-2}	CPE$_2$ / S$^\alpha$ Ω^{-1} cm^{-2}	α_1	α_2
	9.62 x 10^5 (± 2.52%)	9.78 x 10^5 (± 2.38)	1.52 x 10^{-9} (± 4.88%)	2.24 x 10^{-10} (± 10.56%)	0.82 (±1.14%)	0.79 (±1.08%)

Notes: a) EIS data fitting at high frequencies using the EEC, as shown as inset in correspondent Nyquist plots, Figures 2, 4, 5, 6, 7 and 8, respectively; b) EIS data fitting at high frequencies using the EEC, as shown in the correspondent Nyquist plot (Figure 3).

A commonly accepted approach to compare different coating systems is to examine thickness-independent properties, such as relative permittivity εr. This physical property represents the electrical polarization, or the amount of electrical energy that can be stored in a material, which differs from one material to another. The lower the value of the relative permittivity the lower the charge stored within the material, as stated for vacuum or air when it is close to one. Water has a permanent dipole and its relative permittivity at 20 ºC is ≈80.[54] The investigation of dielectric properties of the OIH films show that samples based on A(X) matrices exhibit εr values in a range between 20 and 85. It was found that as Jeffamine® MW increases, the εr values for the undoped A(X) matrices increase with A(400) and A(2000) films showing lower and higher ε_r values, respectively. However, for the matrices doped with Cr(III) it was found that as the MW of Jeffamine® increases, the εr decreases. A(400)_Cr(III) and A(2000)_Cr(III) films show higher and lower εr values, respectively.

Table 4 also shows that A(X) conductivity (expressed by -log σ values) seems not to be influenced by the presence/absence of Cr(III). However, as the MW of Jeffamine® increases, the conductivity values increase by three orders of magnitude for the doped and undoped A(X) matrices.

3.1.2. i_{gal} Measurements

Figure 9 shows the macrocell current density (i_{gal}) collected from the 20 different prepared electrochemical cells involving the HDGS coated samples, plus the control, that were embedded in the mortar during a period of 137 days. All the measured i_{gal} values are higher during the first seven days and a gradual decrease to lower values over time is observed. This behaviour was found in all OIHs based on A(X) matrices. The plots also show that, generally, the control (uncoated HDGS sample) presents higher i_{gal} values when compared to those involving OIH coated HDGS samples.

The lowest i_{gal} values, taken from all sets of samples after 28 days, were obtained for HDGS coated with A(400) (Figures 9a) and 9b)) and A(400)_Cr(III) (Figures 9c) and 9d)) both with either one or three layers. Even though a slight increase to higher values than the control over time is observed for HDGS coated with three layers of A(400)_Cr(III) (Figure 9d), the i_{gal} behaviour evolves over time to lower values than the control. Figure 9 also shows that samples coated with A(230)_Cr(III) and A(400)_Cr(III), either with one or three layers, and A(600)_Cr(III) one layer display lower values between the 10th and 28th day, later rising to higher values. However, they always remain below the control sample with the exception of A(400)_Cr(III) three layers.
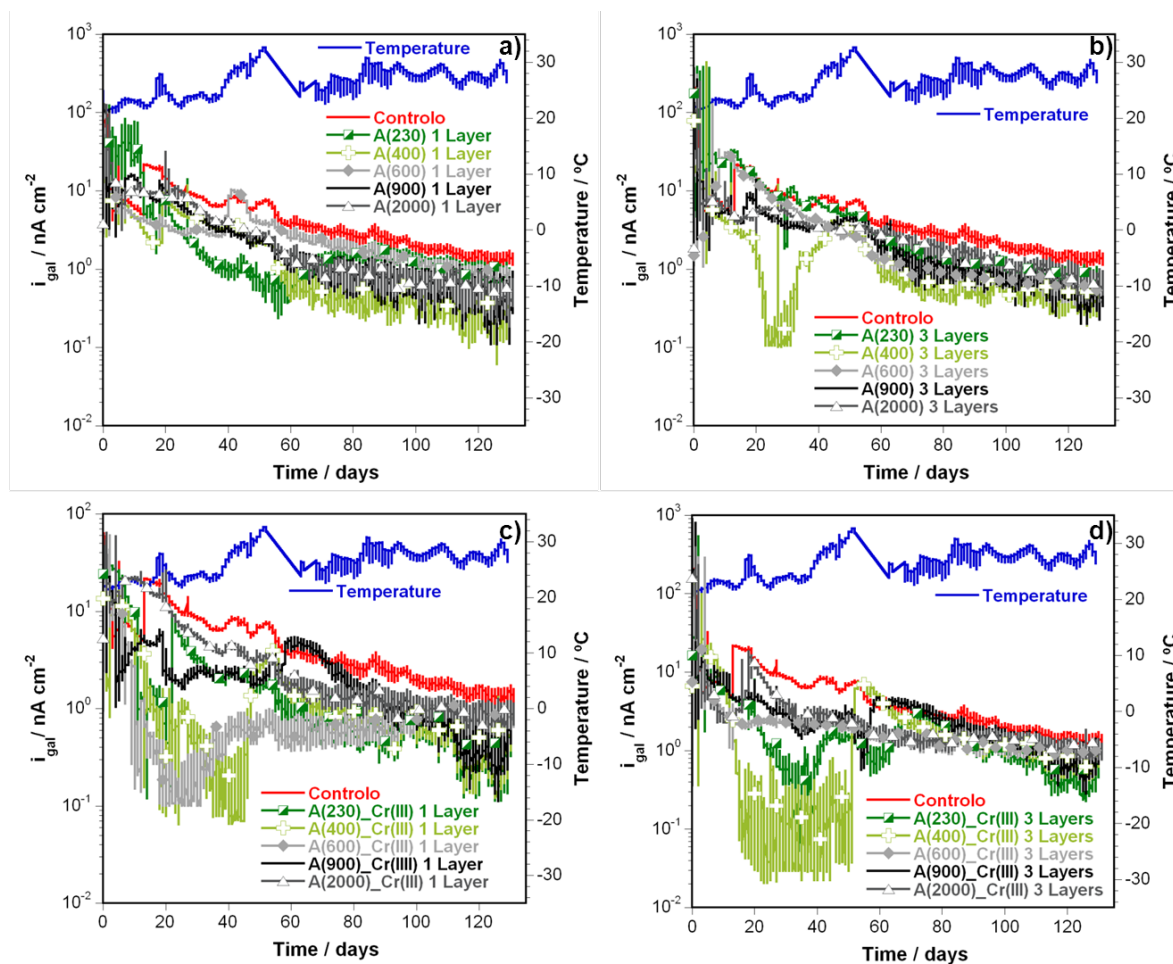
Figure 9. Plots of the macrocell current density (i_{gal}) variation and laboratory temperature over time recorded for the different coated HDGS sample cells (kept embedded in mortar for 137 days). Displayed graphs correspond to different amino-alcohol-silicate matrices. A(X) samples deposited by: a) one dip step (1 layer); b) three dip steps (3 layers) and A(X)_Cr(III) samples deposited by: c) one dip step (1 layer); d) three dip steps (3 layers).

Although the Jeffamine® precursors used have different structures and compositions, they show the same two terminal amine groups. The reaction of Jeffamine® with functionalized siloxane (GPTMS) with one terminal epoxy group led to the opening of the epoxide ring with the formation of an hybrid precursor (step 1, Figure 1) with amino and alcohol functions. The final structure of the A(X) matrices could be described as two blocks co-existing within a network: the rigid inorganic (silicate based) backbones (which give enhanced mechanical properties to the final material) are spaced by a flexible organic (polyether) chain linked by the oxygen from the epoxide group of GPTMS (Figure 1). When the sol-gel precursors, A(X), are applied on HDGS surfaces, a new interface is formed between the components of the amino-alcohol-silicate networks and the metal surface. The nature of the gel precursors suggests that the interaction between the network components and the HDGS substrate

happens preferentially with the silicate groups. The organic part of the OIH is kept away from the metal surface due to its predominant hydrophobic characteristics. Overall, the obtained i_{gal} data highlights that A(X) gels based on Jeffamine® with lower MWs (Figure 9), reveal a more efficient barrier effect than higher Jeffamine® MWs. As observed on Figure 9 lower i_{gal} values correspond to A(X) gels based on low Jeffamine® MWs. For HDGS coated with A(X) samples, no significant difference was found between the use of one and three layers except for the HDGS samples coated with A(400) one layer. Lower i_{gal} values than those observed were expected, which might be due to the limited time left for the reaction between GPTMS and Jeffamine® prior to addition of a catalyst, leading to a less extensive amino-alcohol bonding between functionalized siloxane and Jeffamine and to a poor network crosslinking. This might be explained by the lower reactivity between epoxy and amine groups comparatively with previously studied ureasilicate.[28] When the catalyst or the Cr(III) solution are added to the reactional media, without the reaction between GPTMS and Jeffamine® having reached the end, existent epoxy side reactions could be catalysed, turning the reaction between epoxy and amine group less favourable due to the decrease of available reactive epoxy groups. Simultaneously, the formation of products from the side reactions of the epoxy group could affect the formation of the silicate network by hydrolysis-condensation reaction involving the alkoxide groups. Consequently, the formed OIH material may exhibit a network characterized by a reduced level of polymerization/condensation. This affects primarily the extension of the amino-alcohol bonds between inorganic (silicate) and organic (Jeffamine®) components and may affect the extension of the silicate network formed. The conjugation of these factors may contribute to lower matrix cohesion and integrity, leading to the loss of the barrier properties of the coatings and affecting the electric (conductivity) and dielectric (permittivity) properties of the OIH gel materials. Moreover, all these factors together may also minimize the network-metal surface interactions.

3.1.3. R_p and E_{corr} Measurements

The determination of the R_p and E_{corr} values was performed once a day during the first seven days and then on the 12th, 20th, 27th and 127th days. An exception was made for samples A(230) 1layer, A(600) 1 layer, A(600)_Cr(III) 1 layer and A(2000)_Cr(III) 3 layers where R_p measurements were taken on the 137th day instead on the 127th day. The R_p results obtained for the cells of all sets of HDGS coated samples are presented in Figure 10. An R_p value $\geq 10^6$ Ωcm^2 is considered as the threshold limit value above which steel is passivated in cementitious materials[30] and is represented by a black horizontal line in all plots.
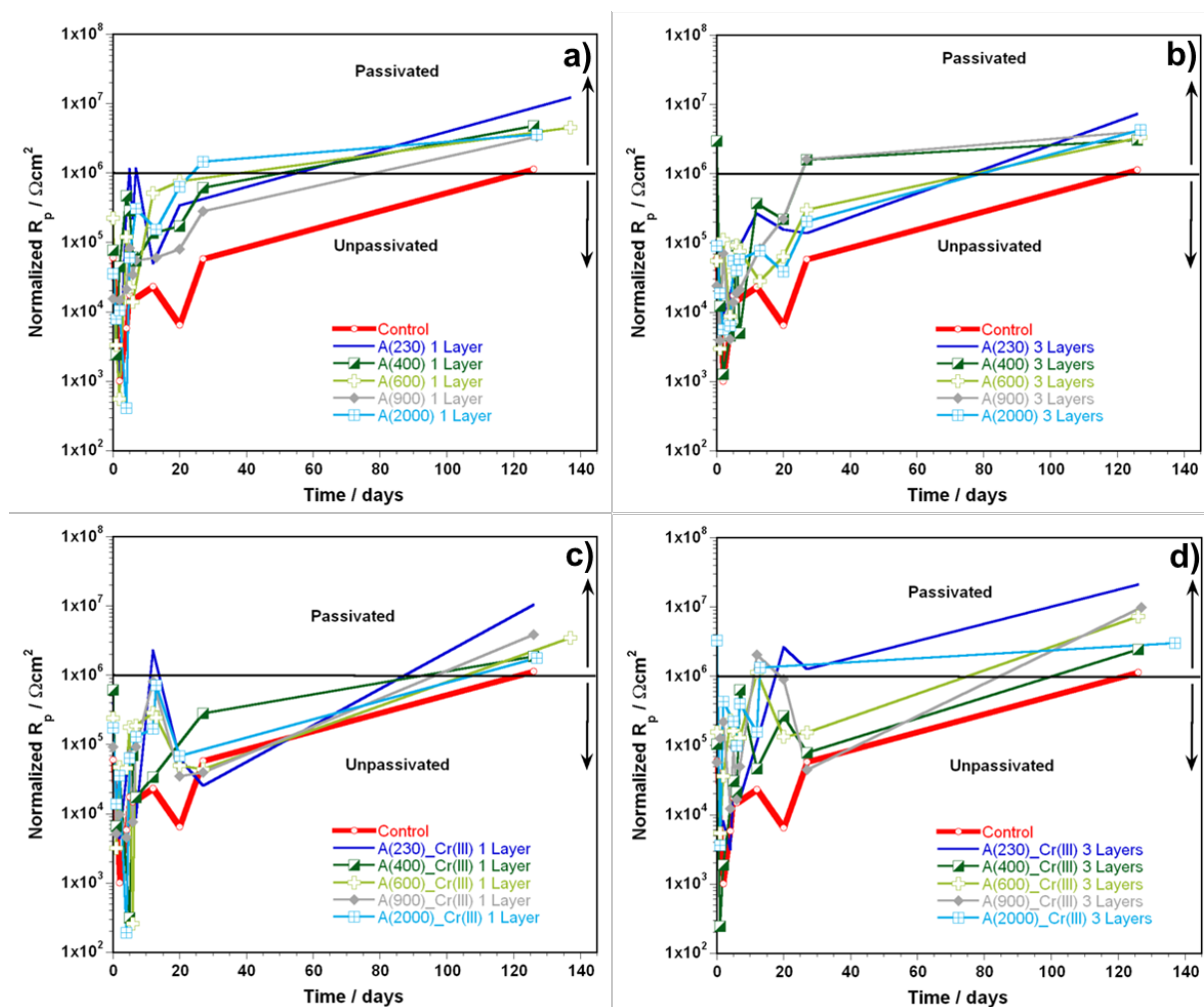
171

Figure 10. Plots of the of normalized polarization resistance (R_p) variation recorded for the different coated HDGS sample cells (kept embedded in mortar for 137 days). Displayed graphs correspond to different amino-alcohol-silicate matrices. A(X) samples deposited by: a) one dip step (1 layer); b) three dip steps (3 layers) and A(X)_Cr(III) samples deposited by: c) one dip step (1 layer); d) three dip steps (3 layers).

The E_{corr} results are presented in Figure 11. In the conditions studied, HDGS coated with OIHs reach passivation earlier than the control, and generally, higher values of i_{gal} correspond to lower R_p data. The results also demonstrate that the R_p and E_{corr} data are in agreement with i_{gal} data measurements. Generally, lower R_p and E_{corr} values were obtained for all cells during the first ten days, suggesting that zinc corrosion occurred, which is also in agreement with the i_{gal} results. After this time, the HDGS coated samples generally show higher E_{corr} and R_p values when compared to the control. However, the OIHs based on A(X)_Cr(III) matrices with the exception of A(400)_Cr(III) and A(2000)_Cr(III), both with one layer (Figure 11c) and A(900)_Cr(III) with three layers (Figure 11d) show lower R_p values on the 27th day when compared to the control sample.
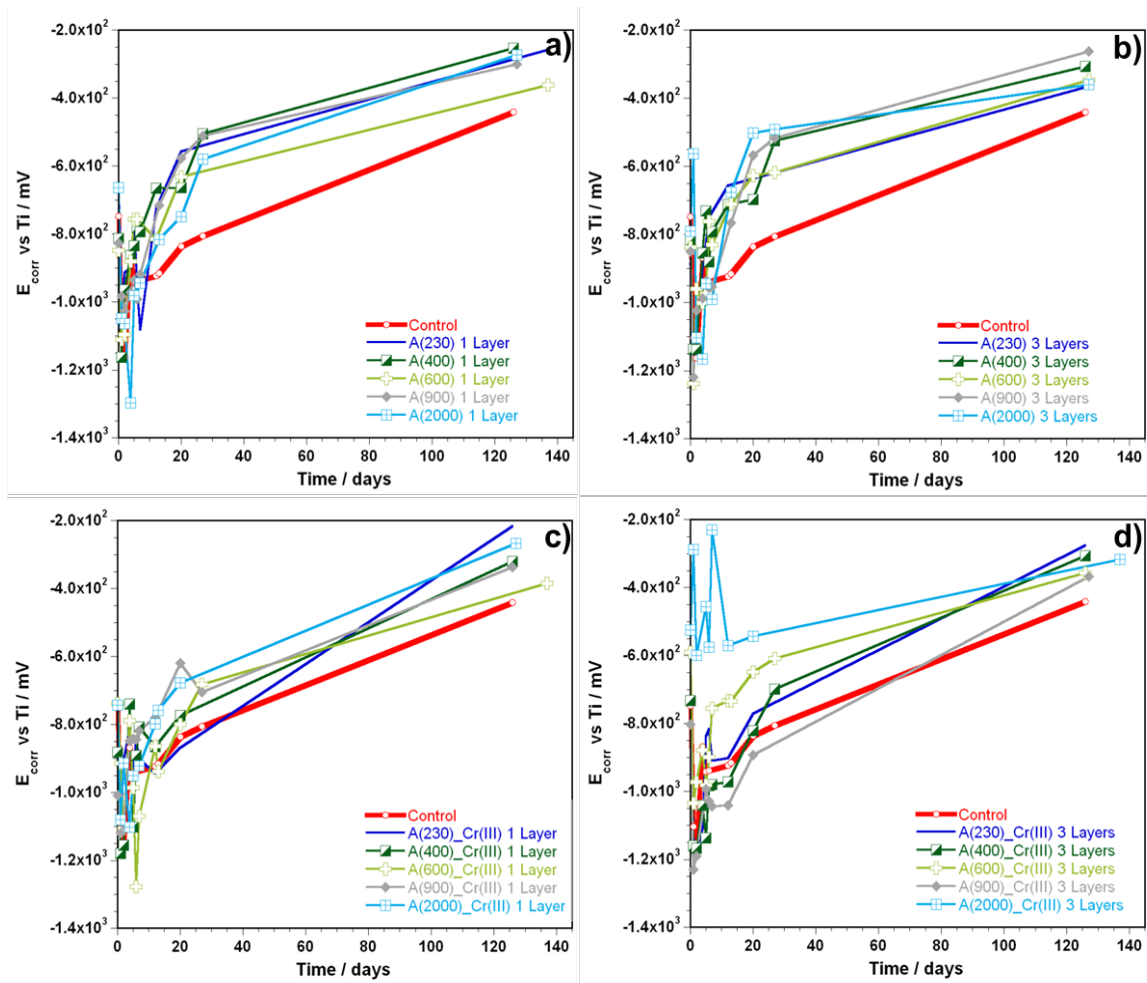
Figure 11. Plots of the of corrosion potential (E_{corr}) variation over time recorded for the different coated HDGS sample cells (kept embedded in mortar for 137 days). Displayed graphs correspond to different amino-alcohol-silicate matrices. A(X) samples deposited by: a) one dip step (1 layer); b) three dip steps (3 layers) and A(X)_Cr(III) samples deposited by: c) one dip step (1 layer); d) three dip steps (3 layers).

For the E_{corr} data only A(230)_Cr(III) one layer (Figure 10c) and A(900)_Cr(III) three layers (Figure 10d) show values lower than the control samples. These results may be explained by the low reaction time between the two gel precursors (Jeffamine® and GPTMS) and/or the presence of Cr(III) ions. In the first case, the OIH material formed might show a network that is characterized by a reduced level of polymerization/condensation, which may contribute to lower network-metal surface bonding and to an increase in matrix permeability, leading to the loss of the barrier properties of the OIH coatings. Another explanation for these results might be oxidation of the Cr(III) ions into high state forms due to the reaction with the functional groups of siloxane-derived precursor (epoxide) that did not previously react, contributing to a net reduction. Consequently, the formation of chemical bonds with free Cr(III) ions within the gel matrix will also compromise the hybrid

network. These results are not in agreement with the conductivity data as the inclusion of Cr(III) ions does not significantly change the conductivity of the OIH films, suggesting that Cr(III) ions do not interact significantly with the OIH network. This behaviour suggests a synergetic effect of the interactions of the OIH coatings and the electrolyte (mortar) and the Cr(III) ions within the OIH network. However, these results are in agreement with other authors.[28,55] It has been shown that the choice of inhibitor, as well the concentration used in the synthesis process, are critical parameters that interfere with the stability of the OIH network, compromising the barrier properties of the OIHs doped with Cr(III). Nevertheless, more studies should be performed in order to evaluate which other possible factors might contribute to the loss of stability of the OIH coatings doped with Cr(III). By analysing the data obtained for HDGS coated with A(230) with and without Cr(III) one layer (Figure 11b), it is observed that the substrate with each one of the OIH coatings passivates in the first few days. However, the R_p values suddenly drop under the limit of passivation for the period between the 10th and 27th day, rising again to values above the passivation limit by the 55th and 90th days, respectively. HDGS samples coated with three layers and one layer of pure OIHs A(400) (Figure 10b), exhibit higher R_p values when compared to the doped matrices. Table 4 summarizes the relevant data about the R_p evolution with time for all the studied cells. The information gathered in this table is: the observed time (in days) necessary for R_p to reach passivation threshold values, the evolution of R_p after the threshold moment and the R_p value at the end of the monitoring period (137 days).

Table 4. Electrical properties of the OIH disc samples based on A(X) matrices

OIH sample	log (R / Ω cm^2)	-log (σ / Scm^{-1})	C / nF cm^{-2}	ε_r
A(400)[a]	8.69 ± 0.10	9.85 ± 0.06	0.035 ± 0.002	26.90 ± 2.36
A(400)_Cr(III)	8.14 ± 0.42	9.37 ± 0.43	0.124 ± 0.017	84.36 ± 11.93
A(600)[b]	5.97 ± 0.34	6.39 ± 0.90	n.a.	n.a.
A(600)_Cr(III)	5.80 ± 0.10	6.85 ± 0.09	0.040 ± 0.004	40.13 ± 5.69
A(900)	4.78 ± 0.13	5.99 ± 0.05	0.041 ± 0.006	28.50 ± 4.00
A(900)_Cr(III)	4.76 ± 0.07	5.98 ± 0.09	0.041 ± 0.002	28.44 ± 1.96
A(2000)	4.78 ± 0.29	5.89 ± 0.40	0.051 ± 0.009	56.75 ± 9.39
A(2000)_Cr(III)	5.09 ± 0.11	6.24 ± 0.11	0.031 ± 0.002	24.33 ± 1.77

Notes: a) Analysis of impedance response at high frequencies based on a EEC, as shown as inset in correspondent Nyquist plots, Figures 2, 4, 5, 6, 7 and 8, respectively; b) Analysis of impedance response at high frequencies based on an EEC, as shown in the correspondent Nyquist plot (Figure 3).

After 10 days, all the coated samples show higher E_{corr} values than the control with the exception of A(230)_Cr(III) and A(600)_Cr(III), both with one layer (Figure 11c), and A(400)_Cr(III) and

A(900)_Cr(III), both with three layers (Figure 11d). Overall, in the conditions studied, HDGS coated with OIHs show that the R_p and E_{corr} data are in agreement with i_{gal} measurements.

3.2. Morphology of the Coatings

The preliminary observations of the surfaces of the HDGS were performed using a stereo-zoom microscope before and after being embedded in a mortar. The images obtained with stereo-zoom microscope for the control samples, A(600)_Cr(III) and A(2000)_Cr(III) after being embedded for 137 days are shown in Figure 12.
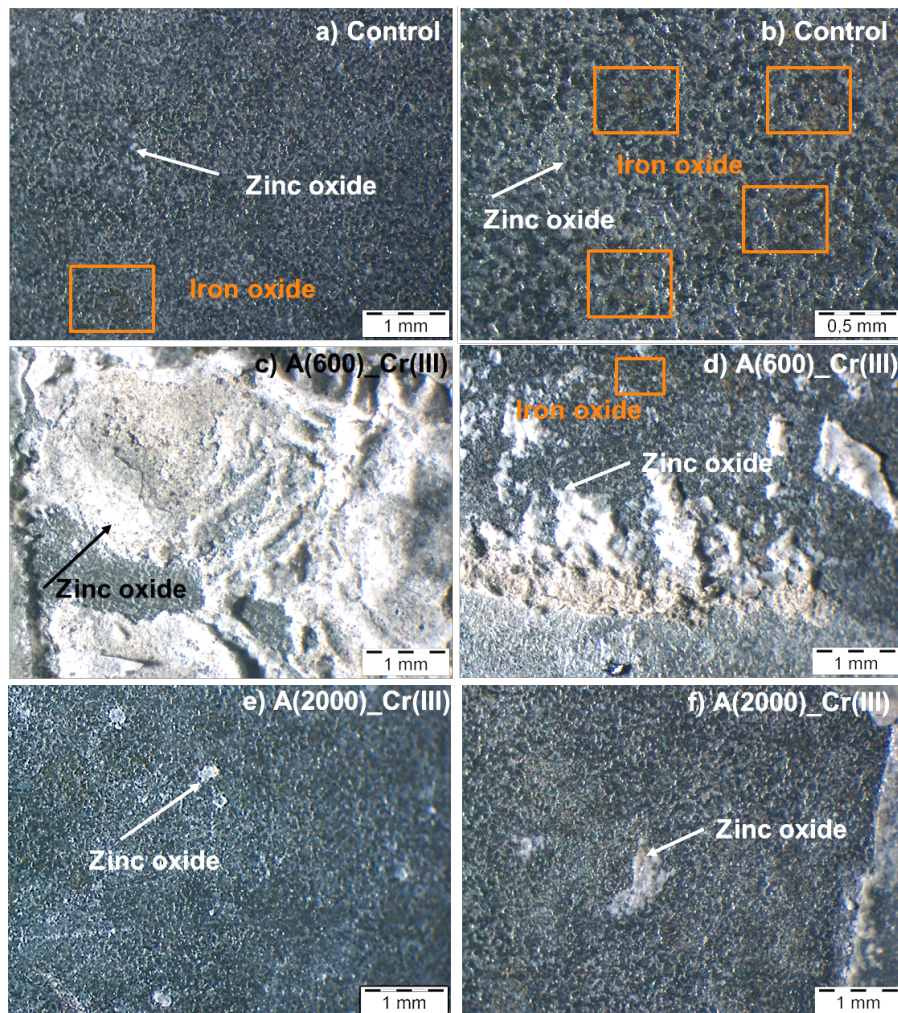

Figure 12. Stereomicroscopic observation of HDGS surfaces: a) uncoated substrate (control) magnified twenty times; b) uncoated substrate (control) magnified forty times; c) and d) HDGS coated with A(600)_Cr(III) 3 layers; e) and f) HDGS coated with A(2000)_Cr(III) 3 layers all magnified twenty times after being embedded in mortar for 137 days.

Images for the control samples are shown at two different magnitudes, Figure 12b is twice the magnification of Figure 12a. As an illustrative examples the photographs of the HDGS coated with A(600)_Cr(III) three layers in Figures 12c and 12d and A(2000)_Cr(III) three layers in Figures 12e and 12f after being embedded in a mortar for 137 days are shown. All HDGS samples coated were obtained with a 20 times magnification. The control sample (Figures 12a and 12b), showed the presence of zinc oxide (white deposits known as white rust10,11) and iron oxide (rusty deposits) on both surfaces after being embedded in a mortar for 137 days. The images obtained for all coated substrates in the same conditions as the control samples showed improved results. The presence of iron oxide was not as clear as in the control samples and only traces of iron oxides were found on the substrate. However, deposits of zinc oxides were evident. The substrates coated with A(600)_Cr(III) three layers (Figures 12c and 12d) exhibited a large amount of zinc oxides when compared either to the uncoated substrates (control) or HDGS coated with A(2000)_Cr(III).

The substrates coated with A(600)_Cr(III) with three layers showed lower R_p and E_{corr} values (Figures 10 and 11). This behaviour seems to be related with the corrosion of zinc that is demonstrated by the large amount of zinc oxides found on the surface (Figures 12c and 12d). The R_p, E_{corr} and i_{gal} values are in agreement with the visual observations. Higher R_p, E_{corr} and lower i_{gal} values were obtained for the coated substrates that showed few oxides on the surface (Figures 12e and 12f) and consequently were less attacked by the electrolyte. Lower R_p and higher i_{gal} values correspond to the surfaces that were attacked more by the electrolyte, such as the case of the large amount of oxides found on the surface of HDGS coated with A(600)_Cr(III) three layers (Figures 12c and 12d). The huge amount of zinc oxides found on these surfaces (Figures 12c and 12d) might be explained, once again, by the low reaction time between the two precursors. The incomplete reaction between the two precursors may lead to the formation of sub products within the OIH matrix network. These sub products are available to react with the zinc and that may cause the production of great amount zinc oxides (Figure 12c).

Surface morphology of coated HDGS samples was assessed by SEM/EDS analysis before and after contact with a high alkaline environment. SEM analyses revealed that A(X) coatings cover the HDGS substrate regardless of the OIH composition and the number of dip steps. Figure 13 is an example of the coated substrate by one dip step. The BSE image shows that the darker areas correspond to the OIH coating and lighter areas to uncoated or barely coated substrate. The presence of Zn, demonstrated by the EDS analysis, corresponds to lighter areas and the presence of OIH coating to high peaks of C, O and Si. The presence of Cr was also confirmed by the SEM/EDS analysis.
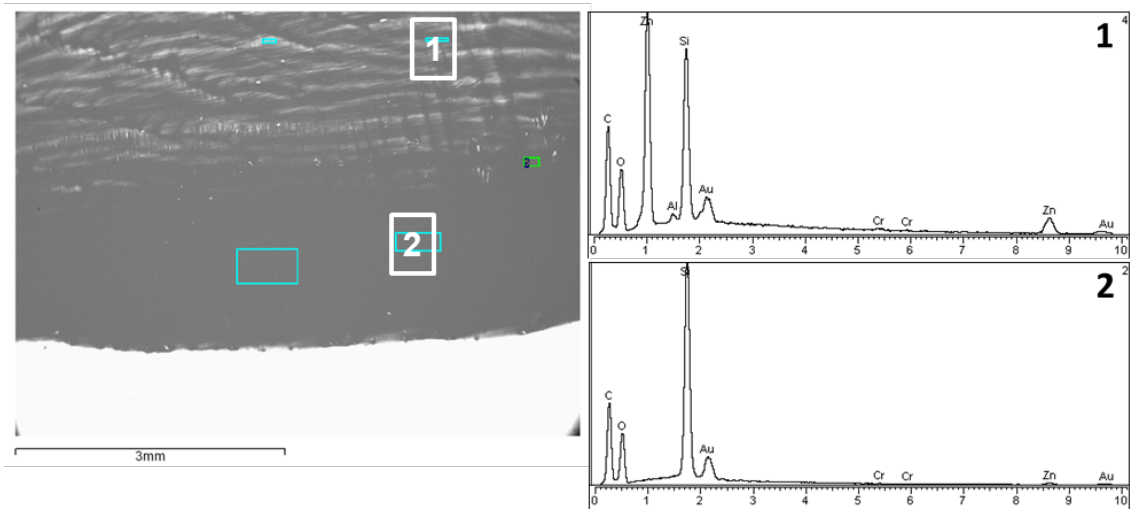
Figure 13. SEM/EDS of HDGS surfaces coated by one dip step with OIH sol-gel before being embedded in mortar.

Figure 13 also shows that the thickness of the coatings on the substrate is not homogenous since multiple shades of grey were found. EDS analysis confirmed that the darker areas present high intensity peaks of Si, C and O, and correspond to thicker coating zones compared to the light grey areas which show lower intensity peaks of Si, C, O and high peaks of Zn (Figure 13) that could be interpreted as the thinnest coating area.
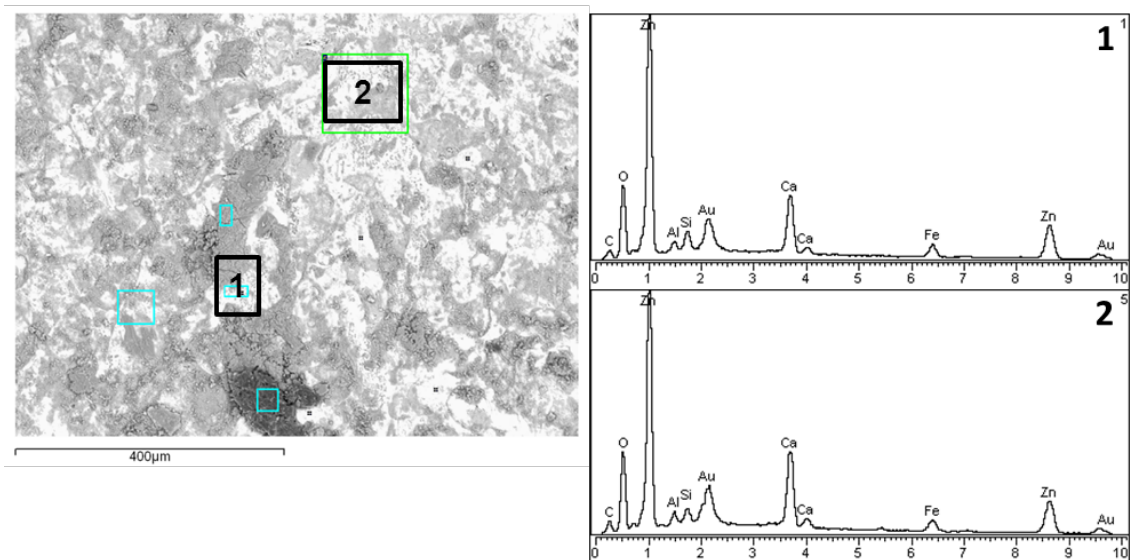

Figure 14. SEM/EDS of HDGS surfaces uncoated (control) after being embedded in mortar for 137 days.

A detailed analysis of the morphological modifications produced on HDGS coated samples, after 137 days exposed to mortar, is highlighted on a representative example of HDGS coated with A(600)_Cr(III). The results for HDGS samples uncoated (control) and coated with OIHs A(600)_Cr(III) with one or three layers, embedded in mortar for 137 days, are displayed in Figures 14 and 15, respectively.
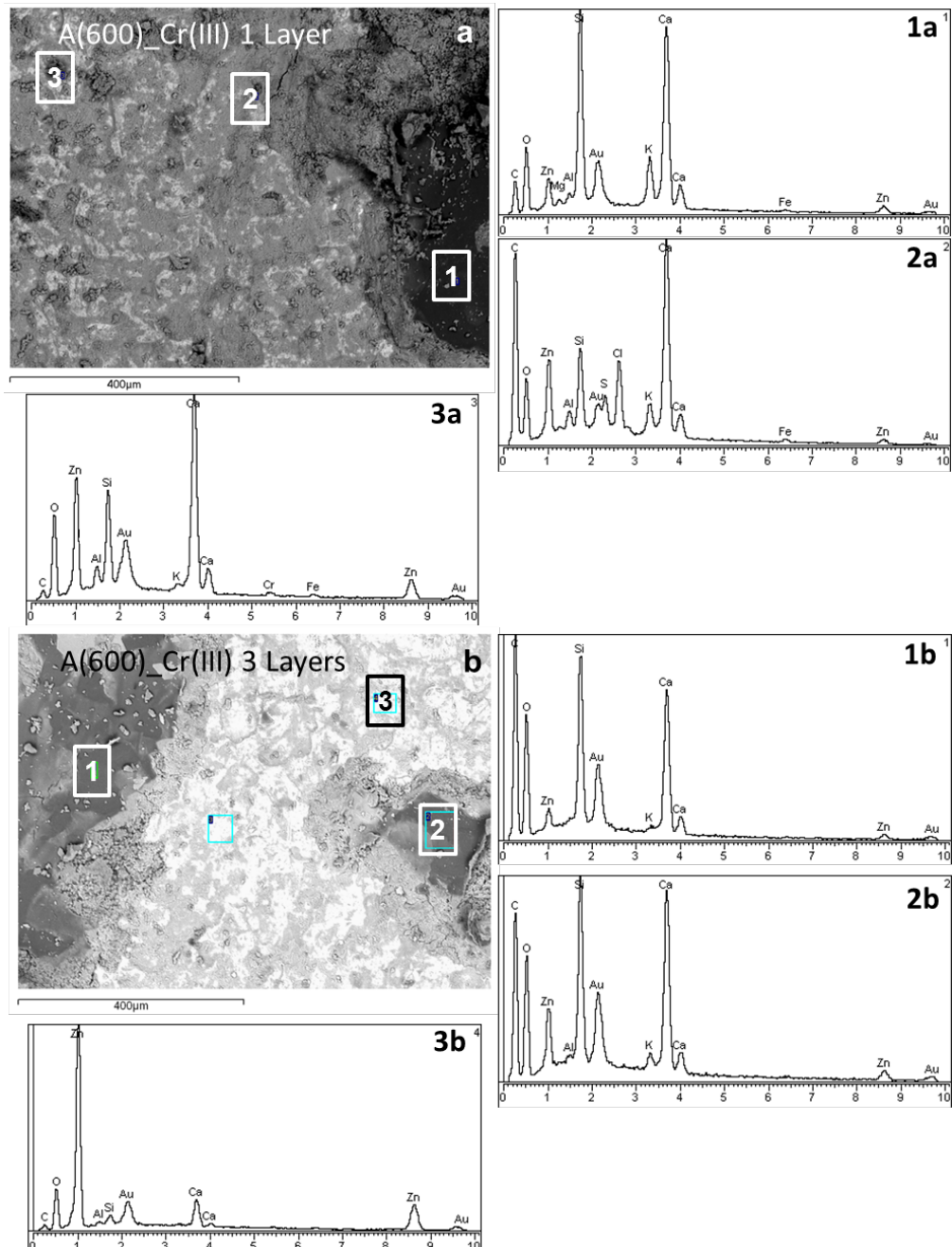

Figure 15. SEM images of HDGS surfaces coated with: a) A(600)_Cr(III) 1 layer; b) A(600)_Cr(III) 3 layers after being embedded in mortar for 137 days. EDS spectra of HDGS coated with A(600)_Cr(III) 1 layer: 1a, 2a and 3a and coated with A(600)_Cr(III) 3 layers: 1b, 2b and 3b.

The obtained images and spectra show that A(600)_Cr(III) deposited by one dip step show traces of Fe (Figure 15a), suggesting that the OIH coating was eroded as well the Zn protective layer. However, these results show less erosion than the control (Figure 14). HDGS coated with three layers of A(600)_Cr(III) (Figure 15b) show an improved behaviour when compared to the substrate coated with one layer of A(600)_Cr(III) and no traces of Fe were found. It has also been demonstrated that the SEM/EDS results are in agreement with the data obtained by i_{gal} and R_p measurements. The R_p, E_{corr} and i_{gal} values are also in agreement with SEM/EDS results.

4. Conclusions

The present work reports the electrochemical study of OIH sol-gel based coatings on HDGS in contact with mortar for 137 days. The OIH coatings were obtained from the reaction of GPTMS with Jeffamine® of different molecular weights (MWs) doped and undoped with Cr(III) ions and deposited on HDGS by a single or a triple dip step method.

The results allow to conclude that the A(230) and A(400), regardless the presence of Cr(III) ions, show electrochemical properties that makes them suitable for consideration as an efficient coating material. A(400) with or without Cr(III) showed resistances that meet the desired requirements for coatings protections (resistances $>10^7$ Ω cm^2).[52-54] The electrochemical results obtained from monitoring cells involving HDGS coated samples exposed to mortar show that all samples, after 137 days, display better performance when compared to the uncoated HDGS sample. It was also noted that the i_{gal} values are in agreement with R_p, E_{corr} and SEM/EDS data.

The results point to the conclusion that the produced OIH film coatings based on A(X) matrices have promising properties to be employed as pre-treatments to reduce corrosion activity during the initial stages of contact of the HDGS samples with the concrete alkaline environment, allowing the formation of protective layers on the surface of the substrate. For the conditions tested in this work, the results suggest that the observed barrier effect introduced by A(230) and A(400) OIH coatings, with or without the presence of Cr(III), could hinder or partially hinder the cathodic reaction involving hydrogen evolution and may be considered potential substitutes for chromium-based pre-treatments systems containing Cr(VI). Future research should take into account modifications on OIH gel coating synthesis procedures by adjusting the sol-gel procedure and optimizing the reaction between the two precursors (GPTMS and Jeffamine®) to improve the structural properties of the matrix. Further studies on the curing conditions of the OIH coatings on HDGS should also be performed to improve the corrosion protection efficiency.

Acknowledgements

References

1. H. Böhni, *Corrosion in reinforced concrete structures*, ed. H. Böhni, Woodhead Publishing Ltd, Cambridge, UK (2005).

2. D. A. Hausmann, *Mater. Prot.*, **6**, 19-23 (1967).

3. C. L. Page and K. W. J. Treadaway, *Nature*, **297**, 109-115 (1982).

4. F. W. Gibson, *Corrosion, Concretes and chlorides – steel corrosion concrete: causes and restraints,* ACI SP-102, American Concrete Institute, Detroit, USA (1987).

5. N. S. Berke, V. Chaker and D. Whiting, *ASTM STP 1065*, American Society for Testing Materials, Philadelphia, USA (1990).

6. *Concrete Reinforcement Corrosion: ICE design and practice*, ed. Thomas Telford Publishing, London, UK (2002).

7. L. Bertolini, B. Elsener, P. Pedeferri, E. Redaelli and R. B. Polder, *Corrosion of Steel in Concrete: Prevention, Diagnosis, Repair*, Wiley-VCH Verlag GmbH & Co KGaA, Weinheim, Germany (2004).

8. N. R. Short, S. Zhou and J. K. Dennis, *Surf. Coat. Technol.*, **79**, 218-224 (1996).

9. U. Nürnberger, *Corrosion of metals in contact with mineral building materials*, M. Raupach, B. Elsener, R. Polder, J. Mietz (Eds.), Corrosion Reinforcements in Concrete (EFC 38), EFC series, Belgium (2006).

10. Fédération Internationale du Béton, *Effect of zinc on prestressing steel*, FIB bulletin Nº. 64 (2012).

11. Comité Euro-International du Béton, *Coating protection for reinforcement: State of the art report*, CEB Bulletin d'Information Nº. 211 (1995).

12. C. Andrade and C. Alonso, *Electrochemical aspects of galvanized reinforcement corrosion*, in: S. R. Yeomans (Ed.), Galvanised steel reinforcement in concrete, Oxford (2004).

13. R. Reisfeld and C. K. JØrgensen, Chemistry, *Spectroscopy and Applications of Sol-Gel glasses*, Springer-Verlag, Berlin, Heidelberg (1992).

14. S. Kozhukharov, V. Kozhukharov, M. Wittmar, M. Schem, M. Aslan, H. Caparrotti and M. Veith, *Prog. Org. Coat.*, **71**, 198-205 (2011).

15. S. Ningshen, U. K. Mudali, R. Krishnan and B. Raj, *Surf. Coat. Tech.*, **205**, 3961-3966 (2011).

16. F. Samiee, K. Raeissi and M. A. Golozar, *Corros. Sci.*, **53**, 1969-1975 (2011).

17. C. Sanchez, G. J. de A. A. Soler-Illia, F. Ribot, T. Lalot, C. R. Mayer and V. Cabuil, *Chem. Mater.*, **13**, 3061-3083 (2001).

18. J. H. Osborne, *Prog. Org. Coat.*, **41**, 280-286 (2001).

19. C. Arunchandran, S. Ramya, R. P. George and U. Kamachi Mudaliz, *J. Electrochem. Soc.*, **159**, C552-C559 (2012).

20. H. Shi, F. Liu and E. Han, *Trans. Nonferrous Met. Soc. China*, **20**, 1928-1935 (2010).

21. M. Fedel, M.-E. Druart, M. Olivier, M. Poelman, F. Deflorian and S. Rossi, *Prog. Org. Coat.*, **69**, 118-125 (2010).

22. B. Nikrooz and M. Zandrahimi, *J Sol-Gel Sci Technol.*, **59**, 640-649 (2011).

23. E. P. Souza, E. Arizab, M. Ballester, I. V. P. Yoshida, L. A. Rocha and C. M. A. Freire, *Mat. Res.*, **9**, 59-64 (2006).

24. European Committee for Standardization, BS EN 196-1 (2005).

25. ASTM G109-07 Standard Test Method for Determining Effects of Chemical Admixtures on Corrosion of Embedded Steel Reinforcement in Concrete Exposed to Chloride Environments. In: Annual book of ASTM standards, 03.02, (2007).

26. C. J. R. Silva and M. J. Smith, *Electrochim. Acta*, **40**, 2389-2392 (1995)

27. R. M. Figueira, E. V. Pereira, C. J. R. Silva and M. M. Salta, *Port. Electrochim. Acta*, **31**, 277-287 (2013).

28. R. B. Figueira, C. J. R. Silva, E. V. Pereira and M. M. Salta, *J. Electrochem. Soc.*, **160**, C467-C479 (2013).

29. E. V. Pereira, R. B. Figueira, M. M. Salta and I. T. E. Fonseca, *Sensors*, **9**, 8391-8398 (2009).

30. J. González, A. Molina, M. Escudero and C. Andrade, *Corros. Sci.*, **25**, 917-930 (1985).

31. C. Andrade, V. Castelo, C. Alonso and J. González, *Corrosion effect of stray currents and the techniques for evaluating corrosion of rebars in concrete*, ASTM STP 906, American Society for Testing and Materials, Philadelphia (1986).

32. European Committee for Standardization, EN ISO 1463 (2003).

33. L. Beaunier, I. Epelboin, J. C. Lestrade and H. Takenouti, *Surf. Technol.*, **4**, 237-254 (1976).

34. M. W. Kendig and H. Leidheiser, *J. Electrochem. Soc.*, **23**, 982-989 (1976).

35. J. D. Scantlebury and K. N. Ho., *JOCCA*, **62**, 89-92 (1979).

36. T. Szauer, *Prog. Org. Coat.*, **10**, 157-170 (1982).

37. F. Mansfeld, M. W. Kendig and S. Tsai, *Corrosion*, **38**, 478-485 (1982).

38. A. Amirudin and D. Thierry, *Prog. Org. Coat.*, **26**, 1-28 (1995).

39. F. Deflorian and L. Fedrizzi, *J. Adhesion Sci. Technol.*, **13**, 629-645 (1999).

40. D. Loveday, P. Peterson and B. Rodgers, *J. Coat. Tech.*, **10**, 88-93 (2004).

41. D. Loveday, P. Peterson and B. Rodgers, *J. Coat. Tech.*, **2**, 22-27 (2005).

42. F. Deflorian and S. Rossi, *Electrochim. Acta*, **51**, 1736-1744 (2006).

43. K. Allahar, Q. Su and G. P. Bierwagen, *Prog. Org. Coat.*, **67**, 180-187 (2010).

44. S. Touzain, *Electrochim. Acta*, **55**, 6190-6194 (2010).

45. T. Breugelmans, E. Tourwé, J. B. Jorcin, A. Alvarez-Pampliega, B. Geboes, H. Terryn and A. Hubin, *Prog. Org. Coat.*, **69**, 215-218 (2010).

46. A. S. Roya, S. Gupta, S. Seethamraju, G. Madras and P. C Ramamurthy, *Composites: Part B*, **58**, 134-139 (2014).

47. S. R. Kunst, H. R. P. Cardoso, C. T. Oliveira, J. A. Santana, V. H. V. Sarmento, I. L. Muller and C. F. Malfatti, *Appl. Surf. Sci.*, **298**, 1-11 (2014).

48. J. Ross Macdonald and W. B. Johnson, *Impedance Spectroscopy*, John Wiley & Sons, New York, USA, (1987).

49. M. E. Orazem and B. Tribollet, *Electrochemical Impedance Spectroscopy*, John Wiley & Sons, Inc., Hoboken, NJ, USA (2008).

50. J. B. Jorcin, M.E. Orazem, N.P. Pébère and B. Tribollet, *Electrochim. Acta* **51**, 1473-1479 (2006).

51. G. Bierwagen, D. Tallmann, J Li, L. He and L. C. Jeffcoate, *Prog. Org. Coat.*, **46**,149-158 (2003).

52. H. Leidheiser, Jr., *Prog. Org. Coat.*, **7**, 79-104 (1979).

53. H. Leidheiser, Jr., *J. Coat. Technol.*, **802**, 21-31 (1991).

54. H. M. Jol, *Ground penetrating radar theory and applications*, Elsevier Science, Amsterdam (2008).

55. M. L. Zheludkevich, R. Serra, M. F. Montemor, K. A. Yasakau, I. M. Miranda Salvado and M. G. S. Ferreira, *Electrochim. Acta,* **51**, 208-217 (2005).

Conclusions

The use and the applicability of the sol-gel method for the production of organic-inorganic hybrid (OIH) coatings on hot-dip galvanized steel (HDGS) for corrosion protection in contact with cementitious materials have been demonstrated for the first time. OIH sol-gel coatings based on ureasilicate (U(X)) and alcohol-aminosilicate (A(X)) matrices doped and undoped with Cr(III) were deposited on HDGS by a dip-coating method.

The U(X) coatings were obtained from the reaction of ICPTES with Jeffamine of different molecular weights (MWs). A(X) coatings were obtained from the reaction of GPTMS with Jeffamine® of different molecular weights (MWs). Both OIHs were deposited on HDGS by a single or a triple dip step method without residence time.

OIH film samples were assessed by Electrochemical Impedance Spectroscopy (EIS). Generally, U(X) based matrices show higher resistance values than A(X) based matrices, with or without an inhibitor. The EIS results allows for the conclusion that A(230), A(400) and all the U(X) coatings, with or without inhibitor, show electrical properties that meet the desired requirements to be considered as efficient pre-treatments for corrosion protection. Moreover, the EIS is a technique that accurately and rapidly evaluates the barrier properties of OIH sol-gel materials.

The OIH coatings on HDGS samples were exposed to cementitious materials and monitored by macrocell current density (i_{gal}) and polarization resistance (R_p). The electrochemical results show that all the samples display better performance when compared to the control. It was also shown that the i_{gal} values are in agreement with R_p data and that both performance parameters are sensitive to the OIH composition as well as the process used to obtain the deposited coatings. Moreover, it was also shown that the i_{gal} values are in agreement with R_p, corrosion potential and SEM/EDS data.

The prepared OIH sol-gel coatings effectively minimize the corrosion of HDGS in the first instants of contact with highly alkaline environments such as concrete. Furthermore, the HDGS coated with the OIH coatings, when in contact with cementitious materials, at room temperature, reaches passivation earlier than the control (non coated) HDGS sample and before the curing period of the concrete (28 days).

The results point to the conclusion that the produced OIH film coatings based on U(X) and A(X) matrices have promising properties to be employed as pre-treatments to reduce corrosion activity during the initial stages of contact of the HDGS samples with highly alkaline environments such as concrete, allowing the formation of protective layers on the surface of the substrate. For the

conditions tested in this work, the results suggest that the observed barrier effect introduced by A(230), A(400) and all the U(X) coatings, with or without the presence of a Cr(III) inhibitor, could hinder or partially hinder the cathodic reaction involving hydrogen evolution and may be considered potential substitutes for chromium-based pre-treatments systems containing Cr(VI).

As a result of this study, further research might well be conducted in order to improve the corrosion behaviour of the A(X) matrices. Furthermore, the coatings coverage obtained throughout this study point to the conclusion that the coating deposition method used can be optimized in order to improve the OIH coating properties and therefore increase their barrier performance. Therefore, new deposition methods should be studied such as spin or spraying or the combination of both. However, the time consumed and the costs associated with the coating deposition method and the used precursors, in order to obtain stable and effective protective coatings should be considered.